TURKISH
JOURNAL OF PHARMACEUTICAL SCIENCES

TURKISH
JOURNAL OF PHARMACEUTICAL SCIENCES

TÜRK
ECZACILIK BİLİMLERİ DERGİSİ

AIMS AND SCOPE

The Turkish Journal of Pharmaceutical Sciences is the only scientific periodical publication of the Turkish Pharmacists' Association and has been published since April 2004.

Turkish Journal of Pharmaceutical Sciences is an independent international open access periodical journal based on double-blind peer-review principles. The journal is regularly published 4 times a year and the publication language is English. The issuing body of the journal is Galenos Yayinevi/Publishing House.

The aim of Turkish Journal of Pharmaceutical Sciences is to publish original research papers of the highest scientific and clinical value at an international level.

The target audience includes specialists and physicians in all fields of pharmaceutical sciences.

The editorial policies are based on the "Recommendations for the Conduct, Reporting, Editing, and Publication of Scholarly Work in Medical Journals (ICMJE Recommendations)" by the International Committee of Medical Journal Editors (2016, archived at http://www.icmje.org/) rules.

Editorial Independence

Turkish Journal of Pharmaceutical Sciences is an independent journal with independent editors and principles and has no commerical relationship with the commercial product, drug or pharmaceutical company regarding decisions and review processes upon articles.

ABSTRACTED/INDEXED IN

Web of Science-Emerging Sources Citation Index (ESCI)
SCOPUS SJR
Directory of Open Access Journals (DOAJ)
ProQuest
Chemical Abstracts Service (CAS)
EBSCO
EMBASE
Analytical Abstracts
International Pharmaceutical Abstracts (IPA)
Medicinal & Aromatic Plants Abstracts (MAPA)
TÜBİTAK/ULAKBİM TR Dizin
Türkiye Atıf Dizini
UDL-EDGE

OPEN ACCESS POLICY

This journal provides immediate open access to its content on the principle that making research freely available to the public supports a greater global exchange of knowledge.

Open Access Policy is based on the rules of the Budapest Open Access Initiative (BOAI) http://www.budapestopenaccessinitiative.org/. By "open access" to peer-reviewed research literature, we mean its free availability on the public internet, permitting any users to read, download, copy, distribute, print, search, or link to the full texts of these articles, crawl them for indexing, pass them as data to software, or use them for any other lawful purpose, without financial, legal, or technical barriers other than those inseparable from gaining access to the internet itself. The only constraint on reproduction and distribution, and the only role for copyright in this domain, should be to give authors control over the integrity of their work and the right to be properly acknowledged and cited.

MATERIAL DISCLAIMER

The author(s) is (are) responsible for the articles published in the JOURNAL.

The editor, editorial board and publisher do not accept any responsibility for the articles.

INSTRUCTIONS TO AUTHORS

Turkish Journal of Pharmaceutical Sciences is the official double peer-reviewed publication of The Turkish Pharmacists' Association. This journal is published every 3 months (4 issues per year; March, June, September, December) and publishes the following articles:

• Research articles

• Reviews (only upon the request or consent of the Editorial Board)

• Preliminary results/Short communications/Technical notes/Letters to the Editor in every field or pharmaceutical sciences.

The publication language of the journal is English.

The Turkish Journal of Pharmaceutical Sciences does not charge any article submission or processing charges.

A manuscript will be considered only with the understanding that it is an original contribution that has not been published elsewhere.

The Journal should be abbreviated as "Turk J Pharm Sci" when referenced.

The scientific and ethical liability of the manuscripts belongs to the authors and the copyright of the manuscripts belongs to the Journal. Authors are responsible for the contents of the manuscript and accuracy of the references. All manuscripts submitted for publication must be accompanied by the Copyright Transfer Form [copyright transfer]. Once this form, signed by all the authors, has been submitted, it is understood that neither the manuscript nor the data it contains have been submitted elsewhere or previously published and authors declare the statement of scientific contributions and responsibilities of all authors.

Experimental, clinical and drug studies requiring approval by an ethics committee must be submitted to the JOURNAL with an ethics committee approval report including approval number confirming that the study was conducted in accordance with international agreements and the Declaration of Helsinki (revised 2013) (http://www.wma.net/en/30publications/10policies/b3/). The approval of the ethics committee and the fact that informed consent was given by the patients should be indicated in the Materials and Methods section. In experimental animal studies, the authors should indicate that the procedures followed were in accordance with animal rights as per the Guide for the Care and Use of Laboratory Animals (http://oacu.od.nih.gov/regs/guide/guide.pdf) and they should obtain animal ethics committee approval.

Authors must provide disclosure/acknowledgment of financial or material support, if any was received, for the current study.

If the article includes any direct or indirect commercial links or if any institution provided material support to the study, authors must state in the cover letter that they have no relationship with the commercial product, drug, pharmaceutical company, etc. concerned; or specify the type of relationship (consultant, other agreements), if any.

Authors must provide a statement on the absence of conflicts of interest among the authors and provide authorship contributions.

All manuscripts submitted to the journal are screened for plagiarism using the 'iThenticate' software. Results indicating plagiarism may result in manuscripts being returned or rejected.

The Review Process

This is an independent international journal based on double-blind peer-review principles. The manuscript is assigned to the Editor-in-Chief, who reviews the manuscript and makes an initial decision based on manuscript quality and editorial priorities. Manuscripts that pass initial evaluation are sent for external peer review, and the Editor-in-Chief assigns an Associate Editor. The Associate Editor sends the manuscript to at least two reviewers (internal and/or external reviewers). The reviewers must review the manuscript within 21 days. The Associate Editor recommends a decision based on the reviewers' recommendations and returns the manuscript to the Editor-in-Chief. The Editor-in-Chief makes a final decision based on editorial priorities, manuscript quality, and reviewer recommendations. If there are any conflicting recommendations from reviewers, the Editor-in-Chief can assign a new reviewer.

The scientific board guiding the selection of the papers to be published in the Journal consists of elected experts of the Journal and if necessary, selected from national and international authorities. The Editor-in-Chief, Associate Editors may make minor corrections to accepted manuscripts that do not change the main text of the paper.

In case of any suspicion or claim regarding scientific shortcomings or ethical infringement, the Journal reserves the right to submit the manuscript to the supporting institutions or other authorities for investigation. The Journal accepts the responsibility of initiating action but does not undertake any responsibility for an actual investigation or any power of decision.

The Editorial Policies and General Guidelines for manuscript preparation specified below are based on "Recommendations for the Conduct, Reporting, Editing, and Publication of Scholarly Work in Medical Journals (ICMJE Recommendations)" by the International Committee of Medical Journal Editors (2016, archived at http://www.icmje.org/).

Preparation of research articles, systematic reviews and meta-analyses must comply with study design guidelines:

CONSORT statement for randomized controlled trials (Moher D, Schultz KF, Altman D, for the CONSORT Group. The CONSORT statement revised recommendations for improving the quality of reports of parallel group randomized trials. JAMA 2001; 285: 1987-91) (http://www.consort-statement.org/);

PRISMA statement of preferred reporting items for systematic reviews and meta-analyses (Moher D, Liberati A, Tetzlaff J, Altman DG, The PRISMA Group. Preferred Reporting Items for Systematic Reviews and Meta-Analyses: The PRISMA Statement. PLoS Med 2009; 6(7): e1000097.) (http://www.prisma-statement.org/);

STARD checklist for the reporting of studies of diagnostic accuracy (Bossuyt PM, Reitsma JB, Bruns DE, Gatsonis CA, Glasziou PP, Irwig LM, et al., for the STARD Group. Towards complete and accurate reporting of studies of diagnostic accuracy: the STARD initiative. Ann Intern Med 2003;138:40-4.) (http://www.stard-statement.org/);

STROBE statement, a checklist of items that should be included in reports of observational studies (http://www.strobe-statement.org/);

MOOSE guidelines for meta-analysis and systemic reviews of observational studies (Stroup DF, Berlin JA, Morton SC, et al. Meta-analysis of observational studies in epidemiology: a proposal for reporting Meta-analysis of observational Studies in Epidemiology (MOOSE) group. JAMA 2000; 283: 2008-12).

Authorship

Each author should have participated sufficiently in the work to assume public responsibility for the content. Any portion of a manuscript that

is critical to its main conclusions must be the responsibility of at least 1 author.

GENERAL GUIDELINES

Manuscripts can only be submitted electronically through the Journal Agent website (http://journalagent.com/tjps/) after creating an account. This system allows online submission and review.

The manuscripts are archived according to ICMJE, Web of Science-Emerging Sources Citation Index (ESCI), SCOPUS, Chemical Abstracts, EBSCO, EMBASE, Analytical Abstracts, International Pharmaceutical Abstracts, MAPA(Medicinal & Aromatic Plants Abstracts), Tübitak/Ulakbim Turkish Medical Database, Türkiye Citation Index Rules.

Format: Manuscripts should be prepared using Microsoft Word, size A4 with 2.5 cm margins on all sides, 12 pt Arial font and 1.5 line spacing.

Abbreviations: Abbreviations should be defined at first mention and used consistently thereafter. Internationally accepted abbreviations should be used; refer to scientific writing guides as necessary.

Cover letter: The cover letter should include statements about manuscript type, single-Journal submission affirmation, conflict of interest statement, sources of outside funding, equipment (if applicable), for original research articles.

The ORCID (Open Researcher and Contributor ID) number of the all authors should be provided while sending the manuscript. A free registration can be done at http://orcid.org.

REFERENCES

Authors are solely responsible for the accuracy of all references.

In-text citations: References should be indicated as a superscript immediately after the period/full stop of the relevant sentence. If the author(s) of a reference is/are indicated at the beginning of the sentence, this reference should be written as a superscript immediately after the author's name. If relevant research has been conducted in Turkey or by Turkish investigators, these studies should be given priority while citing the literature.

Presentations presented in congresses, unpublished manuscripts, theses, Internet addresses, and personal interviews or experiences should not be indicated as references. If such references are used, they should be indicated in parentheses at the end of the relevant sentence in the text, without reference number and written in full, in order to clarify their nature.

References section: References should be numbered consecutively in the order in which they are first mentioned in the text. All authors should be listed regardless of number. The titles of Journals should be abbreviated according to the style used in the Index Medicus.

Reference Format

Journal: Last name(s) of the author(s) and initials, article title, publication title and its original abbreviation, publication date, volume, the inclusive page numbers. Example: Collin JR, Rathbun JE. Involutional entropion: a review with evaluation of a procedure. Arch Ophthalmol. 1978;96:1058-1064.

Book: Last name(s) of the author(s) and initials, book title, edition, place of publication, date of publication and inclusive page numbers of the extract cited.

Example: Herbert L. The Infectious Diseases (1st ed). Philadelphia; Mosby Harcourt; 1999:11;1-8.

Book Chapter: Last name(s) of the author(s) and initials, chapter title, book editors, book title, edition, place of publication, date of publication and inclusive page numbers of the cited piece.

Example: O'Brien TP, Green WR. Periocular Infections. In: Feigin RD, Cherry JD, eds. Textbook of Pediatric Infectious Diseases (4th ed). Philadelphia; W.B. Saunders Company;1998:1273-1278.

Books in which the editor and author are the same person: Last name(s) of the author(s) and initials, chapter title, book editors, book title, edition, place of publication, date of publication and inclusive page numbers of the cited piece. Example: Solcia E, Capella C, Kloppel G. Tumors of the exocrine pancreas. In: Solcia E, Capella C, Kloppel G, eds. Tumors of the Pancreas. 2nd ed. Washington: Armed Forces Institute of Pathology; 1997:145-210.

TABLES, GRAPHICS, FIGURES, AND IMAGES

All visual materials together with their legends should be located on separate pages that follow the main text.

Images: Images (pictures) should be numbered and include a brief title. Permission to reproduce pictures that were published elsewhere must be included. All pictures should be of the highest quality possible, in

JPEG format, and at a minimum resolution of 300 dpi.

Tables, Graphics, Figures: All tables, graphics or figures should be enumerated according to their sequence within the text and a brief descriptive caption should be written. Any abbreviations used should be defined in the accompanying legend. Tables in particular should be explanatory and facilitate readers' understanding of the manuscript, and should not repeat data presented in the main text.

MANUSCRIPT TYPES

Original Articles

Clinical research should comprise clinical observation, new techniques or laboratories studies. Original research articles should include title, structured abstract, key words relevant to the content of the article, introduction, materials and methods, results, discussion, study limitations, conclusion references, tables/figures/images and acknowledgement sections. Title, abstract and key words should be written in both Turkish and English. The manuscript should be formatted in accordance with the above-mentioned guidelines and should not exceed 16 A4 pages.

Title Page: This page should include the title of the manuscript, short title, name(s) of the authors and author information. The following descriptions should be stated in the given order:

1. Title of the manuscript (Turkish and English), as concise and explanatory as possible, including no abbreviations, up to 135 characters

2. Short title (Turkish and English), up to 60 characters

3. Name(s) and surname(s) of the author(s) (without abbreviations and academic titles) and affiliations

4. Name, address, e-mail, phone and fax number of the corresponding author

5. The place and date of scientific meeting in which the manuscript was presented and its abstract published in the abstract book, if applicable

INSTRUCTIONS TO AUTHORS

Abstract: A summary of the manuscript should be written in both Turkish and English. References should not be cited in the abstract. Use of abbreviations should be avoided as much as possible; if any abbreviations are used, they must be taken into consideration independently of the abbreviations used in the text. For original articles, the structured abstract should include the following sub-headings:

Objectives: The aim of the study should be clearly stated.

Materials and Methods: The study and standard criteria used should be defined; it should also be indicated whether the study is randomized or not, whether it is retrospective or prospective, and the statistical methods applied should be indicated, if applicable.

Results: The detailed results of the study should be given and the statistical significance level should be indicated.

Conclusion: Should summarize the results of the study, the clinical applicability of the results should be defined, and the favorable and unfavorable aspects should be declared.

Keywords: A list of minimum 3, but no more than 5 key words must follow the abstract. Key words in English should be consistent with "Medical Subject Headings (MESH)" (www.nlm.nih.gov/mesh/MBrowser.html). Turkish key words should be direct translations of the terms in MESH.

Original research articles should have the following sections:

Introduction: Should consist of a brief explanation of the topic and indicate the objective of the study, supported by information from the literature.

Materials and Methods: The study plan should be clearly described, indicating whether the study is randomized or not, whether it is retrospective or prospective, the number of trials, the characteristics, and the statistical methods used.

Results: The results of the study should be stated, with tables/figures given in numerical order; the results should be evaluated according to the statistical analysis methods applied. See General Guidelines for details about the preparation of visual material.

Discussion: The study results should be discussed in terms of their favorable and unfavorable aspects and they should be compared with the literature. The conclusion of the study should be highlighted.

Study Limitations: Limitations of the study should be discussed. In addition, an evaluation of the implications of the obtained findings/results for future research should be outlined.

Conclusion: The conclusion of the study should be highlighted.

Acknowledgements: Any technical or financial support or editorial contributions (statistical analysis, English/Turkish evaluation) towards the study should appear at the end of the article.

References: Authors are responsible for the accuracy of the references. See General Guidelines for details about the usage and formatting required.

Review Articles

Review articles can address any aspect of clinical or laboratory pharmaceuticals. Review articles must provide critical analyses of contemporary evidence and provide directions of or future research. Most review articles are commissioned, but other review submissions are also welcome. Before sending a review, discussion with the editor is recommended.

Reviews articles analyze topics in depth, independently and objectively. The first chapter should include the title in Turkish and English, an unstructured summary and key words. Source of all citations should be indicated. The entire text should not exceed 25 pages (A4, formatted as specified above).

CORRESPONDENCE

All correspondence should be directed to the Turkish Journal of Pharmaceutical Sciences editorial board;

Post: Turkish Pharmacists' Association

Address: Willy Brandt Sok. No: 9 06690 Ankara, TURKEY

Phone: +90 312 409 8136

Fax: +90 312 409 8132

Web Page: http://turkjps.org/home/

E-mail: onur@pharmacy.ankara.edu.tr

TURKISH
JOURNAL OF PHARMACEUTICAL SCIENCES

CONTENTS

TURKISH
JOURNAL OF PHARMACEUTICAL SCIENCES

CONTENTS

CONTENTS

ORIGINAL ARTICLE

Comparative *In Vitro* Assessment of the Methanol Extracts of the Leaf, Stem, and Root Barks of *Cnidoscolus aconitifolius* on Lung and Breast Cancer Cell Lines

Cnidoscolus aconitifolius'un Yaprak, Gövde ve Kök Kabuklarının Metanol Ekstrelerinin Akciğer ve Meme Kanseri Hücre Hatlarında Karşılaştırmalı *İn Vitro* Değerlendirilmesi

🆔 Emmanuel Oise IKPEFAN[1]*, 🆔 Buniyamin Adesina AYINDE[2], 🆔 Azhar MUDASSIR[3], 🆔 Ahsana Dar FAROOQ[3]

[1]Delta State University, Faculty of Pharmacy, Department of Pharmacognosy and Traditional Medicine, Abraka, Nigeria
[2]University of Benin, Faculty of Pharmacy, Department of Pharmacognosy, Benin City, Nigeria
[3]University of Karachi, International Centre for Chemical and Biological Sciences, Dr. Panjwani Center for Molecular Medicine and Drug Research, Karachi, Pakistan

ABSTRACT

Objectives: *Cnidoscolus aconitifolius* Mill. I.M.Johnst. is a medicinal plant widely used in ethnomedicine for the treatment of cancer and other diseases.

Materials and Methods: The effects of methanol extracts of the leaf, stem, and root barks were evaluated on breast (MCF-7) and lung (NCI-H460) cancer cells at 1-250 µg/mL using the SRB assay and the extracts were screened for phytochemicals using the standard method.

Results: The stem and root extracts showed no activity at the maximum concentration, while the leaf extract at 100 µg/mL showed remarkable cell growth inhibition against breast (-14.50±0.58) and lung cancer (+53.29±4.57) *in vitro*. The extracts showed the presence of saponins, terpenes, cardiac glycosides, and phenolic compounds. Partitioning of the active leaf extract further enhanced its activity as the chloroform fraction exhibited GI_{50}, LC_{50}, and total growth inhibition (TGI) of 22.5, 68.75, and 43.75 µg/mL against breast cancer, respectively, and GI_{50} and TGI of 35.4 and 55.8 µg/mL against lung cancer cells, respectively. However, the aqueous fraction showed no cytotoxicity against either cell line.

Conclusion: These results justified the ethnomedicinal uses of the plant against tumor-related ailments. Isolation of the constituents responsible for the observed activity needs to be carried out to further support this claim.

Key words: Cytotoxicity, *Cnidoscolus aconitifolius*, growth inhibition, MCF-7, NCI-H460, cancer cells

ÖZ

Amaç: *Cnidoscolus aconitifolius* Mill. I.M.Johnst. kanser ve diğer hastalıkların tedavisinde yaygın olarak kullanılan tıbbi bir bitkidir.

Gereç ve Yöntemler: Yaprak, kök ve kök kabuklarının metanol ekstrelerinin etkileri, SRB yöntemi kullanılarak 1-250 µg/mL konsantrasyonda meme (MCF-7) ve akciğer (NCI-H460) kanser hücreleri üzerinde değerlendirilmiş ve ekstrelerin fitokimyasal içeriği standart yöntem kullanılarak taranmıştır.

Bulgular: Gövde ve kök ekstreleri maksimum konsantrasyonda aktivite göstermezken, yaprak ekstresi 100 µg/mL dozda meme (-14,50±0,58) ve akciğer kanserine (+53,29±4,57) karşı belirgin *in vitro* hücre büyümesi inhibisyonu göstermiştir. Ekstrelerde saponinler, terpenler, kardiyak glikozitler ve fenolik bileşiklerin varlığı saptanmıştır. Aktif yaprak ekstresinin fraksiyonlanması ile kloroform fraksiyonunda meme kanseri hücrelerine karşı sırasıyla 22,5, 68,75 ve 43,75 µg/mL GI_{50}, LC_{50} ve toplam büyüme inhibisyonu (TGI) değerleriyle; akciğer kanseri hücrelerine karşı sırasıyla 35,4 ve 55,8 µg/mL GI_{50} ve TGI değerleriyle aktivitenin arttığı tespit edilmiştir. Bununla birlikte, sulu fraksiyon her iki hücre hattına karşı sitotoksik etki göstermemiştir.

Sonuç: Bu sonuçlar, bitkinin tümörle ilgili hastalıklara karşı etnomedikal kullanımını desteklemiştir. Bu kaydın desteklenmesi için ileri çalışmalarda aktiviteden sorumlu bileşiklerin izole edilmesi gerekmektedir.

Anahtar kelimeler: Sitotoksisite, *Cnidoscolus aitifitifolius*, büyüme inhibisyonu, MCF-7, NCI-H460, kanser hücreleri

INTRODUCTION

Traditionally, medicinal plants have found applications in the formulation and production of modern drugs. They are used in the treatment of severe life-threatening ailments including cancer especially in developing countries.[1] Over the years, cancer patients have relied on surgery, radiotherapy, and chemical derived drugs for their treatment, which further damage patients' health and increase their suffering. Hence, there is a need to search for and focus on medicinal plants that are used traditionally in treating tumor-related ailments. One such plant, *Cnidoscolus aconitifolius* (Mill.) I.M.Johnst., has been used as a constituent of herbal preparations for the treatment of cancer patients by Nigerian herbalists.

C. aconitifolius (Euphorbiaceae) originates from southeast Mexico and Guatemala and the southwestern part of Nigeria.[2] It is locally known as Iyana Ipaja.[3] In Nigerian traditional health practices, it is also referred to as "Hospital too far" due to its rapid healing properties against certain health conditions.[4] In ethnomedicine, it has been reported to have a blood boosting effect in both pregnant women and young anemic children,[5] and as an antidote for alcoholism, insomnia, and scorpion bites. Previously, the cytotoxic and antiproliferative activity of the methanol extracts of *C. aconitifolius* leaves, stem, and root barks against tadpoles of *Ranicep ranninus* and radicle length of *Sorghum bicolor* has been reported.[6] The cytotoxicity of ethanol extract of its leaf against the brine shrimp has also been noted.[7] However, there is presently no report on the anticancer activity of this plant. Therefore, the present study was aimed at validating the antitumor ethnomedicinal uses of *C. aconitifolius* using human breast and lung cancer cell lines.

MATERIALS AND METHODS

Chemicals

Dimethyl sulfoxide (DMSO), fetal bovine serum, gentamicin sulfate, $_L$-glutamine penicillin streptomycin solution, Roswell Park Memorial Institute-1640 medium (RPMI-1640), sulforhodamine B (SRB), trichloroacetic acid (TCA), tris base, trypan blue, and trypsin-EDTA were purchased from Sigma (St. Louis, MO, USA). Acetic acid (Lab Scan, Ireland), amphotericin B (Formepharma, Pakistan), and doxorubicin (ICN, USA) were also obtained.

Consumables

The cell culture boats, flasks (25 and 75 cm²), centrifuge tubes (15 and 50 mL), culture plates (96-well, transparent with flat bottom), and serological pipettes (1, 5, and 10 mL) were purchased from Falcon BD (USA). The microcentrifuge tubes (2 mL) were purchased from Kartel (Italy).

Equipment

The equipment included an analytical balance, milligram balance, pH meter (Precisia, Switzerland), centrifuge, CO_2 incubator (Kendro Lab Products, Germany), safety cabinet class 2 (Heraeus Germany), microscope: inverted TS-100 (Nikon, Japan), multiwell microplate reader (Stat fax 2100, Awareness Technology, USA), multiwell plate shaker (PMS 1000, Grant Instruments, UK), ultrasonic bath (MXB6, Grant Instruments), and Neubauer's chamber (0.1 mm and 0.0025 mm², HBG, Germany).

Collection and processing of the plant

The leaves of *C. aconitifolius* (Mill.) I.M.Johnst. were collected in February 2014 at Sabongida-Ora in Edo State, Nigeria, and the identity of the plant was confirmed by Dr. Shasanya Olufemi, a plant taxonomist. It was preserved at the Forest Research Institute of Nigeria, Ibadan, with herbarium specimen number FHI 109574. The plant material was air dried in the laboratory for 5 days at room temperature, followed by oven drying at 40˚C, and subsequently ground to powder form and stored in an air-tight container.

Extraction of plant materials

About 2.5 kg of each plant part was exhaustively extracted in methanol (95%) using a Soxhlet apparatus, and dried using a rotary evaporator maintained at 40˚C.

Preliminary phytochemical screening

Phytochemical screenings of the extracts (leaves stem and root barks) were carried out using standard methods previously described.[8]

Sulforhodamine-B assay

The growth inhibitory activities of methanol extract of *C. aconitifolius* and its fractions were tested using human cancer cell lines [breast (MCF-7) and lung cancer (NCI-H460)].[9]

The stock solutions of plant extracts and fractions were prepared as 40 mg/mL in DMSO. However, doxorubicin (1 mM) was prepared in distilled water. On the experimental day, respective dilutions were prepared in RPMI-1640 containing gentamicin (50 µg/mL).

Monolayer trypsinization, cell viability determination, and cell counting from a confluent flask (75 cm²) were carried out. Cells (10,000 cells/well/100 µL for MCF-7 and NCI-H460) were seeded for monolayer formation and incubated in a CO_2 incubator at 37˚C for 24 h. Various concentrations of methanol extracts of *C. aconitifolius* (1, 10, 50, 100, 200, and 250 µg/mL) and fractions (1, 25, 50, 75, and 100) were added (100 µL/well) in appropriate wells, followed by incubation for 48 h. Appropriate controls and blanks (drug and extract) were also prepared. At the end of 48 h, time zero-1 (T_{z1} plate) and time zero-2 (T_{z2} plate)

plates were fixed with gentle addition of 50% w/v cold TCA (50 µL/well) before and after the addition of extract and fractions in experimental plates. These were left at room temperature for 30 min, washed (3×), and dried overnight. After 48 h, the experimental plates were also fixed in a similar manner.

The dried fixed plates were stained with 100 µL of sulforhodamine solution (0.4% wt/vol prepared in 1% acetic acid) for 10 min, followed by washing (5×) with 1% acetic acid to remove excess stain, and air-dried. Finally, 100 µL of tris base solution (pH 10.2, 10 mM) was added to solubilize protein bound stain and absorbance was recorded at 545 nm using a microplate reader. All the experiments were conducted in triplicate. The results of the extracts and fractions were presented as GI_{50}, TGI, and LC_{50} (µg/mL) values.

Fractionation of methanol extract of the leaf of C. aconitifolius
About 25.0 g of the crude methanol extract was re-dissolved in methanol–water (1:1) and partitioned exhaustively with chloroform (400 mL×4) volumes in a separating funnel. The chloroform layer (lower) was collected first, followed by the aqueous fraction. This was repeated until a clear lower layer was obtained. The aqueous and the chloroform fractions were concentrated to dryness on a rotary evaporator and their respective yields noted.

RESULTS

The 2.5 kg of the powdered leaves, stem, and roots of *C. aconitifolius* yielded 87.65, 71.10, and 68.43 g of the methanol extracts, corresponding to 3.5%, 2.8%, and 2.7%, respectively.

Phytochemical screening of extract of the leaves, stem, and roots of *C. aconitifolius* showed the presence of saponins, tannins, terpenes, and flavonoids in varying intensities. However, alkaloids and anthraquinones were absent (Table 1).

Results of the effect of the methanol extracts on MCF-7 and NCI-H460 cell lines
The methanol extract of leaves produced growth inhibitory and cytotoxic effects on MCF-7 to varying extents. At a concentration of 50 µg/mL, the extract had +63.08±3.63% growth inhibition, which became more cytotoxic at 200 and 250 µg/mL as -14.70±0.76, and -26.25±2.18% were recorded. The

GI_{50} and TGI were recorded as 26.67±3.33 and 95 µg/mL while the LC_{50} was greater than 250 µg/mL (Table 2). At the maximum concentration of 250 µg/mL, stem and root barks extracts of *C. aconitifolius* showed no significant activities against breast cancer cell lines.

Extract of *C. aconitifolius* at 50-100 µg/mL exhibited cell growth inhibitory effects on the lung cells unlike the breast cancer cells. Significant growth inhibition ranging between ~28% and 77% was recorded in a concentration-dependent manner against the human lung cancer cell line (NCI-H460). A GI_{50} value of ~59.67 µg/mL was recorded, while LC_{50} and TGI were greater than 250 µg/mL (Table 3).

Effects of the aqueous and chloroform fractions of C. aconitifolius against breast (MCF-7) and lung cancer (NCI-H460) cell lines
The chloroform fraction at 25 µg/mL displayed significant growth inhibition of ~48.62% against MCF-7 cells, which became cytotoxic at 50-100 µg/mL in a concentration-dependent manner with GI_{50}, LC_{50}, and TGI of 22.50, 68.75, and 43.75 µg/mL, respectively (Table 4).

Similar effects were also observed with the chloroform fraction against NCI-H460 cells, giving GI_{50} and TGI of 35.40 and 55.8

Table 1. Results of the phytochemical screening of methanol extracts of the leaves, stem, and roots of *C. aconitifolius*

Phytochemical groups	Leaves	Stem bark	Root bark
Alkaloids	-	-	-
Anthraquinones	-	-	-
Tannins/phenolic compounds	+++	+	+
Flavonoids	+	-	-
Saponins	++	+	+
Cardiac glycosides	+	+	++
Terpenes	+++	+	++

+++: Appreciable amount, ++: Moderate amount, +: Minute amounts, -: Not detected

Table 2. Cytotoxicity of methanol extract of *C. aconitifolius* against breast cancer cell line (MCF-7)

Extract	(µg/mL)	% Growth inhibition/ cytotoxicity	GI_{50}	LC_{50}	TGI
				(µg/mL)	
	1	+18.04±0.61	+26.67±3.33	>250	95±0
	10	+42.38±2.99			
	50	+63.08±3.63			
	100	-4.07±0.58			
	200	-14.70±0.76			
	250	-26.25±2.18			

Control absorbance in MCF-7 at 545 nm=1.9±0.1
Each value represents % mean ± standard error of mean of three independent experiments as compared to control. Growth inhibition=+ and cytotoxicity=−; GI_{50} and TGI=Concentration of drug causing 50% and 100% growth inhibition of cells. LC_{50}=Lethal concentration of drug that killed 50% cells. The order of activity was significantly different from each other.
TGI: Total growth inhibition

Table 3. Cytotoxicity of methanol extract of *C. aconitifolius* against lung cancer cell-line (NCI-H460)

Methanol extract	Conc. (µg/mL)	% Growth inhibition/ cytotoxicity	GI_{50}	LC_{50}	TGI
				(µg/mL)	
	1	0.00±0.00	+59.67±0.75	>250	>250
	10	+28.45±4.26			
	50	+46.24±3.24			
	100	+53.29±4.57			
	200	+64.73±2.79			
	250	+77.68±1.96			

Control absorbance in NCI-H460 at 545 nm=2.0±0.1
Each value represents % mean ± standard error of mean of three independent experiments as compared to control. Growth inhibition=+ and cytotoxicity=−; GI_{50} and TGI=Concentration of drug causing 50% and 100% growth inhibition of cells. LC_{50}=Lethal concentration of drug that killed 50% cells. The order of activity was significantly different from each other.
TGI: Total growth inhibition

µg/mL with LC_{50}>100 µg/mL. The aqueous fraction did not show any activity at 100 µg/mL on either cell line (Table 5).

Table 4. Cytotoxicity of the aqueous and chloroform fractions of *C. aconitifolius* against breast cancer (MCF-7) cell line					
Chloroform fraction	Conc. (µg/mL)	% Growth inhibition/ cytotoxicity	GI_{50}	LC_{50}	TGI
				(µg/mL)	
	1	+8.32±1.60	22.50	68.75	43.75
	25	+48.62±5.30			
	50	-16.10±2.30			
	75	-58.30±6.70			
	100	-72.00±9.10			
Aqueous fraction	100	‹50	>100	>100	>100

Each value represents % mean ± standard error of mean of three independent experiments as compared to control. Growth inhibition=+ and cytotoxicity=–; GI_{50} and TGI=Concentration of drug causing 50% and 100% growth inhibition of cells. LC_{50}=Lethal concentration of drug that killed 50% cells. The order of activity was significantly different from each other.
TGI: Total growth inhibition

Table 5. Cytotoxicity of the aqueous and chloroform fractions of *C. aconitifolius* against lung cancer (NCI-H460) cell line					
Chloroform fraction	Conc. (µg/mL)	% Growth inhibition/ cytotoxicity	GI_{50}	LC_{50}	TGI
				(µg/mL)	
	1	+3.00±0.72	35.40	>100	55.8
	25	+21.00±2.10			
	50	-2.00±1.30			
	75	-9.60±1.20			
	100	-22.00±11.00			
Aqueous fraction	100	‹50	>100	>100	>100

Control absorbance in NCI-H460 at 545 nm=2.0±0.1
Each value represents % mean ± standard error of mean of three independent experiments as compared to control. Growth inhibition=+ and cytotoxicity=–; GI_{50} and TGI=Concentration of drug causing 50% and 100% growth inhibition of cells. LC_{50}=Lethal concentration of drug that killed 50% cells. The order of activity was significantly different from each other.
TGI: Total growth inhibition

DISCUSSION

Among all human diseases, cancer remains the most deadly and life-threatening pathological condition.[10] The global burden of this disease has continued to surge due to the adoption of high level of cancer-inducing lifestyles such as smoking, eating of a westernized diet, and physical inactivity.[11]

According to global cancer statistics, breast and lung cancers are the most frequently diagnosed cancers in females and males, respectively.[12] The commonly employed treatment includes chemotherapy, radiotherapy, and in some cases surgery, which also exhibit series of side effects among patients.[13] Due to this, research into ethnomedicinal plants with antitumor properties as an alternative medicine at the early stage of the disease has become necessary.

Phytochemical screening of extracts revealed the presence of various phytochemicals including tannins and flavonoids, which

are known to possess free radical scavenging activity, hence preventing the development of diseases. The higher activity demonstrated by the leaf extract over the stem and root extracts could be due to the abundance of one or more secondary metabolites such as terpenes and phenolic compounds, which are known for their antifree radical potentials and inhibition of carcinogenesis.[14,15]

Our previous work demonstrated that the extracts from the leaf, stem, and root barks of *C. aconitifolius* displayed cytotoxic and antiproliferative effects on guinea corn radicle length and tadpoles *in vitro*. The present study further validates the previous results with the leaf extract being most active against breast and lung cancer cells. This could happen due to variation in the chemical constituents of the different morphological parts of the plant occasioned by translocation.

The leaf extract exhibited a concentration-dependent effect with higher growth inhibitory effect against breast cancer by ~2× than that of lung cancer cells. Partitioning of the extract was observed to increase the activity compared to the crude as the chloroform fraction at 100 µg/mL produces cytotoxicities of -72±9.1% and -22±11% as well as GI_{50} of 22.5 and 35 µg/mL against MCF-7 and NCI-H460 cells, respectively. This variation in sensitivities of the crude extracts and fraction could be as a result of the interference of some molecular process at some stages in the cell division processes, e.g., the G2/M phase and the induction of some apoptotic process such as mitochondrial transmembrane depolarization.[14]

The results obtained have validated the traditional uses of this plant in the treatment of cancer. However, further work towards the isolation of the constituents responsible for the observed activities is required.

ACKNOWLEDGEMENTS

Conflicts of interest: No conflict of interest was declared by the authors.

REFERENCES

1. Kolawole AO. Feasible cancer control strategies for Nigeria mini review. Am J Trop Med Pub Health. 2011;1:1-10.

2. Ross-Ibarra J, Molina-Cruz A. The Ethnobotany of Chaya (*Cnidoscolus aconitifolius* ssp. Aconitifolius Breckon): A Nutritious Maya Vegetable. Econ Bot. 2002;56:350-65.

3. Oyagbemi AA, Odetola AA, Azeez O. Ameliorative effects of *Cnidoscolus aconitifolius* on anaemia and osmotic fragility induced by protein energy malnutrition. J Biotech. 2008;7:1721-6.

4. Donkoh A, Kese AG, Atuahene CC. Chemical composition of chaya leaf meal (*Cnidoscolus aconitifolius* (Mill.) Johnston) and availability of its amino acids to chicks. Anim Feed Sci Technol. 1990;30:155-62.

5. Iwalewa EO, Adewunmi CO, Omisore NO Adebanji OA. Pro-anti oxidant effect of vegetables in south west Nigeria. J Med Food. 2005;8:531-4.

6. Ikpefan EO, Ayinde BA, Gita TD. In vitro comparative cytotoxic and growth inhibitory effects of the methanol extracts of the leaf, stem and root barks of *Cnidoscolus acontifolius* (Mill.) Johnst (Euphorbiaceae). Int J Bioassays. 2013;2:445-9.

7. Senjobi CT, Moody JO, Ettu AO. Antimicrobial and cytotoxic effects of *Cnidoscolus aconitifolius*. J Agric Biol Sci. 2011;2:21-5.

8. Khandelwal KR. Practical Pharmacognosy, Techniques and Experiments. 15th ed. New Delhi; Nirali Prakashan; 2006:15-163.

9. Skehan P, Storeng R, Scudiero D, Monks A, McMahon J, Vistica D, et al. New colorimetric cytotoxicity assay for anticancer-drug screening. J Natl Cancer Inst. 1990;82:1107-12.

10. Izevbigie EB, Bryant JL, Walker A. A novel natural inhibitor of extracellular signal-regulated kinases and human breast cancer cell growth. Exp Biol Med (Maywood). 2004;229:163-9.

11. Jemal A, Bray F, Center MM, Ferlay J, Ward E, Forman D. Global cancer statistics. CA Cancer J Clin. 2011;61:69-90.

12. Ferlay J, Soerjomataram I, Dikshit R, Eser S, Mathers C, Rebelo M, et al. Cancer incidence and mortality worldwide: sources, methods and major patterns in GLOBOCAN 2012. Int J Cancer. 2015;136:E359-86.

13. Ayinde BA, Ofeimun JO, Kashif M. Kashif M, Farooq AD, Choudhary MI. Growth Inhibitory Evaluations of Four Nigerian Medicinal Plants Against Cancer Cells, with Active Cytotoxic Fractions from the Leaves of *Parquetina nigrescens*. Can J Pur Appl Sci. 2014;9:3241-5.

14. Miliauskas G, Venskutonis PR, van Beek TA. Screening of radical scavenging activity of some medicinal and aromatic plant extracts. Food Chem. 2004;85:231-7.

15. Zheng W, Wang SY. Antioxidant activity and phenolic compounds in selected herbs. J Agric Food Chem. 2001;49:5165-70.

ORIGINAL ARTICLE

Synthesis and Hypoglycemic and Anti-inflammatory Activity Screening of Novel Substituted 5-[Morpholino(Phenyl)Methyl]-Thiazolidine-2,4-Diones and Their Molecular Docking Studies

Yeni Sübstitüe 5-[Morfolino(Fenil)Metil]-Tiazolidin-2,4-Dionların Sentezi ve Hipoglisemik ve Antienflamatuvar Aktivitelerinin Taranması ile Moleküler Doking Çalışmaları

ⓘ Srikanth Kumar KARUMANCHI[1], ⓘ Lakshmana Rao ATMAKURI[1]*, ⓘ V Basaveswara Rao MANDAVA[2], ⓘ Srikala RAJALA[3]

[1]V. V. Institute of Pharmaceutical Sciences, Department of Pharmaceutical Chemistry, Gudlavalleru, Andhra Pradesh, India
[2]Krishna University, Department of Chemistry, Machilipatnam, Andhra Pradesh, India
[3]Sree Vidyanikethan College of Pharmacy, Department of Pharmaceutical Chemistry, Tirupati, Andhra Pradesh, India

ABSTRACT

Objectives: The aim was the synthesis of novel substituted 5-[morpholino(phenyl)methyl]-thiazolidine-2,4-diones and screening for their *in vivo* hypoglycemic activity and *in vitro* anti-inflammatory activity, as well as molecular docking studies to find out active potential lead molecules.

Materials and Methods: Substituted aromatic aldehydes, thiazolidine-2,4-dione, and morpholine on Mannich reaction gave the title compounds. They were characterized by physical and spectral methods. In vivo hypoglycemic activity was examined in alloxan induced Wistar albino rats by tail tipping method. In vitro anti-inflammatory activity was tested by human red blood cell (HRBC) membrane stabilization and protein denaturation. Using AutoDock, molecular docking studies were carried out to find out the best fit ligands.

Results: Series of substituted 5-[morpholino(phenyl)methyl]-thiazolidine-2,4-diones were synthesized and chemically they were confirmed by spectral techniques. Acute toxic studies of *in vivo* hypoglycemic activity results revealed that compounds 4c, 4h, and 4n exhibited good activity at 35 mg/kg body weight. Chronic toxic study results indicated that compounds 4h and 4n exhibited good activity at 70 mg/kg body weight. Anti-inflammatory activity results indicated the highest inhibition was shown by compounds 4k and 4f at 500 μg/mL in HRBC membrane stabilization. In protein denaturation, the highest inhibition was shown by compound 4k at 500 μg/mL. In molecular docking studies, compounds 4h and 4n exhibited higher binding affinity at PPARγ receptor protein and compound 4k exhibited higher binding affinity at COX-1 and COX-2 actives sites.

Conclusion: Microwave irradiation produced high yield in short reaction times. The presence of electron releasing groups at the para position of the phenyl ring may give the ability to produce hypoglycemic activity and the presence of electron withdrawing groups at the para position of the phenyl ring causes anti-inflammatory activity. The results showed that some compounds exhibited good hypoglycemic and anti-inflammatory activities. Compounds 4h and 4n exhibited higher binding affinity at PPARγ receptor protein and compound 4k exhibited higher binding affinity at COX isoenzymes' active sites in molecular docking studies.

Key words: Thiazolidinediones bearing morpholine, Mannich reaction, *in vivo* hypoglycemic activity, *in vitro* anti-inflammatory activity, docking studies

ÖZ

Amaç: Bu çalışmanın amacı, yeni sübstitüe 5-[morfolino(fenil)metil]-tiyazolidin-2,4-dionların sentezi ve *in vivo* hipoglisemik ve *in vitro* anti-enflamatuvar aktivitelerinin taranması ile olası aktif moleküler için moleküler doking çalışmalarının yapılmasıdır.

Gereç ve Yöntemler: Bileşikler; sübstitüe aromatik aldehidler, tiyazolidin-2,4-dion ve morfolinin mannich reaksiyonu sonucu elde edilmiş, elde edilen bileşikler fiziksel ve spektral yöntemlerle karakterize edilmiştir. *İn vivo* hipoglisemik aktivite, alloxan ile indüklenen Wistar albino farelerde "tail

tipping" yöntemi, *in vitro* anti-enflamatuar aktivite ise, insan kırmızı kan hücrelerinde membran stabilizasyonu ve protein denatürasyon yöntemleri ile gerçekleştirilmiştir. AutoDock kullanarak, en uygun ligandları bulmak için moleküler doking çalışmaları yapılmıştır.

Bulgular: Sübstitüe 5-[morfolino(fenil)metil]-tiyazolidin-2,4-dion serileri sentezlenmiş ve spektral tekniklerle kimyasal yapıları teyit edilmiştir. *İn vivo* hipoglisemik aktivite sonuçlarıyla ilgili akut toksik çalışmaları, 4c, 4h ve 4n bileşiklerinin 35 mg/kg'da, kronik toksisite çalışmaları da, bileşik 4h ve 4n'nin 70 mg/kg'da iyi aktivite sergilediklerini göstermektedir. Antienflamatuar aktivite sonuçları, membran stabilizasyon yönteminde en yüksek inhibisyonunun 500 µg/mL'de 4k ve 4f bileşikleri ile görüldüğünü göstermektedir. Protein denatürasyonunda, 500 µg/mL'de bileşik 4k en yüksek inhibisyonu göstermiştir. Moleküler doking çalışmalarında, 4h ve 4n bileşiklerinin PPARγ reseptör proteinine, 4k bileşiğinin de, COX-1 ve COX-2 aktif bölgelerine daha yüksek bağlanma afinitesi sergilediği görülmüştür.

Sonuç: Mikrodalga tekniği düşük reaksiyon sürelerinde yüksek verim sağlamıştır. Fenil halkasının para pozisyonunda; elektron salıcı grupların hipoglisemik aktivite oluşturabileceği, elektron çekici grupların ise antienflamatuar aktiviteye neden olabileceği belirtilmiştir. Sonuçla, bazı bileşiklerin iyi hipoglisemik ve anti-enflamatuar aktivite sergilediklerini göstermiştir.

Moleküler doking çalışmalarında; bileşik 4h ve 4n, PPARγ reseptör proteininde, bileşik 4k da COX izoenzimleri aktif bölgelerinde daha yüksek bağlanma afinitesi sergilemiştir.

Anahtar kelimeler: Morfolin taşıyan tiyazolidinonlar, mannich reaksiyonu, *in vivo* hipoglisemik aktivite, *in vitro* antienflamatuar aktivite, doking çalışmaları

INTRODUCTION

Diabetes mellitus (DM) is a common chronic metabolic syndrome in which high blood sugar levels occur over a prolonged time and symptoms include frequent urination, increased hunger, and increased thirst. DM is associated with severe degenerative complications such as nephropathy, neuropathy, cataract, retinopathy, accelerated atherosclerosis, stroke, and increased risk of myocardial infarction. Onset of these pathologies is a remarkable event in the course of both type 1 and type 2 diabetes. Prevention and control are still serious challenging therapeutic problems as they stand for the foremost causes of morbidity and mortality for diabetic patients.[1] Type 1 diabetes is characterized by deficient insulin production and symptoms include excessive thirst (polydipsia) and excretion of urine (polyuria), weight loss, constant hunger, fatigue, and vision changes requiring daily administration of insulin. Type 2 diabetes results from the body's ineffective impaired insulin action. The majority of cases around the world are type 2 diabetes and it is principally the result of physical inactivity and excess body weight. Symptoms are similar to type 1 diabetes, but are less marked. In the past this type of diabetes was seen only in the adults but at present it is also happening frequently even in children. Normally in humans up to 80% of insulin stimulated glucose disposal takes place in the skeletal muscle, which is the major site of insulin resistance in type 2 diabetes.[2]

Worldwide the frequency of diabetes for all age groups was estimated to be 2.8% in 2000 and 4.4% in 2030. The total number of people with diabetes is expected to increase from 171 million in 2000 to 366 million in 2030. The occurrence of diabetes is higher in men than in women; however, there are more women with this diabetes than men. In developing countries, the urban population is expected to double between 2000 and 2030. Across the world the most important demographic change to diabetes prevalence appears to be an increase in the proportion of people greater than 65 years of age. Therefore, there is a need to develop novel drug candidates in this region.[3]

Heterocyclic compounds and their derivatives are a fascinating field in medicinal chemistry because of their remarkable biological and pharmacological properties. In the family of heterocyclic compounds, heterocycles with O, S, and N atoms have attracted more attention in chemistry research due to their wide range of biological activities. O and N atoms containing morpholine have a unique position in heterocyclic chemistry. Morpholine is a six-member saturated heterocyclic system having O and N as heteroatoms at the 1st and 4th positions, respectively. Clinically the morpholine ring contains drugs used in the market that have considerable importance, such as timolol (β-adrenergic blocker used in ocular hypertension and glaucoma), moclobemide (mono amino oxidase inhibitor used to treat depression and anxiety), reboxetine (norepinephrine reuptake inhibitor used as an antidepressant), pholcodine (opioid cough suppressant), emorfazone (nonsteroidal anti-inflammatory agent), gefitinib (epidermal growth factor receptor inhibitor used for certain breast, lung, and other cancers), and linezolid (antibiotic used to treat infections caused by gram-positive bacteria).[4]

Similarly, the thiazolidine-2,4-dione (TZD) nucleus is also one of the most important heterocyclics that has received much attention especially in the treatment of diabetes. TZD is a five-member heterocyclic compound that consists of S and N as heteroatoms in the ring at the 1st and 3rd positions, respectively, along with ketone functional groups at the 2nd and 4th positions. The TZD class of drugs includes troglitazone, ciglitazone, rosiglitazone, and ciglitazone with an insulin sensitizing property. Troglitazone was withdrawn from the market in 2000 due to its hepatotoxicity producing nature. TZDs are found to produce hypoglycemic activity by lowering the blood glucose levels significantly through the activation of peroxisome proliferator-activated receptor gamma (PPARγ) receptors.[5] TZDs enhance the insulin action and promote glucose utilization in the peripheral tissues. The exact mechanism of TZDs has not been elucidated, but is expected to exhibit pharmacological actions by binding and agonistic properties at the PPARγ nuclear receptor.[6]

Recently TZDs have been found to possess a wide range of biological activities such as antidiabetic,[7] protein tyrosine phosphatise 1B inhibitory,[8] 15-hydroxyprostaglandin

dehydrogenase (15-PGDH) inhibitory,[9] hypolipidemic,[10] aldose reductase inhibitory,[11] anti-inflammatory,[12] antimicrobial,[13] antitubercular,[14] antioxidant,[15] antitumor,[16] and antiproliferative.[17] From the literature observations, we made an attempt to design and develop novel TZD derivatives bearing morpholine in their structures using the Mannich reaction by both conventional heating and microwave irradiated methods. Microwave techniques give high yields, decrease by-product formation, and decrease the decomposition of products as compared to the conventional heating reaction methods.[18,19] The developed compounds were characterized and screened for biological activities. By using AutoDock molecular docking software the binding energies of the designed ligands and their interactions at the target protein were studied.

MATERIALS AND METHODS

All the chemicals required for the synthesis of novel thiazolidinediones such as reagents and solvents were obtained from commercial suppliers in Merck grade and further they were used without purification. Reaction progress and completion were monitored by thin layer chromatography with the help of 0.25 mm E. Merck grade silica gel 60GF-254 precoated TLC plates; spots were observed under ultraviolet (UV)-light and in an iodine chamber. Fourier Transform Infrared Spectrometer (FT-IR) spectra of the compounds were recorded with a Bruker FT-IR analyzer spectrophotometer by compression of compound with anhydrous KBr under vacuum using the KBr pressed pellet technique. Chemical shifts in δ, ppm of proton nuclear magnetic resonance (^{1}H-NMR) and carbon-13 nuclear magnetic resonance (^{13}C-NMR) spectra were recorded on a Bruker AMX 400 MHz spectrometer using deuterated dimethyl sulfoxide (DMSO) solvent and tetramethylsilane as internal standard. Mass spectra of the compounds were recorded on an Agilent LC-MSD 1200 mass spectrometer. For conventional synthesis normal reflux condenser setup and microwave assisted synthesis was performed on an RGSSIRR model Raga's scientific microwave system having different power levels from 140 W to 700 W. Melting points were determined by electrical melting point apparatus and were uncorrected. The Wistar albino rats used in the hypoglycemic study were divided into various groups and each group contained 6 rats (n=6).

Chemistry

*Synthesis of thiazolidine-2,4-dione (**3**)*

A. Conventional synthesis: Chloroacetic acid (20 mmoL) and thiourea (20 mmoL) were separately dissolved in 5 mL of water. The contents of the vessels were transferred into a three-necked round bottom flask and stirred until white precipitate was obtained. The reaction mixture was cooled and conc. Hydrochloric acid [(HCl) 6 mL] was added slowly to it from the dropping funnel. It was refluxed by applying gentle heat for about 10-12 h at 100-110°C. The contents of the flask were cooled to solidify them and they were filtered to obtain the product by washing with water. Recrystallization was done using ethyl alcohol.[20]

B. Microwave irradiation synthesis: A mixture of chloroacetic acid (10 mmoL) and thiourea (10 mmoL) dissolved in 5 mL of water was transferred into the microwave synthesizer reaction vessel. The reaction vessel was closed with the help of lids and condenser and stirred for about 1 h in cold condition. Then 3 mL of conc. HCl was added to the reaction mixture and irradiated for 6 min using 280 W power level at 120°C. The reaction mixture was cooled to room temperature and the obtained solid was filtered, dried, and recrystallized from ethyl alcohol.[21]

78.42% (conventional synthesis yield), 90.25% (MWI synthesis yield), white crystalline powder, melting point 124-126°C, R$_f$ value 0.62 from using 9:1 v/v of chloroform and methanol. IR [KBr v cm^{-1}]: 3321.46 (-NH-), 1689.94 (C=O), 2968.89 (C-H), 1303.29 (C-N), 626.69 (C-S). ^{1}H-NMR [400 MHz, δ, ppm, DMSO-d_6]: 12.015 (s, 1H, NH), 4.132 (s, 2H, CH$_2$). ^{13}C-NMR [400 MHz, δ, ppm, DMSO-d_6]: 35.80, 173.06, 173.82. ESI-MS: (M$^+$) m/z 117.

*General procedure for synthesis of compounds **4a-4n***

A. Conventional synthesis: 0.01 mol of TZD (**3**) was dissolved in 5 mL of ethanol and 0.01 moL of substituted aromatic benzaldehyde was added to this solution. The mixture was stirred for about 30 min at room temperature. To the reaction mixture 0.01 moL of morpholine and a catalytic amount of conc. HCl (3-5 drops) were added, followed by refluxing for 5-6 h. Completion of the reaction was monitored by TLC using mobile phase n-hexane and ethylacetate (9:1). The reaction mixture was allowed to cool for about 2-4 h and then it was poured into ice cold water. The product was collected by filtration and washed with cold water followed by dry toluene. It was dried and recrystallized with absolute ethanol.[22]

B. Microwave irradiation synthesis: 0.01 moL of TZD (**3**) was dissolved in 5 mL of ethanol and 0.01 moL of substituted aromatic benzaldehyde was added to it. The reaction mixture was stirred for 30 min at RT. To the above solution 0.01 moL of morpholine and 3-5 drops of conc. HCl were added. It was mixed well and placed in a Raga's scientific microwave synthesizer vessel and the reaction mixture was irradiated at 420 W power level for about 6-10 min at 120°C. The reaction mixture was cooled to room temperature and treated with ice cold water for the work up process. The obtained precipitate was filtered, washed, and dried to get the desired compound. Completion of the reaction was monitored by TLC using the same mobile phase mentioned in the above conventional synthesis.[23]

5-[(4-chlorophenyl)-morpholin-4-yl-methyl]-thiazolidine-2,4-dione **(4a)**

IR [KBr v cm^{-1}]: 3331.29 (-NH-), 1660.56 (C=O), 1263.44 (C-N), 2984.21 (C-H), 3045.20 (=C-H), 615.50 (C-S), 1104.13 (C-O-C), 785.56 (C-Cl). ^{1}H-NMR [400 MHz, δ, ppm, DMSO-d_6]: 12.105 (s, 1H, NH), 4.305-4.317 (d, 1H, TZD CH), 4.012-4.041 (d, 1H, N-CH), 7.355-7.421 (d, 2H, 3'-H&5'-H), 6.945-7.014 (d, 2H, 2'-H&6'-H), 3.642-3.685 (t, 4H, CH$_2$-O-CH$_2$), 2.475-2.635 (t, 4H, CH$_2$-N-CH$_2$). ^{13}C-NMR [400 MHz, δ, ppm, DMSO-d_6]: 173.15, 166.56, 138.45, 133.74, 130.32, 126.46, 68.44, 59.20, 56.48, 51.52. ESI-MS: (M$^+$) m/z 326.

5-[(2,4-dichlorophenyl)-morpholin-4-yl-methyl]-thiazolidine-2,4-dione **(4b)**

IR [KBr ν cm^{-1}]: 3456.54 (-NH-), 1672.55 (C=O), 1284.56 (C-N), 2949.85 (C-H), 3084.78 (=C-H), 632.04 (C-S), 1131.45 (C-O-C), 796.74 (C-Cl). ^{1}H-NMR [400 MHz, δ, ppm, DMSO-d_6]: 12.214 (s, 1H, NH), 4.321-4.348 (d, 1H, TZD CH), 4.124-4.168 (d, 1H, N-CH), 7.409 (s, 1H, 3'-H), 7.358-7.414 (d, 1H, 5'-H), 6.984-7.021 (d, 1H, 6'-H), 3.748-3.894 (t, 4H, CH$_2$-O-CH$_2$), 2.546-2.798 (t, 4H, CH$_2$-N-CH$_2$). ^{13}C-NMR [400 MHz, δ, ppm, DMSO-d_6]: 176.15, 167.08, 140.84, 136.56, 133.45, 131.63, 128.23, 125.46, 69.52, 60.45, 54.62, 50.45. ESI-MS: (M$^+$) m/z 361.

5-[(4-fluorophenyl)-morpholin-4-yl-methyl]-thiazolidine-2,4-dione **(4c)**

IR [KBr ν cm^{-1}]: 3425.45 (-NH-), 1673.52 (C=O), 1274.25 (C-N), 2983.44 (C-H), 3063.74 (=C-H), 623.24 (C-S), 1121.47 (C-O-C), 1345.25 (C-F). ^{1}H-NMR [400 MHz, δ, ppm, DMSO-d_6]: 12.046 (s, 1H, NH), 4.215-4.298 (d, 1H, TZD CH), 4.112-4.156 (d, 1H, N-CH), 7.284-7.301 (d, 2H, 3'-H&5'-H), 6.845-7.001 (d, 2H, 2'-H&6'-H), 3.542-3.599 (t, 4H, CH$_2$-O-CH$_2$), 2.546-2.741 (t, 4H, CH$_2$-N-CH$_2$). ^{13}C-NMR [400 MHz, δ, ppm, DMSO-d_6]: 175.26, 168.54, 139.74, 134.52, 130.66, 124.48, 67.47, 58.45, 54.74, 50.62. ESI-MS: (M$^+$) m/z 310.

5-[(4-hydroxyphenyl)-morpholin-4-yl-methyl]-thiazolidine-2,4-dione **(4d)**

IR [KBr ν cm^{-1}]: 3415.41 (-NH-), 1681.46 (C=O), 1264.74 (C-N), 2986.21 (C-H), 3085.46 (=C-H), 631.42 (C-S), 1116.22 (C-O-C), 3505.46 (Ph-OH). ^{1}H-NMR [400 MHz, δ, ppm, DMSO-d_6]: 11.965 (s, 1H, NH), 4.317-4.365 (d, 1H, TZD CH), 9.845 (s, 1H, C$_6$H$_4$-O<u>H</u>), 4.205-4.246 (d, 1H, N-CH), 6.935-7.459 (m, 4H, C$_6$H$_4$-OH), 3.645-3.726 (t, 4H, CH$_2$-O-CH$_2$), 2.685-2.784 (t, 4H, CH$_2$-N-CH$_2$). ^{13}C-NMR [400 MHz, δ, ppm, DMSO-d_6]: 176.46, 167.89, 159.56, 138.46, 133.47, 115.48, 65.32, 59.64, 53.12, 51.32. ESI-MS: (M$^+$) m/z 308.

5-[(4-methylphenyl)-morpholin-4-yl-methyl]-thiazolidine-2,4-dione **(4e)**

IR [KBr ν cm^{-1}]: 3335.66 (-NH-), 1666.22 (C=O), 1272.65 (C-N), 2980.67 (C-H), 3095.26 (=C-H), 615.22 (C-S), 1128.27 (C-O-C). ^{1}H-NMR [400 MHz, δ, ppm, DMSO-d_6]: 12.025 (s, 1H, NH), 4.225-4.308 (d, 1H, TZD CH), 2.865 (s, 3H, C$_6$H$_4$-C<u>H</u>$_3$), 4.056-4.116 (d, 1H, N-CH), 6.849-7.554 (m, 4H, C$_6$<u>H</u>$_4$-CH$_3$), 3.720-3.842 (t, 4H, CH$_2$-O-CH$_2$), 2.784-2.951 (t, 4H, CH$_2$-N-CH$_2$). ^{13}C-NMR [400 MHz, δ, ppm, DMSO-d_6]: 178.66, 165.42, 158.45, 137.45, 134.62, 118.61, 66.30, 60.52, 54.11, 52.55, 30.28. ESI-MS: (M$^+$) m/z 306.

5-[(4-nitrophenyl)-morpholin-4-yl-methyl]-thiazolidine-2,4-dione **(4f)**

IR [KBr ν cm^{-1}]: 3364.22 (-NH-), 1693.45 (C=O), 1274.66 (C-N), 2968.41 (C-H), 3095.45 (=C-H), 618.62 (C-S), 1135.84 (C-O-C), 1362.04, 1546.15 (NO$_2$). ^{1}H-NMR [400 MHz, δ, ppm, DMSO-d_6]: 12.546 (s, 1H, NH), 4.015-4.068 (d, 1H, TZD CH), 4.325-4.366 (d, 1H, N-CH), 6.846-7.387 (m, 4H, C$_6$H$_4$-NO$_2$), 3.862-3.984 (t, 4H, CH$_2$-O-CH$_2$), 2.855-2.948 (t, 4H, CH$_2$-N-CH$_2$). ^{13}C-NMR [400 MHz, δ, ppm, DMSO-d_6]: 178.79, 168.46, 150.62, 143.52, 130.46, 120.84, 68.32, 59.23, 55.74, 50.85. ESI-MS: (M$^+$) m/z 337.

5-[(4-methoxyphenyl)-morpholin-4-yl-methyl]-thiazolidine-2,4-dione **(4g)**

IR [KBr ν cm^{-1}]: 3381.47 (-NH-), 1679.22 (C=O), 1269.61 (C-N), 2971.52 (C-H), 3068.94 (=C-H), 629.41 (C-S), 1130.49 (C-O-C). ^{1}H-NMR [400 MHz, δ, ppm, DMSO-d_6]: 11.985 (s, 1H, NH), 4.211-4.285 (d, 1H, TZD CH), 4.389-4.401 (d, 1H, N-CH), 6.956-7.421 (m, 4H, C$_6$<u>H</u>$_4$-OCH$_3$), 3.986 (s, 3H, 4'-OCH$_3$), 3.745-3.889 (t, 4H, CH$_2$-O-CH$_2$), 2.651-2.894 (t, 4H, CH$_2$-N-CH$_2$). ^{13}C-NMR [400 MHz, δ, ppm, DMSO-d_6]: 180.22, 169.56, 160.55, 133.52, 129.44, 118.22, 68.45, 64.21, 59.45, 54.66, 51.23. ESI-MS: (M$^+$) m/z 322.

5-[(3,4-dimethoxyphenyl)-morpholin-4-yl-methyl]-thiazolidine-2,4-dione **(4h)**

IR [KBr ν cm^{-1}]: 3421.46 (-NH-), 1685.26 (C=O), 1284.62 (C-N), 2979.85 (C-H), 3089.13 (=C-H), 620.45 (C-S), 1115.65 (C-O-C). ^{1}H-NMR [400 MHz, δ, ppm, DMSO-d_6]: 12.264 (s, 1H, NH), 4.145-4.189 (d, 1H, TZD CH), 4.374-4.485 (d, 1H, N-CH), 6.452 (s, 1H, 2'-H), 6.678-6.894 (d, 2H, 5'-H&6'-H), 3.964 (s, 6H, 3'-OCH$_3$&4'-OCH$_3$), 3.745-3.865 (t, 4H, CH$_2$-O-CH$_2$), 2.746-2.894 (t, 4H, CH$_2$-N-CH$_2$). ^{13}C-NMR [400 MHz, δ, ppm, DMSO-d_6]: 177.88, 169.46, 153.56, 149.25, 132.45, 125.26, 118.24, 113.46, 69.05, 61.85, 58.47, 55.62, 50.43. ESI-MS: (M$^+$) m/z 352.

5-[(3,4,5-trimethoxyphenyl)-morpholin-4-yl-methyl]-thiazolidine-2,4-dione **(4i)**

IR [KBr ν cm^{-1}]: 3385.41 (-NH-), 1676.74 (C=O), 1268.46 (C-N), 2959.74 (C-H), 3094.25 (=C-H), 628.71 (C-S), 1134.84 (C-O-C). ^{1}H-NMR [400 MHz, δ, ppm, DMSO-d_6]: 12.114 (s, 1H, NH), 4.058-4.194 (d, 1H, TZD CH), 4.405-4.492 (d, 1H, N-CH), 6.248 (s, 2H, 2'-H&6'-H), 3.954 (s, 9H, 3'-OCH$_3$&4'-OCH$_3$&5'-OCH$_3$...), 3.954 (s, 9H, 3',4',5'-triOCH$_3$), 3.725-3.849 (t, 4H, CH$_2$-O-CH$_2$), 2.652-2.845 (t, 4H, CH$_2$-N-CH$_2$). ^{13}C-NMR [400 MHz, δ, ppm, DMSO-d_6]: 179.05, 168.19, 151.42, 140.74, 135.65, 112.27, 68.91, 63.64, 57.41, 53.44, 50.22. ESI-MS: (M$^+$) m/z 382.

5-[(4-hydroxy-3-methoxyphenyl)-morpholin-4-yl-methyl]-thiazolidine-2,4-dione **(4j)**

IR [KBr ν cm^{-1}]: 3325.41 (-NH-), 1675.64 (C=O), 1291.45 (C-N), 2980.65 (C-H), 3091.47 (=C-H), 622.11 (C-S), 1125.62 (C-O-C), 3512.22 (Ph-OH). ^{1}H-NMR [400 MHz, δ, ppm, DMSO-d_6]: 12.005 (s, 1H, NH), 4.105-4.184 (d, 1H, TZD CH), 4.357-4.462 (d, 1H, N-CH), 6.348 (s, 1H, 2'-H), 6.548-6.754 (d, 1H, 5'-H), 6.874-6.994 (d, 1H, 6'-H), 9.548 (s, 1H, C$_6$H$_4$-O<u>H</u>), 3.895 (s, 3H, 3'-OCH$_3$), 3.765-3.910 (t, 4H, CH$_2$-O-CH$_2$), 2.747-2.897 (t, 4H, CH$_2$-N-CH$_2$). ^{13}C-NMR [400 MHz, δ, ppm, DMSO-d_6]: 175.44, 167.41, 155.22, 148.45, 131.58, 123.21, 119.55, 112.41, 68.08, 62.44, 59.75, 56.32, 50.85. ESI-MS: (M$^+$) m/z 338.

5-[(4-bromophenyl)-morpholin-4-yl-methyl]-thiazolidine-2,4-dione **(4k)**

IR [KBr ν cm^{-1}]: 3389.81 (-NH-), 1686.35 (C=O), 1271.64 (C-N), 2992.67 (C-H), 3089.45 (=C-H), 621.12 (C-S), 1131.83 (C-O-C), 578.63 (C-Br). ^{1}H-NMR [400 MHz, δ, ppm, DMSO-d_6]: 12.158 (s, 1H, NH), 4.317-4.397 (d, 1H, TZD CH), 4.135-4.187 (d, 1H, N-CH), 7.278-7.314 (d, 2H, 3'-H&5'-H), 6.942-7.108 (d, 2H, 2'-H&6'-H), 3.618-3.685 (t, 4H, CH$_2$-O-CH$_2$), 2.612-2.732 (t, 4H, CH$_2$-N-CH$_2$). ^{13}C-NMR [400 MHz, δ, ppm, DMSO-d_6]: 178.54, 166.64, 138.18, 133.79, 130.52, 122.15, 66.35, 57.72, 53.23, 50.48. ESI-MS: (M$^+$) m/z 371.

5-[(3-bromophenyl)-morpholin-4-yl-methyl]-thiazolidine-2,4-dione **(4l)**

IR [KBr ν cm^{-1}]: 3412.54 (-NH-), 1678.75 (C=O), 1269.18 (C-N), 2987.2 (C-H), 3086.23 (=C-H), 619.84 (C-S), 1128.46 (C-O-C), 584.45 (C-Br). ^{1}H-NMR [400 MHz, δ, ppm, DMSO-d_6]: 11.846 (s, 1H, NH), 4.365-4.381 (d, 1H, TZD CH), 4.208-4.299 (d, 1H, N-CH), 7.875 (s, 1H, 2'-H), 7.457-7.510 (d, 1H, 4'-H), 7.108-7.201 (t, 1H, 5'-H), 6.847-6.912 (d, 1H, 6'-H), 3.748-3.8414 (t, 4H, CH$_2$-O-CH$_2$), 2.546-2.698 (t, 4H, CH$_2$-N-CH$_2$). ^{13}C-NMR [400 MHz, δ, ppm, DMSO-d_6]: 175.51, 168.25, 139.17, 136.85, 133.79, 130.52, 126.62, 121.87, 68.55, 58.74, 54.76, 50.08. ESI-MS: (M$^+$) m/z 371.

5-[(4-dimethylaminophenyl)-morpholin-4-yl-methyl]-thiazolidine-2,4-dione **(4m)**

IR [KBr ν cm^{-1}]: 3426.45 (-NH-), 1684.24 (C=O), 1289.47 (C-N), 2992.35 (C-H), 3084.47 (=C-H), 627.74 (C-S), 1118.64 (C-O-C). ^{1}H-NMR [400 MHz, δ, ppm, DMSO-d_6]: 12.248 (s, 1H, NH), 4.462-4.510 (d, 1H, TZD CH), 4.256-4.347 (d, 1H, N-CH), 7.415-7.511 (d, 1H, 2'-H&6'-H), 6.917-7.125 (d, 1H, 3'-H&5'-H), 3.148 (s, 6H, H$_3$C-N-CH$_3$), 3.839-3.990 (t, 4H, CH$_2$-O-CH$_2$), 2.847-2.954 (t, 4H, CH$_2$-N-CH$_2$). ^{13}C-NMR [400 MHz, δ, ppm, DMSO-d_6]: 178.77, 169.71, 152.82, 135.54, 129.64, 119.55, 68.74, 65.46, 59.44, 57.62, 43.25. ESI-MS: (M$^+$) m/z 335.

5-[(4-isopropylphenyl)-morpholin-4-yl-methyl]-thiazolidine-2,4-dione **(4n)**

IR [KBr ν cm^{-1}]: 3386.62 (-NH-), 1693.24 (C=O), 1276.48 (C-N), 2989.42 (C-H), 3090.48 (=C-H), 613.75 (C-S), 1125.64 (C-O-C). ^{1}H-NMR [400 MHz, δ, ppm, DMSO-d_6]: 12.156 (s, 1H, NH), 4.324-4.398 (d, 1H, TZD CH), 4.158-4.205 (d, 1H, N-CH), 7.146-7.205 (d, 1H, 2'-H&6'-H), 7.452-7.512 (d, 1H, 3'-H&5'-H), 2.421-2.564 (dd, 6H, H$_3$C-CH-CH$_3$), 2.875-3.105 (m, 1H, H$_3$C-CH-CH$_3$), 3.754-3.897 (t, 4H, CH$_2$-O-CH$_2$), 2.759-2.851 (t, 4H, CH$_2$-N-CH$_2$). ^{13}C-NMR [400 MHz, δ, ppm, DMSO-d_6]: 174.32, 168.46, 150.41, 136.52, 129.22, 122.48, 67.71, 64.41, 58.32, 54.40, 35.46, 27.56. ESI-MS: (M$^+$) m/z 334.

Biological evaluation

In vivo hypoglycemic activity screening

Wistar albino rats of both sexes weighing 160-200 g for acute and chronic studies were purchased from Sainadh Agencies Laboratory animal suppliers, Hyderabad. Acute and chronic studies were carried out on alloxan induced Wistar albino rats by tail tipping method.[24,25] The rats were acclimatized for a week to the normal laboratory conditions prior to commencing the experiments, with *ad libitum* access to tap water and pellets. The rats were housed in cages with 12 h/12 h dark and light cycle at room temperature. Intraperitoneally alloxan monohydrate 120 mg/kg in normal saline was administered to the acclimatized animals, kept fasting for 24 h with water *ad libitum*. To overcome the early hypoglycemic phase, 5% dextrose solution was given for a day. After 72 h, by tail tipping method a drop of blood from the tail vein was collected and blood glucose levels as well as biochemical parameters were measured using a digital Accu-Chek active digital glucometer and Robonik biochemical analyzer, respectively. Rats having blood glucose levels above 150 mg/dL were selected for the study and

divided into six groups. For the acute study, 36 mg/kg body weight dose was calculated by considering thiazolidinedione derivatives equivalent to average human intake 200 mg/kg. The test compounds were given orally by mixing with CMC-0.25% solution. Rosiglitazone at 30 mg/kg body weight dose was used as the standard drug. At 0 h, 1 h, 2 h, 4 h, 6 h, and 8 h blood samples were withdrawn and analyzed for blood glucose level. Based on the acute study results limited compounds were selected for the chronic study. Doses of 35 and 70 mg/kg body weight were taken into consideration in the chronic study. On day 7 and day 15, decrease in blood glucose was observed by measuring the blood glucose levels.

In vitro anti-inflammatory activity screening

In vitro anti-inflammatory activity was evaluated by human red blood cell (HRBC) membrane stabilization method and protein denaturation method.[26-28]

HRBC membrane stabilization method

Fresh whole blood was collected from a healthy human volunteer who had not used any nonsteroidal anti-inflammatory drug 2 weeks prior to the experiment and mixed with an equal volume of sterilized Alsever's solution (0.8% sodium citrate, 2% dextrose, 0.42% sodium chloride, and 0.05% citric acid in water). At 3000 rpm the blood was centrifuged for 10 min and the packed cells were washed three times with 0.85% isosaline (pH 7.2). The volume of blood was measured and reconstituted with isosaline as 10% v/v suspension. Different concentrations (50, 100, 300, and 500 μg/mL) of the test solutions were prepared in isosaline. To 1 mL of test solution were added 2 mL of hyposaline (0.25% w/v NaCl), 1 mL of 0.15 M phosphate buffer (pH 7.4), and 0.5 mL of 10% HRBC in isosaline. For the test control, 1 mL of distilled water used instead of hyposaline, while the product control lacked red blood cells. The mixtures were incubated at 37°C for 30 min and centrifuged at 3000 rpm for about 20 min. Diclofenac sodium (100 μg/mL and 200 μg/mL) was used as the reference drug. The hemoglobin content in the suspension was estimated using a UV-spectrophotometer at 560 nm. Percentage inhibition activity was calculated as follows:

$$\% \text{ inhibition} = 100 - \left[\frac{\text{OD of test}}{\text{OD of control}} \times 100 \right]$$

where optical density (OD) of test sample is OD or absorbance of the test sample absorbance and OD of control is OD or absorbance of the negative control.

Protein denaturation method

Denaturation of proteins is a well-documented cause of inflammation. Salicylic acid, phenylbutazone, diclofenac, and flufenamic acid are anti-inflammatory drugs that have shown dose dependent ability for thermally induced protein denaturation. Agents that can prevent protein denaturation would be advisable for anti-inflammatory drug development. Each 0.5 mL of test sample solution consists of 0.45 mL of 5% w/v aqueous bovine serum albumin solution and 0.05 mL of test sample of different concentrations (50, 100, 300, and 500

µg/mL), while 0.5 mL of test control solution consists of 0.45 mL of 5% w/v aqueous bovine serum albumin solution and 0.05 mL of distilled water, and 0.5 mL of standard solution consists of 0.45 mL of 5% w/v aqueous bovine serum albumin solution and 0.05 mL of different concentrations (100 and 200 µg/mL) of diclofenac sodium. All the solutions were adjusted to pH 6.3 using 1 N HCl. The samples were incubated at 37°C for 20 min and the temperature was raised to keep the samples at 57°C for 3 min. After cooling, 2.5 mL of phosphate buffer was added to the above solutions. The absorbance was measured using a UV-visible spectrophotometer at 600 nm. The percentage inhibition of protein denaturation was calculated as follows:

$$\% \text{ inhibition} = 100 - \left[\left\{\frac{\text{OD of test} - \text{OD of product control}}{\text{OD of test control}}\right\} \times 100\right]$$

MOLECULAR DOCKING

Docking studies were performed to identify novel insulin sensitizers by observing the molecular interactions of designed ligands with PPARγ receptor protein and to determine the potential anti-inflammatory agents at cyclooxygenase (COX)-1 and COX-2 isoenzymes. The selection of the target protein for docking is based on several factors such as it must possess resolution between 2.0 and 3.0 Å, the structure should be determined by X-ray diffraction, it consists of co-crystallized ligand, and it does not have any protein breaks in the selected protein's 3D structure. PPARγ receptor protein is the most promising target for the identification of antidiabetic drugs possessing a thiazolidinedione nucleus.[29,30] The crystal structure of the PPARγ target receptor protein was obtained from the protein databank PDB ID: 2PRG having resolution of 2.3 Å. COX isoenzymes were the targets for determining the anti-inflammatory activity and the target proteins were downloaded from a protein databank PDB ID: 1EQG (COX-1) and PDB ID: 1CX2 (COX-2) having a resolution of 2.6 Å and 3.0 Å, respectively.[31] AutoDock 4.2.6 software was utilized to know the type of interactions of the designed 3D-structured thiazolidinediones with the 2PRG, 1EQG, and 1CX2 active site regions. ChemDraw Ultra 8.0 software was used to draw the designed structures and they were converted into suitable 3D models. By applying molecular mechanics they were subjected to energy minimizations, which are required for molecular docking and for the preparation of corresponding pdb files. Docking studies were preformed to find out the possible locations for the ligand in the active site region of the receptor. Grid-based docking studies was carried out using default parameters and docking was performed by considering rosiglitazone, indomethacin, and celecoxib as standard ligands at PPARγ receptor protein, COX-1, and COX-2 active sites, respectively.

RESULTS AND DISCUSSION

Chemistry

Initially TZD (**3**) was synthesized conventionally, which on further reaction with various substituted aromatic aldehydes and morpholine as secondary amines underwent the Mannich reaction to yield the series of designed and title Mannich bases represented in Scheme 1. TZD (**3**) and the title Mannich base compounds **4a-4n** were also prepared by microwave-assisted irradiation with 280 W and 420 W power levels at different steps of the synthesis. The physical characterization data, the comparative studies of conventional synthesis and microwave irradiation synthesis with respect to percentage yields, and their reaction time intervals are shown in Table 1.

Table 1. Physical characterization data of synthesized compounds 4a-4n

Compound	R	m.p. (°C)	Molecular formula	m.w.	Conventional synthesis		Microwave synthesis	
					% yield	Reaction time	% yield	Reaction time
4a	4-chloro	186-188	$C_{14}H_{15}N_2ClO_3S$	326.80	63.45	5 h	74.95	8 min
4b	2,4-dichloro	202-204	$C_{14}H_{14}N_2Cl_2O_3S$	361.24	68.42	6 h	74.68	7 min
4c	4-fluoro	192-194	$C_{14}H_{15}N_2FO_3S$	310.34	59.32	5 h	72.35	10 min
4d	4-hydroxy	186-188	$C_{14}H_{16}N_2O_4S$	308.35	70.45	5.5 h	77.46	7 min
4e	4-methyl	204-206	$C_{15}H_{18}N_2O_3S$	306.38	69.15	6.5 h	80.72	6 min
4f	4-nitro	200-202	$C_{14}H_{15}N_3O_5S$	337.35	71.48	6 h	82..94	10 min
4g	4-methoxy	190-192	$C_{15}H_{18}N_2O_4S$	322.38	69.74	6 h	79.48	9 min
4h	3,4-dimethoxy	200-202	$C_{16}H_{20}N_2O_5S$	352.41	64.84	5.5 h	78.22	8 min
4i	3,4,5-trimethoxy	212-214	$C_{17}H_{22}N_2O_6S$	382.43	63.48	5 h	79.18	8 min
4j	4-hydroxy-3-methoxy	234-236	$C_{15}H_{18}N_2O_5S$	338.38	69.23	6 h	80.46	8 min
4k	4-bromo	214-216	$C_{14}H_{15}N_2BrO_3S$	371.25	70.51	6.5 h	79.25	10 min
4l	3-bromo	198-200	$C_{14}H_{15}N_2BrO_3S$	371.25	68.26	5.5 h	80.15	9 min
4m	4-dimethylamino	210-212	$C_{16}H_{21}N_3O_3S$	335.42	69.43	6 h	78.67	8 min
4n	4-isopropyl	216-218	$C_{17}H_{22}N_2O_3S$	334.43	70.24	6 h	81.64	8 min

The designed and synthesized Mannich bases **4a-4n** were confirmed by the IR absorption bands at 3300-3500 cm^{-1} characteristic of -NH- of TZD, 1640-1690 cm^{-1} characteristic of –C=O of TZD, 3000-3100 cm^{-1} characteristic of =C-H stretching of the aromatic phenyl ring, and 1050-1300 cm^{-1} characteristic of C-O stretching of morpholine. The ^{1}H-NMR spectra produced a singlet at 11-12.5 ppm that is characteristic of the NH proton of TZD, triplets at 2-3.8 ppm indicating methylene group protons of morpholine, doublets at 4-4.5 ppm indicating CH of TZD, and N-CH protons, aromatic protons, were exhibited at 6.5-8 ppm. In ^{13}C-NMR, the signal appeared at 165-200 ppm indicating C=O of TZD, signals at 120-160 ppm indicate aromatic carbons, 10-50 ppm signals indicate aliphatic carbons, and 30-60 ppm signals indicate –CH$_2$-N-CH$_2$- carbons.

In vivo hypoglycemic activity

In vivo hypoglycemic activity study protocols were approved by the Institutional Animal Ethics Committee under the supervision of Committee for the Purpose of Control and Supervision of Experiments on Animals (CPCSEA), New Delhi, bearing registration number: 1847/PO/Re/S/16/CPCSEA. Blood glucose levels and body weights were expressed as mean ± standard error of the mean (SEM). The values were analyzed by one-way analysis of variance followed by Dunnet's "t" test and they were considered significant when compared to the normal group. The acute and chronic study results are given in Tables 2 and 3, respectively. The acute study results showed compounds **4c, 4h,** and **4n** exhibited good hypoglycemic activity and they were subjected to the chronic study at 35 and 70 mg/kg body weight. The chronic study results indicate that compounds **4h** and **4n** exhibited good activity at a dose of 70 mg/kg body weight.

In vitro anti-inflammatory activity

As a part of the *in vitro* anti-inflammatory activity investigation, the compounds were tested for HRBC membrane stabilization and protein denaturation by taking diclofenac sodium as

R=
4a: 4-chrolo
4b: 2,4-dichloro
4c: 4-fluoro
4d: 4-hydroxy
4e: 4-methyl
4f: 4-nitro
4g: 4-methoxy

4h: 3,4-dimethoxy
4i: 3,4,5-trimethoxy
4j: 4-hydroxy-3-methoxy
4k: 4-bromo
4l: 3-bromo
4m: 4-dimethylamino
4n: 4-isopropyl

Conventional synthesis: a) H$_2$O, Conc. HCl, 100-110°C, 10-12 hrs
b) aromatic aldehyde, morpholine, ethanol, Conc. HCl, 5-6 hrs
Microwave irradiation: a) H$_2$O, Conc. HCl, 280W, 120°C, 6 min
b) aromatic aldehyde, morpholine, ethanol, Conc. HCl, 420W, 8-10 min

Scheme 1. Reaction conditions and reagents

standard. Percentage inhibition of test compounds at various concentration levels was calculated and the results are given in Tables 4 and 5. HRBC membrane stabilization indicated the standard drug diclofenac sodium showed 90.78±0.87% inhibition at 300 µg/mL concentration. The highest inhibition of 90.64±0.26% and 89.61±0.25% was exhibited by compounds **4k** and **4f**, respectively, at 500 µg/mL concentration. Protein denaturation indicated the standard drug diclofenac sodium showed 95.34±0.92% inhibition at 300 µg/mL concentration. In protein denaturation, the highest inhibition of 93.72±0.61% was exhibited by compound **4k** at 500 µg/mL concentration. All the values were expressed as mean ± SEM, n=3.

Molecular docking

Molecular docking studies at PPARγ receptor protein, COX-1, and COX-2 active site regions give the data of binding energy (kcal/moL), number of hydrogen bonds, hydrogen bond length, and interacted amino acid residues, shown in Tables 6, 7, and 8. In comparison with the standard ligand rosiglitazone (binding energy -8.26 kcal/moL), compounds **4h** and **4n** showed higher

Table 2. Effect of synthesized compounds 3a-3l on blood glucose level in alloxan induced diabetic rats (acute study)

Compound	Mean ± SEM of blood glucose level mg/dL					
	0 h	1 h	2 h	4 h	6 h	8 h
Normal	121.24±2.56	123.64±2.04	122.5±5.11	121.54±3.47	120.5±4.22	120.33±2.3
Standard	398.26±4.22*	242.34±5.48	192.1±4.29*	148.64±3.46*	110.35±4.65	100.55±5.26**
4a	326.45±2.64	294.32±4.41**	265.61±4.68	250.31±8.61	253.12±8.32**	290.5±4.85
4b	315.22±8.15**	254.26±6.78	235.81±6.34*	175.52±3.51	165.45±5.61*	200.61±2.46
4c	325.64±8.55	249.6±5.44**	199.72±7.14*	150.4±6.45	118.12±6.47**	125.47±3.84
4d	322.3±4.22	299.52±6.38*	235.42±4.28**	168.5±2.64	154.8.3±6.55	198.24±5.24**
4e	315.88±5.64	305.11±7.34	296.58±5.42	235.25±2.65**	258.44±6.54	272.05±7.56
4f	305.44±5.26**	297.53±6.48	285±7.12*	252.56±5.29	278.32±5.48*	308±6.24*
4g	316.0±8.54*	291.5±6.44*	252.5±4.62	230.45±4.69	268.2±5.48*	274.68±8.47
4h	335.78±8.95	250.55±4.37**	200.48±5.48**	153.51±4.62**	112.4±5.12	125.42±5.46
4i	334.54±4.18*	309.85±4.68**	295.23±6.18	254±6.47*	289.14±5.61*	306.47±5.28
4j	309.52±2.84	300.15±6.15*	285.3±7.52	265.9±4.28**	273.58±4.35**	298.09±5.51
4k	338.4±6.41*	310.68±3.48	279.5±6.45**	254.30±5.49	281.21±5.41	298.45±6.32**
4l	325.64±2.54	308±5.48	285.46±8.17	265.48±6.48	285.15±5.48**	310.56±4.29*
4m	319.25±5.35*	318.62±4.65	294.32±6.21*	268.48±7.15**	294.54±4.62	300.58±5.42**
4n	320.61±5.16**	260.46±3.16	210.45±4.65*	145.68±5.49	120.64±4.68	130.64±6.48*

All values expressed as mean ± standard error of the mean, n=6. Standard drug: Rosiglitazone; Statistical analysis is done by one-way One-Way Analysis of Variance followed by Dunnet's "t" test; **p<0.01 (considered significant when compared to normal group), *p<0.001.
SEM: Standard error of the mean

Table 3. Effect of synthesized compounds 4c, 4h, and 4n on fasting blood glucose level and body weight in alloxan induced diabetic rats (chronic study 15 days)

Compound	Blood glucose in mg/dL			Body weight in g		
	Day 0	Day 7	Day 15	Day 0	Day 7	Day 15
Standard	368.25±4.24	200.65±3.63	178.91±5.61	196.5±4.27	193.22±3.25	194.2±5.24
4c (35 mg/kg bw)	325.56±2.59*	260.46±3.24*	216.22±2.44	194.20±2.43	196.5±3.34	194.22±5.17**
4c (70 mg/kg bw)	327.18±4.41	228.46±3.54*	209.16±3.28	199.31±2.64*	197.22±2.26*	195.21±2.77
4h (35 mg/kg bw)	336.64±4.22**	250.61±2.64	228.42±5.16	196.31±4.14	198.47±2.67**	195.44±3.12
4h (70 mg/kg bw)	319.61±2.58	205.22±4.51	179.62±3.61**	199.42±3.16	197.61±3.21	198.55±4.67*
4n (35 mg/kg bw)	320.38±4.55	254.35±3.14	211.28±2.45	198.66±2.61*	199.34±2.61	195.24±2.34*
4n (70 mg/kg bw)	320.64±3.27	206.37±2.48**	180.55±3.22**	200.61±3.64	198.46±3.48	197.41±4.54

All values expressed as mean ± standard error of the mean, n=6. Standard drug: rosiglitazone; Statistical analysis is done by one-way One-Way Analysis of Variance followed by Dunnet's "t" test; **p<0.01 (considered significant when compared to normal group), *p<0.001.

Table 4. Effect of compounds 4a-4n on human red blood cell membrane stabilization

Compound	% Inhibition at different concentrations			
	50 µg/mL	100 µg/mL	300 µg/mL	500 µg/mL
Diclofenac sodium	-----	86.79±0.43	90.78±0.87	-----
4a	53.33±0.38	58.67±0.32	61.33±0.46	68.00±0.62
4b	37.33±0.18	48.00±0.46	52.67±0.22	65.33±0.32
4c	42.67±0.32	52.00±0.62	61.33±0.28	68.00±0.32
4d	46.00±0.32	54.67±0.22	65.33±0.46	72.00±0.52
4e	40.00±0.32	46.00±0.52	52.00±0.36	54.00±0.42
4f	64.25±0.45	82.62±0.40	85.46±0.32	89.61±0.25
4g	52.34±0.36	61.48±0.85	72.42±0.60	85.82±0.46
4h	58.64±0.42	70.84±0.23	76.55±0.44	81.12±0.52
4i	51.65±0.75	60.33±0.48	71.64±0.68	78.45±0.72
4j	49.25±0.24	58.64±0.44	65.98±0.52	74.23±0.75
4k	61.42±0.61	80.43±0.64	84.28±0.48	90.64±0.26
4l	54.40±0.44	63.44±0.74	71.68±0.80	78.71±0.64
4m	58.64±0.62	65.49±0.82	70.18±0.42	76.48±0.34
4n	57.82±0.48	62.47±0.62	72.14±0.54	78.91±0.46

All values expressed as mean ± standard error of the mean, n=3

Table 5. Effect of compounds 4a-4n on protein denaturation

Compound	% Inhibition at different concentrations			
	50 µg/mL	100 µg/mL	300 µg/mL	500 µg/mL
Diclofenac sodium	-----	88.89±0.36	95.34±0.92	-----
4a	80.27±0.20	83.47±0.35	86.80±0.15	88.80±0.42
4b	66.53±0.28	84.53±0.42	86.00±0.35	86.80±0.45
4c	54.67±0.18	61.33±0.12	71.93±0.45	84.93±0.13
4d	61.33±0.46	71.80±0.35	78.67±0.38	86.00±0.28
4e	71.47±0.35	78.60±0.42	82.93±0.36	86.80±0.25
4f	83.42±0.35	86.49±0.28	87.42±0.33	94.82±0.44
4g	78.64±0.54	82.66±0.42	88.48±0.40	91.62±0.64
4h	81.80±0.24	86.48±0.22	88.64±0.86	92.75±0.32
4i	74.63±0.26	80.46±0.26	87.42±0.34	90.66±0.28
4j	78.62±0.42	81.66±0.48	86.94±0.55	90.48±0.36
4k	81.26±0.32	85.46±0.46	90.46±0.22	93.72±0.61
4l	81.46±0.62	85.92±0.68	88.33±0.82	92.64±0.46
4m	72.61±0.64	79.45±0.40	84.24±0.28	88.49±0.62
4n	69.46±0.52	72.24±0.64	76.18±0.38	82.81±0.12

All values expressed as mean ± standard error of the mean, n=3

binding energy (-8.32 kcal/moL and -8.29 kcal/moL) at the active site region of PPARγ receptor protein. Figure 1 depicts the 3D structure of PPARγ receptor protein, binding mode of rosiglitazone and compounds **4h** and **4n** at the active site region of PPARγ protein (PDB ID: 2PRG). Compound **4k** gave the highest binding energy (-7.47 kcal/moL and -10.98 kcal/moL) with the two COX targets used in comparison with the binding energy of the standard ligands indomethacin (-7.14 kcal/moL) and celecoxib (-10.89 kcal/moL). Figure 2 depicts the binding mode of indomethacin at the active site region of COX-1 (PDB ID: 1EQG), celecoxib at the active site region of COX-2 (PDB ID: 1CX2), and compound **4k** interaction with the two targets.

PPARγ protein structure from PDB ID: 2PRG

Binding mode of rosiglitazone at active site region of PPARγ protein PDB ID: 2PRG

Binding mode of compound 4 h at active site region of PPARγ protein PDB ID: 2PRG

Binding mode of compound 4 n at active site region of PPARγ protein PDB ID: 2PRG
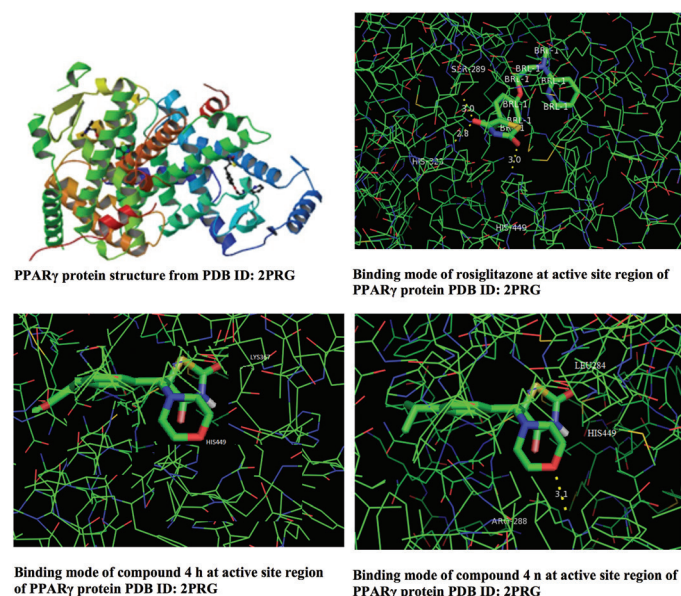
Figure 1. Molecular docking studies at active site region of PPARγ protein receptor (PBD ID: 2PRG)

PPARγ: Proliferator-activated receptor gamma

Binding mode of indomethacin at active site region of COX-1 PDB ID: 1EQG

Binding mode of celecoxib at active site region of COX-2 PDB ID: 1CX2

Binding mode of compound 4k at active site region of COX-1 PDB ID: 1EQG

Binding mode of compound 4k at active site region of COX-2 PDB ID: 1CX2
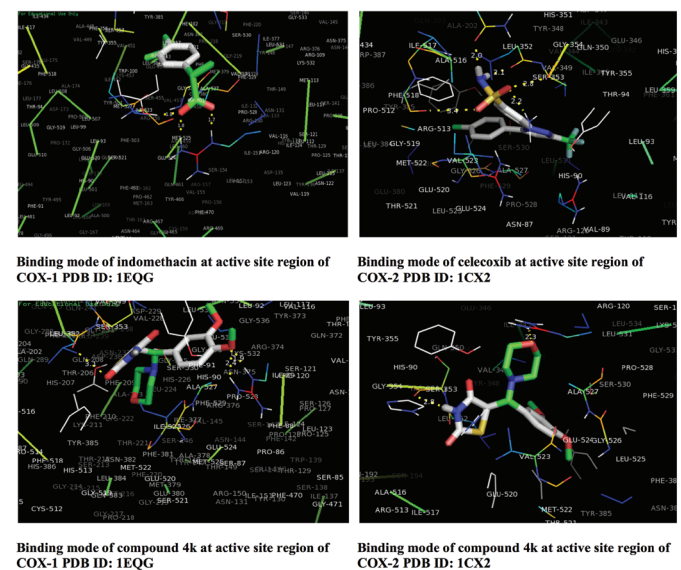
Figure 2. Molecular docking studies at active site region of COX isoenzymes (COX-1 PBD ID: 1EQG & COX-2 PDB ID: 1CX2)

CONCLUSION

In this investigation various thiazolidinedione derivatives possessing morpholine and substituted phenyl appendages that are attached to the common methyl group were developed as Mannich bases by simple Mannich reaction. The title compounds were synthesized by conventional as well as microwave-assisted synthesis. Microwave irradiation produced high yield in a shorter reaction time in comparison with traditional conventional heating synthesis. Characterization of the compounds was done physically and spectrally. They were evaluated for *in vivo* hypoglycemic activity and *in vitro* anti-inflammatory activity because of the existing thiazolidinedione

Table 6. Binding energy and amino acid residues interacted by the compounds 4a-4n with the target PPARγ protein (PDB ID - 2PRG)

Compound	Binding energy (kcal/moL)	Number of hydrogen bonds	Hydrogen bond length	Interacted amino acid residues
Rosiglitazone	-8.26	3	3.11, 3.01, 2.82	Ser289, His449, His323
4a	-7.64	2	3.15, 2.64	Leu284, Ser289
4b	-8.12	2	2.94, 3.22	Ser289, Cys258
4c	-7.64	3	2.84, 3.12, 2.61	Gln284, Tyr388, Met348
4d	-7.86	2	3.26, 2.82	Leu288, His449
4e	-7.85	3	3.24, 2.84, 2.28	Ser289, Met326, Leu284
4f	-7.24	2	2.98, 2.42	Cys258, Tyr471
4g	-7.61	3	1.86, 2.64, 1.91	Thr246, Ser289, His449
4h	-8.32	2	2.93, 3.08	Lys367, His449
4i	-7.12	3	2.48, 2.27, 1.92	Leu284, Ser289, Met298
4j	-7.57	2	3.40, 2.50	Cys255, Gln286
4k	-7.28	2	2.53, 1.94	Ser289, Thr246,
4l	-7.08	3	3.14, 1.92, 2.68	Tyr388, Ser289, His449
4m	-6.89	2	1.96, 2.44	Tyr471, Met348
4n	-8.29	3	3.10, 2.94, 3.22	Arg288, His449, Leu284

PPARγ: Proliferator-activated receptor gamma

Table 7. Binding energy and amino acid residues interacted by the compounds 4a-4n with the target COX-1 isoenzyme (PDB ID: 1EQG)

Compound	Binding energy (kcal/moL)	No. of hydrogen bonds	Hydrogen bond length	Interacted amino acid residues
Indomethacin	-7.14	2	2.62, 3.21	Leu352, Tyr355
4a	-7.01	2	2.32, 2.81	Arg120, Tyr355
4b	-6.58	3	1.87, 2.65, 3.17	Ala527, Ile523, Met522
4c	-6.48	1	2.84	Tyr355
4d	-6.74	3	2.56, 3.11, 1.98	Met522, Leu352, Tyr385
4e	-7.02	2	2.22, 2.95	Tyr385, Ser530
4f	-6.91	4	2.91, 2.05, 3.46, 2.07	Met522, Ile523, Tyr385, Arg120
4g	-6.65	2	1.97, 3.08	Leu352, Tyr355
4h	-6.46	3	1.91, 1.97, 3.12	Tyr385, Met522, Ile523
4i	-7.01	4	2.15, 2.04, 3.26, 1.91	Tyr355, Leu352, Ala527, Ser530
4j	-6.54	1	3.16	Arg120
4k	-7.47	3	1.96, 2.42, 3.17	Arg120, Leu352, Tyr385
4l	-6.22	2	2.64, 1.78	Arg120, Tyr355
4m	-6.81	2	2.74, 3.26	Tyr385, Leu352
4n	-6.74	5	2.08, 2.34, 2.65, 2.84, 2.26	Tyr385, Ser530, Ala527, Ile523, Met522

Compound	Binding energy (kcal/moL)	Number of hydrogen bonds	Hydrogen bond length	Interacted amino acid residues
Celecoxib	-10.89	5	2.25, 2.08, 2.16, 2.84, 3.46	His90, Gln192, Leu352, Ser353, Phe518
4a	-8.59	3	1.95, 2.64, 3.66	Ala527, His90, Ala527
4b	-7.99	3	3.22, 1.94, 2.65	Ala527, Ser530, Val523
4c	-9.47	2	3.42, 2.68	Tyr355, VAL349
4d	-8.98	4	2.31, 3.18,1.97, 3.18	Leu352, Arg120, Ser353, Tyr385
4e	-9.19	2	1.88, 2.86	Ser253, Val349
4f	-9.86	3	1.94, 2.09, 2.72	His90, Arg120, Ser353
4g	-8.89	2	2.55, 3.74	Arg120, Val349
4h	-7.49	3	2.19, 2.92, 3.15	His90, Ser353, Val523
4i	-9.05	3	3.22, 2.10, 1.94	Val349, Ser253, Leu352
4j	-9.39	4	1.89, 2.54, 3.30, 2.38	Tyr355, Tyr385, Ala527, Ser530
4k	-10.98	2	2.32, 2.87	Arg120, Ser353
4l	-8.33	2	1.95, 2.40	Tyr355, Tyr385
4m	-9.81	3	3.62, 2.31, 2.48	Arg120, Val349, Ser353
4n	-7.45	2	2.85, 3.23	Arg120, Val349

Table 8. Binding energy and amino acid residues interacted by the compounds 4a-4n with the target COX-2 isoenzyme (PDB ID: 1CX2)

and morpholine moieties. From the data of *in vivo* hypoglycemic activity screening, compounds **4h** and **4n** exhibited good hypoglycemic activity in both acute and chronic toxic studies. In the *in vitro* anti-inflammatory activity investigation by HRBC membrane stabilization method and protein denaturation method, compound **4k** exhibited good activity among all. From the viewpoint of structure–activity relationship, it was identified that compounds with electron releasing groups at the para position of the phenyl ring may have the ability to produce hypoglycemic activity and the presence of electron withdrawing groups at the para position of the phenyl ring causes anti-inflammatory activity. Molecular docking studies with PPARγ receptor protein (PDB ID-2PRG) and compounds **4h** and **4n** exhibited higher binding affinity. In molecular docking studies with COX isoenzymes (PDB IDs: 1EQG and 1CX2) for potential anti-inflammatory activity, compound **4k** exhibited higher binding affinity.

ACKNOWLEDGEMENTS

Conflicts of interest: No conflict of interest was declared by the authors.

REFERENCES

1. Maccari R, Ottanà R, Ciurleo R, Rakowitz D, Matuszczak B, Laggner C, Langer T. Synthesis, induced-fit docking investigations, and *in vitro* aldose reductase inhibitory activity of non-carboxylic acid containing 2,4-thiazolidinedione derivatives. Bioorg Med Chem. 2008;16:5840-5852.

2. Nazreen S, Alam MS, Hamid H, Yar MS, Dhulap A, Alam P, Pasha MA, Bano S, Alam MM, Haider S, Kharbanda C, Ali Y, Pillai KK. Thiazolidine-2,4-diones derivatives as PPAR-γ agonists: synthesis, molecular docking, *in vitro* and *in vivo* antidiabetic activity with hepatotoxicity risk evaluation and effect on PPAR-γ gene expression. Bioorg Med Chem Lett. 2014;24:3034-3042.

3. Wild S, Roglic G, Green A, Sicree R, King H. Global prevalence of diabetes: estimates for the year 2000 and projections for 2030. Diabetes Care. 2004;27:1047-1053.

4. Gangadhara S, Prasad Ch, Venkateswarlu P. Synthesis, antimicrobial and antioxidant activities of novel series of cinnamamide derivatives having morpholine moiety. Med Chem. 2014;4:778-783.

5. Vijay P, Kalpana T, Sonali M, Rhea M, Ramaa CS. Synthesis and primary cytotoxicity evaluation of new 5-benzylidene-2,4-thiazolidinedione derivatives. Eur J Med Chem. 2010;45:4539-4544.

6. Lee HW, Kim BY, Ahn JB, Kang SK, Lee JH, Shin JS, Ahn SK, Lee SJ, Yoon SS. Molecular design, synthesis, and hypoglycemic and hypolipidemic activities of novel pyrimidine derivatives having thiazolidinedione. Eur J Med Chem. 2005;40:862-874

7. Nazreen S, Alam MS, Hamid H, Yar MS, Dhulap A, Alam P, Pasha MA, Bano S, Alam MM, Haider S, Kharbanda C, Ali Y, Pillai KK. Thiazolidine-2,4-diones derivatives as PPARγ agonists: synthesis, molecular docking, *in vitro* and *in vivo* antidiabetic activity with

hepatotoxicity risk evaluation and effect on *PPARγ* gene expression. Bioorg Med Chem Lett. 2014;24:3034-3042.

8. Wang Z, Liu Z, Lee W, Kim SN, Yoon G, Cheon SH. Design, synthesis and docking study of 5-(substituted benzylidene) thiazolidine-2,4-dione derivatives as inhibitors of protein tyrosine phosphatase 1B. Bioorg Med Chem Lett. 2014;24:3337-3340.

9. Wu Y, Tai HH, Cho H. Synthesis and SAR of thiazolidinedione derivatives as 15-PGDH inhibitors. Bioorg Med Chem. 2010;18:1428-1433.

10. Lee HW, Kim BY, Ahn JB, Kang SK, Lee JH, Shin JS, Ahn SK, Lee SJ, Yoon SS. Molecular design, synthesis, and hypoglycemic and hypolipidemic activities of novel pyrimidine derivatives having thiazolidinedione. Eur J Med Chem. 2005;40:862-874.

11. Maccari R, Ottanà R, Ciurleo R, Vigorita MG, Rakowitz D, Steindl T, Langer T. Evaluation of *in vitro* aldose reductase inhibitory activity of 5-arylidene-2,4-thiazolidinediones. Bioorg Med Chem Lett. 2007;17:3886-3893.

12. Youssef AM, White MS, Villanueva EB, El-Ashmawy IM, Klegeris A. Synthesis and biological evaluation of novel pyrazolyl-2,4-thiazolidinediones as anti-inflammatory and neuroprotective agents. Bioorg Med Chem. 2010;18:2019-2028.

13. Neeru M, Prasad DN. Synthesis and antimicrobial evaluation of N-substituted-5-benzylidene-2,4-thiazolidinedione derivatives. Iran J Pharm Sci. 2012;8:209-214.

14. Pattan S, Kedar M, Pattan J, Dengale S, Sanap M, Gharate U, Shinde P, Kadam S. Synthesis and evaluation of some novel 2,4-thiazolidinedione derivatives for antibacterial, antitubercular and antidiabetic activities. Indian J Chem. 2012;51B:1421-1425.

15. Reddy KA, Lohray BB, Bhushan V, Reddy AS, Kishore PH, Rao VV, Saibaba V, Bajji AC, Rajesh BM, Reddy KV, Chakrabarti R, Rajagopalan R. Novel euglycemic and hypolipidemic agents: Part-2. Antioxidant moiety as structural motif. Bioorg Med Chem Lett. 1998;8:999-1002.

16. Hafez HN, El-Gazzar AR. Synthesis and antitumor activity of substituted triazolo [4,3-*a*] pyrimidin-6-sulfonamide with an incorporated thiazolidinone moiety. Bioorg Med Chem Lett. 2009;19:4143-4147.

17. Fan YH, Chen H, Natarajan A, Guo Y, Harbinski F, Iyasere J, Christ W, Aktas H, Halperin JA. Structure-activity requirements for the antiproliferative effect of troglitazone derivatives mediated by depletion of intracellular calcium. Bioorg Med Chem Lett. 2004;14:2547-2550.

18. Mavandadi F, Pilotti A. The impact of microwave-assisted organic synthesis in drug discovery. Drug Discov Today. 2006;11:165-174.

19. Kidwai M. Dry media reactions. Pure Appl Chem. 2001;73:147-151.

20. Kumar BR, Soni M, Kumar SS, Singh K, Patil M, Baig RB, Adhikary L. Synthesis, glucose uptake activity and structure–activity relationships of some novel glitazones incorporated with glycine, aromatic and alicyclic amine moieties via two carbon acyl linker. Eur J Med Chem. 2011;46:835-844.

21. Prashantha Kumar BR, Nanjan MJ, Suresh B, Karvekar MD, Adhikary L. Microwave induced synthesis of the thiazolidine-2,4-dione motif and the efficient solvent free-solid phase parallel syntheses of 5-benzylidene-thiazolidine-2,4-dione and 5-benzylidene-2-thioxo-thiazolidine-4-one compounds. J Heterocycl Chem. 2006;43:897-903.

22. Jiwane SK, Singh VK, Namdeo KP, Prajapati SK. Synthesis of Some Novel 2,4-Thiazolidinedione Derivatives and Their Biological Screening as Antidiabetic Agents. Asian J Chem. 2009;21:5068-5072.

23. Sivakumar KK, Rajasekaran A, Senthilkumar P, Wattamwar PP. Conventional and microwave assisted synthesis of pyrazolone Mannich bases possessing anti-inflammatory, analgesic, ulcerogenic effect and antimicrobial properties. Bioorg Med Chem Lett. 2014;24:2940-2944.

24. Anna PGN, Dipali D, Hemant DU. Facile synthesis and *in vivo* hypoglycemic activity of novel 2,4-hiazolidinedione derivatives. Eur J Exp Bio. 2012;2:343-353.

25. Shashikant RP, Prajact K, Ashwini P, Ana N, Kittur BS. Studies on the Synthesis of Novel 2,4-Thiazolidinedione Derivatives with Antidiabetic Activity. Iranian J Pharm Sci. 2009;5:225-230.

26. Sachin SS, Archana RJ, Manoj NG. *In vitro* antioxidant and anti-inflammatory activity of methanol extract of *Oxalis corniculata* Linn. Int J Pharm Pharm Sci. 2010;2:146-155.

27. Reshma, Arun KP, Brindha P. *In vitro* anti-inflammatory, Antioxidant and nephroprotective studies on leaves of *Aegle marmelos* and *Ocimum sanctum.* Asian J Pharm Clin Res. 2014;7:121-129.

28. Sangita Ch, Priyanka Ch, Protapaditya D, Sanjib B. Evaluation of *in vitro* anti-inflammatory activity of coffee against the denaturation of protein. Asian Pac J Trop Biomed. 2012;2:S178-S180.

29. Madhuri M, Prasad Ch, Vasudeva Rao A. *In silico* Protein-Ligand Docking Studies on Thiazolidinediones as Potential Anticancer Agents. Int J Comp Appl. 2014;95:13-16.

30. Arifa B, Shaheen B, Prasad KVSRG, Bharathi K. *In silico* studies on functionalized azaglycine derivatives containing original article 2,4-thiazolidinedione scaffold on multiple targets. Int J Pharm Pharm Sci. 2017;9:209-215.

31. Ugwu DI, Okoro UC, Ukoha PO, Gupta A, Okafor SN. Novel anti-inflammatory and analgesic agents: synthesis, molecular docking and *in vivo* studies. J Enzyme Inhib Med Chem. 2018;33:405-415.

Intrinsic Stability Study and Forced Degradation Profiling of Olopatadine Hydrochloride by RP-HPLC-DAD-HRMS Method

RP-YBSK -DAD-HRMS Yöntemi ile Olopatadin Hidrokloridin Gerçek Stabilite ve Zorlanmış Bozunma Profilinin Oluşturulması

Ⓘ Pawan Kumar BASNIWAL[1,2]*, Ⓘ Deepti JAIN[1]

[1]School of Pharmaceutical Sciences, Rajiv Gandhi Technological University, Bhopal, Madhya Pradesh, India
[2]Lal Bahadur Shastri College of Pharmacy, Jaipur, Rajasthan, India

ABSTRACT

Objectives: Forced degradation determines the intrinsic stability of a molecule by establishing degradation pathways in order to identify the likely degradation products (DPs). The objective of the present research was to establish intrinsic stability and forced degradation profiling of olopatadine hydrochloride.

Materials and Methods: The intrinsic stability of olopatadine hydrochloride was evaluated by RP-HPLC, where a mixture of 0.1% formic acid and organic phase (methanol:acetonitrile; 50:50 % v/v) was used as mobile phase at 1.0 mL/min in gradient mode. Different stress conditions were employed to explore the intrinsic stability of olopatadine hydrochloride.

Results: In acidic condition, five DPs, i.e. OLO1, OLO2, OLO3, OLO4, and OLO5, were observed. OLO5 was the major DP that increased with time and the peak area of OLO was decreased. In addition to OLO3 and OLO5, two more DPs were observed in alkaline condition, i.e. OLO6 and OLO7. OLO5 and OLO6 were two major DPs; OLO5 increased with time while OLO6 had a zigzag pattern of peak area with time. All DPs of neutral condition were also found in acidic condition while OLO3 and OLO5 were common in all three types of hydrolytic degradation.

Conclusion: Thus, OLO has similar pattern of degradation profiling in all hydrolytic conditions (acidic, alkaline, and neutral). No degradation was found in thermal, ultraviolet light, or oxidative conditions over 10 days. OLO-Imp was recognized as an analogue structure of OLO and proposed as 11-[(3-dimethylamino)-propylidene]-6,11-dihydro-dibenz[b,e]oxepin-2-propanoic acid in standard drug. OLO1 was identified as (2-(4-(dimethylamino) butyl) phenyl)methanol, which may be formed by cleavage of the tricyclic ring in neutral condition.

Key words: Olopatadine hydrochloride, forced degradation, HPLC

ÖZ

Amaç: Zorlanmış bozunma, muhtemel bozunma ürünlerini (DP) tanımlamak için bozunma yolları oluşturarak bir molekülün gerçek stabilitesini belirler. Bu araştırmanın amacı, olopatadin hidrokloridin gerçek stabilitesini ve zorlanmış bozunma profilini oluşturmaktır.

Gereç ve Yöntemler: Olopatadin hidrokloridin gerçek stabilitesi, %0,1 formik asit ve organik faz karışımı (metanol: asetonitril;% 50:50 h/h) mobil faz olarak 1,0 mL/dak'de gradyan modunda kullanımıyla RP-YBSK ile değerlendirilmiştir. Olopatadin hidrokloridin gerçek stabilitesini araştırmak için farklı stres koşulları kullanılmıştır.

Bulgular: Asidik koşulda, beş DP, yani OLO1, OLO2, OLO3, OLO4 ve OLO5 gözlenmiştir. başlıca DP OLO5 idi, pik süresi artmış ve OLO'nun pik alanı azalmıştır. OLO3 ve OLO5'e ek olarak, alkali koşullarda, iki DP daha, OLO6 ve OLO7 gözlenmiştir. OLO5 ve OLO6 iki ana DP idi; OLO5 zamanla

artarken OLO6 zamanla zikzak bir tepe alanı düzenine sahipti. Nötral koşullardaki bütün DP'ler asidik koşullarda da bulunurken, OLO3 ve OLO5 üç hidrolitik bozunma tipinde de ortaktı.

Sonuç: OLO, tüm hidrolitik koşullarda (asidik, alkali ve nötr) benzer bir bozulma profiline sahiptir. Termal, ultraviyole ışığı veya oksidatif koşullarda 10 gün boyunca hiçbir bozulma bulunamamıştır. OLO-Imp, OLO'nun analog bir yapısı olarak kabul edilmiş ve standart ilaçta 11-[(3-dimetilamino) -propiliden]-6,11-dihidro-dibenz [b, e] oksepin-2-propanoik asit olarak önerilmiştir. OLO1, trisiklik halkanın nötr koşulda bölünmesiyle oluşturulabilecek (2-[4-(dimetilamino) butil] fenil) metanol olarak tanımlanmıştır.

Anahtar kelimeler: Olopatadin hidroklorid, zorlanmış bozunma, YBSK

INTRODUCTION

Forced degradation involves degradation of a new drug substance or drug product at more severe conditions than accelerated conditions. Forced degradation studies afford information for the identification of possible degradants, degradation pathways, and the inherent stability of the active pharmaceutical ingredient. It also yields information about any possible polymorphic or enantiomeric substances and the difference between drug related degradation and excipient interferences. A New Drug Application (NDA) registration requires data of forced degradation studies in the form of forced degradation products (DPs), degradation reaction kinetics, structure, mass balance, drug peak purity, etc. Therefore, forced degradation and impurity profiling is one of the inputs for an NDA registration manuscript.[1] Due to the presence of impurities or DPs The Food and Drug Administration has recalled finished pharmaceutical products; they include adagen (pegademase bovine) injection, azelastine hydrochloride ophthalmic solution, brimonidine tartrate ophthalmic solution, ciclopirox gel, diflorasone diacetate cream, fludeoxyglucose F18 injections, hydroxyzine hydrochloride oral solution, leflunomide tablets, pediatric atropine sulfate injection, prednisolone sodium phosphate oral solution, ropinirole hydrochloride tablets, and topiramate tablets.[2] The intrinsic stability of armodafinil hydrochloride was explored by forced degradation and impurity profiling, where the structures of four DPs were established and a possible pathway was postulated. In the present work, the whole research methodology was adopted from Jain and Basniwal.[3]

Chemically, olopatadine (OLO) is 11-((Z)-3-(dimethyl-amino) propylidene)-6,11-dihydro-dibenz[b,e] oxepin-2-acetic acid[4] and is indicated for allergic rhinitis, urticaria, and itching resulting from skin diseases such as eczema/dermatitis, prurigo, pruritus cutaneous, psoriasis vulgaris, and multiform exudative erythema. OLO primarily acts as a selective histamine H1 receptor antagonist. It also inhibits the production and release of chemical mediators such as leukotriene and thromboxane, and the release of the neurotransmitter tachykinin.[5-9] Analytical methods for OLO determination in different matrices have been reported, i.e. radioimmunoassay,[10] liquid chromatography (LC) with tandem mass spectrometry,[11] LC–ESI-MS–MS,[12,13] capillary zone electrophoretic method,[14] high performance LC (HPLC), and high-performance thin-layer chromatography (HPTLC),[15] but there is no study reported on forced degradation profiling including the intrinsic stability of OLO. The objective of forced degradation is to provide guidance for the development of executing purposeful degradation experiments for

pharmaceutical drug candidates. The International Council for Harmonisation of Technical Requirements for Pharmaceuticals for Human Use (ICH) Guideline provides some guidance on stress testing or purposeful degradation stress testing helps to determine the intrinsic stability of the molecule by establishing degradation pathways in order to identify the likely DPs.[16] The objective of present research was to establish intrinsic stability and forced degradation profiling of OLO by reverse phase (RP) HPLC diode array detector (DAD) high-resolution mass spectrometry (HRMS).

EXPERIMENTAL

MATERIALS AND METHODS

Chemicals and reagent

Working standard of OLO hydrochloride was gifted by Ranbaxy Laboratories Limited, Gurgaon, Harayana. HPLC grade solvents (methanol and acetonitrile), formic acid, hydrochloric acid, sodium hydroxide, and hydrogen peroxide were procured from Merck Specialties Private Limited, Mumbai, India. Triple distilled water was prepared in-house.

Instrument and chromatography

All dilutions, mobile phase, and other solutions were filtered through a 0.2-μm nylon filter and chromatographed by an Agilent Infinity 1260 series system equipped with a 1260 binary pump VL 400 bar, 1260 manual injector 600 bar, Rheodyne 7725i 7-port sample injection valve with 20 μL fixed loop, ZORBAX Eclipse Plus C18 (250×4.6 mm, 5 μm), 1260 DAD VL, 20 Hz detector, standard flow cell 10 mm, 13 μL, 120 bar, OpenLab CDS EZChrom Ed. Workstation, and syringe 50.0 μL, FN, LC tip. Micromass Q-TOF micro (Waters) LC-mass spectrometry (MS) was performed in HRMS mode using electrospray positive ionization. The parameters desolvation gas (500 L/h), cone gas (25 L/h), desolvation temperature (250˚C), source temperature (120˚C), capillary voltage (3000 V), cone voltage (30 V), and collision energy (10 V) were used for HRMS analysis. All dilutions, mobile phase, and other solutions used for the analysis were filtered through a 0.2-μm nylon filter (Ultipor® N66 Nylon 6,6 membrane, Pall Sciences, Pall India Pvt. Ltd. Mumbai, India). The mobile phase was composed of water adjusted to 0.1% formic acid (A) and acetonitrile and methanol (50:50) (B) in gradient mode (Tmin/A:B; T0/70:30; T4/70:30; T14/20:80; T22/80:20; T25/70:30). The flow rate was set to 1.0 mL/min with UV detector wavelength fixed at 300 nm. The injection volume was 20 μL.

Standard solution

An accurately weighed amount of 100 mg of OLO was dissolved in 100 mL of methanol to prepare stock P (1000 μg/mL). An aliquot of stock P was diluted to prepare stock Q (100 μg/mL), which was used to prepare a series of standard dilutions, i.e. 2, 4, 6, 8, and 10 μg/mL OLO.

Method validation

As per ICH guidelines,[17-19] the proposed method was validated for the stability indicating assay and to establish the inherent stability of OLO drug with forced degradation profiling in different conditions by RP-HPLC determination. The developed method was validated to assure the reliability of results of analysis for different parameters, i.e. linearity, range, accuracy, precision, robustness, limit of quantification (LOQ), limit of detection (LOD), and specificity. The serial dilutions (2-10 μg/mL) of the OLO in 50% methanol in triplicate were used for the linearity determination. Accuracy was determined by recovery method by spiking the standard solution into pre-analyzed samples. The precision of the method was studied under the head of repeatability and intermediate precision. The six replicates of 10 μg/mL were chromatographed subsequently to assure repeatability. The intermediate precision was determined by day-to-day analysis variation and analyst-to-analyst variation in the linearity range. The robustness of the method was studied with variation in the temperature (20, 25, and 30°C) and content of formic acid (0.1%) in aqueous phase variation by 5% change. LOD and LOQ were determined by signal-to-noise ratio. The specificity was ascertained by degrading the drug sample in stressed conditions. Sample solution stability was demonstrated by analyzing six replicates of 10 μg/mL OLO standard samples at different time intervals with freshly prepared mobile phase each time.

Forced degradation

Forced degradation studies of bulk drug included appropriate solid state (thermal and photolytic) and solution state stress conditions (hydrolytic and oxidative). The stock solution was used for the forced degradation study to provide an indication of the stability indicating the property and specificity of the proposed method. Accurately weighed about 100 mg of OLO was dissolved in 50 mL of methanol and the volume was made up to 100 mL with water/0.2 N HCl/0.2 N NaOH to perform hydrolytic degradation in neutral (water), acidic (0.1 N HCl), and alkali (0.1 N NaOH) conditions, respectively, followed by refluxing at 60°C. Bulk drug (powder form) was exposed to 60°C (hot air oven) and ultraviolet (UV) light separately for temperature and UV degradation, respectively. Oxidative degradation of OLO was performed in 3% and 10% H_2O_2 solution. Prior to injection, samples were withdrawn at the appropriate time, neutralized (in the case of acid and alkali hydrolysis), and the solutions were diluted with 50% methanol. Thermal and photolytic degraded drug (solid powder) was dissolved in 50% methanol to prepare samples for injection.

RESULTS AND DISCUSSION

Optimization of chromatographic conditions

OLO was eluted at 3.77 min by the mixture of 0.1% formic acid and methanol (35:65) on a ZORBAX Eclipse Plus C18 column (250×4.6 mm, 5 μm) at 1.0 mL/min flow rate and it was successfully applied for determination of the OLO drug in dosage form,[20] but it was not suitable for separation of the DPs along with OLO.

Thus, chromatographic conditions were optimized to develop a stability-indicating assay to separate the related compounds and DPs from the drug content. RP-HPLC mode chromatography was selected based on the solubility and pKa value of OLO. A ZORBAX Eclipse Plus C18 column (250×4.6 mm, 5 μm) was used to separate all degradants along with the drug. The wavelength of 300 nm was selected due to maximum absorbance of all the DP and drug, which was optimized by 1260 DAD VL, 20 Hz detector.

Peak broadening and splitting were observed with both mobile phases, methanol and water (50:50) and acetonitrile and water (50:50). The drug's peak was merged with the diluent's as the organic phase was increased. After using the acidic aqueous phase (pKa of drug 4.29), the broadening and tailing of the OLO peak persisted. It was improved by increasing the organic phase (methanol) up to 65%. Further, methanol content was reduced to 60% to resolve 4-5 grouped peaks in degraded samples, where little separation was found, but the peak shapes were not acceptable. Then acetonitrile content was incorporated in the organic phase along with methanol (50:50). All peaks of degraded samples were very sharp but not well resolved with 0.1% formic acid and above organic phase (40:60). Degradant peaks were well separated up to 6 min when this ratio was reversed (60:40), but high tailing was observed in the drug's peak. Thus, degradants were well resolved in 60:40 ratios while the drug eluted in 40:60; then it was concluded to run gradient mode.

DPs were resolved before the drug peak but a few of them were merged with the drug peak between 11 and 13 min and two DPs were merged with each other at 16.5 min in gradient mode (Tmin/A:B; T0/70:30; T7/70:30; T9/30:70; T17/70:30; T20/70:30). Basically, the above elution mode is not purely gradient; it was a combination of more isocratic and less gradient mode. Fine resolution was observed up to 16 min, when gradient mode was increased (Tmin/A:B; T0/70:30; T5/70:30; T16/30:70; T17/70:30; T20/70:30), but groups of DPs were observed between 16 and 19 min. Therefore, the run time was extended to 25 min with increased gradient mode (Tmin/A:B; T0/70:30; T4/70:30; T20/30:70; T22/70:30; T25/70:30). Most of the DPs were resolved but tailing in the drug peak was seen, which may have been due to less exposure to the organic phase, and so it was decided to increase organic content in the mobile phase (Tmin/A:B; T0/70:30; T4/70:30; T14/20:80; T22/70:30; T25/70:30). In this gradient mode, OLO and all DPs in different forced degradation conditions were well separated with acceptable resolution.

Method validation

The consistence performance of the HPLC system was assured by system suitability parameters. Six replicates of OLO samples were injected, and column performance parameters like tailing factors, retention time, and number of theoretical plates were observed. The values of % relative standard deviation (RSD) for these parameters were within the acceptance criteria of system performance. OLO has better separation in the set of conditions as the higher theoretical plates (59526) with less than one unit of % RSD (0.88). The tailing factor was 0.68 with acceptable % RSD. The capacity factor was 15.02, i.e. OLO has sufficient opportunity to interact with the stationary phase, resulting in differential migrations. The co-elution of impurities or degradants is generally investigated by examining peak purity using a PDA detector. The three-dimensional view of the chromatogram confirmed that there was no peak around the OLO elution time. Here the peak purity at 11.62 min was 1.0; there was no interference with elution of OLO at retention time, or nothing was co-eluting along with OLO at 11.62 min. Thus, all system suitability parameters were within the acceptance criteria.

The linear regression equation was Y=16751x+26.50 with correlation coefficient r^2=0.999 and a calibration graph was plotted for concentration versus area found in the chromatogram. The accuracy of the developed method was assured at all levels of linearity. It was 99.50-100.28% by the recovery method with % RSD of 0.32, which shows the reliability for accuracy of the developed RP-HPLC method. The developed method was performed under two heads: repeatability and intermediate precision. The repeatability of sample injections was measured as the determined amount of OLO in six different serial replicates, which was expressed as 99.89% with % RSD of 0.08, while intermediate precision was evaluated on the heads of interday analysis as well as analyst-to-analyst. Both parameters were determined near to 100% (99.93% and 99.95%) with less than unit % RSD (0.11 and 0.12) at all three levels of concentration.

The robustness of the developed method was assured by the variation in the amount of formic acid (0.1%) in the aqueous phase of mobile phase composition and temperature of real-time analysis. The three variations in formic acid in the aqueous phase (0.105%, 0.100%, and 0.095%) and temperature variation (20, 25, and 30°C) had no significant effect of change in parameters on the results. These were found to be 99.97 and 100.17, with % RSD 0.13 and 0.29, respectively. The LOD and LOQ were determined by signal-to-noise ratio. These were found to be 0.045 µg/mL and 0.149 µg/mL, respectively, which show the sensitivity of the developed method. The % RSD value was less than two. Analysis of degraded drug sample in stressed conditions was evidence for specificity of the method. The retention time, peak symmetry, peak purity, and UV spectrum of the recorded chromatograms of different samples were confirmed to assure the specificity. The AUC of the OLO peak in the chromatogram decreased with an increase in the AUC of the degradant's peak. This experimental evidence confirmed that the developed method was specific for the analysis of OLO. The stability of OLO was assured during analysis by response ratio. The response ratio of the drug at all concentration level varied between 16565.67 and 16973.33 with % RSD of 0.89. This is evidence that the drug is stable in selected solution at room temperature and the RP-HPLC method is continuously sensitive toward the analyte.

Forced degradation profiling

Acidic degradation: Five DPs, i.e. OLO1 (5.17), OLO2 (7.87), OLO3 (11.11), OLO4 (12.65), and OLO5 (12.91), were observed in acidic condition (Figure 1). OLO5 was the major DP that increased with time and the peak area of OLO was decreased. All DPs appeared on the first day except OLO1 and OLO2, which appeared on fourth and second day, respectively. The peak area of OLO3 and OLO4 increased first and then decreased. The other two DPs, OLO1 and OLO2, increased with time.

Alkaline degradation: OLO was gradually degraded into four DPs, i.e. OLO3 (11.11), OLO6 (12.07), OLO5 (12.91), and OLO7 (17.48), in alkaline condition (Figure 2). OLO3 and OLO5 were common DPs in acidic and alkaline conditions, while OLO6 and OLO7 were newer DPs in basic degradation. OLO5 and OLO6 were two major DPs; OLO5 increased with time while OLO6 had a zigzag pattern of peak area with time. Concentrations of both OLO3 and OLO7 increased with time.

Neutral degradation: All DPs in neutral condition were also found in acidic condition, while OLO3 and OLO5 were common in all three types of hydrolytic degradation (Figure 3). OLO5 was the major DP in all conditions. OLO was gradually degraded and the peak area of all DPs increased with time in neutral condition.
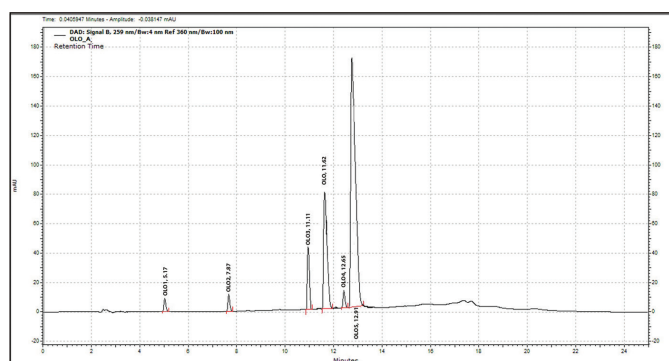
Figure 1. Representative chromatogram of OLO in acidic condition
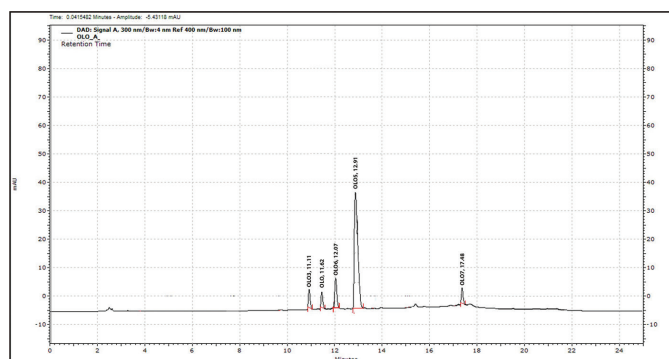
OLO: Olopatadine

Figure 2. Representative chromatogram of OLO in alkaline condition

OLO: Olopatadine

RP-HPLC analysis of stressed samples of OLO in thermal, oxidative, and photolytic degradation showed that there was no degradation in these conditions. It might be possible that due to solid sample in thermal stress condition no degradation was observed.

Thus, in acidic condition, five DPs, i.e. OLO1, OLO2, OLO3, OLO4, and OLO5, were observed. OLO5 was the major DP that increased with time and the peak area of OLO was decreased. In addition to OLO3 and OLO5, two more DPs were observed in alkaline condition, i.e. OLO6 and OLO7. OLO5 and OLO6 were two major DPs; OLO5 increased with time while OLO6 had a zigzag pattern of peak area with time. All DPs of neutral condition were also found in acidic condition, while OLO3 and OLO5 were common in all three types of hydrolytic degradation. Thus, OLO has a similar pattern of degradation profiling in all hydrolytic conditions (acidic, alkaline, and neutral) (Figure 4). No degradation was found in thermal and UV light exposure, as these were performed on solid powder of OLO, and so it is possible that degradation is less likely in the solid powder. Similarly, oxidative degradation was also not observed over 10 days.

Degradation pathway and impurity profiling

Standard drug OLO: LC-MS was performed in positive mode using leucine enkephalin as standard, where OLO and its impurity (OLO-Imp) were observed at relative retention time (RRT) of 1.00 and 1.11, respectively. The ESI mass spectrum of

OLO showed a protonated molecular ion [M+H]$^+$ and its isotopic abundance [M+2H]$^+$ at m/z 338.1671 and 339.1663 with ppm errors in mass 2.08 and 4.45, respectively. It was advocated by its further fragmentation pattern into its daughter products as: 337.1678 → 292.1099 → 221.0961 → 247.1117 → 165.0546 (Table 1, Figure 5).

An impurity, OLO-Imp (OLO5), was observed in the ESI spectrum, and its protonated molecular ion [M+H]$^+$ was observed at m/z 352.1840 along with its isotopic abundance (Figure 6). Its structure was an analogue of OLO and proposed as 11-[(3-dimethylamino)-propylidene]-6,11-dihydro-dibenz[b,e] oxepin-2-propanoic acid (Figure 6). It was also used as internal standard for the metabolite study.[10]

Acidic degradation: In addition to OLO, sodium salt of OLO (OLO3) and OLO5 (OLO-Imp) were observed in the MS spectrum of the acidic condition sample at RRT of 0.96 and 1.11. OLO3 was observed in all three degradation conditions. Its protonated molecular ion [M+H]$^+$ was observed at m/z 360.1502, which showed its carboxylic acid analogue at m/z 338.1684. The MS-MS fragmentation pattern into its daughter products indicated the purposed structure as: 359.1497 → 337.1678 → 279.1623

Figure 3. Representative chromatogram of OLO in neutral condition

OLO: Olopatadine
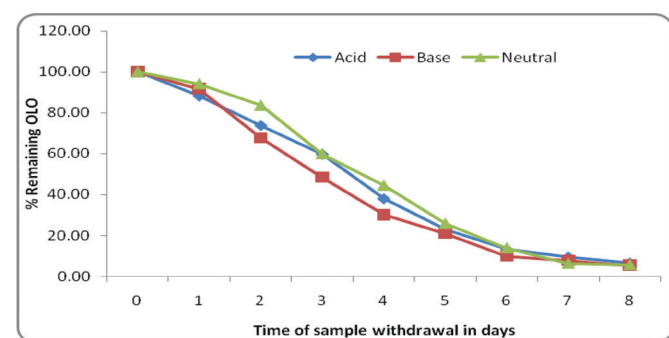
Figure 4. Degradation profiling of OLO in acidic, basic, and neutral conditions
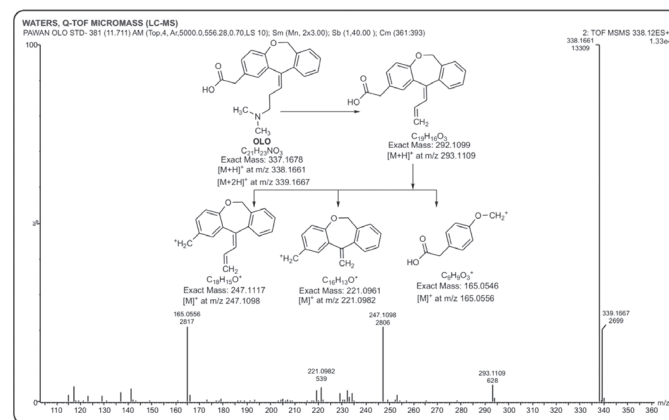
OLO: Olopatadine

Figure 5. Chromatogram of OLO by TOF MS-MS spectrum and proposed fragmentation pattern of OLO

OLO: Olopatadine, MS: Mass spectrometry
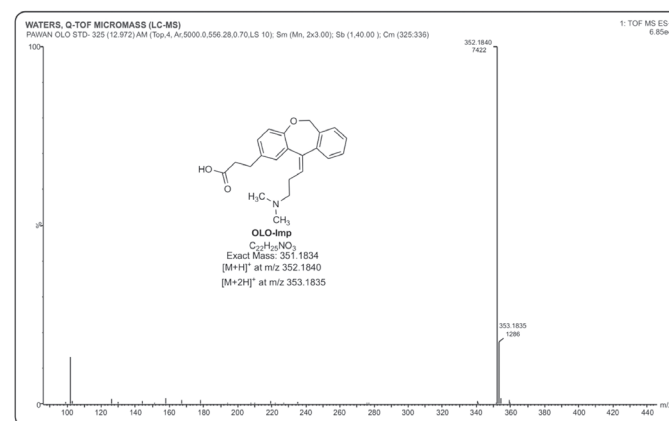
Figure 6. Chromatogram of OLO-Imp by TOF MS-ES+ and proposed structure of OLO-Imp

OLO: Olopatadine, MS: Mass spectrometry, ES: Electrospray
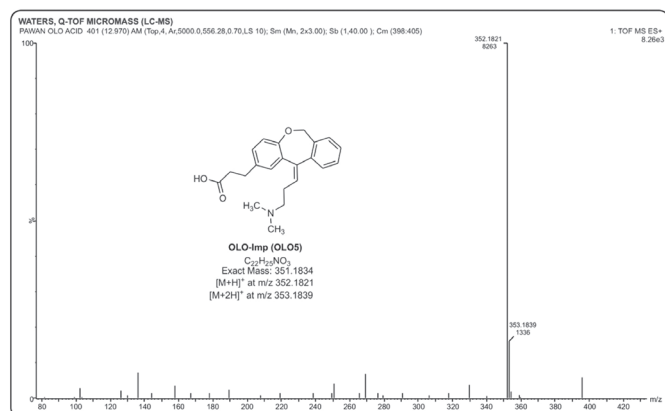
Figure 7. Chromatogram of OLO5 by TOF MS-ES⁺ spectrum and proposed structure of OLO5 in acidic condition

OLO: Olopatadine, MS: Mass spectrometry, ES: Electrospray
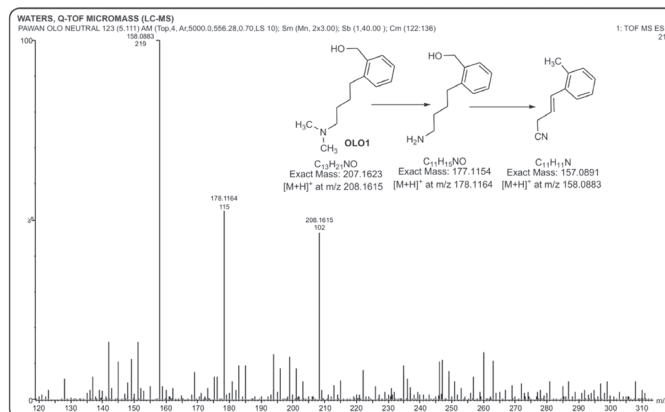
Figure 9. Chromatogram of degraded OLO in neutral condition by TOF MS-ES+ spectrum and proposed fragmentation pattern of OLO1

OLO: Olopatadine, MS: Mass spectrometry, ES: Electrospray
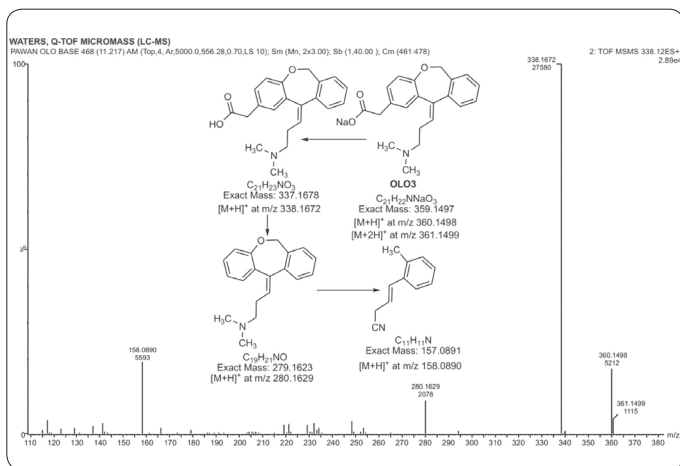
Figure 8. Chromatogram of degraded OLO in alkaline condition by TOF MS-MS spectrum and proposed fragmentation pattern of OLO3

OLO: Olopatadine, MS: Mass spectrometry, ES: Electrospray
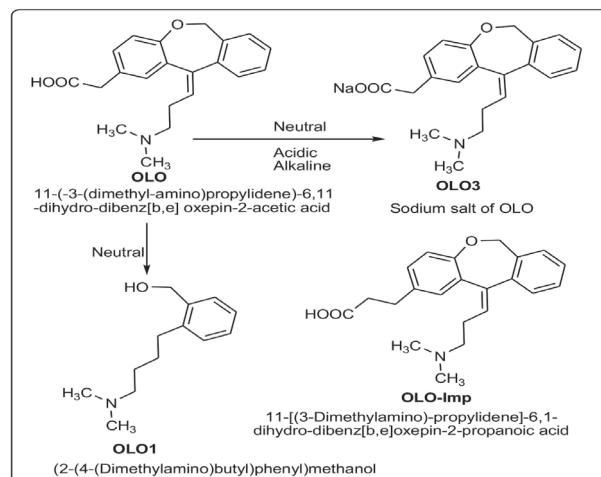
Figure 10. Proposed structure of OLO-Imp and proposed degradation pathway of OLO in acidic, alkaline, and neutral conditions

OLO: Olopatadine

Table 1. Observed m/*z* values for [M+H]⁺ ions and major fragments of OLO and its impurity							
Analyte code	RRT in LC MS	MS-ES or MS-MS	m/z value	Measured mass	Best possible molecular formulae	Exact mass	ppm error
OLO	1.00	MS-ES	338.1671	337.1671	C21H23NO3	337.1678	2.08
			339.1663	337.1663	C21H23NO3	337.1678	4.45
			340.1701	337.1701	C21H23NO3	337.1678	-6.82
	1.00	MS-MS	338.1661	337.1661	C21H23NO3	337.1678	5.04
			339.1667	337.1667	C21H23NO3	337.1678	3.26
			293.1109	292.1109	C19H16O3	292.1099	-3.42
			247.1098	247.1098	C18H15O+	247.1117	7.69
			221.0982	221.0982	C16H13O+	221.0961	-9.50
			165.0556	165.0556	C9H9O3+	165.0546	-6.06
OLO-Imp	1.11	MS-ES	352.1840	351.1840	C22H25NO3	351.1834	-1.71
			353.1835	351.1835	C22H25NO3	351.1834	-0.28

RRT: Relative retention time, OLO: Olopatadine, LC: Liquid chromatography, MS: Mass spectrometry, ES: Electrospray

→ 157.0891 (Table 2). OLO was also characterized in acidic degradation at RRT of 1.00. MS-ES⁺ scanning revealed the protonated molecular ion [M+H]⁺ of OLO at m/z 338.1676 with isotopic abundance. MS-MS of OLO in acidic condition showed the fragmentation pattern in the mass spectrum as: 337.1678 → 292.1099 → 247.1117; 165.0546 (Table 2). The protonated molecular ion [M+H]⁺ of OLO5 was observed at m/z 352.1821 with isotopic abundance at 353.1839 (Figure 7). The ppm error in mass was less than five units (Table 2).

Alkaline degradation: The MS spectrum of the alkaline sample of OLO was similar to the MS spectrum of acidic condition. The degradation pathway and fragmentation pattern of OLO and its DPs were similar to those in acidic condition (Figure 8). Only ppm error in mass varied from acidic condition (Table 3).

Neutral degradation: In neutral condition, the tricyclic ring underwent cleavage and OLO1 was formed (RRT=0.44). OLO3 was also formed in a similar pattern to acidic and alkaline conditions (RRT=0.96). OLO5 (OLO-Imp) was also observed in the MS spectrum similar to all other conditions. Only one additional DP (OLO1) was observed in neutral condition, whose protonated molecular ion [M+H]⁺ was found at m/z 208.1615 and identified as (2-(4-(dimethylamino)butyl) phenyl)methanol (Figure 9). The proposed structure was further advocated by its degradation pattern (207.1623 → 177.1154 → 157.0891) (Table 4). OLO3, OLO, and OLO5 were also characterized in neutral condition similar to above both acidic and alkaline conditions. The ppm error in mass is different from the above conditions but most of the error is below 5 units (Table 4).

Thus, OLO and its impurity (OLO-Imp) were observed at RRT of 1.00 and 1.11, respectively, in the LC-MS study. OLO-Imp was recognized as an analogue structure of OLO and proposed as 11-[(3-dimethylamino)- propylidene]-6, 11-dihydro-dibenz[b,e]oxepin-2-propanoic acid (Figure 10). In addition to OLO, sodium salt of OLO (OLO3) and OLO5 (OLO-Imp) were observed in the MS spectrum of acidic and alkaline conditions samples at RRT of 0.96 and 1.11. OLO3 was observed in all three degradation conditions and identified as sodium salt of OLO (OLO is a carboxylic acid derivative). Additionally, OLO1 (RRT=0.44) was identified as (2-(4-(dimethylamino)butyl) phenyl)methanol, which may be formed by cleavage of the tricyclic ring in neutral condition. OLO is an acetic acid derivative along with oxepin ring and tertiary nitrogen, which is quite a stable form of drug. There is no vulnerable functional group liable to convert or break down into DPs under stressed or forced degradation conditions. Thus, OLO forms relatively slow and fewer DPs.

CONCLUSION

OLO has a similar pattern of degradation profiling in all hydrolytic conditions (acidic, alkaline, and neutral), while no degradation was found in thermal, UV light, and oxidative conditions over 10 days. OLO-Imp was recognized as an analogue structure of OLO and proposed as 11-[(3-dimethylamino)-propylidene]-6,11-dihydro-dibenz[b,e]oxepin-2-propanoic acid. OLO3 was observed in all three degradation conditions and identified as sodium salt of OLO (OLO is a carboxylic acid derivative). Additionally, OLO1 was identified as (2-(4-(dimethylamino)

Table 2. Observed m/z values for the [M+H]⁺ ions and major fragments of OLO and its degradation products in acidic condition							
Analyte code	RRT in LC MS	MS-ES or MS-MS	m/z value	Measured mass	Best possible molecular formulae	Exact mass	ppm error
OLO3	0.96	MS-ES	360.1502	359.1502	$C_{21}H_{22}NNaO_3$	359.1497	-1.39
			338.1684	337.1684	$C_{21}H_{23}NO_3$	337.1678	-1.78
	0.96	MS-MS	360.1491	359.1491	$C_{21}H_{22}NNaO_3$	359.1497	1.67
			361.1488	359.1488	$C_{21}H_{23}NO_3$	359.1497	2.51
			338.1676	337.1676	$C_{21}H_{23}NO_3$	337.1678	0.59
			280.1625	279.1625	$C_{19}H_{21}NO$	279.1623	-0.72
			158.0883	157.0883	$C_{11}H_{11}N$	157.0891	5.09
OLO	1.00	MS-ES	338.1676	337.1676	$C_{21}H_{23}NO_3$	337.1678	0.59
			339.1698	337.1698	$C_{21}H_{23}NO_3$	337.1678	-5.93
	1.00	MS-MS	338.1695	337.1695	$C_{21}H_{23}NO_3$	337.1678	-5.04
			339.1688	337.1688	$C_{21}H_{23}NO_3$	337.1678	-2.97
			293.1102	292.1102	$C_{19}H_{16}O_3$	292.1099	-1.03
			247.1132	247.1132	$C_{18}H_{15}O^+$	247.1117	-6.07
			165.0552	165.0552	$C_9H_9O_3^+$	165.0546	-3.64
OLO5	1.11	MS-ES	352.1821	351.1821	$C_{22}H_{25}NO_3$	351.1834	3.70
			353.1839	351.1839	$C_{22}H_{25}NO_3$	351.1834	-1.42

RRT: Relative retention time, OLO: Olopatadine, LC: Liquid chromatography, MS: Mass spectrometry, ES: Electrospray

Table 3. Observed m/z values for the [M+H]+ ions and major fragments of OLO and its degradation products in alkaline condition

Analyte code	RRT in LC MS	MS-ES or MS-MS	m/z value	Measured mass	Best possible molecular formulae	Exact mass	ppm error
OLO3			360.1507	359.1507	$C_{21}H_{22}NNaO_3$	359.1497	-2.78
	0.96	MS-ES	338.1686	337.1686	$C_{21}H_{23}NO_3$	337.1678	-2.37
			360.1498	359.1498	$C_{21}H_{22}NNaO_3$	359.1497	-0.28
			361.1499	359.1499	$C_{21}H_{23}NO_3$	359.1497	-0.56
			338.1672	337.1672	$C_{21}H_{23}NO_3$	337.1678	1.78
			280.1629	279.1629	$C_{19}H_{21}NO$	279.1623	-2.15
	0.96	MS-MS	158.0890	157.0890	$C_{11}H_{11}N$	157.0891	0.64
OLO			338.1696	337.1696	$C_{21}H_{23}NO_3$	337.1678	-5.34
			339.1688	337.1688	$C_{21}H_{23}NO_3$	337.1678	-2.97
	1.00	MS-ES	340.1675	337.1675	$C_{21}H_{23}NO_3$	337.1678	0.89
			338.1685	337.1685	$C_{21}H_{23}NO_3$	337.1678	-2.08
			339.1688	337.1688	$C_{21}H_{23}NO_3$	337.1678	-2.97
			293.1108	292.1108	$C_{19}H_{16}O_3$	292.1099	-3.08
			247.1110	247.1110	$C_{18}H_{15}O^+$	247.1117	2.83
	1.00	MS-MS	165.0540	165.0540	$C_9H_9O_3^+$	165.0546	3.64
			352.1828	351.1828	$C_{22}H_{25}NO_3$	351.1834	1.71
OLO5	1.11	MS-ES	353.1839	351.1839	$C_{22}H_{25}NO_3$	351.1834	-1.42

RRT: Relative retention time, OLO: Olopatadine, LC: Liquid chromatography, MS: Mass spectrometry, ES: Electrospray

Table 4. Observed m/z values for the [M+H]+ ions and major fragments of OLO and its degradation products in neutral condition

Analyte code	RRT in LC MS	MS-ES or MS-MS	m/z value	Measured mass	Best possible molecular formulae	Exact mass	ppm error
			208.1615	207.1615	$C_{13}H_{21}NO$	207.1623	3.86
			178.1164	177.1164	$C_{11}H_{15}NO$	177.1154	-5.65
OLO1	0.44	MS-ES	158.0883	157.0883	$C_{11}H_{11}N$	157.0891	5.09
			360.1489	359.1489	$C_{21}H_{22}NNaO_3$	359.1497	2.23
			361.1498	359.1498	$C_{21}H_{23}NO_3$	359.1497	-0.28
			338.1666	337.1666	$C_{21}H_{23}NO_3$	337.1678	3.56
			280.1618	279.1618	$C_{19}H_{21}NO$	279.1623	1.79
OLO3	0.96	MS-ES	158.0888	157.0888	$C_{11}H_{11}N$	157.0891	1.91
OLO			338.1681	337.1681	$C_{21}H_{23}NO_3$	337.1678	-0.89
	1.00	MS-ES	339.1685	337.1685	$C_{21}H_{23}NO_3$	337.1678	-2.08
			338.1687	337.1687	$C_{21}H_{23}NO_3$	337.1678	-2.67
			339.1667	337.1667	$C_{21}H_{23}NO_3$	337.1678	3.26
			293.1118	292.1118	$C_{19}H_{16}O_3$	292.1099	-6.50
			247.1119	247.1119	$C_{18}H_{15}O^+$	247.1117	-0.81
			221.0965	221.0965	$C_{16}H_{13}O^+$	221.0961	-1.81
	1.00	MS-MS	165.0551	165.0551	$C_9H_9O_3^+$	165.0546	-3.03
			352.1856	351.1856	$C_{22}H_{25}NO_3$	351.1834	-6.26
OLO5	1.11	MS-ES	353.1825	351.1825	$C_{22}H_{25}NO_3$	351.1834	2.56

RRT: Relative retention time, OLO: Olopatadine, LC: Liquid chromatography, MS: Mass spectrometry, ES: Electrospray

butyl)phenyl)methanol, which may be formed by cleavage of the tricyclic ring in neutral condition.

ACKNOWLEDGEMENTS

Conflicts of interest: No conflict of interest was declared by the authors.

REFERENCES

1.   Jain D, Basniwal PK. Forced degradation and impurity profiling: Recent trends in analytical perspectives. J Pharm Biomed Anal. 2013;86:11-35.

2.   Singh S, Handa T, Narayanam M, Sahu A, Junwal M, Shah RP. A critical review on the use of modern sophisticated hyphenated tools in the characterization of impurities and degradation products. J Pharm Biomed Anal. 2012;69:148-173.

3.   Jain D, Basniwal PK. Intrinsic Stability Study of Armodafinil Hydrochloride by Forced Degradation and İmpurity Profiling. Pharm Anal Acta. 2016;7:466.

4.   Ohshima E, Ohtaki S, Sato H, Kumazawa T, Obase H, Ishii A, Ishii H, Ohmori K, Hirayama N. Synthesis and antiallergic activity of 11-(aminoalkylidene)-6,11-dihydrodibenz [b,e] oxepin derivatives. J Med Chem. 1992;35:2074-2084.

5.   Scoper SV, Berdy GJ, Lichtenstein SJ, Rubin JM, Bloomenstein M, Prouty RE, Vogelson CT, Edwards MR, Waycaster C, Pasquine T, Gross RD, Robertson SM. Perception and quality of life associated with the use of olopatadine 0.2% (Pataday) in patients with active allergic conjunctivitis. Adv Ther. 2007;24:1221-1232.

6.   Kajita J, Inano K, Fuse E, Kuwabara T, Kobayashi H. Effects of olopatadine, a new antiallergic agent, on human liver microsomal cytochrome p450 activities. Drug Metab Dispos. 2002;30:1504-1511.

7.   McGill JI. A review of the use of olopatadine in allergic conjunctivitis. Int Ophthalmol. 2004;25:171-179.

8.   Takahashi H, Zhang Y, Morita E. Evaluation of the antihistamine effects of olopatadine, cetirizine and fexofenadine during a 24 h period: A double-blind, randomized, crossover, placebo-controlled comparison in skin responses induced by histamine iontophoresis. Arch Dermatol Res. 2008;300:291-295.

9.   Ohishi T, Magara H, Yasuzawa T, Kabayashi H, Yamaguchi K, Kobayashi S. Disposition of KW-4679 (4): metabolism of KW-4679 in rats and dogs. Xenobiol Metab Dispos. 1995;10:689-706.

10. Tsunoo M, Momomura S, Masuo M, Iizuka H. Phase 1 clinical study on KW-4679, an antiallergic drug: Safety and pharmacokinetics in the single and repeated administration study to healthy subjects. Kiso To Rinsho. 1995;29:4129-4147.

11. Zhu P, Wen Y, Fan XP, Zhou ZL, Fan RX, Chen JM, Huang KL, Zhu XL, Chen YF, Zhuang J. A rapid and sensitive liquid chromatography-tandem mass spectrometry method for determination of olopatadine concentration in human plasma. J Anal Toxicol. 2011;35:113-118.

12. Fujimaki K, Lee XP, Kumazawa T, Sato J, Sato K. Determination of some antiallergic drugs in human plasma by direct-injection high-performance liquid chromatography-tandem mass spectrometry. Forensic Toxicol. 2006;24:8-16.

13. Fujita K, Magara H, Kobayashi H. Determination of olopatadine, a new antiallergic agent, and its metabolites in human plasma by high-performance liquid chromatography with electrospray ionization tandem mass spectrometry. J Chromatogr B Biomed Sci Appl. 1999;731:345-352.

14. Güray T, Turan T, Tunçel M, Uysal UD. A validated capillary electrophoretic method for the determination of olopatadine and its application to a pharmaceutical preparation of eye drops. J AOAC Int. 2017;100:206-211.

15. Varghese SJ, Kumar AM, Ravi TK. Stability-indicating high-performance column liquid chromatography and high-performance thin-layer chromatography methods for the determination of olopatadine hydrochloride in tablet dosage form. J AOAC Int. 2011;94:1815-1820.

16. ICH "Stability Testing of New Drug Substance and Products", International Conference on Harmonization of Technical Requirement for Registration of Pharmaceutical for Human Use, Geneva, 2000.

17. ICH "Text on Validation of Analytical Procedures"; International Conference on Harmonization of Technical Requirements for Registration of Pharmaceutical for Human Use, Geneva, 2000.

18. ICH "Validation of Analytical Procedure: Methodology"; International Conference on Harmonization of Technical Requirements for Registration of Pharmaceutical for Human Use, Geneva, 2000.

19. Crowther JB. Validation of pharmaceutical test methods. In: Ahuja S, Scypinski S, eds. Handbook of Modern Pharmaceutical Analysis. London; Academic Press;2001:415-444.

20. Basniwal PK, Jain D. ICH guideline practice: application of novel RP-HPLC-DAD method for determination of olopatadine hydrochloride in pharmaceutical products. J Analyt Sci Tech. 2013;4:12.

ORIGINAL ARTICLE

In Vitro Evaluation of the Chemical Composition and Various Biological Activities of *Ficus carica* Leaf Extracts

Ficus carica Yaprak Ekstrelerinin Kimyasal Bileşiminin ve Çeşitli Biyolojik Aktivitelerinin *İn Vitro* Değerlendirilmesi

🆔 Mustafa ERGÜL[1]*, 🆔 Merve ERGÜL[2], 🆔 Nuraniye ERUYGUR[3], 🆔 Mehmet ATAŞ[4], 🆔 Esra UÇAR[5]

[1]Sivas Cumhuriyet University, Faculty of Pharmacy, Department of Biochemistry, Sivas, Turkey
[2]Sivas Cumhuriyet University, Faculty of Pharmacy, Department of Pharmacology, Sivas, Turkey
[3]Selçuk University, Faculty of Pharmacy, Department of Pharmacognosy, Konya, Turkey
[4]Sivas Cumhuriyet University, Faculty of Pharmacy, Department of Microbiology, Sivas, Turkey
[5]Sivas Cumhuriyet University, Sivas Vocational School, Department of Medicinal and Aromatic Plants, Sivas, Turkey

ABSTRACT

Objectives: The present study aimed to investigate the inhibitory activities of enzymes related to diabetes mellitus and Alzheimer's disease of the methanol and water extracts of *Ficus carica* leaf extracts. The bioactive compounds and anticancer, antioxidant, and antimicrobial effects of the extracts were also investigated.

Materials and Methods: The bioactive compounds in the extracts were determined by gas chromatography-mass spectrometry. The antioxidant activity was evaluated by 1,1-diphenyl-2-picrylhydrazyl (DPPH), 2,2'-azino-bis(3-ethylbenzothiazoline-6 sulphonic acid) (ABTS) radical scavenging, total phenol and flavonoid content, ferric reducing power, and iron chelating method. The anticancer, anticholinesterase, and antimicrobial effects were investigated using the XTT assay, Ellman method, and microdilution, respectively.

Results: Our results showed that between the water and methanol extracts there was a difference in terms of chemical composition. The antioxidant results suggested that both extracts have strong antioxidant activity. Similarly, both extracts showed strong α-glucosidase and α-amylase inhibition activity, while the water extract had higher inhibition activity than the methanol extract against acetylcholinesterase and butyrylcholinesterase. The methanol extract of *F. carica* exhibited significant anticancer activity on MDA-MB-231 cells and showed moderate antimicrobial activities against *Escherichia coli* and *Staphylococcus aureus*.

Conclusion: Our results suggest that *F. carica* leaves could be a valuable source for developing a promising therapeutic agent in cancer, diabetes, and Alzheimer's disease.

Key words: *Ficus carica*, Alzheimer's disease, diabetes, antioxidant activity, anticancer and antimicrobial activities

ÖZ

Amaç: Bu çalışmada, *Ficus carica* yapraklarına ait su ve metanol ekstrelerinin diyabet ve Alzheimer hastalığı ile ilişkili enzimlerin inhibisyonu üzerine etkisinin araştırılması amaçlanmıştır. Ayrıca, ekstrelere ait biyoaktif bileşenler, antikanser, antioksidan ve antimikrobiyal etkiler de araştırılmıştır.

Gereç ve Yöntemler: Ekstrelerdeki biyoaktif bileşikler gaz kromatografisi-kütle spektrometresi metodu ile belirlenmiştir. Antioksidan aktivite, 1,1-diphenyl-2-picrylhydrazyl (DPPH), 2,2'-azino-bis(3-ethylbenzothiazoline-6 sulphonic acid) (ABTS) radikal süpürücü, toplam fenol ve flavonoid içeriği, ferrik indirgeme gücü ve demir şelasyon yöntemleriyle değerlendirilmiştir. Antikanser, antikolinesteraz ve antimikrobiyal etkinlikler ise sırasıyla XTT yöntemi, Ellman yöntemi ve mikrodilüsyon tekniği yöntemi ile belirlenmiştir.

Bulgular: Elde ettiğimiz sonuçlar su ve metanol ekstreleri arasında kimyasal bileşim açısından farklılık olduğunu ve her iki ekstrenin de güçlü antioksidan aktiviteye sahip olduğunu göstermiştir. Benzer şekilde, her iki ekstrede güçlü α-glikozidaz ve α-amilaz aktivite gösterirken, su ekstresi metanole göre daha güçlü asetilkolinesteraz ve butirilkolinesteraz inhibisyon etkiye sahiptir. *F. carica* metanol ekstresi MDA-MB-231 hücreleri üzerinde güçlü antikanser etki, *Escherichia coli* ve *Staphylococcus aureus*'e karşı ise orta düzeyde antimikrobiyal etki göstermiştir.

Sonuç: Bulgularımız, *F. carica* yapraklarının kanser, diyabet ve Alzheimer hastalığında umut verici bir terapötik ajan geliştirmek için değerli bir kaynak olabileceğini düşündürmektedir.

Anahtar kelimeler: *Ficus carica*, Alzheimer hastalığı, diyabet, antioksidan aktivite, antikanser ve antimikrobiyal aktivite

INTRODUCTION

Ficus carica L. belongs to the family Moraceae and is a native of southwest Asia. It is cultivated worldwide and has been traditionally used in indigenous systems of medicine, such as Ayurveda and homeopathy, for cardiovascular and hypertensive diseases.[1,2] Its fruit possesses several vitamins, minerals, carbohydrates, and phenolic compounds, for instance, phenolic acids, flavonols, and flavones, which play a significant role in its therapeutic efficiency.[3-5] Many reports also stated that the polyphenolic ingredient of the fruit has anti-inflammatory, antioxidant, antimicrobial, and anticancer effects.[6]

In recent years, due to increasing cancer cases and similar health problems, the demand for products with antioxidant properties has been increasing day by day. In this context, plants that have antioxidant and anticancer properties have attracted wide attention. It is well known that antioxidants have significant inhibitory effects on various free radical species and also neutralize nonradical species such as hydrogen peroxide. Additionally, they can prevent the production of many reactive oxygen species in various diseases such as cancer and diabetes.[7,8]

Diabetes mellitus is a chronic metabolic disease that causes elevation of blood sugar due to insufficient insulin secretion or insulin resistance. α-Glucosidase and α-amylase inhibitors are used in some cases to control the level of postprandial blood glucose in the treatment of diabetes mellitus. These two enzymes are involved in the conversion of food polysaccharides into monosaccharides. However, synthetic hypoglycemic agents have been reported for several side effects such as hepatotoxicity and gastrointestinal disorders. Accordingly, researchers are looking for new potential antidiabetic agents from natural sources with less adverse effects.[9]

Alzheimer's disease (AD) is the most common form of dementia, characterized by memory loss and other cognitive disabilities. Down-regulation of acetylcholine is associated with the development of AD. Acetylcholinesterase (AChE) and butyrylcholinesterase (BChE) are responsible for the hydrolytic metabolism of the neurotransmitter acetylcholine (ACh) into choline and acetate in the brain. Based on the cholinergic hypothesis, a defect in the cholinergic system is involved in the development of AD.[10] Therefore, the current treatment strategy for AD is directed to the inhibition of AChE and BChE. There are some AChE inhibitors such as galantamine, physostigmine, and tacrine approved for the treatment of AD. However, these drugs have side effects, including hepatotoxicity, limiting the use of these drugs in clinical practice. Hence, researchers are looking for new treatments to control the disease and improve the quality of life for people with AD from natural resources.

Cancer is one of the most significant health issues worldwide and the second leading cause of death globally after cardiovascular diseases.[11] Conventional treatments used in the clinic such as chemotherapy, surgery, and radiotherapy have several serious side effects and can cause damage to noncancerous tissues.[12] Moreover, due to increasing drug resistance especially in cancer treatment, plants have become increasingly important in the search for new chemotherapeutic agents. In the clinic, there are many antitumor drugs derived from plants such as vincristine, vinblastine (*Catharanthus* sp.), paclitaxel (*Taxus* sp.), and epipodophyllotoxins (*Podophyllum* sp.).[13] Furthermore, research continues at a great pace for the discovery of new drugs with more effective and less side effect profiles. *F. carica* is one of the medicinally important plants with therapeutic potential. Many researchers have reported the antimicrobial effects of *F. carica* leaf extracts against oral bacteria, nosocomial infectious agents, food poisoning bacteria, fungi, and viruses.[14-17] Moreover, the fruit, root, and leaves of *F. carica* are utilized medicinally for treating various diseases as a respiratory, gastrointestinal, anti-inflammatory, and antispasmodic remedy.[18]

To the best of our knowledge, the fruit and different parts of this plant have been mostly studied, and the number of study on the leaves is limited. Thus, this study was carried out to evaluate differences between water and methanol extracts for antioxidant, antimicrobial, enzyme inhibition activity (AChE, BChE, α-glucosidase, and α-amylase), and anticancer properties *in vitro*. It was also aimed to analyze the content of extracts by gas chromatography-mass spectroscopy (GC-MS).

EXPERIMENTAL

This study was conducted in the laboratories of the Faculty of Pharmacy, Sivas Cumhuriyet University, Sivas, in 2018. The plant materials were collected in July 2017 from the wild flora of Saklıkent/Fethiye. The experiments were performed in a completely randomized design with three replications.

Preparation of extracts

The plant leaves were milled with a grinder and then dried in the shade and the dry leaves were ground in a blender (Blue house). Ten grams of the leaf was soaked in 50 mL of methanol (Sigma) and water for 24 h with intermittent shaking. At the end of the extraction, it was filtered through No. 1 Whatman filter paper. The filtrate was concentrated to dryness under reduced pressure in a rotary evaporator at 40°C and this was repeated three times. The obtained extracts were analyzed using GC-MS.[19]

In vitro antioxidant activity

The antioxidant activity of the methanol and water extracts of *F. carica* leaves was tested using different methods, namely DPPH, ABTS radical scavenging activity, total phenol/flavonoid content, ferric reducing power, and iron chelating method.

DPPH radical scavenging activity

The free radical scavenging activity by methanol extracts was determined according to the method reported by Miser Salihoglu et al.[20] First 150 μL of the extract was mixed with 50 μL of 1.0×10^{-3} M freshly prepared DPPH• methanol solution in 96-well plates. Methanol was used as the control of the experiment. After 30 min of incubation at 25°C, the reduction of the DPPH• was measured reading the absorbance at 517 nm with a microplate reader (Epoch, USA). Butylated hydroxytoluene (BHT) was used for the positive controls and the percentage inhibition was calculated with the following equation:

% Inhibition=[Absorbance of control-Absorbance of test sample/Absorbance of control]×100

ABTS radical scavenging activity

For determining the ABTS radical scavenging activity of the extracts, the method described by Re et al.[21] was followed with slight modification. The stock solution of ABTS was made by reacting 7 mM ABTS solution with 2.4 mM potassium persulfate solution in equal volume for 16 h. The working solution was then prepared by diluting the stock ABTS•+ solution with methanol to give an absorbance of 0.7±0.02 units at 734 nm using a microplate reader (Epoch, USA). In each experiment, the ABTS•+ solution was prepared freshly. Fifty microliters of the extract was mixed with 150 μL of ABTS•+ working solution and the resulting mixture was left for 10 min in a dark place. All the analyses were conducted in triplicate and the results expressed as the mean ± standard deviation. Appropriate blanks (methanol) and standard (BHT) were run simultaneously.

Determination of total phenolic content (TPC)

In order to measure the TPC in the extracts, the spectrophotometric Folin-Ciocalteu method was used as previously described by Clarke et al.,[22] with slight modification. Briefly, 20 μL of extract in DMSO was mixed with 100 μL of freshly 1/10 diluted F-C reagent with distilled water. After 5 min, the solution was mixed with 80 μL of 7.5% Na_2CO_3 solution, and incubated for 30 min at 25°C. The measurement of absorbance was performed at 650 nm in a microplate reader (Epoch, USA). All the analyses were performed in triplicate and the results expressed as the mean ± standard deviation (SD). Appropriate blanks (DMSO) and standard (gallic acid in DMSO) were run simultaneously, after which the TPC was calculated as milligrams gallic acid equivalents per gram of dry extract.

Estimation of total flavonoid content (TFC)

For determination of TFC, the aluminum chloride colorimetric method was used as previously described by Molan and Mahd[23] using catechin as the reference standard. Briefly, 25 μL of 1 mg/mL test sample solution, 100 μL of dd. H_2O, and 7 μL of 5% $NaNO_2$ were mixed together in 96-well plates. After 15 min of incubation at room temperature, 7 μL of 10% $AlCl_3$ was added. After 5 min, 50 μL of 1 M NaOH and 60 μL of distilled water were added to each well. Then the absorbance was measured at 490 nm in a microplate reader (Epoch, USA). All determinations were carried out in triplicate. The content of total flavonoids was expressed as milligrams of catechin equivalent per gram of the dry weight of the extract.

Iron chelating activity

The iron chelating activity of the extracts was determined according to their interaction with the formation of the ferrozine-Fe^{2+} complex. Previously described procedures were used.[24] Briefly, a mixture of 200 μL of 0.1 mM $FeSO_4$, 200 μL of extract, and 400 μL of 0.2 mM ferrozine was allowed to react at 25°C. The mixture absorbance was read after 10 min of incubation at 562 nm. EDTA was used as positive control.

Ferric reducing antioxidant power (FRAP) assay

The FRAP reagent is used as a reducing agent in redox colorimetric reactions of antioxidants. The FRAP assay was conducted according to the previously reported method with a slight modification.[25,26] The stock solution of each extract was prepared in DMSO. The working solution of FRAP reagent was prepared by mixing 0.3 M pH 3.6 acetate buffer and a solution of 10 mM 2,4,6-tripyridyl-s-triazine (TPTZ) in 0.04 M HCl and 0.02 M $FeCl_3$ solution in the ratio of 10:1:1 at the time of use. All solutions were prepared fresh on the day of the experiment. Thirty microliters of the sample solution and 270 μL of FRAP working solution were mixed together in 96-well plates and warmed at 37°C for 4 min. All determinations were performed in triplicate. The absorbance was measured at 593 nm. A standard calibration curve was prepared using different concentrations of $FeSO_4$ solution. The results were expressed as FRAP values.

Acetylcholinesterase/butyrylcholinesterase inhibition assay

The assay was carried out according to the Ellman method[27] as follows. The mixture consisting of 20 μL of test sample/reference standard of various concentrations, 140 μL of 0.1 mM phosphate buffer (pH 6.8), 10 μL of 3 mM 5,5′-dithio-bis-nitrobenzoic acid (DTNB), and 20 μL of enzyme (0.22 U/mL for acetylcholinesterase/0.1 U/mL for butyrylcholinesterase) prepared in phosphate buffer was incubated for 5 min at 25°C. Following preincubation, 10 μL of the substrate (0.71 mM acetylthiocholine iodide/0.2 mM butyrylthiocholine chloride in phosphate buffer) was added to start the reaction, followed by further incubation for 10 min. The developed yellow color was measured at 412 nm (Epoch, USA). Galantamine was used as the positive control.

Alpha-glucosidase inhibition activity

The α-glucosidase inhibition method was reported by Kumar et al.[28] Acarbose was used as a positive control, while phosphate buffer was used as a negative control in place of the sample. Each concentration was carried out in triplicate. Twenty-five microliters of sample solution diluted with buffer was mixed with 25 μL of α-glucosidase (0.5 U/mL) and incubated for approximately 10 min at 25°C. Then 25 μL of 0.5 mM 4-nitrophenyl-β-D-glucuronide (pNPG) was added to each well as substrate and incubated for a 30 min at 37°C. After the incubation period, 100 μL of 0.2 M sodium carbonate was added to terminate the reaction and the absorbance was read at 405 nm.

Alpha-amylase inhibition activity

The α-amylase inhibition method was reported by Kumar et al.[29] Acarbose was used as a positive control, while phosphate buffer (0.02 M PBS, pH 6.9) was used as a negative control in place of the sample. Each sample was tested in triplicate with different concentrations. The reaction mixture containing 50 μL of sample solution diluted with buffer and 25 μL of α-amylase from porcine pancreases (0.5 mg/mL) was incubated for approximately 10 min at 25°C. Then 50 μL of freshly prepared 0.5% starch solution (w/v) was added to each well as substrate and incubated for 10 min at 25°C. After the incubation period,

100 μL of 1% 3,5-dinitrosalicylic acid (DNS) was added as the color reagent, followed by heating in a water bath for 10 min. The absorbance was read at 540 nm.

Antimicrobial activity

Microdilution broth method

The microdilution broth method with slight modification was used to determine the minimum inhibitory concentration (MIC) of the water and methanol extracts of *F. carica* against the microorganism.[30] In the present study, *Staphylococcus aureus* (ATCC 29213), *Enterococcus faecalis* (ATCC 29212), *Pseudomonas aeruginosa* (ATCC 27853), *Escherichia coli* (ATCC 25922), *Klebsiella pneumoniae* (ATCC 13883), and *Candida albicans* (ATCC 10231) strains were used. The extracts were dissolved in 50% dimethyl sulfoxide (DMSO) and the final concentrations of the extracts were 50 mg/mL. Mueller Hinton Broth (Accumix® AM1072) and Sabouraud Dextrose Broth (Himedia ME033) were used for dilution bacteria and *C. albicans* cultures, respectively. In the first row of the plate, 90 μL of broth was added to the wells and 50 μL of broth was added to all other wells. The 11th wells were used as the reproductive controls and 100 μL of broth was added. In the first line of the microtiter plate, 10 μL of extract was added and serial two-fold dilutions were prepared from the diluted extracts to give concentrations ranging from 2.5 to 0.004 mg/mL. The bacteria and fungi suspensions (50 μL) were added to prepared samples. The final inoculum size was 5×10^5 CFU/mL in the bacteria wells and 0.5-2.5×10^3 CFU/mL in the *C. albicans* wells (CLSI, 2002, CLSI, 2012). The plates with the added bacteria and *C. albicans* were incubated at 37°C and 35°C for 16-24 h, respectively. Afterwards, to observe microbial growth, 50 μL of 2,3,5-triphenyltetrazolium chloride (TTC) (Merck, Germany) was added to each well. The microtiter plates were further incubated at 37°C for 2 h. The first well in which the density of formazan's red color was reduced was accepted as showing the MIC. The experiment was performed in duplicate and the standard deviation was zero.

Cytotoxicity

Cell lines and reagents

Human breast adenocarcinoma (MDA-MB-231) cells and mouse fibroblast (L929) cells were obtained from the American Type Culture Collection (ATCC, Manassas, VA, USA). Dulbecco's modified Eagle's medium (DMEM), fetal bovine serum (FBS), and sterile phosphate buffer saline (PBS) were purchased from PAA Ltd. (France). Trypsin-EDTA was supplied from Biological Industries Ltd. (Haemek, Israel). DMEM without phenol red and L-glutamine-penicillin-streptomycin solutions were from Sigma-Aldrich (Steinheim am Albuch, Germany). XTT reagent (2,3-bis-(2-methoxy-4-nitro-5-sulfophenyl)-2H-tetrazolium-5-carboxanilide) was purchased from Roche Diagnostics.

Cell culture

The cytotoxicity of the *F. carica* leaf extracts was tested against MDA-MB-231 and L929 cell lines. During the experiments, both cell lines were grown in DMEM supplemented with 10% FBS, 1% L-glutamine, 100 IU/mL penicillin, and 10 mg/mL streptomycin in 25 cm² polystyrene flasks and maintained in a humidified atmosphere with 5% CO_2 at 37°C. Growth and morphology were monitored, the culture medium was changed every 2 days, and the cells were passaged when they had reached 80-90% confluence.

Cell viability assay

The antiproliferative activity of the *F. carica* leaf extracts was evaluated by XTT colorimetric assay against the MDA-MB-231 and L929 cells. Extracts were dissolved in DMSO and diluted in DMEM prior to treatment. Initially, cancer and control cells were seeded at a density of 5×10^3 cells per well in 96-well culture plates in 100 μL of culture medium and were allowed to attach overnight before treatment. The next day, these cells were treated with serial concentrations (0.0625, 0.125, 0.25, 0.5, 1 mg/mL) of *F. carica* for 24 h. Furthermore, nontreated cells and cells treated with DMSO (0.5%) were used as negative controls and solvent controls, respectively. After that, the treatment medium was removed and wells were washed twice with 200 μL of PBS. At the end of these periods, for determination of living cells, 100 μL of DMEM without phenol red and 50 μL of XTT labeling mixture were added to each well and then the plates were incubated for another 4 h. The absorbance of XTT-formazan was measured using a microplate reader (Epoch, USA) at 450 nm against the control (the same cells without any treatment). All experiments were performed in three independent experiments and cell viability was expressed in % related to the control (100% viability).

Statistical analysis

Data obtained from *in vitro* antioxidant and antidiabetic activity were expressed as the mean ± SD. Cytotoxicity results were evaluated statistically using one-way analysis of variance (ANOVA) at 95% confidence levels for multiple comparisons. The Tukey test was used as the post-hoc test. P values less than or equal to 0.05 were considered to be statistically significant. The 50% inhibitory concentrations of the extract and reference compounds were calculated through an extract dose-response curve in GraphPad Software (San Diego, CA, USA).

RESULTS AND DISCUSSION

GC-MS analysis of the water and methanol extracts of F. carica

The chemical compositions of the water and methanol extracts of *F. carica* leaves were studied using GC-MS and the results are shown in Table 1. According to the GC-MS results, more different components were obtained in the methanol extract than in the aqueous extract of *F. carica*. Namely, six and 28 different compounds were determined in the water and methanol extracts, respectively. While the most abundant components are benzene, methoxy-(3.32%), 4-methyl-1,4-heptadiene (6.85%), 1-pentene, 2,3-dimethyl-(2.72%) for the water extract, they were 2H-furo[2,3-H]-1-benzopyran-2-one (53.64%), bergapten (19.27%), 9,12,15-octadecatrienoic acid, methyl ester, (*Z,Z,Z*)-(4.05%) for the methanol extract.

Table 1. Chemical components of the water and methanol extracts from *F. carica*

Chemical components	RT (min)	Water (%)	Methanol (%)
2-Furanmethanol (CAS)	6.692	---	0.36
2-Cyclopentene-1,4-dione	7.493	---	0.10
Benzene, methoxy-	8.654	3.32	---
1,2-Cyclopentanedione	8.849	---	0.31
Phenol (CAS)	11.298	-0.02	0.14
4H-Pyran-4-one, 2,3-dihydro-3,5-dihydroxy-6-methyl-	16.677	---	0.30
4-Methyl-1,4-heptadiene	17.031	6.85	---
1-Pentene, 2,3-dimethyl-	18.576	2.72	---
2-Furancarboxaldehyde, 5-(hydroxym ethyl)-	19.274	---	0.01
5-Acetyl-2-furanmethanol	20.545	1.13	---
Benzoic acid, 3-hydroxy-, methyl ester (CAS)	26.770	1.47	---
Cyclododecane	28.218	---	0.66
2,7-Naphthalenediol (CAS)	28.630	---	0.82
Phenol, 2,4-bis(1,1-dimethylethyl)-	29.288	---	0.64
1H-Imidazole, 4-methyl-5-nitro-	30.827	---	0.10
6,7-Dimethoxyquinoxaline	31.931	---	0.10
acrylic acid dodecanyl ester	33.436	---	0.69
(-)-Loliolide	35.084	---	0.48
2H-Furo[2,3-H]-1-benzopyran-2-one	36.280	---	53.64
7H-Furo[3,2-g][1]benzopyran-7-one	36.640	---	0.10
Hexadecanoic acid, methyl ester	37.705	---	0.66
Hexadecanoic acid (CAS)	38.357	---	2.30
Bergapten	40.114	---	19.27
9,12,15-Octadecatrienoic acid, methyl ester (CAS)	40.526	---	0.80
7-Oxabicyclo[4.1.0]heptane, 1,5-dimethyl-	40.709	---	1.40
Heptadecanoic acid, 16-methyl-, methyl ester	40.886	---	0.10
9,12,15-Octadecatrienoic acid, methyl ester, (Z,Z,Z)-	41.207	---	4.05
Methyl (Z)-5,11,14,17-eicosatetraenoate	41.424	---	0.10
Ferruginol	43.970	---	0.28
4,8,12,16-Tetramethylheptadecan-4-olide	44.176	---	0.11
Isosteviol methyl ester	45.899	---	0.38
Docosa-2,6,10,14,18-pentaen-22-al, 2,6,10,15,18-pentamethyl-, alltrans	51.272	---	1.07
Vitamin E	55.563	---	0.35

When the extracts of the *F. carica* leaves were compared, we can see that the solubility of the methanol extracts was much greater than that of the water extracts, because the number of components is much higher in the methanol extracts. However, when we compare the enzyme inhibition activities, the water extracts showed higher inhibition activities than the methanol extracts (Table 2). This is most likely caused by the water extracts' components. It is also interesting that almost none of these components are present in the methanol extract. Likewise, in the study conducted by Konyalıoğlu,[31] the amount of alpha-tocopherol in fig leaves was determined by HPLC and correlated with antioxidant activity. In our study, GC-MS analysis of the *F. carica* leaves shows that the antioxidant vitamin alpha-tocopherol (vitamin E) was found in the methanol extract.

In vitro antioxidant activity

In vitro radical scavenging activity

In some physiopathologic circumstances, there is excessive production of free radicals, leading to the occurrence of oxidative stress. This later is related to the appearance of many diseases including Alzheimer's diseases, cardiovascular disease, and cancer.[7,8] Natural antioxidants inhibit their activity by different mechanisms such as scavenging of reactive oxygen species, metal chelating, activation of antioxidant enzymes, and inhibition of oxidase. Therefore, it is necessary to use different methods to evaluate the antioxidant activity of extracts in plants. Previous studies have shown that the fig of *F. carica* has antioxidant activity.[32] In our study, leaf extract of *F. carica* scavenged DPPH and ABTS radicals in a concentration-dependent manner. As shown in Figure 1a and 1b, the IC_{50} of ABTS radical scavenging activity of the methanol and water extract was 559.39 μg/mL and 428.51 μg/mL, while DPPH scavenging activity was 1.45 mg/mL and 1.83 mg/mL, respectively.

The total phenolics (mg GAE/g of sample) and flavonoid (mg CE/g of sample) in the different extract of the *F. carica* leaves are exhibited in Figure 1c. *F. carica* leaf methanol extract (16.11 mg GAE/g) exhibited higher phenolic contents as compared to water extract (6.29 mg GAE/g), while the total flavonoid content was almost the same as that of methanol (11.29 mg CE/g) and water (11.06 mg CE/g) extract. The phenolic compounds in fig leaves were quantitatively determined using HPLC-DAD by

Table 2. Enzyme inhibitory activity (%) of the water and methanol extracts from *F. carica* leaves (at 2 mg/mL concentrations)

	Anticholinesterase activity		Antidiabetic activity	
Extracts	AChE	BChE	α-glucosidase	α-amylase
Methanol	53.33±3.21	57.97±5.61	64.93±1.09	67.32±2.46
Water	62.88±3.65	73.02±4.28	69.56±0.61	69.08±6.05
Reference drugs				
Galantamine hydrobromide	93.87± 0.56	89.89±0.01	---	---
Acarbose	---	---	57.56±0.52	58.40±0.63

AChE: Acetylcholinesterase, BChE: Butyrylcholinesterase

Teixeira et al.[33] We also achieved similar results using a different method in our study. In another study, by Ali et al.,[34] it was shown that antioxidant and anti-inflammatory activities of fig leaves are associated with flavonoids and phenolic compounds found in the leaves.

It is well known that the ferrous and cupric ions stimulate lipid oxidation by breaking down hydrogen and lipid peroxides to reactive free radicals via the Fenton reaction. Therefore, metal chelating agents play an important role in terms of retarding the radical degradation by reducing the concentration of transition metal.[35] According to our results, water extracts exhibited better iron chelating activity than methanol extract (Figure 1e).

In the FRAP assay, the reductants (antioxidants) present in the extract reduce a Fe^{3+}–TPTZ complex to form blue Fe^{2+}–TPTZ. The change in absorbance at 593 nm is proportional to the FRAP value of the antioxidants in the sample.[36] The results of the FRAP assay are given in Figure 1d. In this assay, the higher activity was noted for methanol extract than water extract at higher concentration, but the ferric reducing power was the same at the lower concentration.
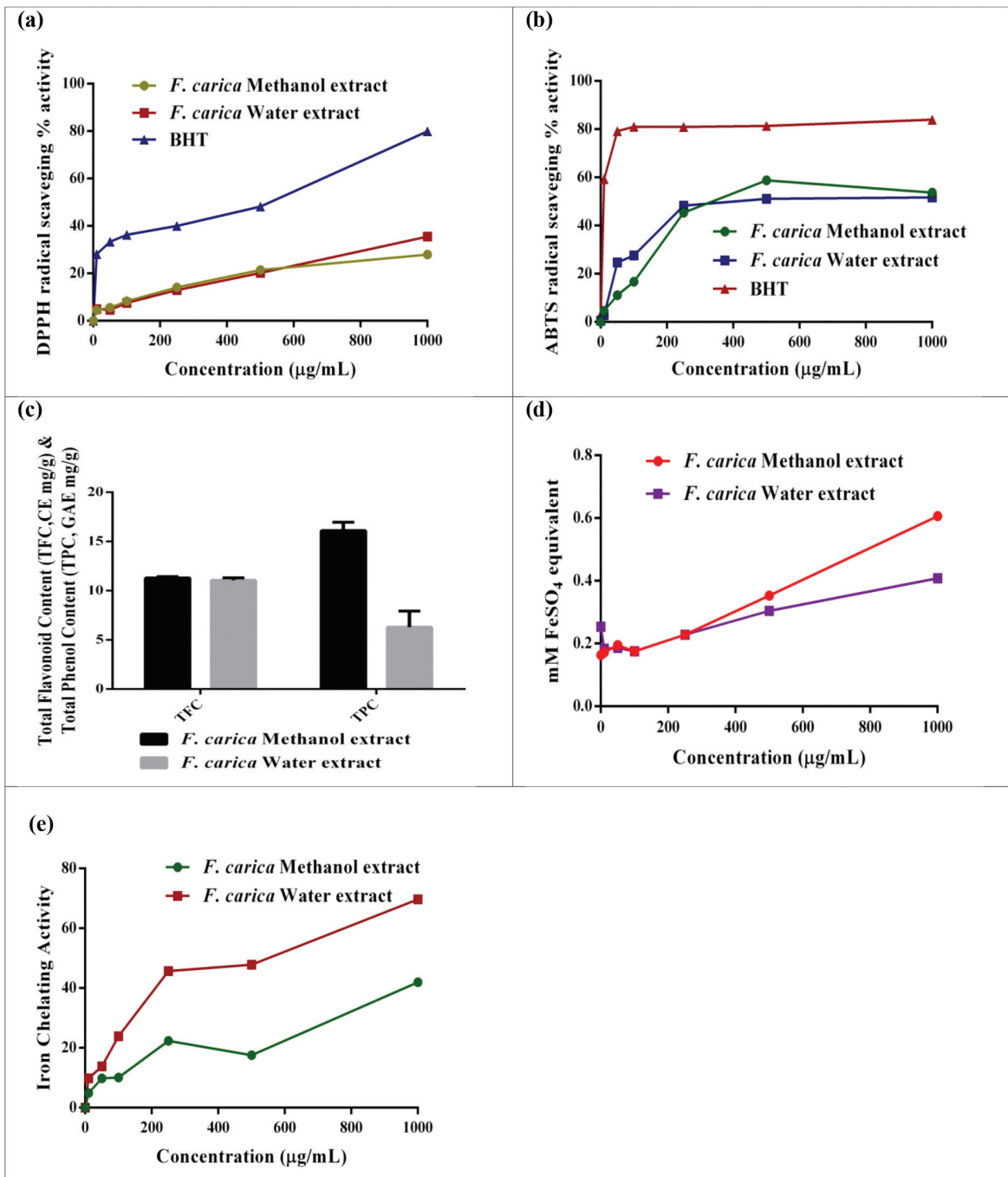

Figure 1. *In vitro* antioxidant activity of the methanol and water extracts from *F. carica* leaves; a) DPPH radical scavenging activity; b) ABTS radical scavenging activity; c) total phenol and total flavonoid contents; d) ferric reducing power as $FeSO_4$ equivalent; e) iron chelating activity.

AChE and BChE inhibition activity

The methanol and water extracts prepared from *F. carica* leaves were evaluated for their inhibitory effects against AChE and BChE, which are Alzheimer's disease-related enzymes. The water extract exhibited stronger activity and showed 63% and 73% inhibition of AChE and BChE, which was lower than the standard drug galantamine (with 93% and 90% inhibition) at the same concentration (Table 2). According to the report by Ahmad et al.[37], the *n*-butanol fractions displayed the best anti-AChE activity, while ethyl acetate soluble fraction demonstrated the best anti-BChE activity among different solvent fractions of *F. carica* fruit. In the study by Orhan et al.,[38] the *n*-hexane and acetone extracts of leaves exhibited notable inhibition activity against both AChE and BChE. However, in our study, the aqueous extract was found to be more active than the methanol in terms of these two enzyme inhibitions. This may be due to the more polar compounds present in the aqueous extract active against AChE and BChE enzyme inhibition.

In vitro α-glucosidase and α-amylase enzyme inhibition activity

It is known that α-amylase and α-glucosidase are enzymes that catalyze the hydrolysis of polysaccharides and disaccharides to monosaccharides. The inhibition of these two enzymes hinders the rapid uptake of blood glucose levels by delaying the digestion of carbohydrates.[39] The results of the inhibitory activity of the *F. carica* leaf methanol and water extracts against α-glucosidase and α-amylase enzyme are presented in Table 2. When compared to each other, the water extract (69.56%

Figure 2. Effects of the water and methanol extracts from *F. carica* on the viability of MDA-MB-231 cell line, after treatment with various concentrations (range: 0.065-1 mg/mL) for 24 h. Both extracts showed no toxicity in normal cells

and 69.08%) was found to be higher than the methanol extract (64.93% and 67.32%) in inhibiting α-glucosidase and α-amylase enzyme activity, and both extracts were found to be potential inhibitors against α-glucosidase and α-amylase compared with the standard antidiabetic drug acarbose (57.56% and 58.4%) at the same concentration (2 mg/mL). In a recent study, similar antidiabetic activities were reported for the ethyl acetate and ethanol extracts of *F. carica* fruit.[39] In another study, the ethyl acetate extract of *F. carica* leaves showed antidiabetic activity by stimulating insulin production from regenerated pancreas beta cells.[40] Similar results were reported for the water and methanol extracts of *F. carica* leaves in our study.

Antimicrobial activity

The antimicrobial activities of *F. carica* methanol and water extracts against *S. aureus*, *E. faecalis*, *P. aeruginosa*, *E. coli*, *K. pneumoniae*, and *C. albicans* were detected using the microdilution technique at the concentration range 0.156 to 2.5 mg/mL (Table 3). It has been reported that the antimicrobial activity of plant extracts was evaluated as significant with MIC value less than or equal to 0.1 mg/mL, moderate with 0.1< MIC ≤0.625 mg/mL, and weak with MIC value greater than 0.625 mg/mL.[41] According to these criteria, the methanol extract of *F. carica* showed moderate antimicrobial activities against *E. coli* (0.625 mg/mL) and *S. aureus* (0.156 mg/mL) and weak antimicrobial activity against the other bacteria and *C. albicans* (≥2.5 mg/mL). Similarly, the water extract of *F. carica* displayed moderate antimicrobial activity against *S. aureus* (0.625 mg/mL) and weak antimicrobial activity against the other bacteria and *C. albicans* (≥2.5 mg/mL).

F. carica methanol extract has been studied against various bacteria and showed moderate to strong antibacterial activity. In an *in vitro* study, Jeong et al.[42] reported that *F. carica* methanol extract had strong antibacterial activity on oral bacteria. In another study, Keskin et al.[43] investigated the antimicrobial activity of different extracts of *F. carica*. Their study reported that the MIC values of the methanol and aqueous extracts of *F. carica* against bacteria and *C. albicans* were MIC 25-400< µg/mL and MIC 200-400< µg/mL, respectively.[43] In the present study, *E. coli* and *S. aureus* were more susceptible to the methanol extract. Our results revealed that the methanol and water extracts of *F. carica* exhibited weak antimicrobial effects against other bacteria and *C. albicans*.

Cell viability

The XTT cell proliferation assay was used to evaluate the antiproliferative effects of the water and methanolic extracts of *F. carica* on MDA-MB-231 and L929 cell lines. As shown in

Table 3. Antimicrobial activity results of *F. carica* methanol and water extracts

Microorganisms and MIC values (mg/mL)

	E. coli	S. aureus	P. aeruginosa	E. faecalis	K. pneumoniae	C. albicans
Methanol	0.625	0.156	>2.5	>2.5	>2.5	2.5
Water	2.5	0.625	>2.5	>2.5	>2.5	2.5

MIC: Minimum inhibitory concantrotion

Figure 2, the methanol extract at all concentrations significantly inhibited MDA-MB-231 cell proliferation ($p<0.05$) in a dose-dependent manner ($IC_{50}=0.081$ mg/mL). On the other hand, concentration of 1 mg/mL of the water extract moderately decreased the cell viability ($IC_{50}>1$ mg/mL) ($p<0.05$). However, neither extract exhibited any significant cytotoxicity on the L929 cell line in the concentrations range (1-0.0625 mg/mL).

Our cytotoxicity results clearly indicated that the methanol extract is more toxic than the water extract of *F. carica*. This may be due to the fact that the methanol extract has richer active ingredients than the water extract, as shown in Table 1. Additionally, the anticancer effects may be associated with antioxidant features due to its polyphenolic components quantity (Figure 1). To the best of our knowledge, this is the first study of the anticancer effect of fig leaf extracts on MDA-MB-231. However, different parts of *F. carica* and different extracts of fig leaf have already been found to be cytotoxic on various cancer cells such as the stomach and cervix.[6,44]

CONCLUSION

Overall, in this study, the components and antioxidant, antimicrobial, anticancer, enzyme inhibition, and antidiabetic effects of *F. carica* leaf methanol and water extracts were investigated. Despite the several antioxidant activities of *F. carica* leaves, to the best of our knowledge there are no reports on the comparative study of extracts with different polarity as well as other antioxidant methods such as iron chelating and ferric reducing power. Our results indicated that especially the methanol extract has strong anticancer, antioxidant, and antidiabetic activities. There is a correlation between anticancer and antioxidant activity and total phenolic content. Moreover, the richer chemical content of the methanol extract may be associated with higher biological activity. Consequently, the methanolic extract of the leaf of *F. carica* may be considered a potential therapeutic agent in cancer and diabetes mellitus. However, further studies, particularly *in vivo* experiments, are needed to verify these effects.

Conflicts of interest: No conflict of interest was declared by the authors.

REFERENCES

1. Manda SC, Mukherjee KP, Saha K, Das J, Pal M, Saba PB. Hypoglycemic activity of *Ficus carica* L. leaves in streptozotocin-induced diabetic rats. Nat Prod Sci. 1997;3:38-41.

2. Alamgeer, Iman S, Asif H, Saleem M. Evaluation of antihypertensive potential of *Ficus carica* fruit. Pharm Biol. 2017;55:1047-1053.

3. Turkoglu M, Pekmezci E, Kilic S, Dundar C, Sevinc H. Effect of *Ficus carica* leaf extract on the gene expression of selected factors in HaCaT cells. J Cosmet Dermatol. 2017;16:54-58.

4. Joseph B, Raj SJ. Pharmacognostic and phytochemical properties of *Ficus carica* Linn - An overview. Int.J. PharmTech Res. 2011;3:8-12.

5. Buenrostro-Figueroa JJ, Velázquez M, Flores-Ortega O, Ascacio-Valdés JA, Huerta-Ochoa S, Aguilar CN, Prado-Barragán LA. Solid state fermentation of fig (*Ficus carica* L.) by-products using fungi to obtain phenolic compounds with antioxidant activity and qualitative evaluation of phenolics obtained. Process Biochem. 2017;62:16-23.

6. Hashemi SA, Abediankenari S, Ghasemi M, Azadbakht M, Yousefzadeh Y, Dehpour AA. The effect of fig tree latex (*Ficus carica*) on stomach cancer line. Iran Red Crescent Med J. 2011;13:272-275.

7. Park EJ, Choi KS, Kwon TK. β-Lapachone-induced reactive oxygen species (ROS) generation mediates autophagic cell death in glioma U87 MG cells. Chem Biol Interact. 2011;189:37-44.

8. Amessis-Ouchemoukh N, Ouchemoukh S, Meziant N, Idiri Y, Hernanz D, Stinco CM, Rodríguez-Pulido FJ, Heredia FJ, Madani K, Luis J. Bioactive metabolites involved in the antioxidant, anticancer and anticalpain activities of *Ficus carica* L., *Ceratonia siliqua* L. and *Quercusilex* L. extracts. Industrial Crops and Products. 2017;95:6-17.

9. Kumkrai P, Weeranantanapan O, Chudapongse N. Antioxidant, α-glucosidase inhibitory activity and sub-chronic toxicity of *Derris reticulata* extract: its antidiabetic potential. BMC Complement Altern Med. 2015;15:35.

10. Rhee IK, van de Meent M, Ingkaninan K, Verpoorte R. Screening for acetylcholinesterase inhibitors from Amaryllidaceae using silica gel thin-layer chromatography in combination with bioactivity staining. J Chromatogr A. 2001;915:217-223.

11. Tayoub G, Al-Odat M, Amer A, Aljapawe A, Ekhtiar A. Antiproliferative effects of *Pancratium maritimum* extracts on normal and cancerous cells. Iran J Med Sci. 2018;43:52-64.

12. Birjandiana E, Motameda N, Yassa N. Crude methanol extract of *Echinophora platyloba* induces apoptosis and cell cycle arrest at S-phase in human breast cancer cells. Iran J Pharm Res. 2018;17:307-316.

13. Sengupta P, Raman S, Chowdhury R, Lohitesh K, Saini H, Mukherjee S, et al. Evaluation of apoptosis and autophagy inducing potential of *Berberis aristata*, *Azadirachta indica*, and their synergistic combinations in parental and resistant human osteosarcoma cells. Front Oncol. 2017;7:296.

14. Jeong MR, Kim HY, Cha JD. Antimicrobial activity of methanol extract from *Ficus carica* leaves against oral bacteria. J Bacteriol Virol. 2009;39:97-102.

15. Wang G, Wang H, Song Y, Jia C, Wang Z, Xu H. Studies on anti-HSV effect of *Ficus carica* leaves. Zhong Yao Cai. 2004;27:754-756.

16. Jeong MR, Cha JD, Lee YE. Antibacterial activity of Korean Fig (*Ficus carica* L.) against food poisoning bacteria. Korean J Food Cookery Sci. 2005;21:84-93.

17. Rashid KI, Mahdi NM, Alwan MA, Khalid LB. Antimicrobial activity of fig (*Ficus carica* Linn.) leaf extract as compared with latex extract against selected bacteria and fungi. JUBPAS. 2014;22:1620-1626.

18. Mawa S, Husain K, Jantan I. *Ficus carica* L. (Moraceae): Phytochemistry, Traditional uses and Biological Activities. Evid Based Complement Alternat Med. 2013;2013:974256.

19. Sacchetti G, Maietti S, Muzzoli M, Scaglianti M, Manfredini S, Radice M, Bruni R. Comparative evaluation of 11 essential oils of different origin as functional antioxidants, antiradicals and antimicrobials in foods. Food Chem. 2005;91:621-632.

20. Miser Salihoglu E, Akaydin G, Caliskan Can E, Yardim Akaydin S. Evaluation of antioxidant activity of various herbal folk medicine. J Nutr Food Sci. 2013;3:1-9.

21. Re R, Pellegrini N, Proteggente A, Pannala A, Yang M, Rice-Evans C. Antioxidant activity applying an improved ABTS radical cation decolorization assay. Free Radic Biol Med. 1999;26:1231-1237.

22. Clarke G, Ting KN, Wiart C, Fry J. High correlation of 2,2-diphenyl-1-picrylhydrazyl (DPPH) radical scavenging, ferric reducing activity potential and total phenolics content indicates redundancy in use of all three assays to screen for antioxidant activity of extracts of plants from the Malaysian rainforest. Antioxidants (Basel). 2013;2:1-10.

23. Molan AL, Mahd AS. Iraqi medicinal plants: Total flavonoid contents, free-radical scavenging and bacterial beta-glucuronidase inhibition activities. IOSR-JDMS. 2014;13:72-77.

24. Chai T, Mohan M, Ong H, Wong F. Antioxidant, iron-chelating and anti-glucosidase activities of *Typha domingensis* Pers (Typhaceae). Trop J Pharm Res. 2014;13:67-72.

25. Wojdylo A, Oszmianski J, Czemerys R. Antioxidant activity and phenolic compounds in 32 selected herbs. Food Chemistry. 2007;105:940-949.

26. Yang H, Dong Y, Du H, Shi H, Peng Y, Li X. Antioxidant compounds from propolis collected in Anhui, China. Molecules. 2011;16:3444-3455.

27. Ellman GL, Courtney KD, Andres Jr. V, Featherstone RM. A new and rapid colorimetric determination of acetylcholinesterase activity. Biochemical Pharmacology. 1961;7:88-95.

28. Kumar D, Kumar H, Vedasiromoni JR, Pal BC. Bio-assay guided isolation of α-glucosidase inhibitory constituents from *Hibiscus mutabilis* leaves. Phytochem Anal. 2012;23:421-425.

29. Kumar D, Gupta N, Ghosh R, Gaonkar RH, Pal BC. α-Glucosidase and α-amylase inhibitory constituent of *Carex baccans*: Bio-assay guided isolation and quantification by validated RP-HPLC-DAD. J Funct Foods. 2013;5:211-218.

30. Eloff JN. A sensitive and quick microplate method to determine the minimal inhibitory concentration of plant extracts for bacteria. Planta Med. 1998;64:711-713.

31. Konyalıoğlu S, Sağlam H, Kıvçak B. α-Tocopherol, flavonoid, and phenol contents and antioxidant activity of *Ficus carica* leaves. J Pharm Biol. 2005;43:683-686.

32. Harzallah A, Bhouri AM, Amri Z, Soltana H, Hammami M. Phytochemical content and antioxidant activity of different fruit parts juices of three figs (*Ficus carica* L.) varieties grown in Tunisia. Ind Crops Prod. 2016;83:255-267.

33. Teixeira DM, Canelas VC, de Canto AM, Teixeira JMG, Dias CB. HPLC-DAD quantification of phenolic compounds contributing to the antioxidant activity of *Maclura pomifera*, *Ficus carica* and *Ficus elastica* extracts. J Anal Lett. 2009;42:2986-3003.

34. Ali B, Mujeeb M, Aeri V, Mir SR, Faiyazuddin M, Shakeel F. Anti-inflammatory and antioxidant activity of *Ficus carica* Linn. leaves. Nat Prod Res. 2012;26:460-465.

35. Halliwell B, Gutteridge JM. Oxygen toxicology, oxygen radicals, transition metals and disease. Biochem J. 1984;219:1-14.

36. Szeto YT, Tomlinson B, Benzie IF. Total antioxidant and ascorbic acid content of fresh fruits and vegetables: implications for dietary planning and food preservation. Br J Nutr. 2002;87:55-59.

37. Ahmad S, Bhatti FR, Khaliq FH, Younas T, Madni MA, Latif A. *In vitro* enzymatic investigation of *Ficus carica* (Fruit). Pak. J. Pharm. Sci. 2016;29:1541-1544.

38. Orhan IE, Ustün O, Sener B. Estimation of cholinesterase inhibitory and antioxidant effects of the leaf extracts of Anatolian *Ficus carica* var. domestica and their total phenol and flavonoid contents. Nat Prod Commun. 2011;6:375-378.

39. Mopuri R, Ganjayi M, Meriga B, Koorbanally NA, Islam MS. The effects of *Ficus carica* on the activity of enzymes related to metabolic syndrome. J Food Drug Anal. 2018;26:201-210.

40. Stephen Irudayaraj S, Christudas S, Antony S, Duraipandiyan V, Naif Abdullah AD, Ignacimuthu S. Protective effects of *Ficus carica* leaves on glucose and lipids levels, carbohydrate metabolism enzymes and β-cells in type 2 diabetic rats. Pharm Biol. 2017;55:1074-1081.

41. Kuete V. Potential of Cameroonian plants and derived products against microbial infections: A review. Planta Med. 2010;76:1479-1491.

42. Jeong MR, Kim HY, Cha JD. Antimicrobial activity of methanol extract from *Ficus carica* leaves against oral bacteria. J Bacteriol Virol. 2009;39:97-102.

43. Keskin D, Ceyhan Guvensen N, Zorlu Z, Ugur A. Phytochemical analysis and antimicrobial activity of different extracts of fig leaves (*Ficus carica* L.) from West Anatolia against some pathogenic microorganisms. J Pure Appl Microbiol. 2012;6:1105-1110.

44. Khodarahmi GA, Ghasemi N, Hassanzadeh F, Safaie M. Cytotoxic effects of different extracts and latex of *Ficus carica* L. on HeLa cell line. Iran J Pharm Res. 2011;10:273-277.

ORIGINAL ARTICLE

Spectrophotometric Quantification of Anti-inflammatory Drugs by Application of Chromogenic Reagents

Anti-enflamatuvar İlaçların Kromojenik Reaktifler Kullanılarak Spektrofotometrik Miktar Tayinleri

🆔 Panikumar Durga ANUMOLU*, 🆔 Sunitha GURRALA, 🆔 Archana GELLABOINA, 🆔 Divya Gayathri MANGIPUDI, 🆔 Sahitya MENKANA,
🆔 Rajesh CHAKKA

Osmania University, Gokaraju Rangaraju College of Pharmacy, Department of Pharmaceutical Analysis and Quality Assurance, Hyderabad, Telangana State, India

ABSTRACT

Objectives: Simple, specific, accurate, precise, sensitive, and cost effective spectrophotometric methods were developed and validated for quantification of the drugs lornoxicam (LOR) and mesalamine (MES) in pure form and in pharmaceutical formulations.

Materials and Methods: A Shimadzu UV-1800 double-beam UV-Visible spectrophotometer having a spectral bandwidth of 0.1 nm with wavelength accuracy ±0.1 nm with a pair of 1 cm path length matched quartz cells was used to measure the absorbance of the resulting solution.

Method I was used for the quantification of LOR, based on measurement of the absorbance of bluish green chromogen complex at 760 nm, which is formed by the reaction of LOR with ferric chloride and potassium ferricyanide (redox technique). Method II was used for the quantification of MES, based on measurement of the absorbance of yellow chromogen at 400 nm, which is formed by the condensation reaction of the primary amino group of MES with salicylaldehyde reagent (SA) (Schiff base formation).

Results: Both methods obeyed Beer's law in the concentration range of 0.5-4.5 μg/mL and 0.2-1.7 μg/mL with good correlation coefficients of 0.9974 and 0.998 for methods I and II, respectively.

Conclusion: The developed method is simple, sensitive, and specific, which was validated statistically as per ICH guidelines, and can be used in the routine analysis of LOR and MES in pharmaceutical dosage forms.

Key words: Ferric chloride, lornoxicam, mesalamine, salicylaldehyde reagent, visible spectrophotometry

ÖZ

Amaç: Lornoksikam (LOR) ve mesalaminin (MES) hem saf formda hemde farmasötik formülasyonlarda tayini için basit, spesifik, doğru, duyarlı ve düşük maliyetli spektrofotometrik yöntemler, geliştirmek ve valide etmektir.

Gereç ve Yöntemler: Elde edilen çözeltilerin absorbansları Shimadzu UV-1800 çift ışınlı spektrofotometrede 0,1 nm spektral bant genişliği ve ±0,1 nm hassasiyetle 1 cm'lik kuvars küvetler kullanılarak ölçüldü.

Bulgular: Metot I, LOR'nin demir III klorür ve potasyum ferrisiyanür (redoks tekniği) ile reaksiyonu sonucu oluşan mavimsi yeşil renkli kromojen kompleksinin absorbansının 760 nm'de ölçümüne dayanan yöntemdir. Metot II, MES'nin primer amino grubunun salisilaldehit reaktifi (SA) (Schiff baz oluşumu) ile kondensasyon reaksiyonundan oluşan sarı renkli kromojenin absorbansının 400 nm'de ölçümüne dayanan yöntemdir. Metot I ve II için; her iki yöntemde de, sırasıyla 0,5-4,5 μg/mL ve 0,2-1,7 μg/mL'lik konsantrasyon aralıklarında, Beer yasasına sırasıyla 0,9974 ve 0,9980'lık korelasyon katsayıları ile iyi bir uygunluk göstermişlerdir.

Sonuç: Geliştirilen yöntemler; LOR ve MES'nin farmasötik dozaj formlarının rutin analizinde kullanılabilecek ve ICH yönergelerine göre valide edilmiş basit, hassas ve spesifik yöntemlerdir.

Anahtar kelimeler: Demir III klorür, lornoksikam, mesalamin, salisilaldehit reaktifi, görünür spektrofotometri

INTRODUCTION

Lornoxicam (LOR) has the IUPAC name 6-chloro-4-hydroxy-2-methyl-N-2-pyridinyl-2H-thieno [2, 3-e]-1,2-thiazine-3-carboximide 1,1-dioxide. It belongs to the class of oxicams and it is a nonsteroidal anti-inflammatory drug with analgesic properties (Figure 1).[1] Mesalamine (MES) has the IUPAC name 5-amino-2-hydroxy benzoic acid (Figure 2). It is an anti-inflammatory drug used to treat inflammation of the digestive tract (Crohn's disease) and mild to moderate ulcerative colitis.

A literature survey revealed that numerous analytical methods have been published for the analysis of both LOR and MES by ultraviolet (UV) spectrophotometric and high performance liquid chromatography (HPLC) methods.[2-18] Most of the reported procedures are not simple for routine analysis and require expensive or sophisticated instruments. Hence, it is always required to develop simple, fast, and inexpensive analytical methods that can be readily adopted for routine analysis at a relatively low cost for the different requirements of analytical problems.

Visible spectrophotometry, because of its simplicity and cost effectiveness, sensitivity and selectivity, fair accuracy, precision, and easy access in most quality control laboratories, has remained competitive in the area of chromatographic techniques for pharmaceutical analysis. Visible spectrophotometric methods based on diverse reactions have been reported for the determination of LOR and MES in pharmaceutical dosage forms.[19,20] However, most of the reported visible spectrophotometric methods suffer from disadvantages like narrow range of determination, poor sensitivity, and temperature and pH maintenance. In the present work, two simple and sensitive extraction-free spectrophotometric methods based on the redox reaction and

Figure 1. Structure of lornoxicam

Figure 2. Structure of mesalamine

condensation reaction are proposed for the determination of LOR and MES in bulk drug and pharmaceutical dosage forms.

MATERIALS AND METHODS

Preparation of reagents and solutions

Ferric chloride solution (3% w/v) was prepared by dissolving 3 g in 100 mL of 0.1 N hydrochloric acid. Potassium ferricyanide (0.3% w/v) was prepared by dissolving 300 mg in 100 mL of distilled water. Salicylaldehyde reagent (5% v/v) was prepared by diluting 0.5 mL to 10 mL using ethanol.

LOR stock solution was prepared by weighing 10.0 mg of LOR and dissolving it in a few milliliters of 0.01 M NaOH and the volume was made up to 100.0 mL with 0.01 M NaOH to acquire 100 µg/mL solution. Further dilutions were made from stock solution to obtain the required concentration for method I.

MES stock solution was prepared by weighing 10.0 mg of MES and dissolving it in a few milliliters of 0.1 M NaOH and the volume was made up to 100.0 mL with 0.1 M NaOH to acquire 100 µg/mL solution. Further dilutions were made from stock solution to obtain the required concentration for method II.

Preparation of sample solutions

Redox-complexation method

Aliquots of standard drug solution of LOR ranging from 0.05 to 0.45 mL were taken into a series of 10.0-mL volumetric flasks. Then 0.5 mL of 3% w/v ferric chloride, 0.5 mL of 0.3% w/v potassium ferricyanide, and 0.5 mL of 1 N hydrochloric acid were added. The volume was made up to the mark with water to prepare a series of standard solutions containing 0.5-4.5 µg/mL. The solutions were kept aside for 30 min and later the absorbance was measured at 760 nm against the corresponding reagent blank.

Condensation method

Aliquots of standard drug solution of MES ranging from 0.02 to 0.17 mL were prepared in a series of 10.0 mL volumetric flasks. To this 1 mL of 5% v/v salicylaldehyde was added. The volume was then made up to the mark with ethanol to prepare a series of standard solutions containing 0.2-1.7 µg/mL. The complete color development was attained after 45 min. Then the absorbance of the colored chromogen was measured at 400 nm against the corresponding reagent blank.

In both methods (I and II), calibration curves were prepared and the linearity in pure solution was checked over concentration of 0.5-4.5 µg/mL for LOR and 0.2-1.7 µg/mL for MES. The relative standard deviation (RSD) and correlation coefficient of the standard curve were calculated.

Assay of pharmaceutical dosage form

Method I

The contents of 20 tablets (Lornoxi 4 and 8; Lorsaid 4 and 8) were weighed and powdered. The equivalent quantity to 4 mg of active ingredient was dissolved in 0.01 N NaOH and the volume was made up to 10.0 mL and was filtered using Whatman filter paper. Appropriate dilutions of the prepared

solution were made to prepare its working solution and the procedures under linearity were followed. The absorbance of the colored chromogen was measured at 760 nm against the corresponding reagent blank.

Method II

The contents of 20 tablets (Mesacol 400 mg) were weighed and powdered. The equivalent quantity to 10 mg of active ingredient was dissolved in 0.1 N NaOH and the volume was made up to 10.0 mL and was filtered using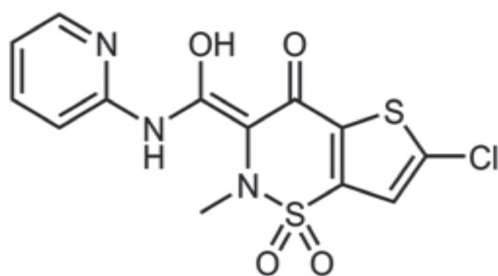 Whatman filter paper. Appropriate dilutions o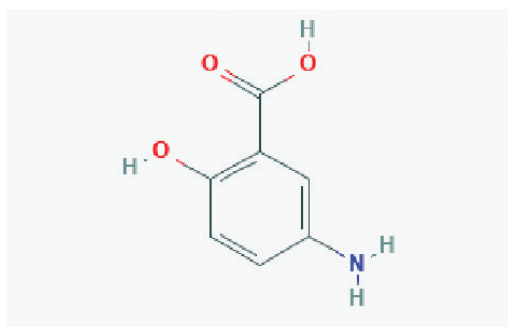f the prepared solution were made to prepare its working solution and the procedures under linearity were followed. The absorbance of the colored chromogen was measured at 400 nm against the corresponding reagent blank.

RESULTS AND DISCUSSION

To attain a sensitive and specific photometric method for quantification of LOR and MES, distinct experimental conditions were investigated such as concentration of chromogenic agent, strength of the medium, concentration of oxidizing agent, temperature conditions, and time for stability of the chromogenic complex.

Redox-complexation method

LOR exhibits a reducing property due to the presence of functional moieties vulnerable to oxidation selectively with oxidizing agents such as ferric chloride. Under controlled experimental conditions when treated with a known excess amount of oxidant, LOR undergoes oxidation, giving products of oxidation (inclusive of reduced form of oxidant Fe(II) from Fe(III) besides unreacted oxidant. It is possible to estimate the drug content colorimetrically, which is equivalent to either reduced oxidant or reduced form of oxidant formed. The reduced form of Fe(III), i.e. Fe(II), has a tendency to give a blue green complex on treatment with potassium ferricyanide. The absorbance of the bluish green complex formed was measured at 760 nm (Scheme 1).

Condensation method

MES undergoes a condensation reaction with salicylaldehyde giving a yellow Schiff base product. MES contains a primary amine group, which reacts with an active carbonyl group in salicylaldehyde forming Schiff bases [compounds containing an imine or azomethine group (-RCH=N-)] of stable yellow exhibiting absorption maxima at 400 nm and the reaction proceeds in ethanol (Scheme 2).

Method validation

Validation of the analytical method was carried out according to International Conference on Harmonisation (ICH) recommendations [ICH, Q1A (R2), 2005].[21]

Linearity and range

The linearity of an analytical method is its ability to elicit test results that are directly or by a well-defined mathematical transformation proportional to the concentration of analyte in samples within a given range. The calibration graph showed that a linear response was obtained over the range of concentrations used in the assay procedure. The linearity ranges are 0.5-4.5 μg/mL and 0.2-1.7 μg/mL for methods I and II respectively (Figures 3 and 4). The correlation coefficients of drugs in methods I and II were 0.9974 and 0.998, respectively. These data clearly demonstrate that the developed methods have adequate sensitivity to the concentration of the analytes in the sample. The optical characteristics of both methods such as absorption maxima, Beer's law limits, molar absorptivity, Sandell's sensitivity, and regression equation are reported in Table 1.

Precision

Precision of the method was determined by intraday and interday precision as per ICH guidelines. Intraday precision was investigated by preparing six replicate sample solutions on the same day. Interday precision was assessed by analyzing newly prepared sample solutions in triplicate over three consecutive
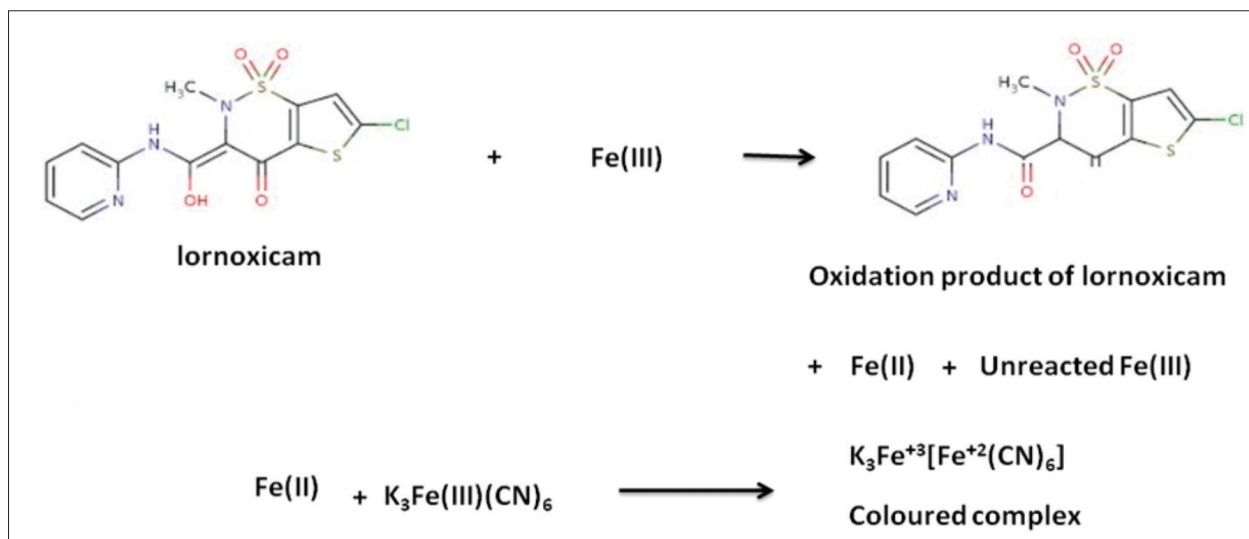
Scheme 1. Reaction mechanism of LOR with potassium ferricyanide in the presence of ferric chloride

LOR: Lornoxicam

days. The obtained RSD % was within the acceptable range. The results of this study are summarized in Table 2.

Accuracy

Accuracy of the methods was assured by applying the standard addition technique where good percentage recoveries were obtained, confirming the accuracy of the proposed methods. The average percentage recovery and RSD % were statistically calculated. The % recovery values for both the methods are shown in Table 3.
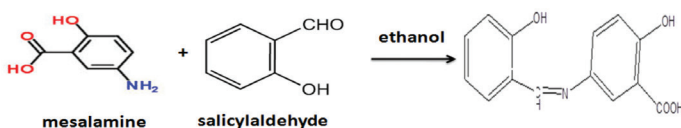
Scheme 2. Reaction mechanism of MES with salicylaldehyde

MES: Mesalamine
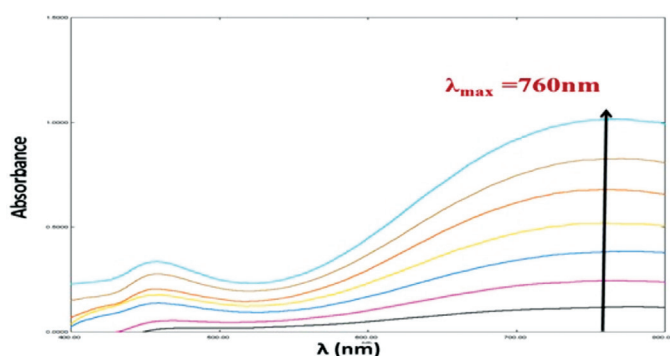
Figure 3. Absorption spectra of lornoxicam with potassium ferricyanide and ferric chloride
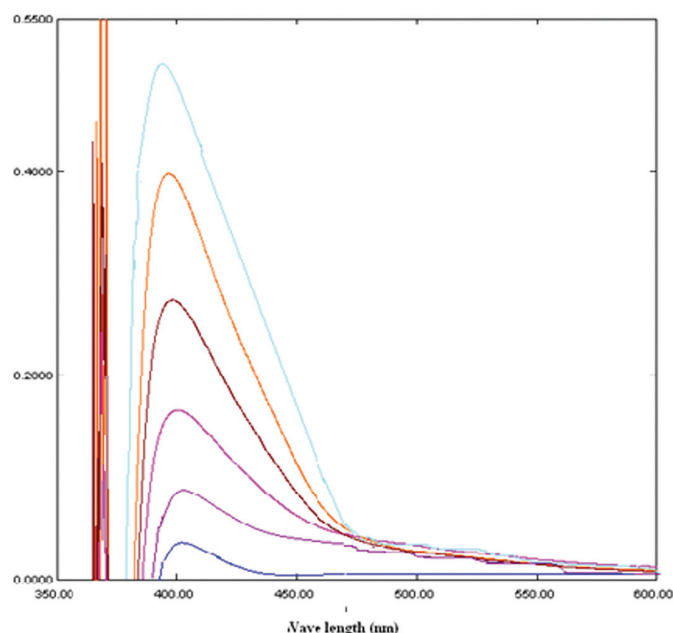
Figure 4. Absorption spectra of mesalamine with salicylaldehyde

Limit of detection (LOD) and limit of quantification (LOQ)

The LOD and LOQ for methods I and II by the proposed method were determined using calibration standards. LOD and LOQ were calculated by using 3.3 σ/s and 10 σ/s, respectively, where s is the slope of the calibration curve and σ is the standard deviation of the y intercept of the regression equation. The LOD and LOQ were 0.0094 µg/mL and 0.0154 µg/mL for method I and 0.0129 µg/mL and 0.0392 µg/mL for method II, respectively.

Application of the proposed method (analysis of commercially available formulations)

The proposed method was successfully applied to the analysis of both the drugs in their respective pharmaceutical formulations. The results obtained were in good agreement with the label claim as concluded from the satisfactory values of % assay and % RSD shown in Table 4. The assay values were compared with

Table 1. Optical parameters for methods I and II

Parameters	Method I	Method II
Absorption wavelength (nm)	760	400
Beer's law range (µg/mL)	0.5-4.5	0.2-1.7
Molar absorptivity (Lcm/mol)	1.1×10^4	1.2×10^4
Sandell's sensitivity (µg/cm^2)	0.0038	0.0048
Limit of detection (µg/mL)	0.0094	0.0129
Limit of quantification (µg/mL)	0.0154	0.0392
Correlation coefficient (r^2)	0.9974	0.9984
Slope (m)	0.2343	0.306
Intercept (c)	0.0083	0.011
Regression equation	Y=0.2343x+0.0083	Y=0.306x-0.011

Table 2. Precision for methods I and II

	Intraday precision		Interday precision	
Concentration (µg/mL)	Concentration estimated (µg/mL) AM ± SD*	% RSD[a]	Concentration estimated (ng/mL) AM ± SD*	% RSD[a]
Precision values for method I				
0.5	0.524±0.002	0.381	0.512±0.0012	0.234
2.5	2.428±0.004	0.164	2.524±0.0045	0.178
4.5	4.621±0.001	0.021	4.545±0.0026	0.057
Precision values for method II				
0.5	0.501±0.004	0.279	0.505±0.0012	0.237
1.1	1.14±0.0028	0.245	1.12±0.0032	0.285
1.7	1.73±0.0056	0.323	1.72±0.0026	0.151

*Mean value of 6 determinations. Relative standard deviation (%).
RSD: Relative standard deviation, SD: Standard deviation

Table 3. Accuracy studies for methods I and II

Brand name	Recovery level (%)	Amount taken (mg)	Amount of drug spiked (mg)	Theoretical amount of drug (mg)	Amount recovered mg ± SD*	% Recovery	% RSD
Accuracy studies for method I							
Lornoxi 4	80	2	1.6	3.6	3.69±0.016	102.5	0.433
	100	2	2.0	4.0	3.82±0.024	95.0	0.628
	120	2	2.4	4.4	4.34±0.074	98.6	1.705
Accuracy studies for method II							
Mesacol -400	80	5	4	9	8.82±0.015	98	0.17
	100	5	5	10	10.03±0.022	100	0.21
	120	5	6	11	11±0.089	100	0.80

RSD: Relative standard deviation, SD: Standard deviation

Table 4. Assay of methods I and II

Formulation	Label claim (mg)	Amount found (mg) AM ± SD*			% Assay	% RSD
		Proposed method	Reference method[6,15]	T-test value		
Lornoxi 4	4	3.92±0.015	4.02±0.008	0.882	99	0.377
Lornoxi 8	8	7.99±0.062	7.95±0.011	0.21	99.8	0.775
Lorsaid 4	4	3.96±0.045	3.93±0.012	0.09	99	0.303
Lorsaid 8	8	7.97±0.012	8.04±0.017	0.5	99.8	0.150
Mesacol	400 mg	399.4±0.6	399.5±0.017	0.01	99.8	0.15

*Mean of three determinations.
RSD: Relative standard deviation, SD: Standard deviation

reference method values using Student's t-test. The calculated values were less than the tabulated t-value (t=2.571 at p≤0.05), which revealed that there is no significant difference between the proposed method and the reference method (similarity of the methods).

CONCLUSION

The contemplated method was simple, sensitive, accurate, and precise for the quantification of LOR and MES in pharmaceutical dosage forms. The assay values were in good concord with their respective dosage form. The developed spectrophotometric methods were found to be enhanced because of their specificity, sensitivity, no extraction procedures, time saving nature, cost effectiveness, and involving very simple procedures. Besides the simplicity and sensitivity of the procedures, the relative inexpensive apparatus and cost effective reagents demonstrate their advantageous characteristics when compared to HPLC techniques. These advantages indicate that the contemplated method can be routinely used in quality control for analysis of LOR and MES in pharmaceutical dosage forms.

ACKNOWLEDGEMENTS

REFERENCES

1.   Maryadale J.O., NF. USP. 2006;679-680.

2.   Aher KB, Bhavar GB, Joshi HP. Rapid RP-HPLC method for quantitative determination of lornoxicam in bulk and pharmaceutical formulations. Int J Chem Tech Res. 2011;3:1220-1224.

3.   Bendale AR, Makwana JJ, Narkhede SP, Narkhede SB, Jadhav AG, Vidyasagar G. Analytical method development and validation protocol for Lornoxicam in tablet dosage form. JOCPR. 2011;3:258-263.

4.   Bhupendra S, Geetanjali S, Devendra NNS, Saumendu DR, Nishant G. Estimation of lornoxicam in tablet dosage form by uv spectrophotometricmethod. Int J Pharm Sci Res. 2011;2:102-106.

5.   Darak VR, Karadi AB, Appalraju A, Appalraju S. Development and Validation of Visible Spectrophotometric methods for the Estimation of Mesalamine in Pharmaceutical Dosage Forms. Der Pharma Chemica. 2011;3:342-346.

6.   Gatkal SH, Mhatre PR, Chopade VV, Chaudhari. Development and validation of stability indicating HPLC assay method for determination of mesalamine in bulk drug and tablet formulation. Int. J Pharm Sci Rev Res. 2013;4:401-406.

7.   Gurupadayya BM, Navya Sloka S, Aswani Kumar Ch. J. Pharm. Res. 2011;4:39-41.

8.   Hanumantha Rao K, Lakshmana Rao A, Chandra Sekhar KB. Validated rp-hplc method for the estimation of mesalamine in bulk and tablet dosage form. IJRPC 2013;3:472-476.

9. Moharana AK, Banerjee M, Panda S, Muduli JN. Development and validation of uv spectrophotometric method for the determination of mesalamine in bulk and tablet formulation. Int J Pharm Sci. 2011;3:19-21.

10. Patel KM, Patel CN, Panigrahi B, Parikh AS, Patel HN. Development and Validation of Spectrophotometric Methods for the Estimation of Mesalamine in Tablet Dosage Forms. Young J Pharm. 2010;2:284-288.

11. Purushotham Reddy M, Prabhavathi K, Rami Reddy N, Raveendra Reddy P. Two simple spectrophotometric methods for the estimation of mesalamine in bulk sample and its pharmaceutical dosage forms. Global J. Pharmacology. 2011;5:101-105.

12. Rakesh KS, Pankaj SP, Pragya G. Int J Pharm Sci Res. 2010;1:44-49.

13. Sivarami Reddy K, Ramachandra B, Naidu NVS. Int. J. Scientific Eng Res. 2014;2:52-56.

14. Narala SR, Saraswathi K. Development and validation of spectrophotometric methods for the estimation of mesalamine in pharmaceutical preparations. J Chem Pharm Res. 2011;3:784-787.

15. Trivedi Rakshit K, Patel Mukesh C, Kharkar Amit. E-J. Chemistry. 2010;8:131-148.

16. Venumadhav E, NeehaT, Bhargavi P, Amreen N, Swetha A, Devala Rao G. Int J Appli Bio Pharm Tech. 2011;2:23-26.

17. Venumadhav E, Neeha T, Bhargav P, Amreen N, Swetha A, Devala Rao G. Int J Pharm Bio Sci. 2010;1:491-494.

18. Moharana AK, Banerjee M, Panda S, Muduli JN., Development and validation of UV spectrophotometric method for the determination of mesalamine in bulk and tablet formulation. Asian J Pharm Clinical Res. 2011;4:71-73.

19. Balram S, Firoz K, Anil B, Sanjay S. Pharmacophore. 2011;2:239-243.

20. Ramya Krishna N, Ramanjaneyulu KV, Deepti M, Kiranmayi A, Sudhakar Babu MS, Venkateswara Rao P, Pramod N. Int J Pharm Bio Archives. 2012;3:1012-1016.

21. ICH, International Conference on Harmonization. Validation of Analytical Procedures: text and methodology Q2 (R1). Harmonized Tripartite Guideline. 2005.

ORIGINAL ARTICLE

Considering the Effect of *Rosa damascena* Mill. Essential Oil on Oxidative Stress and *COX-2* Gene Expression in the Liver of Septic Rats

Rosa damascena Mill. Uçucu Yağının Sepsis Oluşturulmuş Sıçanların Karaciğerinde Oksidatif Stres ve *COX-2* Gen Ekspresyonu Üzerine Etkilerinin Değerlendirilmesi

Abolfazl DADKHAH[1]*, Faezeh FATEMI[2], Mohammad Reza Mohammadi MALAYERI[3], Mohammad Hassan Karvin ASHTIYANI[4], Sakineh Kazemi NOUREINI[4], Azadeh RASOOLI[5]

[1]Islamic Azad University, Qom Branch, Faculty of Medicine, Department of Medicine, Qom, Iran
[2]Nuclear Science and Technology Research Institute, Materials and Nuclear Fuel Research School, Tehran, Iran
[3]Islamic Azad University, Garmsar Branch, Faculty of Veterinary Medicine, Department of Pathobiology, Garmsar, Iran
[4]Hakim Sabzevari University, Faculty of Science, Department of Biology, Sabzevar, Iran
[5]Payame-e-Noor University, Faculty of Sciences, Department of Biochemistry, Tehran, Iran

ABSTRACT

Objectives: Sepsis is a clinical illness with a high rate of mortality all over the world. Oxidative stress is considered the main phenomenon that occurs in sepsis. *Rosa damascena* Mill. is an ancient herbal plant with high pharmacological activities.

Materials and Methods: Cecal ligation and puncture (CLP) as a standard model was used to induce sepsis in rats. Male adult rats were randomly divided into 5 groups. Different doses of *R. damascena* essential oil (50 and 100 mg/kg.bw) were gavaged orally for 14 days and on day 15 CLP was performed. After 24 h, blood samples and liver tissues were removed in order to measure oxidative stress [myeloperoxidase (MPO), malondialdehyde (MDA), glutathione (GSH), glutathione-S-transferase, and ferric reducing ability of plasma (FRAP)] and biochemical parameters [alkaline phosphatase (ALP), aspartate transaminase (AST), alanine transaminase (ALT), and bilirubin] together with plasma prostaglandin E_2 (PGE_2) and COX-2 expression.

Results: The essential oil was capable of modulating all of the oxidative stress, antioxidant, and anti-inflammatory parameters induced by CLP as characterized by elevations in MPO and MDA levels as well as increases in AST and ALT concentrations concomitant with PGE_2 and COX-2 increments. The antioxidant defense system such as GSH and FRAP was also increased in the essential oil treated groups.

Conclusion: Our results showed that the essential oil has antioxidative and hepatoprotective activities through reducing the oxidative injury in sepsis caused by CLP.

Key words: Sepsis, *Rosa damascena Mill.*, oxidative stress, CLP, hepatoprotective activity

ÖZ

Amaç: Sepsis, tüm dünyada yüksek ölüm oranına sahip klinik bir hastalıktır. Oksidatif stres sepsiste ortaya çıkan önemli bir olgu olarak kabul edilir. *Rosa damascena* Mill., farmakolojik aktiviteleri yüksek olan eski bir bitkidir.

Gereç ve Yöntemler: Standart bir model olarak çekal ligasyon ve ponksiyon (CLP), sıçanlarda sepsis oluşturmak için kullanılmıştır. Erkek yetişkin sıçanlar rastgele 5 gruba ayrılmıştır. *R. damascena* uçucu yağları (50 ve 100 mg/kg) 14 gün boyunca oral yolla verilmiş ve 15. günde CLP uygulanmıştır. Yirmi dört saat sonra, plazma plazma prostaglandin E_2 (PGE_2) ve COX-2 ekspresyonu ile birlikte oksidatif stres (MPO, MDA, GSH, GST ve FRAP) ve biyokimyasal parametreleri [alkalen fosfataz, aspartate transaminase (AST), alanin transaminaz (ALT) ve bilirubin] ölçmek için kan örnekleri ve karaciğer dokuları çıkarılmıştır.

Bulgular: Uçucu yağ, MPO ve MDA seviyelerinde yükselme, PGE$_2$ ve COX-2 artışı, AST ve ALT konsantrasyonlarındaki artışla sonuçlanan CLP-nedenli tüm oksidatif stres, antioksidan ve anti-enflamatuvar parametreleri düzenlemiştir. GSH ve FRAP gibi antioksidan savunma sistemi de uçucu yağ verilen gruplarda artmıştır.

Sonuç: Elde ettiğimiz sonuçlar, uçucu yağın, CLP'nin neden olduğu sepsiste oksidatif hasarı azaltarak antioksidan ve hepatoprotektif aktivitelere sahip olduğunu gösterdi.

Anahtar kelimeler: Sepsis, *Rosa damascena*, oksidatif stres, CLP, hepatoprotektif aktivite

INTRODUCTION

Sepsis is an ancient and serious clinical disease with high mortality in critically ill patients.[1,2] Although all parasites and microorganisms have the potential to cause sepsis, the best known and most effective causes of pathogenesis of sepsis are Gram-negative and Gram-positive bacteria and fungi.[3] Sepsis is the result of assaulting microbial pathogens or their products, like toxins in the bloodstream, expressed by the systemic inflammatory response to infection.[4,5]

In the initial stages of sepsis, a pathogenic microorganism stimulates the body to produce large amounts of chemokine and cytokines.[6] The imbalance between pro-inflammatory and anti-inflammatory parameters is responsible for the susceptibility to and outcome of sepsis.[7] By increasing oxidative stress and reactive oxygen species (ROS), the body's antioxidant system is impaired, leading to effects on the cells and mitochondria and finally causing organ dysfunction.[8]

To investigate the pathogenesis of sepsis and its mechanisms, three methods are usually utilized: 1) injection and using lipopolysaccharides (LPS) and other exogenous toxin like zymogens; 2) applying different fatal and vivid pathogens; 3) elimination or changing the endogenous protective barrier, like cecal ligation and puncture (CLP) and colon ascendens stent peritonitis.[9] All of them try to simulate pathophysiological changes, which are very similar to septic shock.[10] Among them, CLP is the most accepted method to imitate human sepsis; it is considered a gold standard model. For the first time, Chaudhry in 1970 developed CLP among others.[11] It is surgery involving cecum ligation and piercing, which can cause penetration microbial and pathogen factors, and finally causing sepsis.[12]

Due the increase of oxidant and inflammatory elements, a substitute for chemical drugs with high curative features and less side effects is noteworthy.[13] The Damask rose (*Rosa damascena* Mill.) is an ancient herbal drug used for treatment of illnesses in the past.[14] It belongs to the family Rosaceae, is considered an ornamental plant, and is known as the king of flowers.[15] Nowadays, this plant is cultivated all over the world for its products, essential oil and rosewater.[16]

On the other hand, previous research has confirmed some pharmacological properties such as antioxidant, anti-HIV, and antibacterial activities.[17] Different features of *R. damascena* were proposed in the distant past to cure bleeding and digestive problems and to treat abdominal pain in traditional medicine.[16] Many studies have proved the antioxidant activity and other therapeutic effect of extract or essential oils of *R. damascena*.[18,19] It was reported that hydroalcoholic extract of *R. damascena* has analgesic and anti-inflammatory effects by the formalin-induced method.[13] The *R. damascena* essential oils as a natural antioxidant showed preventive effects against oxidative damage.[20] However, there is no research on the therapeutic effect of *R. damascena* on hepatic injuries especially induced by sepsis. Thus, the present study was performed to evaluate the hepatoprotective and antioxidant activities of *R. damascena* essential oils against oxidative stress caused by CLP in the rat.

MATERIALS AND METHODS

Essential oil extraction

R. damascena essential oils were purchased from Barij Essence Pharmaceutical Co, Kashan Iran. A voucher specimen (Batch No: 714043, sample Serial No: AE932009) has been deposited at the Barij Essence company.

GC and GC-mass analysis of Rosa damascena essential oils

The *R. damascena* essential oils were qualitatively and quantitatively determined by GC of a Thermo Finnegan Trace GC (Thermo Electron, Waltham, MA, USA), consisting of an AI/AS 3000 auto sampler equipped with a Thermo Finnegan Auto Mass quadruple mass spectrometer (Thermo Electron).

The GC analyzer was equipped with a TR5 fused silica column (30 m, 0.025 mm, 0.025 m coating thick). The analytical conditions were as follows: the column temperature was initiated at 50°C for 1 min, then planned to rise to 280°C at a rate of 10°C/min held by isothermal process. Helium was used as the carrier gas at the rate of 1.0 mL/min. Identification of the constituent was based on the comparison of GC retention with those stored in the Wiley mass spectra library.

Free radical scavenging activity (DPPH assay)

The radical scavenging activity of *R. damascena* essential oils was determined by DPPH assay. The absorbance of DPPH was read against the blank at 517 nm. The inhibitory effect of the essential oils in percent (I %) was calculated by the following equation:

I %=(Ablank-Asample/Ablank)×100

β-Carotene/linoleic acid bleaching assay

To determine the antioxidant activity of *R. damascena* essential oils, the β-carotene/linoleic acid bleaching assay was performed. The oxidation of the β-carotene was monitored spectrophotometrically by measuring absorbance at 470 nm over 60 min. The antioxidant activity of the essential oils was expressed as inhibition percentage with reference to the control after 60 min of incubation using the following equation:

AA=100(DRC-DRS)/DRC

where AA=antioxidant activity; DRC=degradation rate of control=[ln(a/b)/60]; DRS=degradation rate of sample=[ln(a/b)/60]; a=absorbance at time 0; b=absorbance at 60 min.

Treatment of animals

Two-month-old male Wistar rats (200-250 g) were purchased from the animal breeding house of the Pasteur Institute, and were kept in the animal facility at the Qom Azad University animal room. The animals were acclimatized for 2 weeks in standard conditions and kept in a photoperiod of 12 h light/12 h dark at 20-25°C. All the rats were fed a laboratory pellet diet and drinking water *ad libitum*.

The animals were divided into 5 groups (n=10): 1) Negative control (C): in the negative control group, dimethyl sulfoxide (DMSO), as solvent of essential oils, was orally administrated to the rats for 14 days following laparotomy surgery.

2) CLP group: as the control group, the rats received DMSO for 14 days following CLP surgery.

3 & 4) CLP+*R. damascena* essential oils (50 and 100 mg/kg bw): the rats received orally essential oil of *R. damascena* once a day for 14 days dissolved in DMSO following CLP surgery.

5) CLP+IND (2 mg/kg bw): the rats were treated with indomethacin once a day for 14 days along with CLP.

Sepsis induction

Sepsis was induced by CLP. The rats were anesthetized by i.p. injection of ketamine and xylazine. Under sterile conditions, the cecum was exposed through a 1- to 2-cm incision in the lower left abdomen, ligated on the ileocecal valve with 3-0 silk, and then was punctured twice with a 20-gauge needle. The cecum was replaced in the peritoneum and the abdomen was closed with surgical staples. The rats were injected with 5 mL of saline s.c. for fluid resuscitation and were placed on a warming pad until they recovered from anesthesia.

Preparation of tissue homogenate and plasma

At 24 h after CLP induction, the rats in all groups were anesthetized with diethyl ether. Blood samples were withdrawn by heparinized syringe, followed by centrifugation at 3000 × *g* for 10 min. Plasma samples were collected and maintained at -20°C for biochemical purposes. In addition, the liver tissues were removed and homogenized completely with buffer phosphate in an ice bath to evaluate oxidative stress biomarkers. A portion of that was also fixed in 10% formalin, for histopathological studies.

Determination of the oxidative stress and antioxidant parameters in the liver homogenate

Glutathione (GSH) estimation

The level of reduced GSH, as an antioxidant factor, was measured in liver homogenate as described by Sedlak and Lindsay.[21] The GSH level in samples was calculated by plotting a standard curve of absorbance against different concentration of GSH standard solution.

Measurement of tissue myeloperoxidase (MPO) activity

The extent of neutrophil accumulation in the liver was evaluated by assaying MPO activity. MPO activity in the liver was measured by the procedure reported by Hillegass et al.[22]

Measurement of tissue malondialdehyde (MDA)

To investigate the rate of lipid peroxidation, the concentration of MDA was measured spectrophotometrically according the method of Buege and Aust.[23]

Measurement of tissue glutathione-S-transferase (GST) activity

GST activity was measured according to Habig et al.[24] by investigating the conjugation of 1-chloro-2, 4-dinitrobenzene with reduced glutathione. The conjugation was done by an increase in the absorbance at 340 nm.

Ferric reducing ability of plasma (FRAP)

The total antioxidant activity of plasma was measured by FRAP assay based on the Benzie method.[25] According to this, at low pH, ferric tripyridyltriazine complex (Fe_3-TPTZ) is reduced to the ferrous (Fe_2) form. In this reaction, an intense blue color is created with absorption at 593 nm.

Determination of prostaglandin E_2 (PGE$_2$) concentration

PGE_2 was assessed by ELISA kit (BioAssay System) according to the kit's instructions.

Determination of COX-2 gene expression using quantitative real time-polymerase chain reaction (RT-PCR)

Total RNA extracted from the rat livers, by RNA total kit (BioBasic Inc, Canada), was surveyed quantifiably by Nano Drop 2000. Then to synthetic cDNA, each sample was reverse transcribed into compulsory DNA (cDNA), using a PrimeScript™ RT reg Kit (TaKaRa and oligo dt primers). The cDNA was stored at -20°C until use.

In order to use specific primers of COX-2, Gene Runner software version 3.05 and primer 3 servers were applied.

Expression of COX-2 genes was investigated by real-time PCR system (Rotor-Gene Q-QIAGEN). The RT-PCR analyses were done using SYBER green real-time PCR Master Mix. The reaction compositions were Taq polymerase, dNTP, $MgCl_2$, SYBER green I dye, 0.2 μL of primers, 0.5 μL of cDNA, and 10 μL of H_2O. The reaction condition was designed by an initial degeneration stage at 95°C for 2 min, 40 cycles at 95°C for 15 s, 60°C for 20 s, and then held 72°C for 20 s. Each sample was measured in triplicate. At the completion of each run, melting curves for the amplicons were measured by raising the temperature by 0.3°C from 57 to 95°C while monitoring fluorescence. The comparative cycle threshold Ct method was used for the relative quantification of gene expression. Evaluation of the relative expression of mRNA was done and normalized to GAPDH reported as a housekeeping gene.

Assessment of liver injury parameters

To determine the functional injuries to the liver caused by polymicrobial sepsis, the plasma levels of alanine transaminase (ALT), aspartate transaminase (AST), alkaline phosphatase

(ALP), and total bilirubin were evaluated by Pars Azmoon kit (Iran).

Histological analysis

Tissue samples were fixed with 10% buffered formaldehyde, dehydrated, and embedded in paraffin. A liver section (5 μm) was stained with hematoxylin and eosin and examined under light microscopy (Olympus CX31RBSF) to assess the hepatic changes.

Quantitative and semiquantitative histological analysis was also used for scoring the histopathological variables by a veterinary pathologist. The mean numbers of marginated and infiltrated neutrophils were counted in 10 random high power fields of the microscope. Thereafter, scoring was performed between 0 and 4 as follows: score 0=0 up to 9 neutrophils, score 1=10 up to 19 neutrophils, score 2=20 up to 29 neutrophils, score 3=30 up to 39 neutrophils, score 4=more than 40 neutrophils. In addition, mononuclear cell infiltrations and Kupffer cell hyperplasia scoring were as follows: score 0=normal condition, score 1=mild changes, score 2=average changes, score 3=severe changes, score 4=more severe changes.

Statistical analysis

The data of this study were analyzed statistically with SPSS v.19. The data were expressed as mean ± standard deviation. One-way analysis of variance was applied to compare the mean values. The significance was considered as p value <0.05.

RESULTS

Essential oil analysis and antioxidant activities

As a result of the GC and GC-mass analysis, 24 chemical components were identified. The major constituents of *R. damascena* essential oils were characterized which were citronellol (66.11%), trans-geraniol (11.56%), phenylethyl alcohol (5.33%), and other constituents such as linalool, pinene, citral, methyl eugenol, and geranene, presented in Table 1.

The DPPH and β-carotene-linoleic acid bleaching assays were used to evaluate the antioxidant activities of *R. damascena* essential oils. Essential oil was capable of reducing the concentration of DPPH free radicals, which was higher compared to Trolex (Figure 1). In addition, the β-carotene-linoleic acid bleaching test showed high antioxidant activity in comparison with the positive control (BHT) (Figure 2).

The effect of R. damascena essential oil on the oxidative stress and antioxidant parameters

According to the data presented in Table 2, hepatic GSH level was decreased due to CLP (p<0.05). Accordingly, similar to the indomethacin treated group, *R. damascena* essential oils (50 and 100 mg/kg bw) followed by CLP increased the level of GSH to reach the level in the control group (p<0.05).

Table 1. GC and GC-mass analysis of the *R. damascena* essential oils			
	Compound	Percentage	RI
1	α-Pinene	1.81	920.967742
2	Sabinene	0.08	953.225806
3	β-Pinene	0.3	956.989247
4	Myrcene	0.36	965.591398
5	Linalool	1.42	1056.45161
6	Rose oxide (Isomer)	0.47	1065.5914
7	Phenylethyl alcohol	5.33	1072.04301
8	Rose oxide (Isomer)	0.22	1079.56989
9	Citronellol	66.11	1162.84153
10	Carvone	0.76	1176.50273
11	Trans Geraniol	11.56	1181.42077
12	Citral	1.11	1194.53552
13	Citronellol acetate	0.69	1252.40964
14	Eugenol	0.83	1263.25301
15	Nerol acetate	0.89	1277.71084
16	Methyl eugenol	2.36	1297.59036
17	Caryophyllene (isomer)	0.69	1315.06024
18	a-Guaiene	0.54	1326.50602
19	Caryophyllene (isomer)	0.52	1340.96386
20	Germacrene	1.44	1362.04819
21	Bisabolene	0.25	1373.49398
22	Bulenensene	0.41	1378.31325
23	Tetradecane	1.41	1510.13514
24	Farnesol	0.45	1534.45946

Table 2. Effect of *R. damascena* essential oil on oxidative stress parameters					
Groups	GST (nmol/min/mg protein)	GSH (nmol/mg protein)	MDA (nmol/mg protein)	MPO (U/mg protein)	FRAP (μmol/L)
Control	1126±61.61	11.42±1.1	10.34±1.18	9.46±0.7	407±21.76
CLP	1173±32.11	7.28±0.67*	18.51±1.53*	26.13±0.7*	257±10.98*
RD50	1838±38.39	13.51±0.78**	12.66±0.93**	11.06±0.92**	377±9.8**
RD100	2044±85.88	13.58±0.61**	11.78±0.84**	10.46±0.98**	367±12.18**
IND	1076±48.22	11.26±0.95**	11.8±0.87**	6.58±0.2**	280±18.2

*p<0.05 is considered significant between the control group and cecal ligation and puncture group. **p<0.05 is considered significant between the cecal ligation and puncture group and treated groups. Data are presented as mean ± standard deviation
CLP: Cecal ligation and puncture, IND: Indomethacin

CLP induced significant increases in MPO activity as compared to the control group ($p < 0.05$). On the other hand, decreases in MPO activity were seen in both groups treated by *R. damascena* essential oils (50 and 100 mg/kg bw) ($p < 0.05$) as shown in the indomethacin group (Table 2).

Hepatic MDA level was significantly evaluated as an indicator of lipid peroxidation in the CLP group in comparison to the control group ($p < 0.05$, Table 2). Treatment of rats with the essential oils significantly decreased the level of MDA in the liver ($p < 0.05$, Table 2).

Concerning the effect of sepsis on FRAP level (Table 2), CLP caused a significant decrease in FRAP level in comparison to the control group ($p < 0.05$). In addition, treatment of rats with *R. damascena* essential oils in doses of 50 and 100 mg/kg bw increased the level of FRAP to the ideal condition ($p < 0.05$, Table 2).

CLP did not change the GST activity (Table 2), but treatment of rats with 50 and 100 mg/kg bw of *R. damascena* essential oils increased the activity of GST compared to the control and CLP groups ($p < 0.05$).
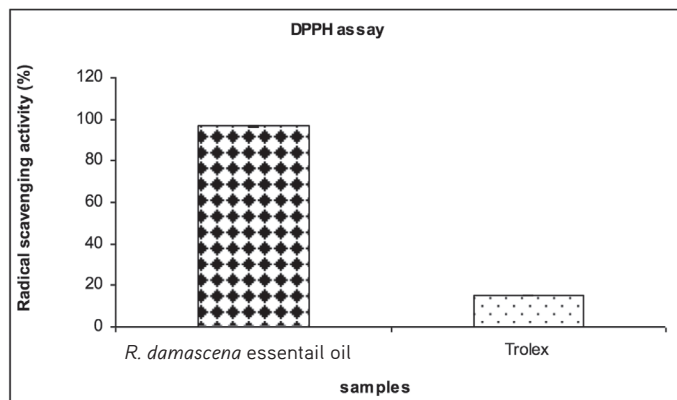
Figure 1. DPPH radical-scavenging activity of *R. damascena* essential oil. The different letters are significantly different at the $p < 0.05$ level. Samples were done in triplicate (n=3)
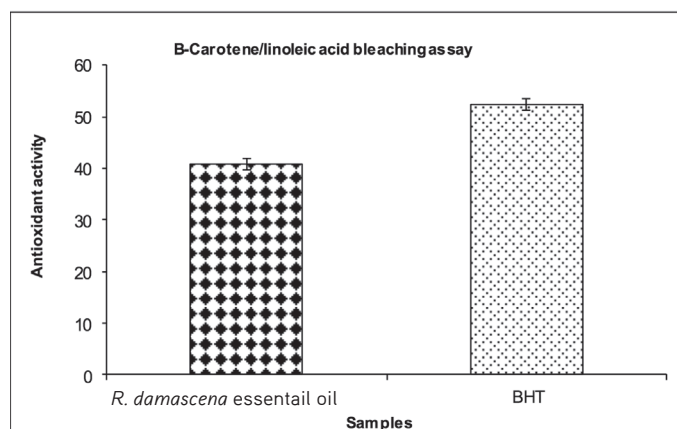
Figure 2. β-Carotene/linoleic acid bleaching assay of *R. damascena* essential oil. The different letters are significantly different at the $p < 0.05$ level. Samples were done in triplicate (n=3)

R. damascena essential oils inhibited CLP-induced concentration of PGE-$_2$

In the present study, the evaluation of PGE$_2$ concentration clearly indicated that CLP caused a significant increase in plasma level of PGE$_2$ as compared to the control group ($p < 0.05$, Table 3). On the contrary, treatment of rats with *R. damascena* essential oils (50 and 100 mg/kg bw) significantly decreased plasma PGE$_2$ concentration in comparison to the CLP group ($p < 0.05$).

R. damascena essential oil inhibited CLP-induced expression of COX-2

Table 3 shows the alteration of COX-2 expression in the different groups. The rats which received CLP showed a significant increase ($p < 0.05$) in COX-2 expression as compared to the control group. On the contrary, the rats that received *R. damascena* essential oils in 50 and 100 mg/kg bw followed by CLP had higher levels of COX-2 expression ($p < 0.05$, Table 3), which were also seen in indomethacin treated group, their levels were lower than the CLP group.

The effect of R. damascena essential oils on plasma biomarker for liver injuries

As shown in Figure 3, the plasma levels of AST and ALT significantly increased ($p < 0.05$) in the CLP group in comparison with the control group (Figures 3A and B), but, after treatment with the essential oils in doses of 50 and 100 mg/kg bw, the
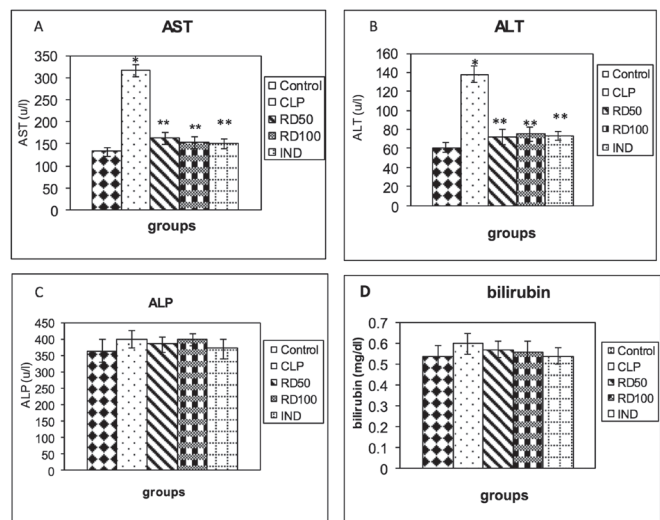
Figure 3. A) concentration of aspartate transaminase in different groups; B) concentration of alanine transaminase in different groups; C) concentration of alkaline phosphatase in different groups; D) concentration of bilirubin in different groups. In the control group the rats underwent just laparotomy after 14 days administering DMSO orally. In the cecal ligation and puncture (CLP) group the animals received just DMSO for 14 days. RD50 and RD100 essential oil (50 and 100 mg/kg bw) was administered orally in 14 days and CLP was done. IND, treated as CLP group, with the difference that the rats received indomethacin orally incubation. Values represent mean ± SD of the each group: *$p < 0.05$ is considered significantly different from the control group within each parameter. *$p < 0.05$ is considered significantly different from the CLP group within each parameter

RD: *Rosa damascena* ALT: Alanine transaminase, AST: Aspartate transaminase, ALP: Alkaline phosphatase, CLP: Cecal ligation and puncture
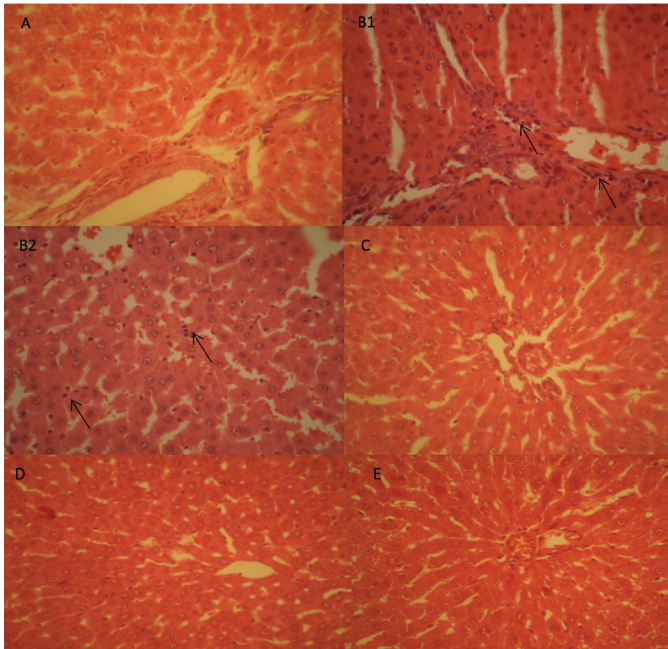
Figure 4. Histopathological studies. A) Control group, the portal tract and the hepatocytes in normal condition. B1) cecal ligation and puncture (CLP) group, neutrophil infiltration in the portal tract (arrows). B2) CLP group, neutrophil infiltration in the sinusoids, which can be seen easily with their dark nuclei (arrows). C) RD 50, the liver in normal condition without any neutrophil infiltration. Hematoxylin and eosin (H&E), 400×. D) RD 100 group, the portal tract and parenchyma in normal condition without any neutrophil infiltration. H&E, 400×. E) Indomethacin group, there is no sign of neutrophil infiltration in the portal tract or in the parenchyma. H&E, 400×

Table 3. Effect of *R. damascena* essential oil on COX-2 expression and PGE2 level in CLP rats

Groups	PGE2 (ng/mL)	COX-2 expression ($\log_{10}$)
Control	508±26.7	0±0.03
CLP	796±20.7*	0.43±0.05*
RD50	632±23.9**	0.21±0.03**
RD100	531±8.2**	0.25±0.04**
IND	536±32.8**	0.15±0.01**

*$p < 0.05$ is considered significant between the control group and cecal ligation and puncture group. **$p < 0.05$ is considered significant between the cecal ligation and puncture group and treated groups. Data are presented as mean ± standard deviation
CLP: Cecal ligation and puncture, IND: Indomethacin

Table 4. Mean values and standard error of histopathologic variables of the liver specimens in the study groups

Study groups	Neutrophil margination and infiltration	Granular degeneration	Inflammatory foci	Mononuclear cells infiltration & Kupffer cell hyperplasia	Portal inflammation
Control	0±0	0.4±0.24	0±0	0±0	0±0
CLP	2.75±0.25*	0.75±0.75	1.5 ± 0.86	3±0.4*	2.25±0.25*
RD50	1.4±0.24**	0.2±0.2	0.2±0.2	1.2±0.2**	0.6±0.24**
RD100	0.8±0.2**	0.2±0.2	0±0	1.6±0.24**	1±0**
IND	0.5±0.28**	0±0	0±0	1±0**	0.25±0.25**

*: Having significant difference in comparison with the control group, **: Having significant difference in comparison with the cecal ligation and puncture group
CLP: Cecal ligation and puncture, IND: Indomethacin

levels of these markers were decreased ($p < 0.05$). Meanwhile, plasma ALP and total bilirubin had no considerable differences during the experiment in all groups (Figures 3C and D).

Histological findings

Histopathologic assessment of the liver specimens revealed that there were some mild changes consisting of congestion and granular degeneration of the hepatocytes in the control group (Figure 4A), whereas severe congestion, interstitial edema, and margination of neutrophils in the venules and sinusoids were observed in the CLP group. Neutrophils and mononuclear cells were also infiltrated in the portal tracts and sinusoids in the septic group. Kupffer cell hyperplasia and granular degeneration were the other observed changes in the CLP group. There were no signs of necrosis in hepatocytes. All the changes in the CLP group revealed a kind of hepatitis called nonspecific reactive hepatitis (Figures 4B1 and B2). However, the essential oil treatments obviously reduced neutrophil infiltration in the portal tract and parenchyma of the liver tissues (Figures 4C and D). In addition, in the indomethacin group, there was no sign of neutrophil infiltration in the portal tract or in the parenchyma (Figure 4E).

As shown in Table 4, the CLP group obviously showed neutrophil margination and infiltration, mononuclear cell infiltration, and Kupffer cell hyperplasia as compared with the control group ($p \leq 0.05$). Concerning portal inflammation, it was also meaningful in the CLP group in comparison with the control group ($p \leq 0.05$). However, there were no obvious difference regarding granular degeneration and inflammatory foci between all the study groups ($p > 0.05$). To confirm the results seen in Figure 4, all the treatment groups had prominently reduced neutrophil margination and infiltration, mononuclear cells infiltration, Kupffer cell hyperplasia, and portal inflammation in comparison with the CLP group ($p \leq 0.05$).

DISCUSSION

Sepsis is a generalized inflammatory response of different parasites and their toxins in the body and can be regarded as a main part of the systemic inflammatory response system. Nowadays, sepsis is the major causes of death in intensive care units. The importance of sepsis in terms of mortality and morbidity and treatment difficulties makes it a public health concern.[26] Oxidative stress can define an incongruence between

oxidants and the body's antioxidant system.[27] It can activate immune systems that promote a destructive effect on lipid, protein, and DNA. The antioxidant defense system can confront sepsis and its consequences by combating free radicals. The role of antioxidant agents in treating sepsis was proved by different studies. Therefore, in the current study, the antioxidant and hepatoprotective activities of *R. damascena* essential oils were investigated, for the first time, through assessing the main antioxidant/oxidative stress and anti-inflammatory parameters. In the present study, the levels of ALT, AST, MPO, and MDA as well as PGE_2 and COX-2 expression ($p < 0.05$) significantly rose FRAP and GSH levels ($p < 0.05$) fell in the septic rats (Tables 2 and 3 and Figure 3), but they were modulated the *R. damascene* essential oils.

Polymorphonuclear leukocyte infiltration following systemic inflammatory response could be created during sepsis, which can result in vascular as well as parenchymal cell dysfunctions. Leucocyte aggregation and activated neutrophils leading to tissue injuries were increased due to the rise of ROS elements. Activated neutrophils can cause MPO secretion and free radical production,[28] meaning the MPO assay is a valuable indicator to evaluate neutrophil accumulation and severity of inflammation in sepsis, which was reversed in rats treated with antioxidative *R. damascena* essential oils (50 and 100 mg/kg bw) ($p < 0.05$) (Table 2). Our results were in agreement with other studies, which showed that MPO activity as neutrophil accumulations was elevated by sepsis, while pretreatment with selenium, *n*-acetylcysteine, and simvastatin decreased MPO activity by scavenging free radical generation, which suppressed the severity of sepsis.[10,29,30]

One of the consequences of sepsis is an event called lipid peroxidation, which is considered as the main oxidative stress parameter and which was increased by the impact of free radicals and MPO increment.[10] Lipid peroxidation can cause cell and mitochondria damage, which initiate protein degeneration, cell lysis, and necrosis.[31] Treatment of rats with the essential oils decreased ($p < 0.05$) lipid peroxidation, which eventually resulted in diminishing MDA level (Table 2). Our results were confirmed by, Ozdulger et al.[32] who reported that MPO activity and MDA concentration were increased in the lungs by sepsis, which showed the intensity of neutrophil infiltration and oxidative stress in rats. Applying estrogen could diminish MDA concentration and as a result of decreasing lipid peroxidation, which protected the ileum and liver from the sepsis-induced and oxidative stress condition.

It is thought that there is a direct link between lipid peroxidation and GSH depletion in sepsis. GSH is considered an important natural antioxidant system that can deal with ROS production by neutralizing them. By establishing the oxidative stress condition in the body, ROS changed the antioxidant power. In other words, the antioxidant defense system in the body was compromised, leading to increased lipid peroxidation concomitant with changes in GSH and antioxidant enzymes such as GST, CAT, and SOD.[33] In our study, we observed that CLP induction caused a decrease in GSH level in comparison to the control group ($p < 0.05$, Table 2).

On the contrary, treatment rats with *R. damascena* essential oil restored the level of GSH in ideal concentration ($p < 0.05$), indicated that inhibiting GSH depletion has curative efficiency that increases the defense ability system, which protects the body from oxidative stress by preventing lipid peroxidation. Our results are in agreement with those published by Bouzenna et al.[34] who reported that the administration of *Citrus limon* essential oil had a hepatoprotective effect on the oxidative stress caused by aspirin as revealed by decreasing lipid peroxidation and amplifying the antioxidant defense system (GSH, CAT, and GPx). Moreover, the present study revealed a significant decline in FRAP in sepsis, while administration of the essential oils caused a significant increase ($p < 0.05$) in the plasma FRAP (Table 2). A decrease in FRAP levels, as a factor in oxidative stress/antioxidant balancing, led to increase resistance and/or decreased susceptibility of the liver to free radical attack.[35] On the contrary, GST activities in the liver did not change ($p > 0.05$) in the treated groups (Table 2), which indicated no probable effective role of this enzyme in the detoxification of septic rats.

On the other hand, in sepsis, changes in cytokine levels were clearly seen, showing the imbalances between pro-inflammatory and anti-inflammatory cytokines.[36] It seems that expression of COX-2 increased by pro-inflammatory cytokines, which simulate PGE_2 level (Table 3). COX-2 is an enzyme that could simulate production of prostaglandins like PGE_2, which can initiate oxidative damage in tissue.[37] Increases in COX-2 expression stimulated the production of PGE_2, resulting in increases in its plasma level. In other words, COX-2 expression is the key principle to immunologic disharmony in septic rats, and so ceasing the COX-2 expression diminishes the effect of oxidative stress.[38] In our study, the treatment of rats with *R. damascena* essential oils had an inhibitory effect on the production of cytokines and ROS, leading to decreased COX-2 expression together with plasma PGE_2 level. Huang et al.[37] reported that LPS has a negative effect on COX-2 expression and PGE_2 production. LPS significantly increased PGE_2 levels and COX-2 transcription and also production of tumor necrosis factor-α, interleukin (IL)-1β, IL-6, and IL-10. They proved that *Bupivacaine* significantly decreases COX-2 expression and PGE2 and cytokine production.

In addition, the plasma levels of ALT and AST, which are considered the most important biomarkers of liver enzymes, could be considerably elevated by hepatocellular injuries.[39] Hepatic injuries are characterized by irregular biomarkers of liver that can be confirmed by elevations in AST and ALT levels. Elevations in the concentrations of these enzymes indicated loss of integrity of the liver, apoptosis, and necrosis. Due to the induction of CLP, the concentrations of these enzymes increased compared to the control group ($p < 0.05$, Figures 3A and B). Liver injuries in the pathologic study confirmed these changes (Figure 4). After hepatic injuries, these enzymes released by cellular necrosis and the elevation of these enzymes showed the rate of damage on integrity of the liver. Treatment of rats with *R. damascena* essential oils as well as indomethacin had ability to reduce hepatoinjuries by diminishing these biomarkers (Table 4 and Figures 3 and 4).

On the other hand, ALP is related to injuries in the bile duct and integrity of the cell membrane. Total bilirubin is also considered a parameter of liver injuries.[39] In the present study, there was no difference in the serum level of ALP and total bilirubin did not differ between the CLP-induction group and the other groups (p<0.05, Figures 3C and D), indicating that CLP does not cause considerable damage to the liver or biliary ducts.

The present study indicated a significant relationship between *in vitro* antioxidative effects of *R. damascena* essential oils and *in vivo* anti-inflammatory effects. Citronellol (66.11%), trans geraniol (11.56%), and phenylethyl alcohol (5.33%) are the main constituents of the essential oils (Table 1), which possessed antioxidant activities proved by DPPH and β-carotene/linoleic acid bleaching assays. According to recent studies, these components are completely related to the antioxidant and radical scavenging ability of the essential oil as it was reported that fresh juice of *R. damascena* has antioxidant potential against rats that received CCl_4 as a toxic material that can cause hepatoinjuries.[18]

CONCLUSION

This study confirmed that *R. damascena* essential oils had antioxidative and hepatoprotective effects against CLP-induced sepsis caused by reactive species. The essential oils decreased oxidative stress parameters, improving the antioxidant defense system, and restoring the ideal concentration of inflammatory parameters and it was confirmed by histopathology assessment.

ACKNOWLEDGEMENTS

REFERENCES

1. Angus DC, van der Poll T. Severe sepsis and septic shock. N Engl J Med. 2013;369:840-851.

2. Peters K, Unger RE, Brunner J, Kirkpatrick CJ. Molecular basis of endothelial dysfunction in sepsis. Cardiovasc Res. 2003;60:49-57.

3. Peters J, Cohen J. Sepsis. Med J. 2013;41:667-669.

4. Cho SY, Choi JH. Biomarkers of sepsis. Infect Chemother. 2014;46:1-12.

5. Nelson GE, Mave V, Gupta A. Biomarkers for sepsis: A review with special attention to India. Biomed Res Int. 2014;2014:264351.

6. Li S, Zhu FX, Zhao XJ, An YZ. The immunoprotective activity of interleukin-33 in a mouse model of cecal ligation and puncture-induced sepsis. Immunol Lett. 2016;169:1-7.

7. Koh HJ, Joo J, Cho ML, Her YM, Hwang JE, Lee J. Proinflammatory and anti-inflammatory cytokine balance in patients with cirrhotic hepatitis during live-donor liver transplant. Exp Clin Transplant. 2013;11:39-43.

8. Lowes DA, Webster NR, Murphy MP, Galley HF. Antioxidants that protect mitochondria reduce interleukin-6 and oxidative stress,

9. Dejager L, Pinheiro I, Dejonckheere E, Libert C. Cecal ligation and puncture: the gold standard model for polymicrobial sepsis? Trends Microbiol. 2011;19:198-208.

10. Song T, Yin H, Chen J, Huang L, Jiang J, He T, Huang H, Hu X. Survival advantage depends on cecal volume rather than cecal length in a mouse model of cecal ligation and puncture. J Surg Res. 2016;203:476-482.

11. Schabbauer G. Polymicrobial sepsis models: CLP versus CASP. Drug Discov Today Dis Models. 2012;9:17-21.

12. Cuenca AG, Delano MJ, Kelly-Scumpia KM, Moldawer LL, Efron PA. Cecal ligation and puncture. Curr Protoc Immunol. 2010;91:19.13.1-19.13.11.

13. Hajhashemi V, Ghannadi A, Hajiloo M. Analgesic and anti-inflammatory effects of *Rosa damascena* hydroalcoholic extract and its essential oil in animal models. Iran J Pharm Res. 2010;9:163-168.

14. Mahboubi M. *Rosa damascena* as holy ancient herb with novel applications. J Tradit Complement Med. 2015;6:10-16.

15. Dolati K, Rakhshandeh H, Shafei MN. Antidepressant-like effect of aqueous extract from *Rosa damascena* in mice. Avicenna J Phytomed. 2011;1:91-97.

16. Akbari M, Kazerani HR, Kamrani A, Mohri M. A preliminary study on some potential toxic effects of *Rosa damascena* Mill. Iran J Vet Res. 2013;14:232-236.

17. Gholamhoseinian A, Fallah H, Sharifi far F. Inhibitory effect of methanol extract of *Rosa damascena* Mill. flowers on ▯-glucosidase activity and postprandial hyperglycemia in normal and diabetic rats. Phytomedicine. 2009;16:935-941.

18. Achuthan CR, Babu BH. Padikkala J. Antioxidant and hepatoprotective effects of *Rosa damascena*. Pharm Biol. 2003;41:357-361.

19. Baydar NG, Baydar H. Phenolic compounds, antiradical activity and antioxidant capacity of oil-bearing rose (*Rosa damascena* Mill.) extracts. Ind Crops Prod. 2013;41:375-380.

20. Yassa N, Masoomi F, Rohani Rankouhi SE, Hadjiakhoondi A. Chemical composition and antioxidant activity of the extract and essential oil of *Rosa damascena* from Iran, population of Guilan. DARU J Pharm Sci. 2009;17:175-180.

21. Sedlak J, Lindsay RH. Estimation of total, protein-bound, and nonprotein sulfhydryl groups in tissue with Ellman's reagent. Anal Biochem. 1968;25:192-205.

22. Hillegass LM, Griswold DE, Brickson B, Albrightson-Winslow C. Assessment of myeloperoxidase activity in whole rat kidney. J Pharmacol Methods. 1990;24:285-295.

23. Buege JA, Aust SD. Microsomal lipid peroxidation. Methods Enzymol. 1978;52:302-310.

24. Habig WH, Pabst MJ, Jakoby WB. Glutathione S-transferases. The first enzymatic step in mercapturic acid formation. J Biol Chem. 1974;249:7130-7139.

25. Benzie IF, Strain JJ. The ferric reducing ability of plasma (FRAP) as a measure of "antioxidant power": the FRAP assay. Anal Biochem. 1996;239:70-76.

26. Zolali E, Hamishehkar H, Maleki-Dizaji N, Majidi Zolbanin N, Ghavimi H, Kouhsoltani M, Asgharian P. Selenium effect on oxidative stress factors in septic rats. Adv Pharm Bull. 2014;4:289-293.

27. Abd El Tawab AM, Shahin NN, AbdelMohsen MM. Protective effect of *Satureja montana* extract on cyclophosphamide-induced testicular injury in rats. Chem Biol Interact. 2014;224:196-205.

28 Makled MN, El-Awady MS, Abdelaziz RR, Atwan N, Guns ET, Gameil NM, Shehab El-Din AB, Ammar EM. Pomegranate protects liver against cecal ligation and puncture-induced oxidative stress and inflammation in rats through TLR4/NF-B pathway inhibition. Environ Toxicol Pharmacol. 2016;43:182-192.

29. Cuzzocrea S, Mazzon E, Dugo L, Serraino I, Ciccolo A, Centorrino T, De Sarro A, Caputi AP. Protective effects of n-acetylcysteine on lung injury and red blood cell modification induced by carrageenan in the rat. FASEB J. 2001;15:1187-1200.

30. Mohamadin AM, Elberry AA, Abdel Gawad HS, Morsy GM, Al-Abbasi FA. Protective effects of simvastatin, a lipid-lowering agent, against oxidative damage in experimental diabetic rats. J Lipids. 2011;2011:167958.

31. Sener G, Arbak S, Kurtaran P, Gedik N, Yeğen BC. Estrogen protects the liver and intestines against sepsis-induced injury in rats. J Surg Res. 2005;128:70-78.

32. Ozdulger A, Cinel I, Koksel O, Cinel L, Avlan D, Unlu A, Okcu H, Dikmengil M, Oral U. The protective effect of N-acetylcysteine on apoptotic lung injury in cecal ligation and puncture-induced sepsis model. Shock. 2003;19:366-372.

33. Zhong W, Qian K, Xiong J, Ma K, Wang A, Zou Y. Curcumin alleviates lipopolysaccharide-induced sepsis and liver failure by suppression of oxidative stress-related inflammation via PI3K/AKT and NF-kB related signaling. Biomed Pharmacother. 2016;83:302-313.

34. Bouzenna H, Dhibi S, Samout N, Rjeibi I, Talarmin H, Elfeki A, Hfaiedh N. The protective effect of *Citrus limon* essential oil on hepatotoxicity and nephrotoxicity induced by aspirin in rats. Biomed Pharmacother. 2016;83:1327-1334.

35. Dadkhah A, Fatemi F, Kazemnejad S, Rasmi Y, Ashrafi-Helan J, Allameh A. Differential effects of acetaminophen on enzymatic and non-enzymatic antioxidant factors and plasma total antioxidant capacity in developing and adult rats. Mol Cell Biochem. 2006;281:145-152.

36. Frencken JF, van Vught LA, Peelen LM, Ong DSY, Klein Klouwenberg PMC, Horn J, Bonten MJM, van der Poll T, Cremer OL; MARS Consortium. An unbalanced inflammatory cytokine response is not associated with mortality following sepsis: A prospective cohort study. Crit Care Med. 2017;45:e493-e499.

37. Huang YH, Tsai PS, Huang CJ. Bupivacaine inhibits COX-2 expression, PGE2, and cytokine production in endotoxin-activated macrophages. Acta Anaesthesiol Scand. 2008;52:530-535.

38. Li B, Li YM, Li X, Shi B, He MY, Zhu XL, Zhou WC, Wachtel MS, Frezza E. COX-2 inhibition improves immune system homeostasis and decreases liver damage in septic rats. J Surg Res. 2009;157:43-47.

39. Hussein RRS, Soliman RH, Abdelhaleem Ali AM, Tawfeik MH, Abdelrahim MEA. Effect of antiepileptic drugs on liver enzymes. Beni-Seuf Univ J Appl Sci. 2013;2:14-19.

Effect of Surfactant on Azithromycin Dihydrate Loaded Stearic Acid Solid Lipid Nanoparticles

Azitromisin Yüklü Stearik Asit Katı Lipit Nanopartiküllerde Sürfaktan Etkisi

🆔 Sayani BHATTACHARYYA*, 🆔 Priyanka REDDY

Krupanidhi College of Pharmacy, Department of Pharmaceutics, Bangalore, India

ABSTRACT

Objectives: Azithromycin dihydrate is a macrolide antibiotic used for the treatment of several types of bacterial infections. The drug shows low oral bioavailability due to its low solubility. In the present work solid lipid nanoparticles of azithromycin dihydrate were formulated, keeping in view enhancement of the solubility and rate of dissolution of the drug.

Materials and Methods: Azithromycin dihydrate loaded stearic acid nanoparticles were formulated by high shear homogenization using three different surfactants, namely Tween 20, poloxamer 188, and poloxamer 407, at a varied lipid surfactant ratio while keeping the quantities of the active ingredient constant. Twelve such formulations were prepared. The nanoparticles obtained were evaluated for drug content, % drug loading, % entrapment efficiency, particle size analysis, zeta potential, surface morphology, Fourier transmission infrared spectroscopy, *in vitro* drug release, and stability.

Results: All the formulations showed good entrapment efficiency and high percentage of *in vitro* release with a particle size suitable for lymphatic absorption. The nanoparticles formulated with poloxamer 188 showed better characteristics compared to the other surfactants.

Conclusion: This study indicates that stearic acid nanoparticles of azithromycin dihydrate prepared by high shear homogenization can be successively used for improvement of dissolution and thereby oral bioavailability of the drug.

Key words: Azithromycin dihydrate, solid lipid nanoparticles, zeta potential, particle size, entrapment efficiency, drug release

ÖZ

Amaç: Azitromisin dihidrat, çeşitli bakteriyel enfeksiyon tiplerinin tedavisinde kullanılan bir makrolid antibiyotiktir. Etkin madde düşük çözünürlüğü nedeniyle düşük oral biyoyararlanım gösterir. Bu çalışmada, etken maddenin çözünürlüğünü ve çözünme hızını arttırmaya yönelik olarak azitromisin dihidratın katı lipit nanopartikülleri formüle edilmiştir.

Gereç ve Yöntemler: Azitromisin dihidrat yüklü stearik asit nanopartikülleri, etken madde miktarını sabit tutarken, farklı lipit yüzey aktif madde oranında üç farklı yüzey aktif madde, Tween 20, Poloksamer 188 ve Poloksamer 407 kullanılarak yüksek hızlı homojenizasyon yöntemi ile formüle edilmiştir. Bu yöntemle on iki formülasyon hazırlanmıştır. Elde edilen nanopartiküller etken madde içeriği, % etken madde yükleme, % enkapsülasyon etkinliği, partikül boyutu analizi, zeta potansiyeli, yüzey morfolojisi, Fourier Transmisyon kızılötesi spektroskopisi, *in vitro* etken madde salımı, stabilite çalışması için değerlendirilmiştir.

Bulgular: Tüm formülasyonlar, iyi yükleme etkinliği ve lenfatik absorpsiyon için uygun bir partikül büyüklüğü ile yüksek oranda *in vitro* salım göstermiştir. Poloksamer 188 ile formüle edilen nanopartiküller, diğer sürfaktanlara kıyasla daha iyi özellikler göstermiştir.

Sonuç: Bu çalışma, yüksek hızlı homojenizasyon yöntemiyle hazırlanan azitromisin dihidratın stearik asit nanopartiküllerinin, çözünmenin ve dolayısıyla ilacın oral biyoyararlanımının iyileştirilmesi için kullanılabileceğini göstermiştir.

Anahtar kelimeler: Azitromisin dihidrat, katı lipit nanopartiküller, zeta potansiyeli, partikül büyüklüğü, enkapsülasyon verimi, ilaç salımı

INTRODUCTION

In recent years, solid lipid nanoparticles (SLNs) have received a lot of attention in drug delivery systems with the aim to improve solubility and bioavailability and to provide controlled delivery of drugs.[1] They are submicron colloidal carriers. The particle size varies in a wide range between 50 and 1000 nm.[2] They are biodegradable and biocompatible, possess low toxicity, and are preferred as potential carriers for a wide variety of poorly soluble drugs. The solid lipid core matrix of SLNs can be used to solubilize lipophilic molecules. They are characterized by their unique properties of smaller size, large surface area, and high drug loading. They have higher potentials than polymeric nanoparticles, fat emulsions, micelles, and liposomes. The suitability of SLNs as carriers is seen in the improvement of biopharmaceutical parameters of poorly soluble drugs, mainly enhancement of bioavailability, drug stability, drug targeting and thereby minimizing toxicity. From the manufacturing point of view they offer limited or no use of organic solvents and ease of scale up for large-scale production.[3-5]

Azithromycin dihydrate (AZT) is a new generation macrolide antibiotic. It is an azalide with a 15-membered azalactone ring. It is derived from erythromycin and possesses enhanced antimicrobial activity. It is prescribed for once daily dosing because of its long half-life. According to the Biopharmaceutical Classification System, AZT can be classified as a class II drug; therefore, the rate-limiting step in the process of drug absorption is the dissolution of the drug, which accounts for its low bioavailability.[6,7] Furthermore, it is a substrate of the p-glycoprotein transport system, which is further responsible for its low bioavailability due to ileal clearance (biliary plus intestinal excretion clearance).[8,9]

Therefore, the present investigation aimed to prepare and characterize azithromycin loaded SLNs using stearic acid with different surfactant combinations with a view to improve the solubility of AZT. It can be used as an alternative carrier transport system to improve the dissolution and bioavailability of AZT.

MATERIALS AND METHODS

Materials

AZT was a gift sample from Strides Ltd, Bangalore. Stearic acid was procured from Loba Chemicals Pvt. Ltd, Mumbai, India. Tween 20 was procured from SD Fine Chem Ltd. Poloxamer 188 and poloxamer 407 were obtained from Dr. Reddy's Laboratories. All other reagents and solvent used were of analytical grade.

Methods

Preparation of AZT SLNPs by high shear homogenization

The SLNs of AZT were prepared using stearic acid and different surfactants in varied proportions by high shear homogenization.[10] Table 1 reports the composition of AZT loaded SLNs. The selected lipid and the different surfactants were varied in ratio from 1:1 to 2:1. Melting of stearic acid was

carried out above its melting point. The drug was dispersed in the molten lipid. A solution of surfactant in distilled water at the same temperature of the molten drug lipid mixture was added to the drug lipid mixture and emulsified by a high shear homogenizer (Polytron PT 1600E Kinematica AG, Switzerland) at 25,000 rpm for 20 min. The nanoemulsion thus formed was subjected to cooling at room temperature. Azithromycin loaded SLNs were finally obtained and stored in a desiccator for further evaluation.

Evaluation of solid lipid nanoparticles

Drug content

For determining drug content, 250 mg of SLN was weighed accurately and dissolved in phosphate buffer pH 6.0 up to 250 mL. Then 1 mL was taken and diluted to 100 mL with phosphate buffer pH 6.0 and the solution was analyzed spectrophotometrically at 482 nm using 13.5 mol/L sulfuric acid as color developing agent. Percentage drug content was calculated using the formula;[11]

$$\%\text{Drug content} = \frac{\text{Absorbance of test}}{\text{Absorbance of standard at the same dilution}} \times 100$$

Determination of entrapment efficiency and drug loading

The entrapment efficiency was determined by centrifugation. SLN dispersion equivalent to 10 mg drug was centrifuged at 15,000 rpm for 60 min using a Remi cooling centrifuge (Mumbai, India). The supernatant layer was diluted with phosphate buffer pH 6.0 and the absorbance was measured at 482 nm in a ultraviolet visible spectrophotometer (Shimadzu 1800, Japan) using 13.5 mol/L sulfuric acid as color developing agent.[12] The

Table 1. Compositions of azithromycin dihydrate loaded solid lipid nanoparticles

Formulation code	AZT –SLN dispersion (% w/w)*			
	Stearic acid	Tween 20	Poloxamer 188	Poloxamer 407
F1	2	1	-	-
F2	2	2	-	-
F3	2	3	-	-
F4	3	2	-	-
F5	2	-	1	-
F6	2	-	2	-
F7	2	-	3	-
F8	3	-	2	-
F9	2	-	-	1
F10	2	-	-	2
F11	2	-	-	3
F12	3	-	-	2

For each formulation azithromycin dihydrate concentration is 1% w/w. AZT: Azithromycin dihydrate, SLN: Solid lipid nanoparticles

percentage entrapment efficiency and percentage drug loading were calculated from the following equations:[13,14]

$$\% \text{ Entrapment efficiency} = \frac{(\text{Weight of initial drug-Weight of free drug})}{\text{Weight of initial drug}} \times 100$$

$$\% \text{ Drug loading} = \frac{\text{Amount of entrapped drug in SLNs}}{\text{Total weight of SLNs}} \times 100$$

In vitro dissolution studies

The *in vitro* release of different SLN dispersions of azithromycin was carried out using a USP type II apparatus (paddle type). Formulation equivalent to 250 mg of drug was taken in the dissolution chamber containing 900 mL of phosphate buffer pH 6.0. The temperature of the dissolution chamber was maintained at 37±0.5℃, samples were withdrawn at predetermined intervals for 45 min, and the same were replenished with fresh buffer to maintain the sink condition. The drug content of each sample was determined spectrophotometrically at 482 nm after suitable dilution with phosphate buffer pH 6.0 using 13.5 mol/L sulfuric acid as color developing agent. The amount of drug released from the nanoparticles was calculated.[15]

Particle size analysis

The mean particle size and polydispersity index (PDI) were determined by dynamic light scattering (Zetasizer nano ZS, Malvern Instruments, UK). Samples after appropriate dilutions in Milli Q water were taken for analysis.[16] Particle size analysis for the formulations was carried out following proper dilutions in Milli Q water at 25.1℃ with equilibration time 70 s in triplicate.

Zeta potential analysis

Electrophoretic light scattering was used to achieve the electrophoretic mobility of nanoparticles using a Zetasizer nano ZS (Malvern Instruments, UK). Measurements were carried out in triplicate at 25.1℃ using water as a dispersant (refractive index: 1.330) in a clear disposable zeta cell.

Scanning electron microscopy

To study the surface morphology scanning electron microscopy was used.[17] The study was carried out at low accelerating voltage of about 15 kV with load current about 80 mA and working distance WD=9.1 mm using a standard error mean (SEM) (Model JSM 840 A, Jeol, Japan).

Fourier transform infrared spectroscopy

The compatibility study of AZT, stearic acid, and the other surfactants was performed by attenuated total reflection (ATR) at ambient temperature using a Bruker Model Alpha E (USA) through direct sampling. The microfine powered drug was sprinkled on the ATR crystal. This facilitated the refraction. The fourier transform infrared spectroscopy (FTIR) spectra of the physical mixture of drug and excipients thus obtained ascertained the compatibility of the drug with the excipients.[18]

Stability studies

The nanoparticles of AZT were stored in capped glass vials at 40±2℃/75% RH±5% RH for 90 days. Samples were evaluated periodically for particle size, drug content, and % release at the end of 30, 60, and 90 days.[14]

Differential scanning calorimetric study

The differential scanning calorimetric (DSC) thermograms of pure drug, stearic acid, blank formulation, and AZT loaded SLNs were recorded using a Mettler-Toledo differential scanning calorimeter (Mumbai, India). A suitable quantity of sample was weighed and heated in a closed pierced aluminum pan at a scanning rate of 10℃/min between 30 and 200℃ and with 20 mL/min nitrogen flow.

RESULTS AND DISCUSSION

Drug content

The drug content of nanoparticles of AZT was in the range of 88.03% to 97.86%. The high shear homogenization method for preparing SLNs of azithromycin with varied proportion of stearic acid and different surfactants at different concentrations was found to be effective. The results are summarized in Table 2.

Entrapment efficiency and drug loading

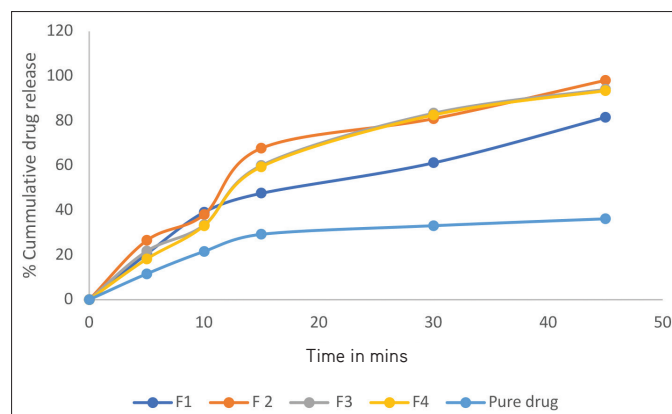To achieve high entrapment of drug in the different concentration of lipid matrix of stearic acid, the type and

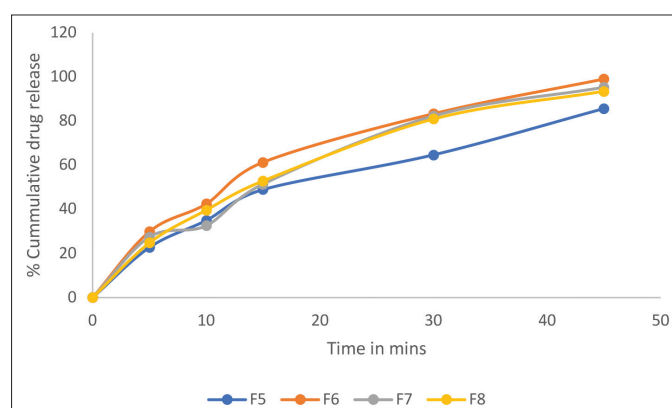**Figure 1.** *In vitro* drug release profile (pure drug, F1 to F4)

Figure 2. *In vitro* drug release profile (F5 to F8)

concentration of surfactants were varied in the ratio from 1:1 to 2:1. It was observed that as the drug was moderately lipophilic the entrapment efficiency of the drug in the matrix was highly satisfactory. The range of the percentage entrapment and drug loading was in the range from 69% to 89% and 23% to 30%, respectively, and is summarized in Table 2.
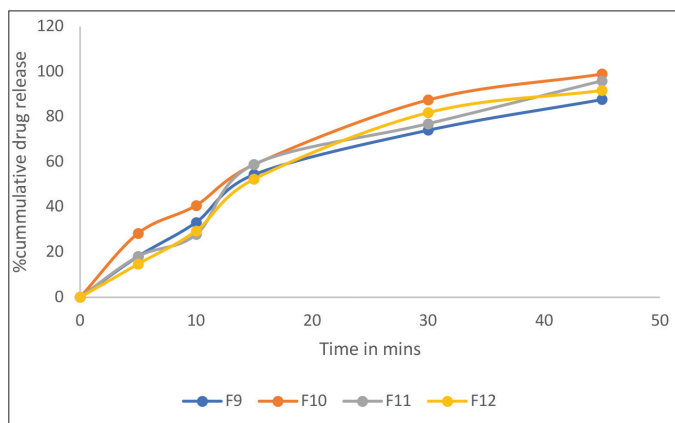

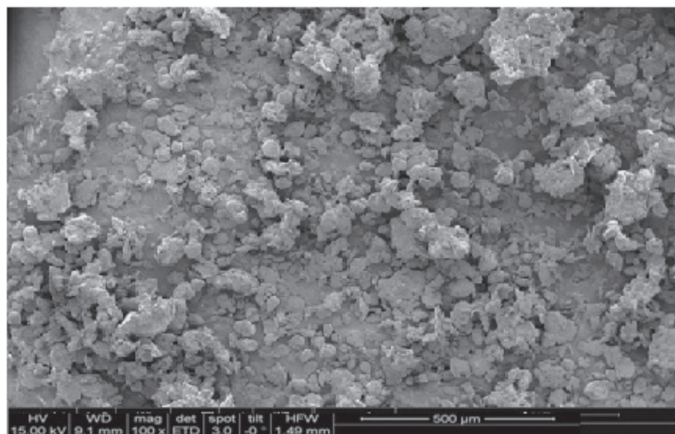**Figure 3.** *In vitro* drug release profile (F9 to F12)

Figure 4. SEM of F2 formulation
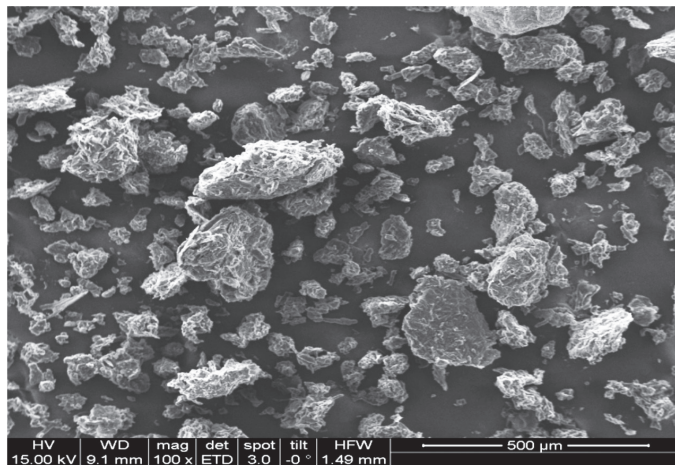
SEM: Scanning electron microscopy

Figure 5. SEM of F6 formulation

SEM: Standard error mean

Cumulative drug release

In vitro release of the AZT loaded nanoparticles in phosphate buffer pH 6 was studied in a USP type II dissolution apparatus over 45 min. Data from the percentage release of drug from the SLNs are illustrated in Figures 1, 2, and 3. Formulations (F1, F5, F9, F4, F8, and F12) containing high lipid surfactant ratios showed less drug release within 45 min. This may be attributed to the hydrophobicity of the matrix and affinity of the drug to the lipid component. Formulations containing relatively high amounts of surfactant (F3, F7, and F11) showed improved dissolution probably due to a reduction in interfacial tension with the increase in surfactant concentration. Better release was obtained from formulations with 1:1 ratio of lipid and surfactant. Formulations F2, F6, and F10 showed better release than any other formulations. This may be attributed to the effect of the concentration of surfactant on the physical properties of the nanoparticles. Poloxamer 188 was the best probably due to its low molecular weight and thereby low viscosity and high HLB compared to other surfactants, which enhanced the release of drug from the lipid matrix.[19,20]

Table 2. Drug content, entrapment efficiency, and drug loading of AZT-SLN dispersions

Sl. no.	Formulation code	Drug content (%) ±SD	Entrapment efficiency (%) ± SD	Drug loading (%) ± SD	% Drug release at 45 min ± SD
1	F1	90.59±0.03	69.38±1.78	24.7±0.57	81.54±0.22
2	F2	93.16±0.02	88.5±1.56	29.9±0.98	98.10±0.38
3	F3	92.93±0.02	79.57±2.53	23.07±1.26	94.03±0.64
4	F4	93.16±0.04	85.97±2.23	29±0.78	93.45±0.43
5	F5	88.03±0.02	71.53±2.89	24.78±0.63	85.66±0.13
6	F6	97.86±0.04	89.79±1.56	30.08±1.98	99.06±0.36
7	F7	89.74±0.02	72±0.89	25.2±2.36	95.31±0.19
8	F8	93.16±0.03	86.3±2.67	25.2±0.94	93.50±0.19
9	F9	96.5±0.03	71.82±3.25	25.64±0.81	87.61±0.28
10	F10	97±0.03	83.84±1.86	29.9±1.94	98.90±0.45
11	F11	94.01±0.02	81±2.31	26.4±0.63	95.93±0.36
12	F12	94.27±0.03	82.31±2.78	23.93±2.13	91.65±0.47

*All results are measured in triplicate, AZT: Azithromycin dihydrate, SLN: Solid lipid nanoparticles, SD: Standard deviation

Table 3. Particle size and zeta potential of AZT-SLN dispersion

Formulation code	Particle size (nm) ± SD	Zeta potential (mV) ± SD	Polydispersity index
F2	143.1±3.91	-30.1±0.35	0.24
F6	144.7±2.72	-31.8±1.10	0.20
F10	167.2±2.70	-30.6±0.26	0.25

*All the results are taken in triplicate, AZT: Azithromycin dihydrate, SLN: Solid lipid nanoparticles, SD: Standard deviation
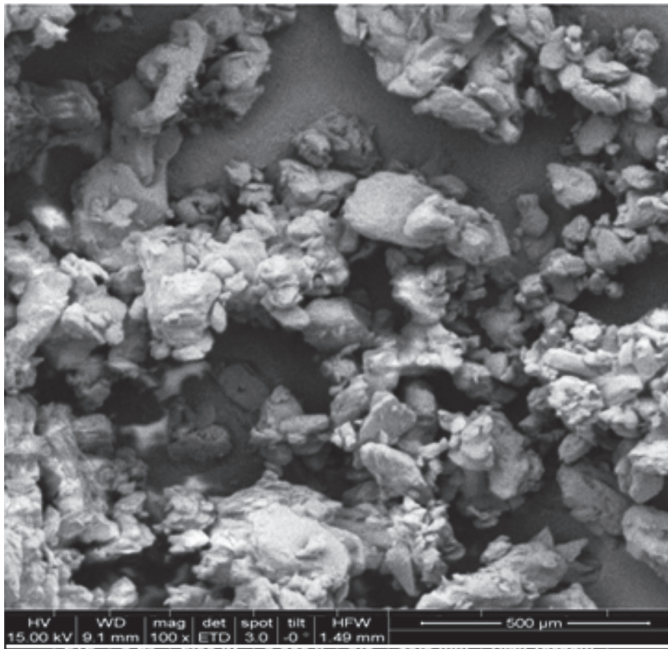
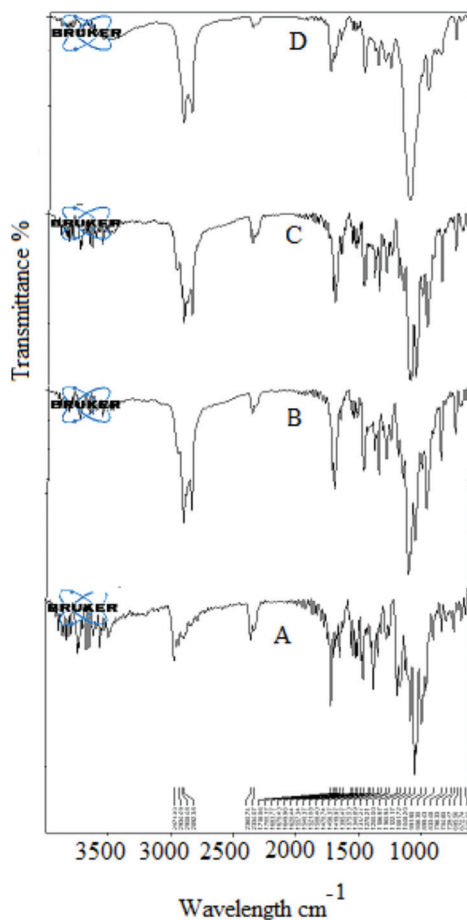**Figure 6.** SEM of F10 formulation

SEM: Standard error mean

Particle size, PDI, and zeta potential measurement

AZT loaded SLNs that showed the highest entrapment efficiency and drug release were subjected to further characterization of particle size, zeta potential, and PDI as shown in Table 3. The selected formulations showed a mean particle size between 143 and 167 nm. The particles were in an acceptable nanometer range, favored for lymphatic uptake. A PDI less than 1 indicated that the formulations were monodisperse in the system. Estimation of zeta potential helps in determining surface charge and potential stability of the dispersed system. Usually high positive or negative zeta potential is required for SLNs as the same charge results in electrostatic repulsion and thereby avoids aggregation of particles. The zeta potential of the selected formulations F2, F6, and F10 was -30.1 mV, -31.8 mV, and -30.6 mV, respectively.

Scanning electron microscopy

The surface morphology of the SLNs was studied by SEM. Formulations F2, F6, and F10 were subjected to size and morphology studies. The photographs (Figures 4, 5, and 6) revealed that all particles were discrete entities, slightly spherical with a smooth surface. Thus the employed method of preparation of SLNs by hot homogenization was found to be appropriate for formulation of nanoparticles.
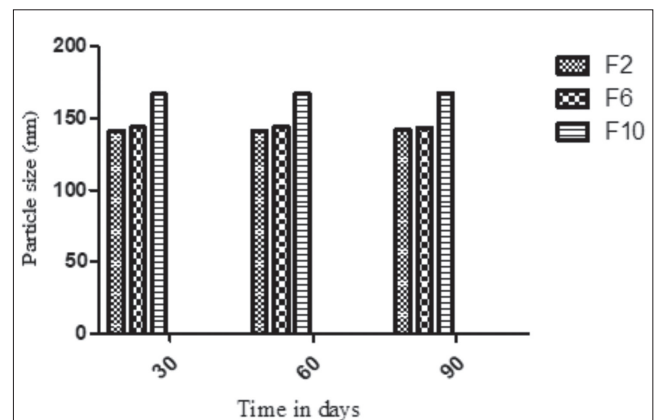

Figure 8. Stability study data of formulations F2, F6, and F10 on particle size

Figure 7. FTIR spectra of pure azithromycin dihydrate (a), physical mixture of drug with stearic acid and poloxamer 188 (b), drug with stearic acid and poloxamer 407 (c), drug with stearic acid and Tween 20 (d)

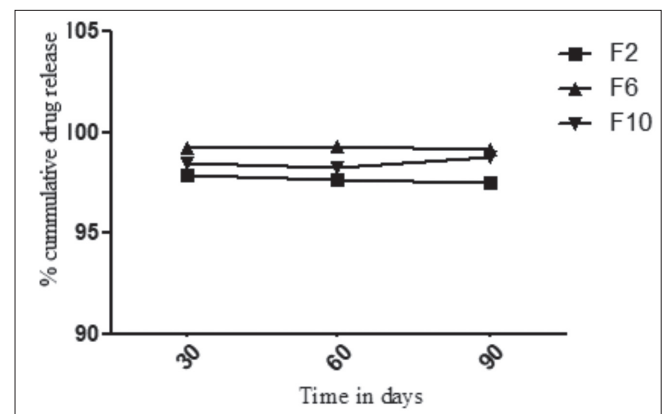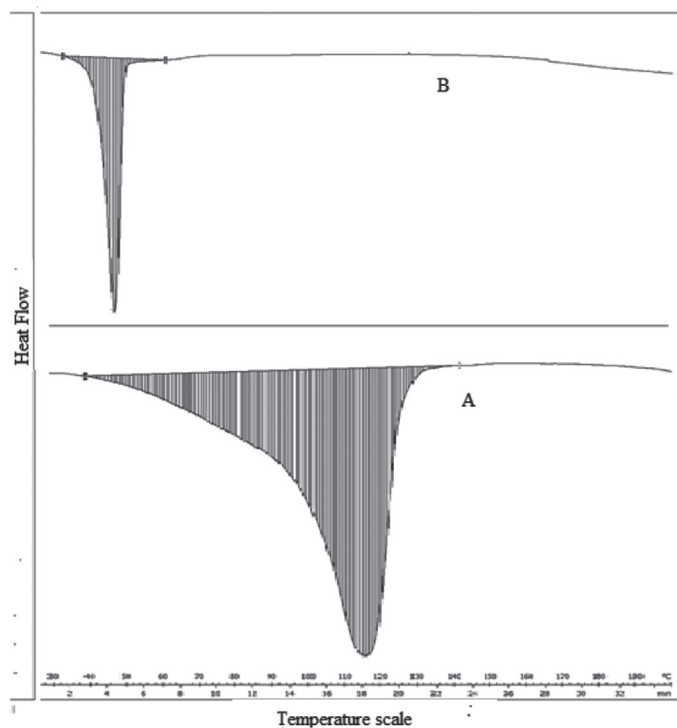FTIR: Fourier transform infrared spectroscopy

**Figure 9.** Stability study data of formulations F2, F6, and F10 on drug release

FTIR studies

The FTIR spectrum of pure AZT showed the characteristic peaks at 2971.30 cm^{-1} (C-H stretching), 1718.56 cm^{-1} (C=O ketone), 1375.53 cm^{-1} (C-H deformation in alkane), and 1186.97 cm^{-1} (C-O-C ether stretching).

Figure 10. DSC thermogram of pure azithromycin dihydrate (a) and formulation F6 (b)

DSC: Differential scanning calorimetry
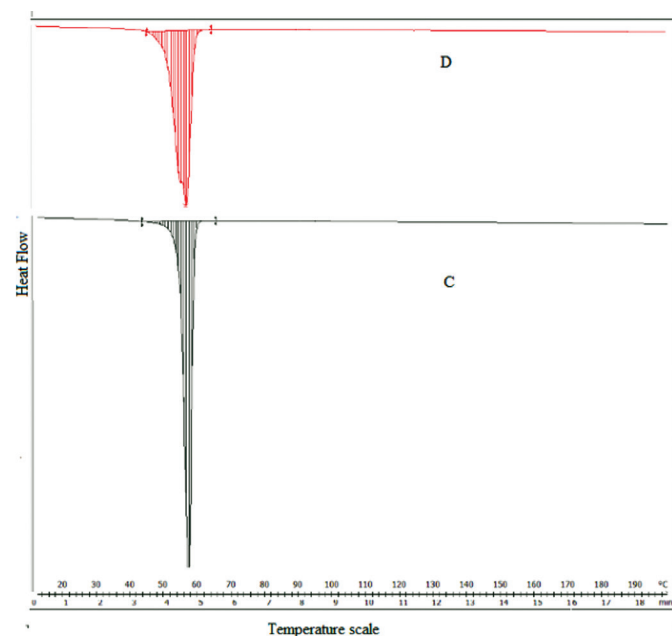
Figure 11. DSC thermogram of stearic acid (c) and blank formulation F6 (d)

DSC: Differential scanning calorimetry

The FTIR spectra of the 1:1 physical mixtures of drug, stearic acid, and surfactants had all the characteristic peaks (Figure 7) and the band values of AZT confirming that all the functional groups were well preserved.

This study clearly indicated the absence of any chemical interaction between the drug and the excipients, and they were compatible with each other.

Stability studies

The selected formulations were subjected to short-term stability studies for 90 days at 40±2°C/75%±5% RH. Both physical and chemical changes were observed during the study at an interval of 30 days. Physical stability was analyzed in terms of particle size, whereas chemical stability was analyzed by the determination of drug content and change in the release profile. The drug content was found to be 93.21%, 97.53%, and 97.11% for formulations F2, F6, and F10, respectively, at the end of the study. Figures 8 and 9 reveal that all the formulations retained their size and release profile during the study period. Therefore, the formulations were found to be stable at 40±2°C/75%±5% RH.

DSC studies

DSC was used to investigate the thermal behavior of the pure drug in the lipid surfactant mixture. AZT showed an endothermic peak at 115.77°C with onset at 93.11°C and end set at 125.54°C corresponding to the melting point of AZT as shown in Figure 10a. It was noted that there was a shift in the melting point from 115.77°C to 47.07°C (Figure 10b), indicating that AZT must be molecularly dispersed in the formulations.[21] The complete fusion of drug in the matrix was further proved by the thermograms of pure stearic acid and the blank SLN corresponds to F6 as shown in Figure 11.

CONCLUSIONS

This study demonstrated that AZT loaded SLNs were successfully prepared and characterized. All the formulations showed improved dissolution of AZT with satisfactory entrapment efficiency and drug loading. The characterization of formulations in terms of their particle size, zeta potential, PDI, surface morphology, and enhancement of dissolution proved the suitability of high shear homogenization to entrap AZT successfully in SLN carriers. From this study it can be concluded that poloxamer 188 is the best surfactant among the three surfactants used for improvement of solubility of AZT in the formulation of SLNs.

ACKNOWLEDGEMENTS

Conflict of Interest: No conflict of interest was declared by the authors.

REFERENCES

1. Müller RH, Mäder K, Gohla S. Solid lipid nanoparticles (SLN) for controlled drug delivery - a review of the state of the art. Eur J Pharm Biopharm. 2000;50:161-177.

2. Ekambaram P, Sathali AAH, Priyanka K. Solid lipid nanoparticles: a review. Sci Revs Chem Commun. 2012;2:80-102.

3. Mehnert W, Mäder K. Solid lipid nanoparticles production, characterization and applications. Adv Drug Deliv Rev. 2001;47:165-196.

4. Mukherjee S, Ray S, Thakur RS. Solid lipid nanoparticles: A modern formulation approach in drug delivery system. Indian J Pharm Sci. 2009;71:349-358.

5. Yadav N, Khatak S, Sara UVS. Solid lipid nanoparticles - A review. Int J Appl Pharm. 2013;5:8-18.

6. Lode H, Borner K, Koeppe P, Schaberg T. Azithromycin--review of key chemical, pharmacokinetic and microbiological features. J Antimicrob Chemother. 1996;37:1-8.

7. Timoumi S, Mangin D, Peczalski R, Zagrouba F, Andrieu J. Stability and thermophysical properties of azithromycin dihy drate. Arabian J Chem. 2014;7:189-195.

8. Idkaidek NM, Najib N, Salem I, Jilani J. Physiologically-based IVIVC of azithromycin. Am J Pharmacol Sci. 2014;2:100-102.

9. Amin ML. P-glycoprotein inhibition for optimal drug delivery. Drug Target Insights. 2013;7:27-34.

10. Ekambaram P, Abdul HS. Formulation and evaluation of solid lipid nanoparticles of ramipril. J Young Pharm. 2011;3:216-220.

11. Padhye SG, Nagarsenker MS. Simvastatin solid lipid nanoparticles for oral delivery: formulation development and *in vivo* evaluation. Indian J Pharm Sci. 2013;75:591-598.

12. Sultana N, Arayne MS, Hussain F, Fatima A. Degradation studies of azithromycin and its spectrophotometric determination in pharmaceutical dosage form. Pak J Pharm Sci. 2006;19:98-103.

13. El-Housiny S, Shams Eldeen MA, El-Attar YA, Salem HA, Attia D, Bendas ER, El-Nabarawi MA. Fluconazole-loaded solid lipid nanoparticles topical gel for treatment of pityriasis versicolor: formulation and clinical study. Drug Deliv. 2018;25:78-90.

14. Bhalekar M, Upadhaya P, Madgulkar A. Formulation and characterization of solid lipid nanoparticles for an anti-retroviral drug darunavir. Appl Nanosci. 2017;7:47-57.

15. Parvin S, Rafshanjani AS, Kader A. Formulation and evaluation of dexamethasone loaded stearic acid nanoparticles by high shear homogenization method. Please check the abbreviation. 2014;3:331-335.

16. Soma D, Attari Z, Reddy MS, Damodaram A, Koteshwara KBG. Solid lipid nanoparticles of irbesartan: preparation, characterization, optimization and pharmacokinetic studies. Braz J Pharm Sci. 2017;53:e15012.

17. Kommavarapu P, Maruthapillai A, Palanisamy K. Preparation, characterization and evaluation of Elvitegravir loaded solid lipid nano particles for enhanced solubility and dissolution rate. Trop J Pharm Res. 2015;14:1549-1556.

18. Singh S, Kamal SS, Sharma A, Kaur D, Katual MK, Kumar R. Formulation and *in-vitro* evaluation of solid lipid nanoparticles containing Levosulpiride. The Open Nanomed J. 2017;4:17-29.

19. Shi L, Li Z,Yu L, Jia H, Zheng L. Effects of Surfactants and Lipids on the Preparation of Solid Lipid Nanoparticles Using Double Emulsion Method. J Dispers Sci Technol. 2011;32:254-259.

20. Bnyan R, Khan I, Ehtezazi T, Saleem I, Gordon S, O'Neill F, Roberts M. Surfactant effects on lipid-based vesicles properties. J Pharm Sci. 2018;107:1237-1246.

21. Londhe V, Save S. Zaltoprofen loaded solid lipid nanoparticles for topical delivery: Formulation design, *in vitro* and *ex vivo* evaluation. MOJ Bioequiv Availab. 2017;4:248-254.

ORIGINAL ARTICLE

Some New Hydrazone Derivatives Bearing the 1,2,4-Triazole Moiety as Potential Antimycobacterial Agents

Antimikobakteriyel Etki Göstermesi Beklenen Yeni Bazı 1,2,4-Triazol Yapısı Taşıyan Hidrazon Türevleri

Keriman ÖZADALI SARI[1], Oya ÜNSAL TAN[1]*, Dharmarajan SRIRAM[2], Ayla BALKAN[1]

[1]Hacettepe University, Faculty of Pharmacy, Department of Pharmaceutical Chemistry, Ankara, Turkey
[2]Birla Institute of Technology and Science – Pilani, Pharmacy Group, Medicinal Chemistry and Antimycobacterial Research Laboratory, Hyderabad Campus, Jawahar Nagar, Hyderabad, Andhra Pradesh, India

ABSTRACT

Objectives: The aim of this study was to synthesize, characterize, and screen some new 1-(4-((2-(4-substitutedphenyl)hydrazono)methyl)phenyl)-1H-1,2,4-triazole derivatives for their antimycobacterial activities.

Materials and Methods: The target compounds (**2a-h**) were gained by condensation of 4-(1H-1,2,4-triazol-1-yl)benzaldehyde with appropriate phenylhydrazines. Their structures were elucidated by IR, ¹H-NMR, and mass spectrometry. The antimycobacterial activities of the compounds were determined *in vitro* against *Mycobacterium tuberculosis* H37Rv.

Results: The biological assay results showed that the methylsulfonyl-substituted derivative **2f** displayed the highest antimycobacterial activity in this series.

Conclusion: Although the methylsulfonyl-substituted derivative exhibited significant antimycobacterial activity, none of the synthesized compounds was as effective as isoniazid, rifampin, ethambutol, and ciprofloxacin against *M. tuberculosis*.

Key words: Hydrazone, 1,2,4-triazole, antimycobacterial activity

ÖZ

Amaç: Bu çalışma, 1-(4-((2-(4-sübstitüefenil)hidrazono)metil)fenil)-1H-1,2,4-triazol türevlerinin sentezlerini yaparak yapılarını aydınlatmayı ve antimikobakteriyel aktivitelerini incelemeyi amaçlamaktadır.

Gereç ve Yöntemler: Bu çalışmada hedef bileşikler (**2a-h**), 4-(1H-1,2,4-triazol-l-il)benzaldehidin uygun fenilhidrazinlerle kondenzasyonu ile elde edilmiştir. Bileşiklerin yapıları, IR, 1H-NMR ve kütle spektrometrisi ile aydınlatılmıştır. Antimikobakteriyel aktiviteleri, *Mycobacterium tuberculosis* H37Rv'ye karşı *in vitro* olarak incelenmiştir.

Bulgular: Aktivite sonuçları incelendiğinde, metilsülfonil sübstitüe türevin **2f** serinin en aktif üyesi olduğu bulunmuştur.

Sonuç: Metilsülfonil sübstitüe türevin dikkate değer antimikobakteriyel aktivite göstermesine rağmen, sentezlenen bileşiklerin hiçbirinin *M. tuberculosis*'e karşı izoniazit, rifampin, etambutol ve siprofloksazin kadar etkili olmadıkları bulunmuştur.

Anahtar kelimeler: Hidrazon, 1,2,4-triazol, antimikobakteriyel aktivite

INTRODUCTION

Tuberculosis (TB), caused by *Mycobacterium tuberculosis*, is the ninth leading cause of death worldwide and the leading cause from a single infectious agent. In 2016, there were an estimated 10.4 million newly infected persons with 600,000 of the cases resistant to rifampicin (RIF), the most effective first-line drug, of which 490,000 had multidrug-resistant TB (MDR-TB). MDR-TB is characterized by resistance to at least the two most powerful first-line anti-TB drugs, isoniazid and RIF. Moreover, extensively drug-resistant TB (XDR-TB), defined as additional resistance to at least one fluoroquinolone and one second-line injectable drug (amikacin, kanamycin), is spreading rapidly all over the world.[1] The World Health Organization declared an urgent need to develop new drugs and strategies for efficient treatment because of the increasing resistance of *M. tuberculosis* strains.[2]

RIF, isoniazid, ethambutol (EMB), and pyrazinamide have been used as first-line drugs for TB chemotherapy for more than 50 years.[3,4] Second-line and third-line drugs, which are expensive, less effective, and more toxic than the first-line anti-TB drugs, are administered in combination for the treatment of MDR-TB.[5,6] Treatment approaches for MDR-TB have shown that increasing the number of medications used is more successful than increasing the duration of treatment.[7-9] Current treatment regimens have not been able to reduce the number of MDR-TB and XDR-TB infections while achieving reductions in the number of TB infections and death. Despite all this knowledge and notable efforts, only two new anti-TB drugs, bedaquiline and delamanid, were approved for TB therapy in the last half-century.[10-12] However, the adaptation of *M. tuberculosis* has already led to the emergence of resistant strains for these drugs. For this reason, more chemotherapeutic agents are still needed.[13]

Azole antifungal/antimycobacterial drugs, containing one of the most important classes of heterocycles, such as econazole, miconazole, and clotrimazole, stop the growth of bacteria by inhibiting P450 enzymes (CYP51, CYP121, and CYP130) and show inhibitory potential against MDR-TB *in vitro* and *in vivo* (infected mice).[14-16] It was also shown that some azole derivatives display a mixed-function oxidase on sterol synthesis in eukaryotic organisms.[17]

Hydrazones possessing an azometine -NHN=CH- moiety have been extensively investigated for their potential as anti-TB drug candidates as well as for other biological and pharmacological activities.[18-23]

In the light of above-mentioned considerations, we designed and synthesized new hydrazone compounds carrying a 1,2,4-triazole ring in order to investigate of their antimycobacterial activity against *M. tuberculosis*.

MATERIALS AND METHODS

Chemistry

Melting points were determined with a Thomas-Hoover Capillary Melting Point Apparatus and are uncorrected. Attenuated total reflection-fourier transform infrared (ATR-FTIR) spectra were obtained using the MIRacle ATR accessory (Pike technologies) in conjunction with a Spectrum BX FTIR spectrometer (PerkinElmer) and are reported in cm^{-1}. The ^{1}H-NMR (400 MHz) spectra (DMSO-d$_6$) were recorded on a Varian Mercury 400 FT NMR spectrometer using TMS as an internal reference (chemical shift represented in δ ppm). The electrospray-ionization-mass spectrometry (ESI-MS) spectra were measured on a Micromass ZQ-4000 single quadruple mass spectrometer.

Synthesis of 1-(4-((2-(4-substitutedphenyl)hydrazono)methyl) phenyl)-1H-1,2,4-triazole derivatives (*2a-h*)

Equimolar amounts of 4-(1*H*-1,2,4-triazol-1-yl)benzaldehyde (**1**) and an appropriate phenylhydrazine derivative were refluxed in ethanol in the presence of acetic acid (1-2 drops) as a catalytic reagent for 4 h. The solid precipitate was filtered and crystallized from acetonitrile.

1-(4-((2-phenylhydrazono)methyl)phenyl)-1H-1,2,4-triazole (*2a*)

Yield 44% (white solid). Mp 184-187˚C. IR (ATR, cm^{-1}); 3232, 3124, 3038, 1603, 1591, 1563, 1517, 1494, 1266. ^{1}H-NMR (DMSO-d$_6$, ppm); δ 10.45 (1H; br; -NH-), 9.27 (1H; s; triazole), 8.22 (1H; s; triazole), 7.85 (2H; d; ar. *J*: 8.8 Hz), 7.84 (1H; s; -N=CH-), 7.78 (2H; d; ar. *J*: 8.8 Hz), 7.20 (2H; t; ar. *J*: 7.6 Hz), 7.06 (1H; d; ar. *J*: 7.8 Hz), 6.74 (2H; t; ar.). ESI-MS (m/z); 286 [M+Na]$^+$, 264 [M+H]$^+$. Anal. Calcd. for C$_{15}$H$_{13}$N$_5$: C, 68.43; H, 4.98; N, 26.60. Found: C, 68.71; H, 4.57; N, 26.77.

1-(4-((2-(4-methoxyphenyl)hydrazono)methyl)phenyl)-1H-1,2,4-triazole (*2b*)

Yield 42% (white solid). Mp 212-216˚C. IR (ATR, cm^{-1}); 3174, 3112, 3020, 1608, 1540, 1503, 1223, 1137. ^{1}H-NMR (DMSO-d$_6$, 400 MHz, ppm); δ 9.33 (1H; s; triazole), 8.24 (1H; s; triazole), 7.84-7.82 (3H; m; ar. and -N=CH-), 7.74 (2H; d; ar. *J*: 8.8 Hz), 7.01 (2H; d; ar. *J*: 8.8 Hz), 6.81 (2H; d; ar. *J*: 8.8 Hz), 3.79 (3H; s; -OCH$_3$). ESI-MS (m/z); 316 [M+Na]$^+$, 294 [M+H]$^+$. Anal. Calcd. for C$_{16}$H$_{15}$N$_5$O: C, 65.52; H, 5.15; N, 23.88. Found: C, 65.65; H, 5.43; N, 23.64.

1-(4-((2-(4-carboxyphenyl)hydrazono)methyl)phenyl)-1H-1,2,4-triazole (*2c*)

Yield 41% (white solid). Mp>265˚C. IR (ATR, cm^{-1}); 3418, 3255, 3049, 1680, 1649, 1598, 1519, 1264. ^{1}H-NMR (DMSO-d$_6$, 400 MHz, ppm); δ 12.29 (1H; br; COOH), 10.90 (1H; br; -NH-), 9.31 (1H; s; triazole), 8.22 (1H; s; triazole), 7.96 (1H; s; -N=CH-), 7.88-7.79 (6H; m; ar.), 7.11 (2H; d; ar.; *J*: 8.8 Hz). ESI-MS (m/z); 330 [M+Na]$^+$, 308 [M+H]$^+$. Anal. Calcd. for C$_{16}$H$_{13}$N$_5$O$_2$: C, 62.53; H, 4.26; N, 22.79. Found: C, 62.90; H, 4.38; N, 23.06.

1-(4-((2-(4-cyanophenyl)hydrazono)methyl)phenyl)-1H-1,2,4-triazole (*2d*)

Yield 71% (white solid). Mp>265˚C. IR (ATR, cm^{-1}); 3232, 3112, 3036, 2209, 1610, 1599, 1572, 1521, 1503, 1276. ^{1}H-NMR (DMSO-d$_6$, 400 MHz, ppm); δ 11.11 (1H; br; -NH-), 9.35 (1H; s; triazole), 8.25 (1H; s; triazole), 8.01 (1H; s; -N=CH-), 7.92-7.85 (4H; m; ar.), 7.62 (2H; d; ar. *J*: 9.2 Hz), 7.18 (2H; d; ar. *J*: 8.4 Hz).

ESI-MS (m/z); 311 [M+Na]+, 289 [M+H]+. Anal. Calcd. for $C_{16}H_{12}N_6$: C, 66.66; H, 4.20; N, 29.15. Found: C, 67.00; H, 4.61; N, 29.23.

1-(4-((2-(4-sulfamoylphenyl)hydrazono)methyl)phenyl)-1H-1,2,4-triazole (2e)

Yield 76% (white solid). Mp>265°C. IR (ATR, cm⁻¹); 3359, 3272, 3130, 1591, 1572, 1515, 1308, 1132, 1094. ¹H-NMR (DMSO-d₆, 400 MHz, ppm); δ 10.96 (1H; br; -NH-), 9.34 (1H; s; triazole), 8.24 (1H; s; triazole), 7.98 (1H; s; -N=CH-), 7.89-7.83 (4H; m; ar.), 7.65 (2H; d; ar. J: 8.8 Hz), 7.16 (2H; d; ar. J: 8.8 Hz), 7.05 (2H; br; -NH₂). ESI-MS (m/z); 365 [M+Na]+, 343 [M+H]+. Anal. Calcd. for $C_{15}H_{14}N_6O_2S$: C, 52.62; H, 4.12; N, 24.55. Found: C, 52.89; H, 4.47; N, 24.83.

1-(4-((2-(4-(methylsulfonyl)phenyl)hydrazono)methyl)phenyl)-1H-1,2,4-triazole (2f)

Yield 77% (white solid). Mp>265°C. IR (ATR, cm⁻¹); 3269, 3134, 3082, 1591, 1572, 1518, 1263, 1124, 1087. ¹H-NMR (DMSO-d₆, 400 MHz, ppm); δ 11.03 (1H; br; -NH-), 9.32 (1H; s; triazole), 8.23 (1H; s; triazole), 7.99 (1H; s; -N=CH-), 7.90-7.84 (4H; m; ar.), 7.72 (2H; d; ar. J: 8.4 Hz), 7.21 (2H; d; ar. J: 8.8 Hz), 3.09 (3H; s; CH₃). ESI-MS (m/z); 364 [M+Na]+, 342 [M+H]+. Anal. Calcd. for $C_{16}H_{15}N_5O_2S$: C, 56.29; H, 4.43; N, 20.51. Found: C, 56.08; H, 4.68; N, 20.87.

1-(4-((2-(4-nitrophenyl)hydrazono)methyl)phenyl)-1H-1,2,4-triazole (2g)

Yield 59% (white solid). Mp>265°C. IR (ATR, cm⁻¹); 3191, 3126, 3038, 1609, 1592, 1521, 1306, 1274, 1109. ¹H-NMR (DMSO-d₆, 400 MHz, ppm); δ 11.37 (1H; br; -NH-), 9.33 (1H; s; triazole), 8.23 (1H; s; triazole), 8.11 (2H; d; ar. J: 9.6 Hz), 8.06 (1H; s; -N=CH-), 7.92-7.87 (4H; m; ar.), 7.18 (2H; d; ar. J: 8.4 Hz). ESI-MS (m/z); 331 [M+Na]+, 309 [M+H]+. Anal. Calcd. for $C_{15}H_{12}N_6O_2$: C, 58.44; H, 3.92; N, 27.26. Found: C, 58.76; H, 4.01; N, 27.33.

1-(4-((2-(2,4-dinitrophenyl)hydrazono)methyl)phenyl)-1H-1,2,4-triazole (2h)

Yield 68% (white solid). Mp>265°C. IR (ATR, cm⁻¹); 3286, 3097, 1608, 1583, 1497, 1321, 1270, 1134, 1085. ¹H-NMR (DMSO-d₆, 400 MHz, ppm); 11.69 (1H; br; -NH-), 9.37 (1H; s; triazole), 8.84 (1H; d; ar. J: 2.4 Hz), 8.72 (1H; s; -N=CH-), 8.35 (1H; dd; ar. J_1: 2.8 J_2: 9.8 Hz), 8.26 (1H; s; triazole), 8.11 (1H; d; ar. J: 10 Hz), 7.98-7.93 (4H; m; ar.). ESI-MS (m/z); 376 [M+Na]+, 354 [M+H]+. Anal. Calcd. for $C_{15}H_{11}N_7O_4$: C, 51.00; H, 3.14; N, 27.75. Found: C, 51.36; H, 3.46; N, 28.02.

Antimycobacterial activity assay

In vitro antimycobacterial activity assays of the synthesized compounds were carried out using the microplate Alamar blue assay method against *M. tuberculosis* H37Rv in duplicate.[24] Ciprofloxacin, isoniazid, EMB, and rifampin were used as reference compounds. The stock solutions of the compounds were prepared in DMSO. Sterile deionized water (200 µL) was added to all outer-perimeter wells of sterile 96-well plates to minimize evaporation of the medium in the test wells during incubation. The wells received 100 µL of Middlebrook 7H9GC broth and two-fold serial dilutions of the target compounds/positive controls were prepared in a volume of 100 µL directly on the plate to get final concentrations of 25, 12.5, 6.25, 3.13, 1.56,

and 0.78 µg/mL. The inoculum was adjusted to a McFarland tube No. 1 and diluted 1:20. Then 100 µL of *M. tuberculosis* inoculum was added to the wells. The plates were incubated at 37°C for 5 days. Next, 50 µL of a freshly prepared 1:1 mixture of Alamar Blue (Accumed International, Westlake, Ohio) reagent and 10% Tween 80 was added to the plates, followed by incubation at 37°C for 24 h. A blue color in the well was interpreted as no growth, and a pink color was scored as growth. The MIC was determined as the lowest drug concentration that prevented a color change from blue to pink. MICs of the compounds are reported in Table 1.

RESULTS

The starting compound, 4-(1H-1,2,4-triazol-1-yl)benzaldehyde (1), was synthesized by the method described in the literature.[25] The target compounds (2a-h) were obtained by condensation of 4-(1H-1,2,4-triazol-1-yl)benzaldehyde with appropriate phenylhydrazines in ethanol in the presence of acetic acid (Scheme 1).

The structures of the target compounds were characterized using spectral methods (IR, ¹H-NMR, and ESI-MS). The bands at around 1610 and 3200 cm⁻¹ in the IR spectra of the compounds (2a-h) were evidence of the presence of a hydrazone moiety. In the ¹H-NMR spectra of 2a-h, the signals belonging to imine and N-H protons were observed at around 8.00 and 11.30 ppm, respectively. Moreover, signals were seen at 12.29, 7.05, 3.79, and 3.09 ppm according to substituted moieties (COOH, SO₂NH₂, OCH₃, and SO₂CH₃, respectively) in the ¹H-NMR spectra. Additionally, the structures of all the target compounds were confirmed by the peaks belonging to [M+Na]+ and [M+H]+ seen in the ESI mass spectra.

The target compounds 2a-h were evaluated for their antimycobacterial activity *in vitro* against *M. tuberculosis* H37Rv using the microplate Alamar blue assay method. The results of the antimycobacterial activity (MIC values) are

Table 1. Antimycobacterial activities of the compounds

Compound	R	MIC in µM
2a	H	190.11
2b	OCH₃	85.32
2c	COOH	>162.87
2d	CN	173.61
2e	SO₂NH₂	146.20
2f	SO₂CH₃	73.31
2g	NO₂	>162.34
2h	2,4-diNO₂	>141.64
INH	-	0.36
Rifampin	-	0.12
Ethambutol	-	7.65
Ciprofloxacin	-	4.71
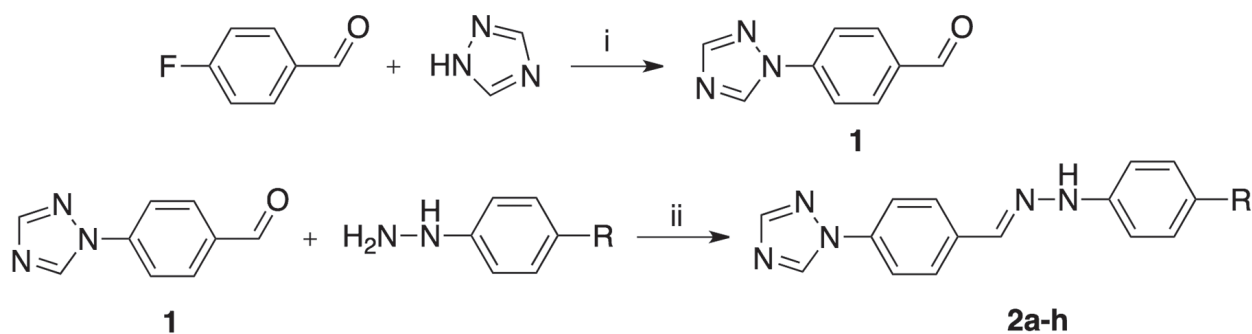
Scheme 1. Synthetic route of the compounds. Reagents and conditions: (i) K_2CO_3, DMSO, ultrasonic irradiation, (ii) CH_3COOH_{cat}, MeOH, reflux

reported in Table 1. As can be seen, the best antimycobacterial activity was obtained by compound **2f** (MIC= 73.31 µM) in the series. **2f** possessed a methylsulfonyl group that is an electron acceptor moiety connected to the phenyl ring. However, the introduction of electron acceptor groups (COOH, CN, NO_2) other than methylsulfonyl moiety to the phenyl ring deteriorated antimycobacterial activity. Furthermore, replacing the methylsulfonyl moiety with sulfamoyl reduced the antimycobacterial activity of **2e** (MIC= 146.20 µM). In the case of nitro-substituted compounds (**2g** and **2h**), increasing the number of nitro groups on the phenyl ring did not improve the antimycobacterial activity. It was interesting that methoxy-substituted compound **2b** showed antimycobacterial activity similar to that of **2f**, independent of electronic properties of substituents in the series.

CONCLUSIONS

In conclusions, a series of 1,2,4-triazole-containing hydrazone compounds were synthesized as potential antimycobacterial agents. The biological assay results showed that the methylsulfonyl-substituted derivative **2f** showed the highest antimycobacterial activity in the series. Based on the preliminary results, compound **2f** was considered a lead antimycobacterial compound for further optimization.

Conflict of Interest: No conflict of interest was declared by the authors

REFERENCES

1. Zhenkun MA, Lienhardt C, McIlleron H, Nunn AJ, Wang X. Global tuberculosis drug development pipeline: the need and the reality. Lancet. 2010;375:2100-2109.

2. World Health Organization (WHO) – Global Tuberculosis Report 2017. Available at http://www.who.int/tb/publications/global_report/en/

3. Saltini C. Chemotherapy and diagnosis of tuberculosis. Respir Med. 2006;100:2085-2097.

4. Tiberi S, Scardigli A, Centis R, D'Ambrosio L, Muñoz-Torrico M, Salazar-Lezama MÁ, Spanevello A, Visca D, Zumla A, Migliori GB, Caminero Luna JA. Classifying new anti-tuberculosis drugs: rationale and future perspectives. Int J Infect Dis. 2017;56:181-184.

5. Hoagland DT, Liu J, Lee RB, Lee RE. New agents for the treatment of drug-resistant *Mycobacterium tuberculosis*. Adv Drug Deliv Rev. 2016;102:55-72.

6. Ahmad S, Mokaddas E. Current status and future trends in the diagnosis and treatment of drug-susceptible and multidrug-resistant tuberculosis. J Infect Public Health. 2014;7:75-91.

7. Franke MF, Becerra MC, Tierney DB, Rich ML, Bonilla C, Bayona J, McLaughlin MM, Mitnick CD. Counting pyrazinamide in regimens for multidrug-resistant tuberculosis. Ann Am Thorac Soc. 2015;12:674-679.

8. Kuaban C, Noeske J, Rieder HL, Aït-Khaled N, Abena Foe JL, Trébucq A. High effectiveness of a 12-month regimen for MDR-TB patients in Cameroon. Int J Tuberc Lung Dis. 2015;19:517-524.

9. Van Deun A, Maug AKJ, Salim MAH, Das PK, Sarker MR, Daru P, Rieder HL. Short, highly effective, and inexpensive standardized treatment of multidrug-resistant tuberculosis. Am J Respir Crit Care Med. 2010;182:684-692.

10. Wallis RS, Maeurer M, Mwaba P, Chakaya J, Rustomjee R, Migliori GB, Marais B, Schito M, Churchyard G, Swaminathan S, Hoelscher M, Zumla A. Tuberculosis—advances in development of new drugs, treatment regimens, host-directed therapies, and biomarkers. Lancet Infect Dis. 2016;16:e34-e46.

11. Jones D. Tuberculosis success. Nat Rev Drug Discov. 2013;12:175-176.

12. Skripconoka V, Danilovits M, Pehme L, Tomson T, Skenders G, Kummik T, Cirule A, Leimane V, Kurve A, Levina K, Geiter LJ, Manissero D, Wells CD. Delamanid improves outcomes and reduces mortality in multidrug-resistant tuberculosis. Eur Respir J. 2013;41:1393-1400.

13. Kumar K, Abubakar I. Clinical implications of the global multidrug-resistant tuberculosis epidemic. Clin Med (Northfield Il). 2015;15(Suppl6):s37-s42.

14. Cochrane JR, White JM, Wille U, Hutton CA. Total synthesis of mycocyclosin. Org Lett. 2012;14:2402-2405.

15. Podust LM, Ouellet H, von Kries JP, de Montellano PRO. Interaction of *Mycobacterium tuberculosis* CYP130 with heterocyclic arylamines. J Biol Chem. 2009;284:25211-25219.

16. Ahmad Z, Sharma S, Khuller GK, Singh P, Faujdar J, Katoch VM. Antimycobacterial activity of econazole against multidrug-resistant strains of *Mycobacterium tuberculosis*. Int J Antimicrob Agents. 2006;28:543-544.

17. Podust LM, Poulos TL, Waterman MR. Crystal structure of cytochrome P450 14-sterol demethylase (CYP51) from *Mycobacterium tuberculosis* in complex with azole inhibitors. Proc Natl Acad Sci. 2001;98:3068-3073.

18. Koçyiğit-Kaymakçıoğlu B, Ünsalan S, Küçükgüzel SG, Şener G, Rollas S. HPLC analysis of in vivo metabolites of 4-nitrobenzoic acid [(5-nitro-2-thiopheneyl)methylene]hydrazide in rats. Eur J Drug Metab Pharmacokinet. 2007;32:197-203.

19. Gülerman NN, Oruç EE, Kartal F, Rollas S. In vivo metabolism of 4-fluorobenzoic acid [(5-nitro-2-furanyl) methylene] hydrazide in rats. Eur J Drug Metab Pharmacokinet. 2000;25:103-108.

20. Kaymakçıoğlu BK, Aktan Y, Süzen S, Gökhan N, Koyunoğlu S, Erol K, Yeşilada A, Rollas S. In vivo metabolism of 2-[1′-phenyl-3′-(3-chlorophenyl)-2′-propenylyden]hydraz   ino-3-methyl-4(3H)-quinazolinone in rats. Eur J Drug Metab Pharmacokinet. 2005;30:255-260.

21. Savini L, Chiasserini L, Gaeta A, Pellerano C. Synthesis and anti-tubercular evaluation of 4-quinolylhydrazones. Bioorg Med Chem. 2002;10:2193-2198.

22. Sonar VN, Crooks PA. Synthesis and antitubercular activity of a series of hydrazone and nitrovinyl analogs derived from heterocyclic aldehydes. J Enzyme Inhib Med Chem. 2009;24:117-124.

23. Ferreira ML, Candea ALP, Henriques MGMO, Kaiser CR, Lima CHS, De Souza MVN. Synthesis and cytotoxic evaluation of disubstituted N-acylhydrazones pyrazinecarbohydrazide derivatives. Lett Drug Des Discov. 2010;7:275-280.

24. Collins LA, Franzblau SG. Microplate alamar blue assay versus BACTEC 460 system for high-throughput screening of compounds against *Mycobacterium tuberculosis* and *Mycobacterium avium*. Antimicrob Agents Chemother. 1997;41:1004-1009.

25. Mečiarová M, Toma Š, Magdolen P. Ultrasound effect on the aromatic nucleophilic substitution reactions on some haloarenes. Ultrason Sonochem. 2003;10:265-270.

ORIGINAL ARTICLE

Flavonoids Isolated from *Vitex grandifolia*, an Underutilized Vegetable, Exert Monoamine A & B Inhibitory and Anti-inflammatory Effects and Their Structure-activity Relationship

Az Kullanılan Bir Bitki, *Vitex grandifolia*'dan İzole Edilen Flavonoidlerin Monoamin A & B İnhibitör ve Anti-enflamatuvar Etkileri ve Yapı-aktivite İlişkisi

ⓘ Oluwasesan M. BELLO[1,2]*, ⓘ Abiodun B. OGBESEJANA[1], ⓘ Charles Oluwaseun ADETUNJI[3], ⓘ Stephen O. OGUNTOYE[2]

[1]Federal University Dutsin-Ma, Department of Applied Chemistry, Katsina State, Nigeria
[2]University of Ilorin, Department of Chemistry, Kwara State, Nigeria
[3]Edo University Iyamho, Department of Microbiology, Applied Microbiology, Biotechnology and Nanotechnology Laboratory, KM [7], Auchi-Abuja Road, Iyamho, Edo State, Nigeria

ABSTRACT

Objectives: *Vitex grandifolia* belongs to family Lamiaceae; it consists of flowering plants and it is also called the mint family. The Yoruba people of southwest Nigeria called it "Oriri" or "Efo oriri". This plant is classified as an underutilized vegetable and little is known about its phytochemistry or its biological evaluations.

Materials and Methods: Methanol extracts of the dried leaves and stem of the plant were subjected to fractionation and isolation using vacuum layer and column chromatography methods. The structures of the compounds were elucidated using spectroscopic techniques including IR, 1D-, and 2D-NMR and by comparison with the data reported in the literature. They were evaluated *in vitro* for the inhibition of monoamine recombinant human MAO-A and -B and anti-inflammatory activities.

Results: Three known flavonoids were isolated from the methanolic extract of the leaves of *V. grandifolia* for the first time to the best of our knowledge, i.e. isoorientin **(1)**, orientin **(2)**, and isovitexin **(3)**. Most of the isolated compounds showed selective inhibition of monoamine oxidase B, inhibition of MAO-B by isoorientin **(1)** and orientin **(2)** were 9-fold more potent (IC$_{50}$ (µg/mL) of 11.08 and 11.04) compared to the inhibition of MAO-A (IC$_{50}$ (µg/mL) of >100), while clorgyline and deprenyl were used as positive standards. The isolated flavonoids displayed good activity against the NF-κb assay with IC$_{50}$ (µg/mL) of 8.9, 12, and 18. This study establishes a link between the structure and the biological activities on the basis of the different patterns of substitution, particularly the C2=C3 double bond and the position of glucose moiety.

Conclusion: This study is the first to establish the phytochemistry of the polar part of *V. grandifolia* and the anti-inflammatory and neuroprotective role of these isolated compounds.

Key words: *Vitex grandifolia*, underutilized vegetable, lupeol, MAO-A and B, neurodegenerative

ÖZ

Amaç: *Vitex grandifolia*, Lamiaceae familyasına aittir; çiçekli bitkilerden oluşur ve aynı zamanda nane ailesi olarak da bilinir. Güneybatı Nijerya'daki Yoruba halkı bitkiyi "Oriri" veya "Efo oriri" olarak adlandırmaktadır. Bu bitki az kullanılan bir bitki olarak sınıflandırılır ve fitokimyası veya biyolojik etkileri hakkında çok az bilgi bulunmaktadır.

Gereç ve Yöntemler: Kurutulmuş yaprak ve gövdelerden hazırlanan metanol ekstreleri üzerinde, vakum ve açık kolon kromatografisi metotları kullanılarak fraksiyonlama ve izolasyon çalışmaları yapılmıştır. Bileşiklerin yapıları, IR, 1D- ve 2D-NMR teknikleri kullanılarak ve literatürdeki verilerle

karşılaştırılarak aydınlatılmıştır. Bileşikler, monoamin rekombinant insan MAO-A ve -B inhibisyonu ve anti-enflamatuvar aktiviteleri yönünden *in vitro* olarak değerlendirilmiştir.

Bulgular: *V. grandifolia*'nın yapraklarının metanollü ekstresinden bilinen üç flavonoid bileşiği izoorientin **(1)**, orientin **(2)** ve isoviteksin **(3)** ilk kez izole edilmiştir. İzole edilen bileşiklerin çoğu, monoamin oksidaz B'ye karşı seçici inhibisyon etki göstermiştir, MAO-B'nin izoorientin **(1)** ve orientin **(2)** tarafından inhibisyonu (IC_{50} (µg/mL), 11.08 ve 11.04), MAO-A'nın inhibisyonuna (IC_{50} (µg/mL) >100) kıyasla 9 kat daha etkili bulunmuştur. Kloril ve deprenil pozitif standartlar olarak kullanılmıştır. İzole edilen flavonoiler NF-ϰb testine karşı 8.9, 12 ve 18 IC_{50} (µg/mL) değerleri ile yüksek aktivite göstermiştir. Bu çalışma, yapıdaki değişik sübstitüsyonlara, özellikle C2=C3 arasındaki çifte bağ ve glukozun konumuna bağlı olarak yapı ile biyolojik aktivite arasında bir bağlantının olduğunu ortaya koymuştur.

Sonuç: Bu çalışma *V. grandifolia*'nın polar fraksiyonunun fitokimyasal profilini ortaya koyan ve izole edilen bileşiklerin anti-enflamatuvar etkisini ve nöroprotektif rolünü gösteren ilk çalışmadır.

Anahtar kelimeler: *Vitex grandifolia*, az kullanılan bitki, lupeol, MAO-A ve B, nörodejeneratif

INTRODUCTION

Pathological and neurodegenerative paths, cancer, and Alzheimer, coronary and Parkinson diseases are the result of free radical-mediated reactions and reactive oxygen species from the human body.[1,2] In the many epidemiological studies carried out, it was discovered that there is a strong connection between people whose diets are rich in fresh fruits and leafy vegetables and low incidence of cardiovascular diseases, neurodegenerative diseases, and some particular forms of cancer.[3] Many studies and investigations have been dedicated to the antioxidant effects of compounds in fruits, medicinal plants, and vegetables so as to improve human health and regulate physiological functions. Monoamine oxidases (MAO-A and MAO-B) are mitochondrial enzymes that oxidatively deaminate monoaminergic neurotransmitters and (potentially harmful) dietary monoamines. Their major purpose is the regulation of noradrenaline, dopamine, serotonin, and adrenaline in the brain.[4] The study of MAO-A and -B has been of significant pharmacological attention recently and their inhibitors (MAOIs) have found extensive medical use for the management of numerous neurological and psychiatric maladies. These enzymes remove as well as catalyze exogenous amines. The MAO-A inhibitors are important in managing anxiety and depression while the MAO-B inhibitors are effective in inhibiting and treating Alzheimer and Parkinson diseases.[5-7]

Medicinal plants, i.e. vegetables, botanical extracts, and herbal products from natural sources, have been viewed as an important and primary basis for MAOs' inhibitors and this validates the cultural application of many botanicals as substitutes for the management of depression, Parkinson disease, and other neuropsychiatric as well as neurological disorders.[8] Flavonoids as secondary metabolites are one of the most popular polyphenols present in medicinal plants, they are broadly distributed in many plant species, and they can be found in various parts of these plants, i.e. bark, flowers, fruits, leaves and stems.[9-12] Flavonoids have been reported to display a large variety of biological activities; some of these are antioxidants and enzyme inhibitors, while others have anti-inflammatory, anticancer, antihyperglycemic, and hepatoprotective activities.[13-16]

In recent times, research on medicinal plants has globally increased tremendously, and volumes of reputable evidence have been gathered to portray the enormous prospects of medicinal plants used in traditional systems.[17,18] Many of these herbal plants have been identified and studied using current scientific methods, and the results revealed the immense promise of medicinal plants in the field of medical science.[19] *Vitex grandifolia*, which belongs to the family *Lamiaceae*, bears fruit that is edible and used to make an alcoholic drink by the locals, while the bark is used to treat stomachache, diarrhea, bronchial complaints, rickets, sores, and fever. It is also used in the treatment of colic, infections of the umbilical cord, toothache, rheumatism, and orchitis. Epidi and Odili[20] (2009) reported the biocidal effect of the powdered leaf of *V. grandifolia* against *Tribolium castaneum* in stored groundnut *Arachis hypogaea*. The plant is a shrub or small tree about 10-12 cm in length and 5-7 cm in width, trunk to 60 cm girth, bearing a spreading crown, in high deciduous forest or secondary jungle. Local names of this plant species are Oori ọdan (Yoruba, Nigeria), ofonma (Egun, Republic of Benin), and ofofrin (Setangun, Republic of Benin).[21] Surprisingly, this plant's phytochemistry has not being looked into although it is a vegetable. Thus, its study and that of the isolated compounds, i.e. biological activities from this plant, will be considered worthwhile. Hence, the present study reports the isolation, characterization, and *in vitro* inhibition of MAO-A and -B of the constituents from polar extract of *V. grandifolia*.

MATERIALS AND METHODS

Collection of plant samples

The leaves with the stem of *V. grandifolia* was collected in April-October 2015 from Ilorin metropolis, Kwara State, Nigeria. The collected plant was identified by a taxonomic botanist in the department of Plant Biology, University of Ilorin, Ilorin, where a voucher number was obtained after the deposit of the specimen. The leaves and stem were air dried, powdered, and stored for further analysis.

Extraction of the plant materials

The air-dried and powdered plant material was defatted with hexane and then was prepared by maceration (1.5 kg) with 7 L of methanol (MeOH) at ambient temperature for 24 h. The process was repeated three times, and the filtrates were combined and evaporated under vacuum to dryness.

General experimental procedure

Precoated TLC plates (AluO); Silica gel 60 F_{254}; layer thickness 0.25 mm (Merck). Precoated TLC plates (Glass); RP-18 F_{254};

layer thickness 0.25 mm (Merck); Silica gel 60; 40-63 µm mesh size (Merck); RP-18; 40-63 µm mesh size; Sephadex LH 20; 25-100 µm mesh size (Merck). Silica gel 60 and RP C-18, Diaion HP-20 was used for column chromatography. ^{1}H NMR, ^{13}C NMR, and 2D NMR were recorded on 400, 500, and 600 (MHz) instruments (Agilent and Bruker Inc., California, USA). Chemical shifts were expressed in parts per million (δ) using TMS as internal standard. Values of coupling constant *J* are reported in Hz. Infrared spectroscopy was performed using a PerkinElmer FT-IR Spectrum Two spectrometer and the masses of the compounds were determined using an Agilent 1260 liquid chromatography system (Agilent, USA) equipped with a quaternary solvent delivery system, and a Triple quad 6410 MS system and Agilent Technologies 6540 UHD Accurate Mass Q-TOF liquid chromatography-mass spectrometer (Agilent, USA).

Fractionation and isolation

The extract of *V. grandifolia* was defatted using hexane and then extracted with MeOH. MeOH extract of *V. grandifolia* was added to reverse phase silica gel (RP-18) using vacuum layer chromatography (VLC) for fractionation. Water with increasing MeOH was used as eluting solvent and the eluates were collected and concentrated on a Rotavapor. TLC was used to check and monitor the isolates and combine the eluates. Eleven fractions were obtained; the first fraction (H_2O only) was picked for further fractionation because the TLC revealed promising compounds. This fraction was subjected to a Diaion HP-20 column for isolation. The column was eluted with water first and then with increasing MeOH and the eluates were collected and concentrated. Twelve fractions were obtained. All fractions were collected, concentrated, and monitored by TLC. The eighth fraction was loaded onto the column in CH_3Cl using 65:35:10 (CH_3Cl: MeOH: H_2O) as eluting solvent. Six fractions were obtained; the third fraction gave compound **3**, which was purified using CC in CH_3Cl with 65:35:10 (CH_3Cl: MeOH: H_2O) as eluting solvent. Fractions 1 and 2 were combined using TLC and two compounds (**1** and **2**) were isolated from the first fraction after further purification with CC in CH_3Cl with 8:2:0.5 (CH_3Cl: MeOH: H_2O) as eluting solvent. Compounds **1** (19 mg), **2** (14.7 mg) and **3** (10.5 mg) (Figure 1) were isolated in pure form after purification.

Monoamine oxidase inhibition assays (MAO)

To evaluate the outcome of the isolated compounds from *V. grandifolia* on MAO-A and MAO-B, the kynuramine deamination assay was used for 96-well plates as expressed previously.[22] The method used was adapted from the reported literature.[23,24] The isolated constituents did not display any interference with fluorescence measurement, but clorgyline and deprenyl were used as positive controls for the experiment.

Anti-inflammatory activity

Inhibition of iNOS activity

The assay was performed using mouse macrophages 915 (RAW 264.7, obtained from ATCC). Cells were cultured in phenol 916 red

free RPMI medium supplemented with 10% bovine calf serum, 100 U/mL penicillin G sodium, and 100 µg/mL streptomycin at 37°C in an atmosphere of 5% CO_2 and 95% humidity. Cells were seeded in 96-well plates at 5×10^4 cells/well and incubated for 24 h. Test compounds diluted in serum-free medium were added to the cells. After 30 min of incubation, LPS (5 µg/mL) was added and the cells were further incubated for 24 h. The concentration of nitric oxide (NO) was determined by measuring the level of nitrite released in the cell culture supernatant using Griess reagent.[25] Percent inhibition of nitrite production by the test compound was calculated in comparison to the vehicle control. IC_{50} values were obtained from dose curves. Parthenolide was used as a positive control.[26,27]

Inhibition of NF-κB activity

The assay was performed in human chondrosarcoma (SW1353, obtained from ATCC) cells as described earlier. Cells were cultured in 1:1 mixture of DMEM/F12 supplemented with 10% FBS, 100 U/mL penicillin G sodium, and 100 µg/mL streptomycin at 37°C in an atmosphere of 5% CO_2 and 95% humidity. Cells (1.2×10^7) were washed once in an antibiotic and FBS-free DMEM/F12, and then reintroduced in 500 µL of antibiotic-free DMEM/F12 containing 2.5% FBS. NF-κB luciferase plasmid construct was added to the cell suspension at a concentration of 50 µg/mL and incubated for 5 min at room temperature. The cells were electroporated at 160 V and one 70-ms pulse using BTX disposable cuvettes, model 640 (4-mm gap), in a BTX Electro Square Porator T 820 (BTX I, San Diego, CA, USA). After electroporation, cells were plated onto the wells of 96-well plates at a density of 1.25×10^5 cells per well. After 24 h, cells were treated with different concentrations of test compound for 30 min prior to the addition of PMA (70 ng/mL) and incubated for 8 h. Luciferase activity was measured using the Luciferase Assay kit (Promega). Light output was detected on a Spectra-Max plate reader. Percent inhibition of luciferase activity was calculated as compared to vehicle control and IC_{50} values were obtained from dose curves. Sp-1 was used as a control transcription factor that is unresponsive to inflammatory mediators (such as PMA). This is useful in detecting agents that nonspecifically inhibit luciferase expression due to cytotoxicity or inhibition of luciferase enzyme activity.[27]
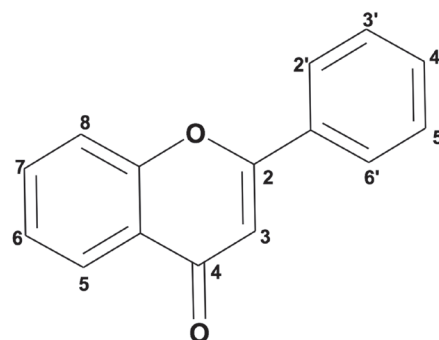

Figure 1. Basic skeleton or structure of flavonoids

RESULTS

MAO-A and -B

Most of the isolated compounds showed selective inhibition of either MAO-A or MAO-B as shown in Table 1. The inhibition of MAO-B by both isoorientin (**1**) and orientin (**2**), two of the flavonoids isolated from *V. grandifolia*, was 9-fold more potent (IC_{50} (µg/mL) of 11.08 and 11.04) compared to the inhibition of MAO-A (IC_{50} (µg/mL) of >100). Isovitexin (**3**), a flavonoid isolated from this wild vegetable for the first time displayed fair selective activity against MAO-A (IC_{50} (µg/mL) of >100) to MAO-B (IC_{50} (µg/mL) of 21.3) like the other two flavonoids, while clorgyline and deprenyl were used as positive standards.

Anti-inflammation

The isolated flavonoids, i.e. isoorientin (**1**), orientin (**2**), and isovitexin (**3**), from *V. grandifolia* displayed good activity against the NF-κb assay (IC_{50} (µg/mL) of 8.9, 12, and 18), although orientin (**2**) showed moderate activity against the Sp-1 assay with IC_{50} of 23 µg/mL, while the others displayed poor activity when compared with the positive standard with IC_{50} of 8 µg/mL as shown in Table 2. Isovitexin (**3**) exhibited moderate activity against the iNOS assay, while the others, i.e. isoorientin (**1**) and orientin (**2**), displayed poor activity with IC_{50} of 48 and 54 µg/mL. The positive standard used in this study was parthenolide.

Isolated compounds

Compound 1

Compound **1** (Figure 1) was isolated as a yellow solid. Its molecular formula was deduced to be $C_{21}H_{20}O_{11}$ from a combination of ^1H NMR and ^{13}C NMR data. ^1H NMR (600 MHz, DMSO-d6) d: 13.2 (1H, brs, 5-OH), 7.55 (1H, *dd*, *J*=2.5, 9.0 Hz, 60-H), 7.45 (1H, *d*, *J*=2.5 Hz, 20-H), 6.85 (1H, *d*, *J* =9.0 Hz, 50-H),

Table 1. IC₅₀ values of isolated compounds as MAO-A and -B inhibitory agents

	Sample name	MAO-A (IC_{50})	MAO-B (IC_{50})
1	Isoorientin (1)	>100	11.08
2	Orientin (2)	>100	11.04
3	Isovitexin (3)	>100	21.3
4	Clorgyline	1.6	NT
5	Deprenyl	NT	0.48

Table 2. IC₅₀ values of isolated compounds as anti-inflammatory agents

	Test compounds	NF-κB	SP-1	iNOS	% Cell death at the highest conc (100 µg/mL)
1	Isoorientin (1)	8.9	63	48	63.89
2	Orientin (2)	12	23	54	
3	Isovitexin (3)	18	41	21	
4	Parthenolide	0.9	6.5	0.18	
5	Parthenolide	0.6	8	0.15	

6.63 (1H, s, 3-H), 4.7 (1H, *d*, *J*=9.7 Hz, 100-H). ^{13}C NMR (150 MHz, DMSO-d6) d: 163.24 (C-2), 102.68 (C-3), 182.32 (C-4), 160.74 (C-5), 108.88 (C-6), 164.41 (C-7), 98.53 (C-8), 156.36 (C-9), 102.68 (C-10), 122.24 (C-1′), 114.34 (C-2′), 146.22 (C-3′), 150.16 (C-4′), 116.00 (C-5′), 119.71 (C-6′), 73.76 (C-1″), 70.13 (C-2″), 79.12 (C-3″), 70.06 (C-4″), 82.35 (C-5″), 62.01 (C-6″). Compound **1** was identified as isoorientin, by NMR analysis and comparison with its literature data.[28]

Compound 2

Compound **2** (Figure 1) was obtained as a yellow solid. Its molecular formula was deduced to be $C_{21}H_{20}O_{11}$ from a combination of ^1H NMR and ^{13}C NMR data. ^1H NMR (400 MHz, DMSO-d6) d: 3.22-3.88 (6H, m, glucosyl-H), 4.69 (1H, *d*, *J* =9.9 Hz, H-1″), 6.25 (1H, s, H-6), 6.64 (1H, s, H-3), 6.86 (1H, *d*, *J* = 8.4 Hz, H-5′), 6.86 (1H, *dd*, *J*=2, 8.4), 7.48 (1H, *d*, *J*=2.0 Hz, H-2′), 7.54 (1H, *dd*, *J*=2.0, 8.4 Hz, H-6′), 13.20 (1H, s, 5-OH). ^{13}C NMR (100 MHz, DMSO-d6) d: 164.4 (C-2), 102.7 (C-3), 182.3 (C-4), 160.74 (C-5), 98.53 (C-6), 163.24 (C-7), 104.91 (C-8), 156.86 (C-9), 104.28 (C-10), 122.24 (C-1′), 114.34 (C-2′), 146.22 (C-3′), 150.16 (C-4′), 116.00 (C-5′), 119.71 (C-6′), 73.76 (C-1″), 71.13 (C-2″), 79.12 (C-3″), 71.06 (C-4″), 82.35 (C-5″), 62.04 (C-6″). Compound **2** was identified as orientin by NMR analysis and comparison with its literature data.[29]

Compound 3

Compound **3** (Figure 1) (19 mg) was isolated as a yellow amorphous powder and the melting point is 219-221°C; IR v max (cm⁻¹): 3320 (-OH), 1697 (C=O), 1645 (C=O); the molecular formula was deduced to be $C_{21}H_{19}O_{10}$ from a combination of ^1H NMR and ^{13}C NMR data. ^1H NMR (DMSO-d6): δ_H : 13.55 (1H, brs, 5-OH), 7.93 (2H, *d*, *J*=8.8 Hz, 3′, 5′ -H), 6.93 (2H, *d*, *J* = 8.4 Hz, 2′, 6′ -H), 6.78 (1H, s, 3-H), 6.51 (1H, s, 8-H), 4.55 (1H, *d*, *J*=9.8 Hz, 1″- H), 3.11-4.03 (6H, m, glucosyl-H). ^{13}C NMR (500 MHz, DMSO-d6) δ_C: 164.36 (C-2), 104.25 (C-3), 182.81 (C-4), 161.52 (C-5), 109.75 (C-6), 164.17 (C7), 94.48 (C-8), 157.08 (C-9), 103.65 (C-10), 121.96 (C-1′), 129.34 (C-2′, 6′), 116.84 (C-3′, 5′), 162.04 (C-4′), 73.91 (C1″), 71.47 (C-2″), 79.80 (C-3″), 71.06 (C-4″), 82.46 (C-5″), 62.34 (C-6″). Compound **3** was identified as isovitexin by NMR analysis and comparison with its literature data.[30-32]

Structure–activity relationship

Anti-inflammatory activity

The following preliminary structure–activity relationship (SAR) profile is proposed based on the anti-inflammatory effects of the flavonoids that were isolated from *V. grandifolia*; these are summarized as the following: (a) the $C_2=C_3$ double bond might contribute to the activity of these flavonoids as anti-inflammatory agents; Wang et al.[33] reported that the $C_2=C_3$ double bond might contribute to molecular planarity, and this was discovered from the more significant anti-inflammatory effect displayed by diosmetin than hesperetin, and its nonexistence ($C_2=C_3$ double bond) resulted in a greater volume/ratio;[34] (b) Hydroxylation substitution (-OH) noted at both C-3′ and 4′, i.e. tertiary increases activity especially at ring B moiety, i.e. isoorientin (**1**), orientin (**2**); Wang et al.[33] reported the hydroxylation pattern, its importance in C- 3′-hydroxylation in

the case of fisetin and 5-hydroxylation in the case of isoflavones gives significant effects for inducing cell delineation (apigenin vs. chrysin) especially ring B moiety;[34] (c) the position of the sugar moiety and glycosides on ring A gives better anti-inflammatory activity than on rings B and C; Isoda et al. gave an assessment that glycosides with significant hydrophilicity displayed lower anti-inflammatory activity, which may be due to lower hydrophobicity as well as steric interference, lessening membrane permeability.[35]

MAO-A and -B

The following preliminary SAR profile is proposed based on the inhibitory effects of the flavonoids against MAO-A and -B isolated from *V. grandifolia*; these are summarized as follows: (a) Hydroxylation substitution pattern (-OH) noted at both C-3′ and 4′, i.e. tertiary increases inhibitory activity of MAO-A and -B mostly at ring B moiety, i.e. isoorientin (**1**) and orientin (**2**) (Figure 2) but reduced activity was noted in isovitexin (**3**) (Figure 2), although Spencer et al. attested to the fact that both unsaturation degree of the $C_2=C_3$ double bond and the hydroxylation pattern on ring B moiety have great significant on the anti-neurodegenerative effects on flavonoids in general.[36]

DISCUSSION

Compounds **1-3** (Figure 2) were known based on their 1D and 2D NMR and by comparison of their NMR data with those reported in the literature.[28,29] Isoorientin (**1**), orientin (**2**), and isovitexin (**3**) were isolated from *V. grandifolia* for the first time to the best of our knowledge. The observation in the UV spectrum was an indication of the presence of hydroxyl groups at C-4′, C-5, and C-7. Compound **1** showed hydroxyl (3376 cm⁻¹), carbonyl (1660 cm⁻¹), and aromatic groups C=C, CH_2, and C-H bending at 1561, 1446, 845, and 800 cm⁻¹ absorptions in its IR spectrum. The ¹H NMR spectrum of compound **1** indicated that B ring protons H-2′ and H-6′ gave a multiplet at δ 7.80 and an H-5′ proton signal was observed at 6.8 ppm as a doublet (*J*=9 Hz). H-8 and H-3 protons were at δ 6.75 (1H, s) and δ 6.25 (1H, s), respectively. An anomeric proton was observed at δ 4.93 (1H, *d*, *J*=7 Hz, C-glucosyl H-1″) and sugar proton signals overlapped at δ 3.5-4.8. The spectroscopic results correlated well to the reported data; hence compound **1** is isoorientin. The complete ¹H and ¹³C NMR assignments of compound **2** were

conducted by a combination of ¹H, ¹³C, ¹³C DEPT, COSY, HSQC, and HMBC experiments and by comparing with assignments published in the literature as orientin. The presence of a -OH group at C-5′ and C-4′ in flavonoid was confirmed. In the ¹³C NMR spectrum, **2** displayed one anomeric carbon signal at δ 104.8 and other sugar moiety signals due to glucopyranoside, indicating that there was one glucose unit. The UV spectrum in MeOH showed absorption at 345 nm, which is a characteristic absorption of orientin.[37-39] Compound **3** was elucidated by a combination of ¹H, ¹³C, ¹³C DEPT, COSY, HSQC, and HMBC experiments and by comparing with assignments previously reported for isovitexin.[40,41] The UV spectrum of compound **2** was an indication of hydroxyl groups at C-4′, C-5, and C-7 because of the presence of a bathochromic shift with NaOMe, NaOAc, and $AlCl_3$/HCl in its UV spectrum. The IR spectrum of compound **3** showed absorptions at 3440 cm⁻¹ (OH), 1660 cm⁻¹ (C=O), 1620 cm⁻¹ (C=C), 1523, 1475 cm⁻¹ (aromatic group), and 1017 cm⁻¹ (C-O). The ¹H NMR spectrum of compound **3** showed six aromatic proton resonances from δ 6 to 8. A set of four AA′BB′ proton signals at δ 7.62 (2H, *d*, *J*=8 Hz, H-2′ and H-6′) and 6.84 (2H, *d*, *J*=8 Hz, H-3′, H-5′) were located on ring B, and H-8 and H-3 protons were observed as singlets at δ 6.5 (1H) and 6.25 (1H), respectively. The anomeric proton showed a doublet at 4.88 ppm (1H, *d*, *J*=8 Hz, glucosyl H-1″). Sugar proton signals overlapped at 3.5-4.7 ppm. This ion was formed by the loss of $C_5H_{10}O_5$ from the molecular ion. On the basis of UV, IR, NMR, and EI mass data, which correlated with the literature, compound **3** was identified as isovitexin.

Extracts and concoctions from medicinal plants still play vital functions in managing primary health requirements in most developing countries. Most of the world's population (80%) depends on these herbs and botanicals as reported by the World Health Organization, and there are active chemical constituents present in these plants responsible for the biological activity.[42] It is therefore of immense concern to evaluate these plants in order to validate their employment in old-age medicine and to reveal the secondary metabolites responsible for pharmacological activity. Most of these medicinal plants reportedly contain flavonoids. Various flavonoids have been isolated from such, i.e. apigenin, galangin, kaempferol, quercetin, luteolin, naringenin, and other flavonoids, and many
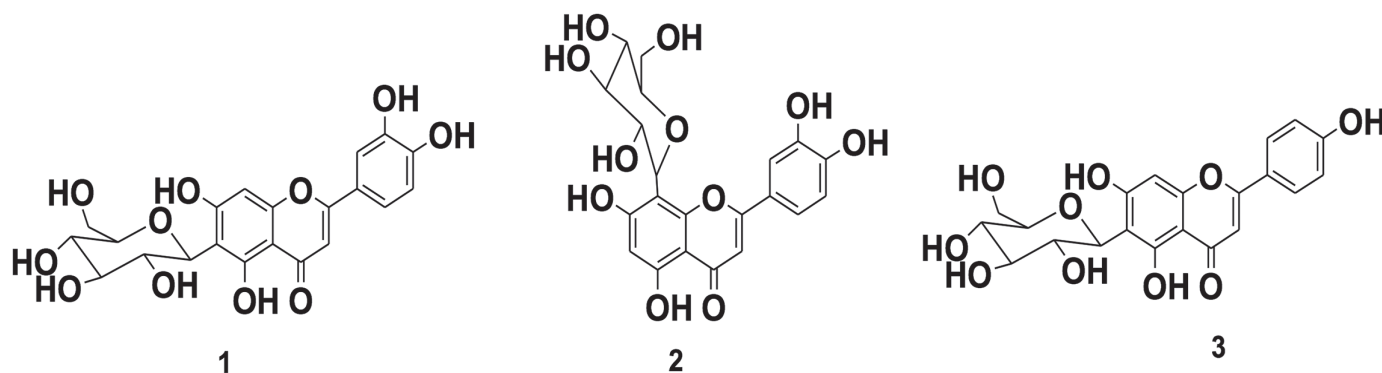

Figure 2. Isolated flavonoids from *Vitex grandifolia*

are MAO inhibitors.[43] Zarmouh et al.[44] reported the selective MAO-B inhibitors of isolated compounds from the ethanolic extract of *Psoralea corylifolia* seeds, a medicinal plants known for its antiaging effects. In that work, human recombinant MAO-B and MAO-A iso-enzymes were employed for the inhibition of enzymes studies. The authors discovered that, out of the eight compounds isolated, only two flavonoids, i.e. bavachinin and genistein, showed significant selectivity of MAO-B inhibition; these two flavonoids showed significant reduction in H_2O_2 produced by MAO-B as compared to MAO-A.[44] Lee et al.[45] isolated four flavonoids, namely isoquercitrin, quercitrin, quercetin, and rutin from the leaves of *Melastoma candidum* D. Don for the first time. These flavonoids displayed selective inhibitory activity against MAO-B with IC_{50} values of 19.06, 11.64, 3.89, and 10.89 μM, respectively.[45] Monoamine oxidase inhibitors (MAOIs) differ by their selectivity of the MAO receptor. Some MAOIs inhibit both MAO-A and MAO-B equally. Other MAOIs have been developed and found to target one over the other.[46] Some studies here corroborate our work that some flavonoids from natural sources can selectively inhibit MAO-B.

CONCLUSION

There is growing attention on the assessment of medicinal plants especially for inhibition of MAO, owing to the likely daily and cultural use as food and vegetables. Chemical constituents in medicinal plants help in the management of disorders associated with the nervous system together with their likely connections with medicines and the diet abundant in dietary monoamines. The present study ascertained that the isolated compounds from *V. grandifolia* are moderate MAO-B inhibitors, and this result could be of importance for better application of this wild vegetable in traditional neuropharmacological use. The use of *V. grandifolia* as a vegetable is widely accepted although tagged as a "poor man's" food, and this study hopes to promote its pivotal role as a source for the development of nutraceutical products. No work or study has reported the inhibition of MAO-A and -B by constituents of this plant with anti-inflammatory activity.

Conflict of Interest: No conflict of interest was declared by the authors

REFERENCES

1. Ames BN, Shigenaga MK, Hagen TM. Oxidants, antioxidants and degenerative diseases of aging. Proc Natl Acad Sci. 1993;90:7915-7922.

2. Shih JC, Chen K, Ridd MJ. Monoamine oxidase: From genes to behaviour. Annu Rev Neurosci. 1999;22:197-217.

3. Salah N, Miller NJ, Paganga G, Tijburg L, Bolwell GP, Rice-Evans C. Polyphenolic flavanols as scavengers of aqueous phase radicals and as chain breaking antioxidants. Arch Biochem Biophy. 1995;322:339-346.

4. Liu YH, Wu WC, Lu YL, Lai YJ, Hou WC. Antioxidant and amine oxidase inhibitory activities of *Hydroxyurea*. Biosci Biotech Biochem. 2010:74:1256-1260.

5. Silverman RB, Ding CZ, Gates KS. Design and mechanism of monoamine oxidase inactivators from an organic chemical perspective. In: Testa B, Kyburz E, Fuhrer W, Giger R, eds. Perspectives in Medicinal Chemistry.

6. Kanazawa I. Short review on monoamine oxidase and its inhibitors. European Neurology. 1994;34:36-39.

7. Abell CW, Kwan SW. Molecular characterization of monoamine oxidase A and B. Prog Nucleic Acids Res Mol Biol. 2009;65:129-156.

8. Viña J, Sastre J, Pallardó F, Borrás C. Mitochondrial theory of aging: importance to explain why females live longer than males. Antioxid Red Signal. 2003;5:549-556.

9. Bratkov VM, Shkondrov AM, Zdraveva PK, Krasteva IN. Flavonoids from the genus *Astragalus*: Phytochemistry and biological activity. Pharmacogn Rev. 2016;10:11-32.

10. Yadav P, Malpathak N. Estimation of antioxidant activity and total phenol, flavonoid content among natural populations of caper (*Capparis moonii*, Wight) from Western Ghats region. Indian J Pharm Educ Res. 2016;50:495-501.

11. Oliveira FGS, Gomes de Lima-Saraiva SR, Oliveira AP, Rabêlo SV, Rolim LA, Silva Almeida JRG.Influence of the extractive method on the recovery of phenolic compounds in different parts of *Hymenaea martiana* Hayne. Pharmacog Res. 2016;8:270-275.

12. El-gizawy HA, Hussein MA. Isolation, structure elucidation of ferulic and coumaric acids from *Fortunella japonica* swingle leaves and their structure antioxidant activity relationship. Free Rad Antioxid. 2017;7:23-30.

13. Venkatesan A, Kathirvel A, Prakash S, Sujatha V. Antioxidant, antibacterial activities and identification of bioactive compounds from *Terminalia chebula* bark extracts. Free Rad Antioxid. 2017;7:43-49.

14. Dutta S, Das S. A study of the anti-inflammatory effect of the leaves of *Psidium guajava* Linn. on experimental animal models. Pharmacog Res. 2010;2:313-317.

15. Middleton EJ, Kandaswami C, Theoharides TC. The effects of plant flavonoids on mammalian cells: Implications for inflammation, heart disease, and cancer. Pharmacol Rev. 2000;52:673-751.

16. Havsteen BH. The biochemistry and medical significance of the flavonoids. Pharmacol Ther. 2002;96:67-202.

17. Fiala ES, Reddy BS, Weisburger JH. Naturally occurring anticarcinogenic substances in foodstuffs. Annu Rev Nutr. 1985;5:291-321.

18. Tapsell LC, Hemphill IL, Cobiac CS, Patch CS, Sullivan DR, Fenech M, Roodenrys S, Keogh JB, Clifton PM, Williams PG, Fazio VA, Inge KE. Health benefits of herbs and spices: The past, the present, the future. Med J Aust. 2006;185:S4-S24.

19. Triggiani V, Resta F, Guastamacchia E, Sabbà C, Licchelli B, Ghiyasaldin S, Tafaro E. Role of antioxidants, essential fatty acids, carnitine, vitamins, phytochemicals and trace elements in the treatment of diabetes mellitus and its chronic complications. Endocr Metab Immune Disord Drug Targets. 2006;6:77-93.

20. Epidi TT, Odili EO. Biocidal activity of selected plant powders against *Triboleum castaneum* Herbst in stored groundnut (*Arachis hypogaea* L.). African J Env Sci Tech. 2009;3:1-5.

21. Burkill HM. The Useful Plants of West Tropical Africa. (2nd ed). Vol. 3. Families J-L. Royal Botanic Gardens, Kew. 1995;857.

22. Samoylenko V, Rahman MM, Tekwani BL, Tripathi LM, Wang YH, Khan SI, Khan IA, Miller LS, Vaishali, CJ, Muhammad I. *Banisteriopsis caapi*, a unique combination of MAO inhibitory and antioxidative constituents for

Basel, Weinheim, New York; Verlag Helvetica Chomica Acta; 1993;73-86.

the activities relevant to neurodegenerative disorders and Parkinson's disease. J Ethnopharm. 2010;127:357-367.

23. Narayan DC, Mohamed AI, Ilias M, Larry AW, Babu LT. Monoamine oxidase inhibitory constituents of propolis: kinetics and mechanism of inhibition of recombinant human MAO-A and MAO-B. Molecules. 2014;19:18936-18952.

24. Bankova V, Popova M, Trusheva B. Propolis volatile compounds: Chemical diversity and biological activity: A review. Chem Cent J. 2014;8:28.

25. Quang DN, Harinantenaina L, Nishizawa T, Hashimoto T, Kohchi C, Soma G, Asakawa Y. Inhibition of nitric oxide production in RAW 264.7 cells by azaphilones from Xylariaceous fungi. Biol Pharm Bull. 2006;29:34-37.

26. Zhao J, Khan SI, Wang M, Vasquez Y, Yang MH, Avula B, Wang YH, Avonto C, Smillie TJ, Khan IA. Octulosonic acid derivatives from Roman chamomile (*Chamaemelum nobile*) with activities against inflammation and metabolic disorder. J Nat Prod. 2014;77:509-515.

27. Al-Taweel AM, El-Shafae AM, Perveen S, Fawzy GA, Khan SI. Anti-inflammatory and cytotoxic constituents of *Bauhinia retusa*. Int J Pharm. 2015;11:372-376.

28. Li YL, Ding CX, Liao ZX. Glycosides from *Swertia erythrosticta.* Chin Trad Herb Drugs. 2002;33:104-106.

29. Song DM, Sun QS. Chemical studies on constituents of *Trollius altaicus* CA. Mey Medi Chem. 2004;14:233-235.

30. Ju Y, Sacalis JN, Still CC. Bioactive flavonoids from endophyte-infected blue grass (*Poa ampla*). J Agric Food Chem. 1998;46:3785-3788.

31. Kumazawa TT, Minatogawa S, Matsuba S. Sato S, Onodera J. An effective synthesis of isoorientin: the regioselective synthesis of a 6-C-glucosylflavone. Carbohydr Res. 2000;329:507-513.

32. Cheng G, Bai Y, Zhao Y, Tao J, Liu Y, Tu G, Ma L, Liao N, Xu X. Flavonoids from *Ziziphus jujuba* Mill var. spinosa. Tetrahedron. 2000;56:8915-8920.

33. Wang TY, Li Q, Bi KS. Bioactive flavonoids in medicinal plants: structure, activity and biological fate. Asian J Pharm Sci. 2018;13:12-23.

34. Çelik H, Koşar M. Inhibitory effects of dietary flavonoids on purified hepatic NADH-cytochrome b5 reductase: structure-activity relationships. Chem Biol Interact. 2012;197:103-109.

35. Isoda H, Motojima H, Onaga S, Samet I, Villareal MO, Han J. Analysis of the erythroid differentiation effect of 574 flavonoid apigenin on K562 human chronic leukemia cells. Chemico-biol Interact. 2014;575:269-277.

36. Spencer JP, Vafeiadou K, Williams RJ, Vauzour D. Neuroinflammation: modulation by 635 flavonoids and mechanisms of action. Molecular Aspects Med. 2012;33:83-97.

37. Yang J, Kwon YS, Kim MJ. Isolation and characterization of bioactive compounds from *Lepisorus thunbergianus* (Kaulf.) Arabian J Chem. 2015;8:407-413.

38. Zhou X, Peng J, Fan G, Wu Y. Isolation and purification of flavonoid glycosides from *Trollius ledebouri* using high-speed counter-current chromatography by stepwise increasing the flow-rate of the mobile phase. J Chromatography A. 2015;1092:216-221.

39. Sharma KK, Sharma AK, Sharma MC, Tanwar K. Isolation of orientin and vitexin from stem bark of *Parkinsonia aculeata* (Caesalpiniaceae) and their successive blending on sheep wool fiber. Inter J Pharm Phy Res. 2014;6:557-561.

40. Hosoya T, Yun YS, Kunugi A. Five novel flavonoids from *Wasabia japonica.* Tetrahedron. 2005;61:7037-7044.

41. Peng J, Fan G, Hong Z, Chai Y, Wu Y. Preparative separation of isovitexin and isoorientin from *Patrinia villosa* Juss by high-speed counter-current chromatography. J Chromatogr A. 2005;1074:111-115.

42. Endo Y, Hayashi H, Sato T, Maruno M, Ohta T, Nozoe S. Confluentic acid and 2′-O-methylperlatolic acid, monoamine oxidase B inhibitors in a Brazilian plant, *Himatanthus sucuuba*. Chem Pharm Bull. 1994;42:1198-1201.

43. Lin RD, Hou WC, Yen KY, Lee MH. Inhibition of monoamine oxidase B (MAO-B) by Chinese herbal medicines. Phytomed. 2003;10:650-656.

44. Zarmouh N, Eyunni S, Mazzio E, Messeha S, Elshami F, Soliman K. Bavachinin and genistein, two novel human monoamine oxidase-B (MAO-B) inhibitors in the *Psoralea Corylifolia* seeds. The FASEB J. 2015; 29:(Supple1).

45. Lee MH, Lin RD, Shen LY, Yang LL, Yen KY, Hou WC. Monoamine oxidase B and free radical scavenging activities of natural flavonoids in *Melastoma candidum* D. Don. J Agric Food Chem. 2001;49:5551-5555.

46. Ficarra R, Ficarra P, Tommasini S, Carulli M, Melardi S, Di Bella MR, Calabrò ML, De Pasquale R, Germanò MP, Sanogo R, Casuscelli F. Isolation and characterization of *Guiera senegalensis* J. F. Gmel. active principles. Boll Chim Farm. 1997;136:454-459.

ORIGINAL ARTICLE

Antibacterial and Antibiofilm Activities of Ceragenins against *Pseudomonas aeruginosa* Clinical Isolates

Cerageninlerin Klinik *Pseudomonas aeruginosa* Suşlarına Karşı Antibakteriyel ve Antibiyofilm Aktiviteleri

Çağla BOZKURT GÜZEL[1], Mayram HACIOĞLU[1]*, Gözde İNCİ[1], Paul B. SAVAGE[2]

[1]İstanbul University, Faculty of Pharmacy, Department of Pharmaceutical Microbiology, İstanbul, Turkey
[2]Brigham Young University, Department of Chemistry and Biochemistry, Provo, Utah, USA

ABSTRACT

Objectives: *Pseudomonas aeruginosa* can cause life-threatening infections that are difficult to treat due to its high resistance to antibiotics and its ability to form antibiotic tolerant biofilms. Ceragenins, designed to mimic the activities of antimicrobial peptides, represent a promising new group of antibacterial agents that display potent anti-*P. aeruginosa* activity. The aim of this study was to evaluate the antibacterial and antibiofilm activities of ceragenins in comparison to colistin and ciprofloxacin against *P. aeruginosa* strains.

Materials and Methods: Biofilm formation and determination of minimum inhibitory concentration (MIC) values of ceragenins (CSA-13, CSA-44, CSA-131, and CSA-138), ciprofloxacin, and colistin were evaluated against 25 *P. aeruginosa* isolates. Four good biofilm-producing strains were chosen for biofilm studies, and sessile MICs and inhibition of molecule adhesion and biofilm formation were evaluated.

Results: The MIC_{50} (µg/mL) values of CSA-13, CSA-44, CSA-131, CSA-138, ciprofloxacin, and colistin were 8, 8, 8, 16, 1, and 2, respectively. The sessile MICs for molecules were greater than planktonic MICs. CSA-13, CSA-44, and CSA-131 were more efficient after 4 h incubation while CSA-138, ciprofloxacin and colistin were more efficient after 1 h incubation. The most efficient agent for inhibition of adhesion was colistin (up to 45%). CSA-131, CSA-138, and colistin were the most efficient agents for inhibition of biofilm formation (up to 90%).

Conclusion: Our study highlights the potential of CSA-131 and CSA-138 as potential alternative agents to conventional antibiotics for the eradication of biofilms of *P. aeruginosa*.

Key words: *Pseudomonas aeruginosa*, biofilm, ceragenin

ÖZ

Amaç: *Pseudomonas aeruginosa*, antibiyotiklere oldukça dirençli ve biyofilm oluşturma yeteneği nedeniyle hayatı tehdit eden enfeksiyonlara neden olabilmektedir. Antimikrobiyal peptidlerin aktivitelerini taklit eden cerageninler, *P. aeruginosa*'ya karşı da güçlü etki gösteren yeni umut verici ajanlardır. Çalışmamızın amacı, cerageninlerin *P. aeruginosa* suşlarına karşı antibakteriyel ve antibiyofilm aktivitelerini değerlendirerek, kolistin ve siprofloksasinle karşılaştırmaktır.

Gereç ve Yöntemler: Yirmi beş *P. aeruginosa* suşunun biyofilm oluşturma özellikleri ve CSA-13, CSA-44, CSA-131, CSA-138, siprofloksasin ve kolistine karşı duyarlılıkları araştırılmış ve antimikrobiyal ajanların minimal inhibitör konsantrasyon (MİK) değerleri belirlenmiştir. Biyofilm çalışmaları için kuvvetli biyofilm oluşturan dört suş seçilerek, antimikrobiyal ajanların sesil MİK değerleri ve adezyon ve biyofilm oluşumuna etkileri araştırılmıştır.

Bulgular: CSA-13, CSA-44, CSA-131, CSA-138, siprofloksasin ve kolistinin $MİK_{50}$ (µg/mL) değerleri sırasıyla 8, 8, 8, 16, 1 ve 2, olarak bulunmuştur. Sesil MİK değerlerinin ise planktonik MİK değerlerinden daha büyük olduğu bulunmuştur. CSA-13, CSA-44 ve CSA-131'in, 4 saatlik inkübasyondan sonra, CSA-138, siprofloksasin ve kolistinin ise 1 saatlik inkübasyondan sonra biyofilme karşı daha etkili oldukları tespit edilmiştir. Adezyon inhibisyonu için kolistinin (%45'e kadar inhibisyon), biyofilm oluşumu inhibisyonu için ise yine kolistin, CSA-131 ve CSA-138'in (%90'a kadar inhibisyon) en etkili ajanlar oldukları tespit edilmiştir.

Sonuç: Çalışmamızda CSA-131 ve CSA-138'in *P. aeruginosa*'nın biyofilmlerine karşı konvansiyonel antibiyotiklere alternatif olarak kullanılabileceği vurgulanmıştır.

Anahtar kelimeler: *Pseudomonas aeruginosa*, biyofilm, ceragenin

INTRODUCTION

Biofilms are communities of bacterial cells surrounded by an extracellular matrix.[1] According to the National Institutes of Health, biofilms are estimated to account for over 80% of all nosocomial infections and are particularly common with device implants, such as contact lenses, ventricular assist devices, vascular and urinary catheters, and endotracheal tubes.[2-4] *Pseudomonas aeruginosa* forms a highly virulent biofilm that has been associated with higher mortality rates compared with other bacterial pathogens, and there are growing concerns over its increased antimicrobial and multidrug resistance. Because the use of conventional antimicrobial compounds in many cases cannot eradicate biofilms, there is an urgent need to develop alternative compounds and approaches to combat biofilm-based infections.[5-9] One frequently studied target is the bacterial membrane. Most antimicrobial peptides display broad-spectrum antibacterial activities and target the bacterial membrane. However, many antimicrobial peptides are difficult to synthesize and purify due to their complexity and size. In addition, antimicrobial peptides can be substrates for proteases, which limit their *in vivo* half-lives.[10] Recently, a series of cationic derivatives of cholic acid have been synthesized and have been found to have properties that may make them useful antimicrobial agents. The ceragenins, designed to mimic the activities of antimicrobial peptides, are a new class of antimicrobial agent. Ceragenins are not peptide based, are not salt sensitive, and are relatively simple to prepare and purify on a large scale.[11] CSAs, which stands for cationic steroidal antimicrobials, are strongly associated with anionic cell surfaces and in the formation of transient pores in the membrane, resulting in membrane depolarization and cell death. As well as their antibacterial activities against resistant strains of *P. aeruginosa*, *Acinetobacter baumannii*, and *Staphylococcus aureus*, these molecules can also display candidacidal, antiviral, antiparasitic, and anticancer effects.[12-18] Additionally, previous studies have demonstrated the efficacy of ceragenins, especially the leading ceragenin CSA-13, on sessile cells including *P. aeruginosa*.[11-13] However, there has been no study in the literature describing the efficacy of CSA-44 and CSA-131 against *P. aeruginosa* biofilms. The present work examines the *in vitro* antibiofilm activities of CSA-13, CSA-44, CSA-131, and CSA-138 in comparison to colistin and ciprofloxacin against *P. aeruginosa* strains.

MATERIALS AND METHODS

Bacterial isolates

A total of 25 *P. aeruginosa* isolates from various sources including blood, catheters, urine, endotracheal aspirate, esophageal aspirate, ears, sputum, abscesses, and bronchoalveolar lavage fluid submitted to the Clinical Microbiology Laboratories of Cerrahpaşa Faculty of Medicine Hospitals in Turkey (2011) were used. All the strains were identified using API 20 NE (BioMérieux, France) systems. *P. aeruginosa* ATCC 27853 strain was used as the quality control strain.

Antimicrobial agents

The CSAs CSA-13, CSA-44, CSA-131, and CSA-138 were synthesized from a cholic acid scaffold technique as previously described (Figure 1).[19] Colistin and ciprofloxacin were kindly provided by their respective manufacturers. Stock solutions of CSAs from dry powders were prepared in water and the antibiotics were prepared according to the manufacturers' recommendation and stored frozen at -80°C for up to 6 months. Final concentrations of antimicrobials were prepared in cation-adjusted Mueller-Hinton broth (CAMHB, Difco Laboratories, Franklin Lakes, NJ, USA) prior to use.

Media

Tryptic soy broth supplemented with 1% glucose (TSB-glucose, Difco Laboratories) was used for biofilm production and to determine minimum biofilm eradication concentration (MBEC) values, CAMHB was used to determine the minimum inhibitory concentration (MIC), and tryptic soy agar (TSA, Difco Laboratories) was used for culturing bacteria.

MIC determinations

MICs of CSA-13, CSA-44, CSA-131, CSA-138, ciprofloxacin, and colistin were determined against *P. aeruginosa* (planktonic forms) by the microbroth dilution technique as described by CLSI.[20] MIC_{50} is the MIC that inhibits 50% of isolates.

Biofilm formation

Biofilm formation by *P. aeruginosa* strains was evaluated using a crystal violet staining method.[21,22] Briefly, populations of suspensions of bacteria were adjusted with TSB-glucose. Biofilms were formed by pipetting cell suspensions into wells of microtiter plates (Greiner Bio-One, Kremsmuenster, Austria) followed by incubation for 24 h at 37°C. After incubation, the remaining medium was aspirated gently, nonadherent cells were removed, and the wells were stained with 0.1% crystal violet, followed by measurement of optical density (OD) at 600 nm. For each isolate, biofilm production was measured in triplicate and *P. aeruginosa* ATCC 27853 was used as a standard strain. The extent of biofilm production (weak, moderate, and strong) was calculated. Four strong biofilm-producing clinical isolates of *P. aeruginosa* (PA-1, PA-2, PA-3, PA-4) and control strain biofilms were selected. Biofilms were formed in the wells of microtiter plates as previously described by Dosler and Karaaslan[22] with some modifications. An overnight culture of isolates from 24 h growth in TSA was inoculated in TSB-glucose in an orbital shaker at 37°C overnight. Cultures were

centrifuged (about 3000 rpm, 5-10 min) and washed twice with sterile phosphate-buffered saline (PBS) and resuspended in TSB-glucose to a cellular density equivalent to 1×10^6 cells/mL. Biofilms were formed by pipetting 200 μL of the standardized cell suspension into selected wells of sterilized polystyrene flat-bottomed 96-well tissue culture microtiter plates and incubated for 24 h at 37°C. After incubation, the waste medium was aspirated gently, and nonadherent cells were removed by washing the biofilms three times with sterile PBS.

Biofilm attachment assay

Biofilm attachment assays were performed using a previously described method with some modifications.[22,23] The overnight cultures of isolates were prepared to cellular density equivalent to 1×10^6 cells/mL, as described above. Four strong biofilm producing clinical isolates of *P. aeruginosa* were added to each well of 96-well tissue culture microtiter plates with 1X MIC of CSAs and antibiotics. A positive control without antimicrobial agent and a negative control without cells were also prepared. The plates were incubated for 1, 2, and 4 h at 37°C. After incubation, the wells were washed twice with PBS and were measured spectrophotometrically at OD 450 nm on a microplate reader (BioRad Novapath).

Inhibition of biofilm formation

Four strong biofilm producing clinical isolates of *P. aeruginosa* strains (1×10^6 cells/mL) were added to each well of 96-well tissue culture microtiter plates with 1X MIC, 1/10X MIC, and 1/100X MIC of ceragenins and antibiotics.[22,23] A positive control without antimicrobial agent and a negative control without cells were prepared. The plates were incubated for 24 at 37°C. After incubation, the wells were washed twice with PBS and were measured spectrophotometrically at OD 450 nm on a microplate reader (BioRad Novapath).

MBEC determinations

To evaluate the activities of antimicrobial agents on 24-h-old mature *P. aeruginosa* biofilms, biofilms were formed as described above and metabolic activities of the biofilms were assessed using the standardized static microtiter plate model and measured by 2,3-bis (2-methoxy-4-nitro-5-sulfophenyl)-5-[8phenylamino) carbonyl]-2H-tetrazolium hydroxide (XTT, Sigma-Aldrich, St. Louis, MO, USA) reduction assay.[24] The 24-h biofilms in 96-well tissue culture microtiter plates were washed three times with 200 μL of PBS solution and air-dried. Doubling concentrations of antimicrobials were added to the pre-formed biofilms. Aliquots of 200 μL of each concentration were added to each corresponding well and the plates were incubated for 24 h at 37°C. Drug-free biofilm wells containing only TSB-glucose were used as controls. After incubation, the medium was aspirated and washed with PBS three times. An XTT solution was prepared as previously published and added to each well. The microtiter plates were incubated in the dark for 6 h at 37°C. Biofilm growth was measured spectrophotometrically at 480 nm on a microplate reader (BioRad Novapath). MBECs were determined as the minimum antibacterial drug concentration that caused 50% reduction of biofilm compared to drug-free untreated biofilm controls. Each experiment was performed in four wells and was repeated twice.

RESULTS

Susceptibility results against planktonic cells (MIC)

The *in vitro* activities of the studied antimicrobials against 25 *P. aeruginosa* isolates are summarized in Table 1. Susceptibility testing demonstrated that the MIC_{50} (μg/mL) values of CSA-13, CSA-44, CSA-131, CSA-138, ciprofloxacin, and colistin were 8, 8, 8, 16, 1, and 2, respectively (Table 1). CSA-13, CSA-44, and CSA-131 showed similar MIC_{50} results. The highest MIC_{50} results were obtained with CSA-138.
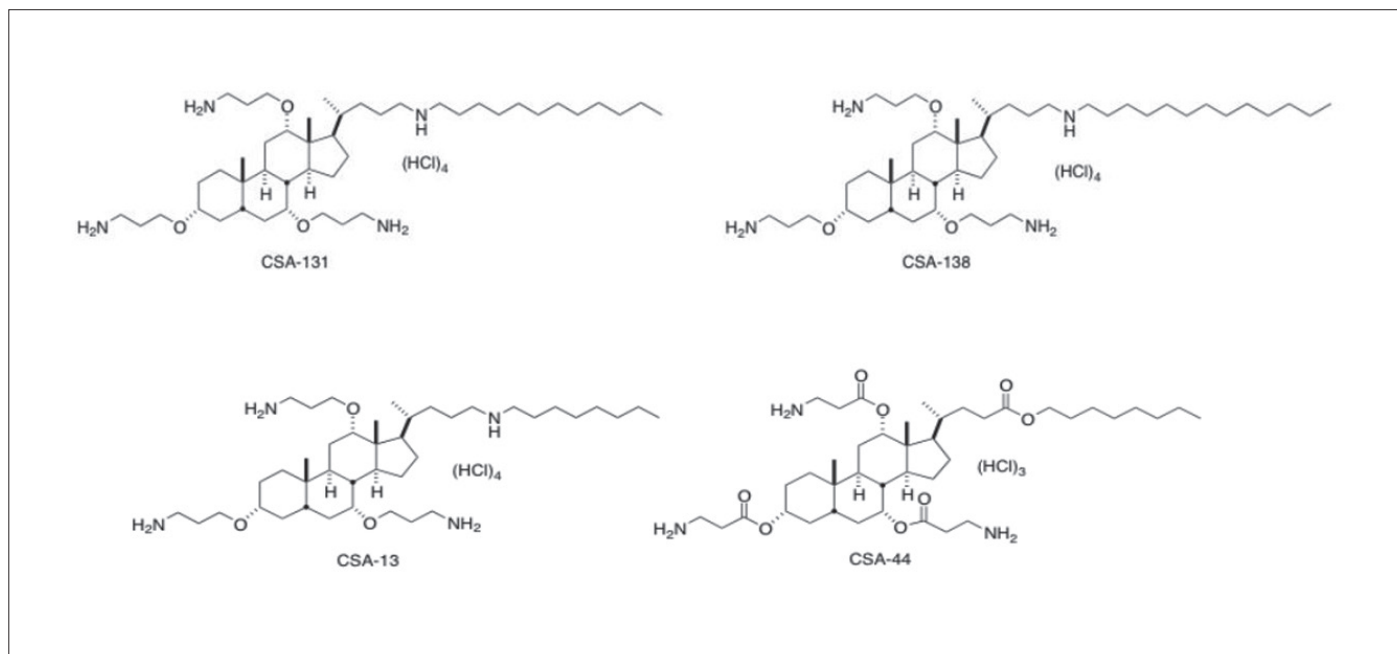

Figure 1. Chemical structures of CSA-13, CSA-44, CSA-131, and CSA-138

Inhibition of adhesion

Inhibition of adhesion rates depended on time. CSA-13, CSA-44, and CSA-131 were more efficient after 4 h incubation, while CSA-138, ciprofloxacin, and colistin were more efficient after 1 h incubation. The most efficient agent for inhibition of adhesion was colistin (up to 45%) (Figure 2).
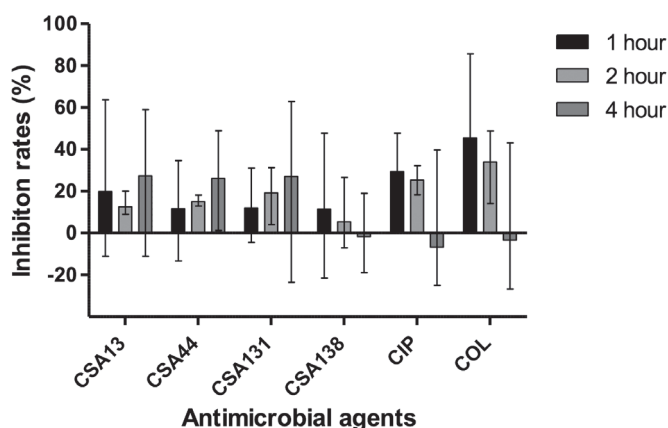
Inhibition of biofilm formation

Inhibition of biofilm formation rates depended on concentration; the highest inhibition rates were shown at MICs for all agents, as expected. CSA-131, CSA-138, and colistin were the most efficient agents for inhibition of biofilm formation (up to 90%) (Figure 3).

Susceptibility results against biofilm cells (MBEC)

We showed that ceragenins are also active against four biofilm producing clinical isolates of *P. aeruginosa* and ATCC 27853 strains. However, MBECs were greater than MICs; ceragenins' MBEC values differ from 16 to 512 µg/mL. Susceptibility results demonstrated that the MBECs (µg/mL) of CSA-13, CSA-44, CSA-131, and CSA-138 were 32-64, 32-256, 16-128, and 128-512, respectively. Ciprofloxacin and colistin showed similar MBEC

Table 1. MICs and MIC$_{50}$s of the tested antimicrobial agents (µg/mL)			
Antimicrobial agents	MIC	Number of isolates	MIC$_{50}$
CSA-13	4	4	8
	8	12	
	16	7	
	32	2	
CSA-44	8	17	8
	16	5	
	32	3	
CSA-131	4	8	8
	8	15	
	16	2	
CSA-138	4	1	16
	8	9	
	16	8	
	32	7	
CIP	0.5	4	1
	1	10	
	2	5	
	4	6	
COL	0.5	1	2
	1	2	
	2	17	
	4	5	

CIP: Ciprofloxacin, COL: Colistin, MIC: Minimum inhibitory concentration
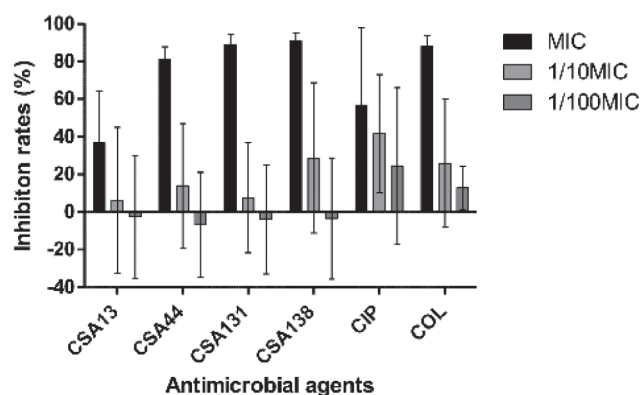
Figure 3. Inhibition of biofilm formation rates of antimicrobials at different concentrations

Table 2. MBECs of the tested antimicrobial agents (µg/mL)						
	CSA-13	CSA-44	CSA-131	CSA-138	CIP	COL
PA-1	64	256	128	256	16	16
PA-2	64	512	16	128	32	8
PA-3	32	32	64	256	8	8
PA-4	64	64	128	128	64	64
P. aeruginosa ATCC 27853	64	64	128	512	32	32

CIP: Ciprofloxacin, COL: Colistin, MBEC: Minimum biofilm eradication concentration

values (8-64 µg/mL) (Table 2). Among the tested ceragenins, CSA-13 was the most effective agent against mature biofilms.

DISCUSSION

Ceragenins are unique, low molecular mass, cationic steroid compounds. These compounds mimic the activity of naturally occurring antimicrobial peptides. Previous studies have shown that ceragenins, especially CSA-13, are potent antimicrobials against various microorganisms including multidrug-resistant *P. aeruginosa*.[11-13] In the present work, in addition to CSA-13, we investigated the effect of CSA-44, CSA-131, and CSA-138 on the formation and adhesion of a biofilm by five good biofilm forming strains of *P. aeruginosa* using the crystal violet staining method. Ciprofloxacin and colistin were used as comparative conventional antibiotics. Here we report that the MIC$_{50}$ (µg/mL) values of CSA-13, CSA-44, CSA-131, CSA-138, ciprofloxacin,

Figure 2. Inhibition of adhesion rates of antimicrobials after 1, 2, and 4 h incubation

and colistin were 8, 8, 8, 16, 1, and 2, respectively, for 25 *P. aeruginosa* strains and these results are similar to those of other published studies.

Chin et al.[11] investigated the efficacy of CSA-13 against 50 clinical isolates of *P. aeruginosa*, and compared them with various antibiotics. CSA-13 was shown to have a 1-32 µg/mL MIC range and 16 µg/mL MIC_{50}. Bozkurt Guzel et al.[25] showed the antibacterial activities of CSA-13 against clinical isolates of *P. aeruginosa* with 8-16 µg/mL MIC range and 8 µg/mL MIC_{50} (Poster presentation, ECCMID, 2017). In another study, Vila-Farrés et al.[26] determined the MIC_{50} (µg/mL) values of CSA-13, CSA-44, CSA-131, and CSA-138 against *P. aeruginosa* strains as 4, 4, 1, and 2, respectively. As shown in previous studies and our study, CSA-13, CSA-44, and CSA-131 showed similar MIC_{50} results. In our study the highest MIC and MIC_{50} results were obtained with CSA-138 against *P. aeruginosa*.

Biofilms are specific and organized communities of cells under the control of signaling molecules, rather than random accumulations of cells resulting from cell division. It is well known that biofilm embedded microorganisms possess resistance to both antimicrobial agents and host immune responses when compared to their planktonic forms.[1] In the present study, MBECs of ceragenins and antibiotics were higher than MICs, as expected. Ciprofloxacin's and colistin's MBECs were less than those of ceragenins, but among the ceragenins CSA-13 was the most effective agent against mature biofilms. In contrast to the antimicrobial effects against bacteria and fungi, the antibiofilm activity of ceragenins is not well defined against biofilms. Only a few studies showed that ceragenins, especially CSA-13, have antibiofilm effects against *P. aeruginosa*.[27-29]

Novel approaches to biofilm control might take one of three main forms: effective reduction of planktonic cells before biofilm formation, inhibition of cell adhesion and biofilm formation, or removal of established biofilm.[22,30] A novel field of research has accordingly focused on preventing biofilm development and adherence. For this purpose in the present study, we investigated the inhibition of bacterial attachment to the surfaces, as well as the inhibition of biofilm production by MIC or subMIC values of ceragenins, ciprofloxacin, and colistin. Although inhibition of adhesion and biofilm formation rates depended on time and concentration, it was shown that CSA-131 and CSA-138 were the most efficient agents with inhibition rates of adhesion of 11.38 and 11.97 and biofilm formation of 90.7 and 88.69 (%), respectively, at MIC. Our results clearly showed that ceragenins are much more effective on biofilm formation rather than attachment. These results indicated that biofilm formation can be prevented by inhibiting not only attachment but also other mechanisms.

In one of our studies the effects of CSA-13, CSA-8, CSA-44, CSA-131, and CSA-138 were evaluated on adhesion and biofilm formation of *C. albicans* and it was shown that all of the studied CSAs inhibited *C. albicans* biofilm formation in a concentration-dependent manner.[15]

Recently, Olekson et al.[30] also showed antibiofilm activities of various ceragenins including CSA-13, CSA-44, CSA-131,

CSA-138, CSA-142, and CSA-192 against preformed mixed-species biofilms of *P. aeruginosa* and *S. aureus*. Nagant et al.[27,29] demonstrated that CSA-13 affected biofilm formation, the surface of biofilms, and the inside of established biofilms of *P. aeruginosa*. Gu et al.[28] showed that CSA-138 also inhibited biofilm formation of *P. aeruginosa* on lenses. Our results were similar to those of these studies.

CONCLUSION

To the best of our knowledge this is the first report to evaluate the antibiofilm activities of CSA-44 and CSA-131 against *P. aeruginosa*. According to our results, ceragenins, especially CSA-13, CSA-131, and CSA-138, appear to be good candidates in the treatment of *Pseudomonas* infections as well as biofilm-related ones. Therefore, CSAs are promising candidates for further research as antibacterial drugs and as agents for treatment of biofilm infections. Future studies should be performed to correlate the safety, efficacy, and pharmacokinetic parameters of these molecules.

ACKNOWLEDGEMENTS

Conflict of Interest: No conflict of interest was declared by the authors.

REFERENCES

1. Branda SS, Vik S, Friedman L, Kolter R. Biofilms: the matrix revisited. Trends Microbiol. 2005;13:20-26.

2. Bryers J. Medical biofilms. Biotechnol Bioeng. 2008;100:1-18.

3. Taylor PK, Yeung AT, Hancock RE. Antibiotic resistance in *Pseudomonas aeruginosa* biofilms: towards the development of novel anti-biofilm therapies. J Biotechnol. 2014;191:121-130.

4. Association for the Advancement of Wound Care (AAWC). Advancing your practice: understanding wound infection and the role of biofilms. Malvern, PA, USA. 2008.

5. Aloush V, Navon-Venezia S, Seigman-Igra Y, Cabili S, Carmeli Y. Multidrug-resistant *Pseudomonas aeruginosa*: risk factors and clinical impact. Antimicrob Agents Chemother. 2006;50:43-48.

6. Jakobsen TH, Bjarnsholt T, Jensen PØ, Givskov M, Høiby N. Targeting quorum sensing in *Pseudomonas aeruginosa* biofilms: current and emerging inhibitors. Future Microbiol. 2013;8:901-921.

7. Driscoll JA, Brody SL, Kollef MH. The epidemiology, pathogenesis, and treatment of *Pseudomonas aeruginosa* infections. Drugs. 2007;67:251-268.

8. Osmon S, Ward S, Fraser VJ, Kollef MH. Hospital mortality for patients with bacteremia due to Staphylococcus aureus or Pseudomonas aeruginosa. Chest. 2004;125:607-616.

9. del Pozo JL, Patel R. The challenge of treating biofilm associated bacterial infections. Clin Pharmacol Ther. 2007;82:204-209.

10. Savage PB, Li C, Taotafa U, Ding B, Guan Q. Antibacterial properties of cationic steroid antibiotics. FEMS Microbiol Lett. 2002;217:1-7.

11. Chin JN, Jones RN, Sader HS, Savage PB, Rybak MJ. Potential synergy activity of the novel ceragenin, CSA-13, against clinical

isolates of Pseudomonas aeruginosa, including multidrug-resistant P. aeruginosa. J Antimicrob Chemother. 2008;61:365-370.

12. Bozkurt-Guzel C, Savage PB, Akcali A, Ozbek-Celik B. Potential synergy activity of the novel ceragenin, CSA-13, against carbapenem-resistant *Acinetobacter baumannii* strains isolated from bacteremia patients. Biomed Res Int. 2014:710273.

13. Bozkurt-Guzel C, Savage PB, Gerceker AA. *In vitro* activities of the novel ceragenin, CSA-13, alone or in combination with colistin, tobramycin and ciprofloxacin against *Pseudomonas aeruginosa* strains isolated from cystic fibrosis patients. Chemother. 2011;57:505-510.

14. Chin JN, Rybak MJ, Cheung CM, Savage PB. Antimicrobial activities of ceragenins against clinical isolates of resistant *Staphylococcus aureus.* Antimicrob Agents Chemother. 2007;51:1268-1273.

15. Bozkurt-Guzel C, Hacioglu M, Savage PB. Investigation of the in vitro antifungal and antibiofilm activities of ceragenins CSA-8, CSA-13, CSA-44, CSA-131, and CSA-138 against *Candida* species. Diagn Microbiol Infect Dis. 2018;91:324-330

16. Lara D, Feng Y, Bader J, Savage PB, Maldonado RA. Anti-trypanosomatid activity of ceragenins. J Parasitol. 2010;96:638-642.

17. Bucki R, Niemirowicz K, Wnorowska U, Byfield FJ, Piktel E, Wątek M, Janmey PA, Savage PB. Bactericidal activity of ceragenin CSA-13 in cell culture and an animal model of peritoneal infection. Antimicrob Agents Chemother. 2015;59:6274-6282.

18. Howell MD, Streib JE, Kim BE, Lesley LJ, Dunlap AP, Geng D, Feng Y, Savage PB, Leung DY. Ceragenins: a class of antiviral compounds to treat orthopox infections. J Invest Dermatol. 2009;129:2668-2675.

19. Lai XZ, Feng Y, Pollard J, Chin JN, Rybak MJ, Bucki R, Epand RF, Epand RM, Savage PB. Ceragenins: cholic acid- based mimics of antimicrobial peptides. Acc Chem Res. 2008;41:1233-1240.

20. Clinical and Laboratory Standards Institute. Methods for dilution antimicrobial susceptibility tests for bacteria that grow aerobically. Approved standard M7-A7. 7th edition Wayne, PA, USA: Clinical and Laboratory Standards Institute; 2006.

21. Ochoa SA, Cruz-Córdova A, Rodea GE, Cázares-Domínguez V, Escalona G, Arellano-Galindo J, Hernández-Castro R, Reyes-López A, Xicohtencatl-Cortes J. Phenotypic characterization of multidrug-resistant *Pseudomonas aeruginosa* strains isolated from pediatric patients associated to biofilm formation. Microbiol Res. 2015;172:68-78.

22. Dosler S, Karaaslan E. Inhibition and destruction of *Pseudomonas aeruginosa* biofilms by antibiotics and antimicrobial peptides. Peptides. 2014;62:32-37.

23. Hadley EB, Hancock RE. Strategies for the discovery and advancement of novel cationic antimicrobial peptides. Curr Top Med Chem. 2010;10:1872-1881.

24. Sabaeifard P, Abdi-Ali A, Soudi MR, Dinarvand R. Optimization of tetrazolium salt assay for *Pseudomonas aeruginosa* biofilm using microtiter plate method. J Microbiol Methods. 2014;105:134-140.

25. Bozkurt Guzel C, Oyardi O, Savage P. Comparative in vitro antimicrobial activities of CSA-142 and CSA-192, second-generation ceragenins, with CSA-13 against various microorganisms. J Chemother. 2018;30:332–337.

26. Vila-Farrés X, Callarisa AE, Gu X, Savage PB, Giralt E, Vila J. CSA-131, a ceragenin active against colistin-resistant *Acinetobacter baumannii* and *Pseudomonas aeruginosa* clinical isolates. Int J Antimicrob Agents. 2015;46:568-571.

27. Nagant C, Pitts B, Stewart PS, Feng Y, Savage PB, Dehaye JP. Study of the effect of antimicrobial peptide mimic, CSA-13, on an established biofilm formed by *Pseudomonas aeruginosa*. Microbiologyopen. 2013;2:318-325.

28. Gu X, Jennings JD, Snarr J, Chaudhary V, Pollard JE, Savage PB. Optimization of ceragenins for prevention of bacterial colonization of hydrogel contact lenses. Invest Ophthalmol Vis Sci. 2013;54:6217-6223.

29. Nagant C, Feng Y, Lucas B, Braeckmans K, Savage P, Dehaye JP. Effect of a low concentration of a cationic steroid antibiotic (CSA-13) on the formation of a biofilm by *Pseudomonas aeruginosa*. J Appl Microbiol. 2011;111:763-772.

30. Olekson MA, You T, Savage PB, Leung KP. Antimicrobial ceragenins inhibit biofilms and affect mammalian cell viability and migration in vitro. FEBS Open Bio. 2017;7:953-967.

ORIGINAL ARTICLE

Investigation of the Voltammetric Behavior of Methyldopa at a Poly (*p*-Aminobenzene Sulfonic Acid) Modified Sensor

Poli (*p*-Aminobenzen Sülfonik Asit) Modifiye Sensör ile Metildopanın Voltametrik Davranışının İncelenmesi

ⓘ Gamze ERDOĞDU[1]*, ⓘ Şevket Zişan YAĞCI[1], ⓘ Ebru KUYUMCU SAVAN[2]

[1]İnönü University, Faculty of Arts and Sciences, Department of Chemistry, Malatya, Turkey
[2]İnönü University, Faculty of Pharmacy, Department of Basic Pharmaceutical Sciences, Division of Analytical Chemistry, Malatya, Turkey

ABSTRACT

Objectives: The aim was to modify carbon electrodes with (*p*-aminobenzene sulfonic acid) and use them as a sensor for sensitive and reliable detection of methyldopa (MD) and ascorbic acid.

Materials and Methods: Electropolymerization was performed by cyclic voltammetry in 0.1 M KCl solution. The modified sensor has a high electrocatalytic effect for oxidation of MD, which appeared in the pH range of 2-11 by differential pulse voltammetry (DPV) techniques.

Results: For the voltammetric determination of MD, the best results were acquired by DPV in phosphate buffer solution (PBS) (pH 3). The calibration plot of the proposed sensor is linear in two concentration ranges of 1.0-30 and 30.0-300.0 μM. The calibration equations over these ranges are I_{pa} (μA)=1.21×C (μM)+30.81, R^2=0.994 and I_{pa} (μA)=0.53×C (μM)+53.30, R^2=0.9975, respectively. In the sensitivity studies, the limit of quantification and the limit of detection were 10.6 nM and 5.0 nM, respectively. The modified sensor was used for the simultaneous determination of interfering substances such as MD and ascorbic acid in real samples.

Conclusion: The obtained results revealed that the prepared modified electrode and the proposed method have good sensitivity, repeatability, reproducibility, and stability.

Key words: Methyldopa, voltammetry, poly (*p*-aminobenzene sulfonic acid), ascorbic acid, glassy carbon electrode

ÖZ

Amaç: Karbon elektrotların poli (*p*-aminobenzen sülfonik asit) ile modifikasyonu ve metildopa (MD) ve askorbik asitin hassas ve güvenilir bir şekilde tayini için bir sensör olarak kullanılması.

Gereç ve Yöntemler: Elektropolimerizasyon, 0.1 M KCl çözeltisi içerisinde dönüşümlü voltametri (CV) ile gerçekleştirildi. Modifiye edilmiş sensör metildopanın oksidasyonu için yüksek elektrokatalitik etkiye sahiptir, bu da 2-12 pH aralığında diferansiyel puls voltametri tekniği ile gözlenmiştir.

Bulgular: MD'nin voltametrik tayini için, en iyi sonuçlar fosfat tampon çözeltisinde (PBS) (pH 3) DPV tekniği ile elde edildi. Bu aralıklarda kalibrasyon denklemi sırasıyla: I_{pa} (μA)=1,21×C (μM)+30,81, R^2=0,994 ve I_{pa} (μA)=0,53xC(μM)+53,30, R^2=0,9975. Duyarlılık çalışmalarında, kantitatif tayin sınırı (LOQ) ve en küçük tayin sınırı sırasıyla 10,6 nM ve 5,0 nM'dir. Duyarlılık çalışmalarında, tayin alt sınırı ve tayin sınırı sırasıyla 10.6 nM ve 5.0 nM idi. Modifiye edilmiş sensör, MD ile askorbik asit gibi girişim yapan maddelerin gerçek örneklerde eş zamanlı tayini için kullanıldı.

Sonuç: Elde edilen sonuçlar, modifiye edilmiş elektrot ve önerilen yöntemin iyi duyarlılık, tekrarlanabilirlik, tekrar üretilebilirlik ve kararlılığa sahip olduğunu ortaya çıkardı.

Anahtar kelimeler: Metildopa, voltametri, poli (*p*-amino benzen sülfonik asit), askorbik asit, camsı karbon elektrot

INTRODUCTION

Methyldopa (MD) is a catecholamine that is known by its chemical name 2-methyl-3-(3,4-dihydroxyphenyl)-DL-alanine (Figure 1), and it is widely used to lower blood pressure. MD is a centrally acting adrenal receptor that reduces high blood pressure and sympathetic tone.[1] In adrenergic nerve terminals, it is converted to α-methyl noradrenaline, and its antihypertensive effect seems to be due to this agent stimulating the central adrenoreceptors.[2]

Various methods like high-performance liquid chromatography with ultraviolet (UV) detection,[3] polarography,[4] potentiometry,[5] UV visible spectrophotometry,[6] and flow injection techniques[7,8] were reported previously for the determination of MD. However, many of these techniques require expensive equipment and are time consuming. In addition, since these catecholamines are electrochemically active, it is also possible to determine the nature of the molecules that provide neurotransmission by electrochemical methods. Therefore, it is important to detect MD in the presence of ascorbic acid (AA) by a reliable method that has good selectivity and sensitivity.

AA (vitamin C) is a biologically and industrially important substance.[9] The coexistence of AA, MD, and other catecholamines with very similar oxidation potentials leads to the response obtained by electrochemical techniques. For this reason, the increased sensitivity and selectivity of the new sensors produced to the MD has long been the subject of research. Using polymer modified electrodes solves this problem. The electrochemical behavior of MD was studied at various polymer electrodes.[10-17]

However, some disadvantages exist in the previously reported modified electrodes. AA exists as an anion in physiological pH (7.4), whereas MD exists as a cation. There are high electron density sulfo groups and electron-rich N atoms in the structure of p-aminobenzene sulfonic acid (ABSA). For this reason, a negatively charged polymer film is required to eliminate the interference of AA in the determination of MD. The p-ABSA molecule has high electron density sulfo groups and p-ABSA films are negatively charged. Due to the electrostatic repulsion between the negatively charged sulfo groups and the AA anions in the modified sensor, the AA shifts to a more negative potential and the dopaminic acid can be easily separated from it. The p-ABSA modified sensor can show high selectivity against MD.[18]

In the present study, electroanalytical methods were developed to detect MD in drug samples rapidly, reliably, and sensitively using an electrode modified with poly (p-ABSA). It has been determined that the modified sensor can be utilized for MD determination even in the presence of AA at the same time. Another significant advantage of these techniques over other ones is that they can be applied directly to the analysis of pharmaceutical dosage forms and biological samples without the need for extensive sample preparation, as there is no interaction between the adjuvants and the endogenous substances.
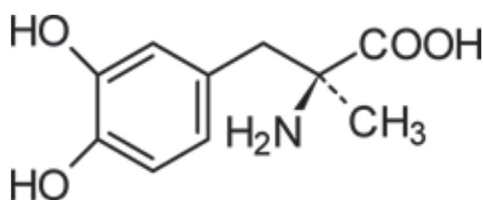
The analytical determination parameters such as the limit of detection (LOD), the limit of quantification (LOQ), and the concentration range were determined, and the amount of MD in the drug tablets and blood serum was found. To test the accuracy of the applied voltammetric method, MD recovery studies were performed in real samples.

MATERIALS AND METHODS

Materials

Alfamet tablets containing 250 mg of MD were kindly supplied by I.E. Ulagay (Turkey). All chemicals were of analytical purity and were procured from Merck (Darmstadt, Germany) or Sigma Chemical Company. Prior to the polymerization the solutions of monomer were held in nitrogen gas atmosphere for about 10 min, and during the electropolymerization the electrochemical cell was covered with nitrogen gas. Voltammetric experiments were carried out in phosphate buffer solution (pH 3.0). MD and AA solutions were freshly prepared before the experiments. All solutions were prepared with ultrapure water.

Instrumentation

In the voltammetry experiments, a BAS (Bioanalytical Systems, Inc.) 100BW electrochemical analyzer was used. This analyzer is connected to a personal computer and the device is controlled and data stored and processed by means of software loaded and running under MS Windows. An electrode system consisting of a Ag/AgCl reference electrode (CHI), a glassy carbon disc working electrode (geometric area: 6.85 mm^2, CHI) and a Pt wire coil as auxiliary electrode (CHI) was used.

Modification of poly (p-ABSA) sensor

Before modification, the working glassy carbon electrode (GCE) was cleaned using 0.3 and 0.05 μm Al_2O_3 slurry on polishing materials. Then the polished GCE was sonicated in 1:1 nitric acid solution for 10 min and washed with ultrapure water. Afterwards, the GCE was electrochemically cleaned by cycling 20 times in the potential range of -0.7 to 1.7 V with a scan rate of 100 mV/s in 0.5 M H_2SO_4. After that, the electrode was plunged into 0.1 M KCl solution containing 5.0 mM p-ABSA and the modification procedure was performed by cyclic sweeping from -1.5 to 2.5 V for 14 cycles at 50 mV/s. Then the modified sensor was conditioned by cyclic voltammetry in the potential range of -0.5 to 0.5 V with 100 mV/s in pH 3.0 phosphate buffer solution (PBS) and was stored in PBS (pH 3.0).

Preparation of real samples

Tablets of MD with the commercial name Alfamet were prepared. Each tablet contains 250 mg of MD. Five MD tablets were finely

Figure 1. Molecular structure of methyldopa

powdered using a mortar and pestle and then an appropriate amount of this sample containing a known amount of the active material was weighed and dissolved with double distilled water. The prepared mixture was filtered using filter paper and diluted to appropriate amounts with double distilled water. The serum samples were collected from a research hospital and were sonicated (15 min with 5000 rpm) and then diluted 10 times with double distilled water without any additional pretreatment. Before voltammetric determination, appropriate amounts of the prepared real samples were added to 10 mL of phosphate buffer solution with optimum pH (pH 3.0), followed by transfer to the electrochemical cell for electrochemical measurements. The standard addition method was used to determine MD in the real and spiked samples.

RESULTS

Electropolymerization of p-aminobenzene sulfonic acid

Figure 2 shows the electropolymerization of *p*-ABSA at the GCE surface. The electropolymerization was performed in 0.1 M KCl solution containing 5.0 mM *p*-ABSA at a GCE by cyclic voltammetry in the potential range of -1.5 to 2.5 V. In the first cycle, two reduction peaks were obtained at 0.452 V (peak A) and 0.449 V (peak B), which might be related to the reduction of *p*-ABSA. Again, in the first cycle, an oxidation peak was observed at 0.824 V (peak C). In the next and subsequent cycles, following the continuous scan, broader peaks were monitored, indicating that the polymer film was constantly growing. It could be observed that film growth was faster for the first five cycles than for the other cycles and also the next cycles no longer existed. These findings show that *p*-ABSA was coated on the GCE surface by electrodeposition. A brown polymer was formed that was properly bonded on the GCE surface.

The effect of film thickness on MD response

The film thickness, which is determined by the number of cycles of electropolymerization, is one of the most important factors
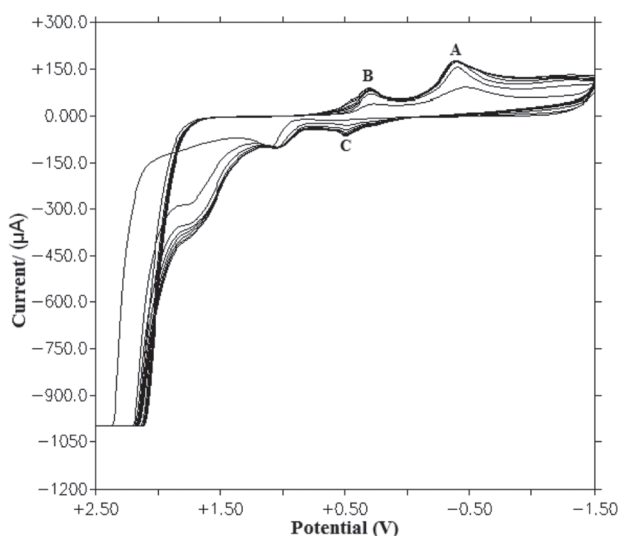
determining the polymer film selectivity property. By altering the amount of charge consumed during electropolymerization, it is possible to obtain poly (*p*-ABSA) films at desired thicknesses. Different film thicknesses were obtained by varying the cycles of the cyclic voltammetry. The selectivity of poly (*p*-ABSA) sensors prepared in the range of 8-18 cycles to MD and AA was systematically examined. From the DPV results of MD, it was observed that regular and repetitive responses could be obtained at 14 cycle film thickness. This can be seen from Figure 3. Furthermore, the effect of the number of cycles on the electropolymerization was calculated as 64.42%. This value was calculated from the ratio of the highest peak current to the peak current of the first polymer film.

Electrochemical behavior of MD at poly (p-ABSA) modified sensor

The voltammograms achieved by cyclic voltammetry of MD show a reduction wave at a potential of nearly 200 mV and an oxidation peak of nearly 220 mV (Figure 4). The electrochemical oxidation of MD was studied by cyclic voltammetry at the surface of the bare and poly (*p*-ABSA) modified GCE. The oxidation of MD shows a weak peak on the bare GC at nearly 0.590 V but the experimental results for the modified GCE show a well-defined anodic peak at the peak potential of 0.220 V with respect to the Ag/AgCl reference electrode. The peak current and peak potential values recorded at the GCE electrode were 0.61 µA and 0.590 mV, respectively. However, at the poly (*p*-ABSA) electrode these values were observed to be 30.48 µA and 0.220 mV, respectively (Figure 4). Consequently, in comparison with the data recorded from the bare GCE electrode, an increase in peak current and a decrease in overpotential of MD were obtained at the modified GC electrode. Therefore, it was assessed as an electrocatalytic effect for the oxidation of MD on the modified surface. It could be observed that the oxidation peak current for the modified electrode significantly increased and it was almost 50 times higher than that for the unmodified electrode. This behavior is due to adsorption of

Figure 2. Cyclic voltammetries of 5 mM *p*-aminobenzene sulfonic acid in 0.1 M KCl at glassy carbon electrode, scan rate: 50 mV/s, 14 cycles
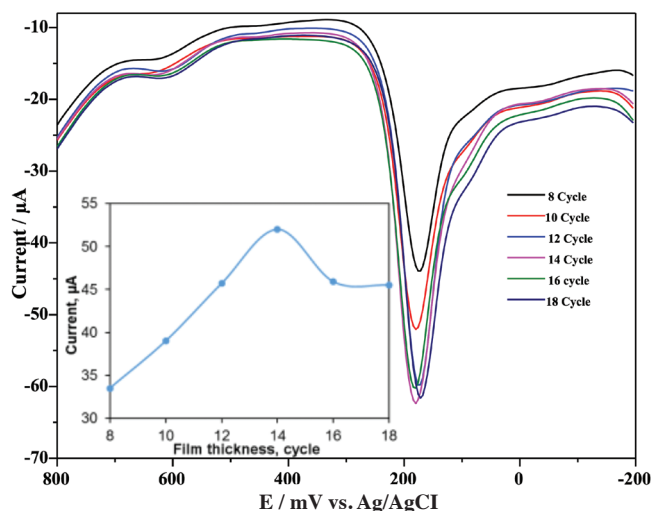
Figure 3. Differential pulse voltammetries of increasing film thicknesses of 0.01 mM methyldopa (MD) in 0.1 M phosphate buffer solution (pH 3.0) at poly (*p*-aminobenzene sulfonic acid) modified sensor. The relationship between film thickness and the peak current of MD (inset)
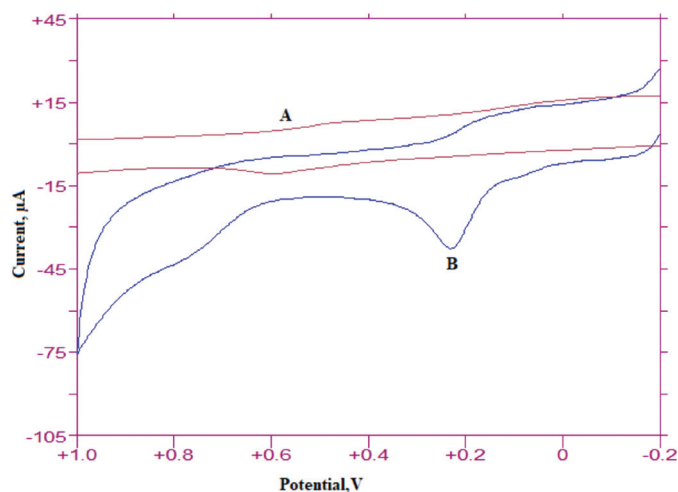
MD on the surface of *p*-ABSA by interaction of MD functional groups such as NH$_2$, COOH, and OH with carboxyl groups of activated *p*-ABSA on the surface of the electrode. Thus sensitivity was significantly enhanced due to preconcentration of MD on the active surface of *p*-ABSA. Moreover, as shown in Figure 4B, the onset potential for MD oxidation at the poly (*p*-ABSA) electrode is lower than its oxidation at the bare GCE (Figure 4B) because of the catalytic behavior of the modified electrode. However, the potential peak at the bare GCE (0.59 V) is higher than the potential peak at the modified GCE (0.220 V). The effect of scan rate on the oxidation peak current of 0.01 mM MD was studied. With the scan rate increasing, the anodic peak current increased. A good linearity between the square root of scan rate and peak current was obtained in the range of 10-250 mV s^{-1}. The linear regression equation was I_p(μA)= $0.502v^{1/2}$–0.899 with correlation coefficient R^2=0.998. The correlation coefficient is very close to 1.0, showing that the oxidation process is diffusion controlled. Furthermore, the plot of the logarithm of peak current versus logarithm scan rate has a slope of 0.63, which is almost the theoretical value of 0.56. The equation was $\log I_p$(μA)=0.63logv–0.7041 (R^2=0.998) on the modified electrode. This indicates a diffusion controlled electron process of MD oxidation at the poly (*p*-ABSA) modified GCE.

DISCUSSION

The electrostatic interaction between the modified GCE electrode and MD contributed to the enhancement of sensitivity and electroactivity. The oxidation peak of MD at pH 3.0 is irreversible and thus with an increase in peak height the peak potential shifts to lower potential. However, onset potential, which shows the kinetic of the reaction, decreased for the modified GCE compared to the bare GCE and thus sensitivity and selectivity increased because of these effects.

Electrolyte type effect on voltammetric behavior of MD
By selecting an appropriate supporting electrolyte solution, a conductive environment is created between the submerged electrodes.

The choice of supporting electrolyte depends on MD's resolution, dissociation degree, and nucleophilic character. For this purpose, voltammograms of MD in Na$_2$SO$_4$, PBS (pH 7.0), NaNO$_3$, NaClO$_4$, NaCl, and KCl supporting electrolytes (electrolytes concentration, 0.1 M) were recorded (Figure 5). While a voltammogram was taken at pH 7.0 for PBS, voltammograms were taken at the native pH of the other electrolyte species.

Effect of pH on the peak potential and peak current of MD
The peak current and potential are dependent on the pH of the solution. To find the optimum pH, the influence of pH over the range of 2.0-11.0 on the performance of the sensor was investigated. Experimental results for MD are shown in Figure 6. It was found that the anodic peak current of MD increased with increment of acidity, and reached its maximum value at pH 3.0. Therefore, pH 3.0 was selected as the optimum pH for the determination of MD. Increasing peak current with the increase in acidity showed that the mechanism for oxidation of MD was a proton dependent reaction.

It was observed that as the pH of solution was increased, the oxidation peak potential shifted to negative potential values. The negative shift and the peak potential showed a linear relationship with a slope of -52.4 mV/ pH in the pH range of 2.0-5.0. This slope approximately revealed that the number of protons in the process was equal with the number of electrons transferred in the oxidation reaction of MD.

Determination of MD in the presence of AA
Determination of MD in poly (*p*-ABSA) was done with differential pulse voltammetry. Differential pulse voltammograms of different concentrations of MD on the poly (*p*-ABSA) modified GCE are shown in Figure 7. The data of the obtained calibration charts are shown in Table 1. The calibration plot of the proposed sensor is linear in two concentration ranges of 1.0-30.0 and 30.0-300.0 μM.

Figure 4. Cyclic voltammetries of 0.01 mM methyldopa in 0.1 mM phosphate buffer solution (pH 3.0) (A) glassy carbon electrode, (B) at poly (*p*-aminobenzene sulfonic acid) modified sensor. Scan rate: 50 mV/s
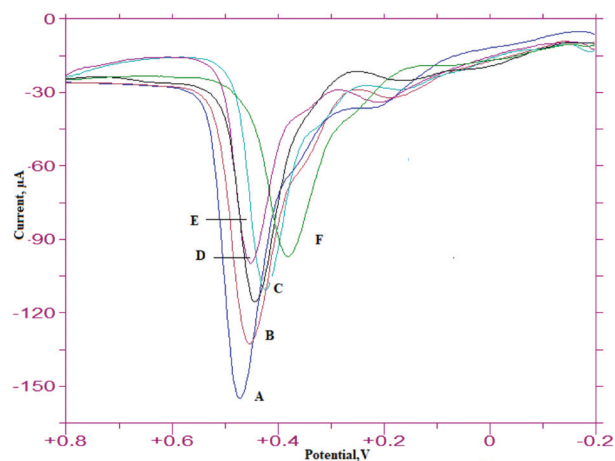
Figure 5. Electrolyte effect on voltammetric analysis of 0.01 mM methyldopa at poly (*p*-aminobenzene sulfonic acid) sensor. A) Phosphate buffer solution (pH 7.0), B) NaClO$_4$, C) KCl, D) NaCl, E) NaNO$_3$, and F) Na$_2$SO$_4$. Electrolyte concentration was 0.1 M
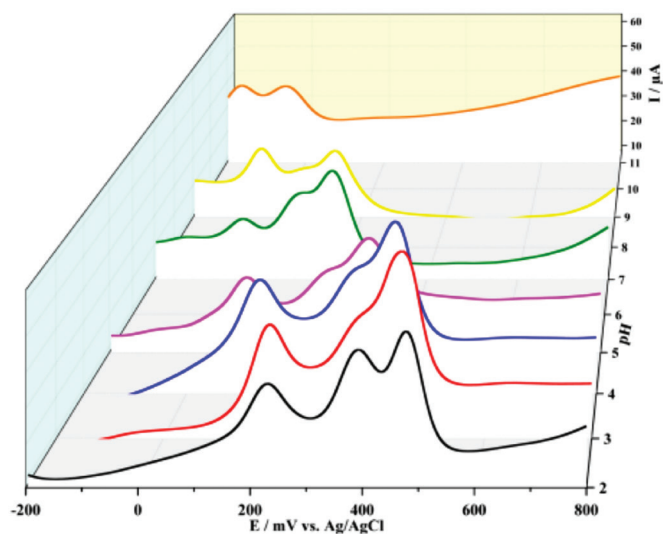
Figure 6. Differential pulse voltammetry responses of 0.01 mM methyldopa and 1.0 mM AA at modified sensor in phosphate buffer solution medium at different pHs: 2.0, 3.0, 4.0, 5.0, 7.0, 9.0, 11.0. Scan rate, 50 mV/s
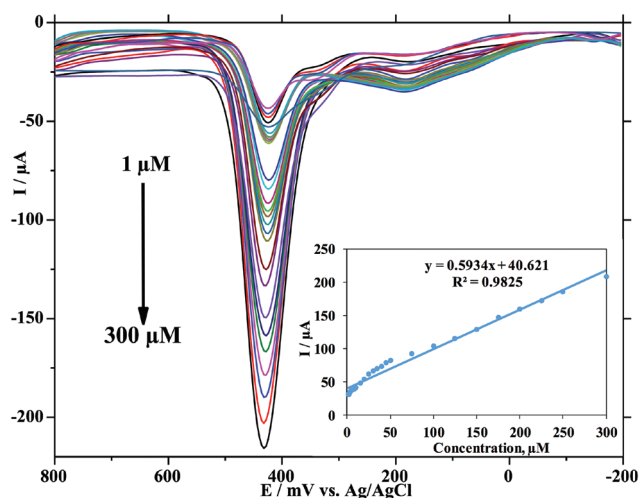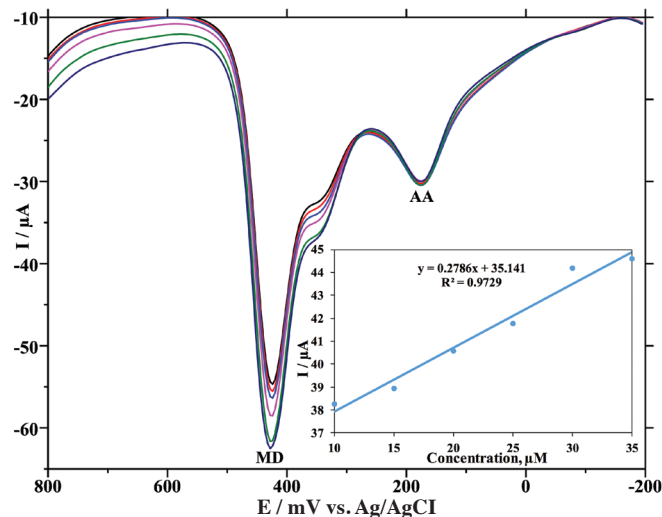

Figure 7. Differential pulse voltammograms and calibration graphs in increasing concentration of methyldopa in 0.1 M phosphate buffer solution (pH 3.0) at poly (*p*-aminobenzene sulfonic acid) modified sensor. The calibration chart of 1.0-300.0 µM methyldopa (inset)

Table 1. The data of calibration charts

	Linear concentration range (µM)	
Parameters	1.0-30.0	30.0-300.0
Correlation coefficient	0.9944	0.9975
Standard error of slope	0.0263	0.0075
Standard error of intercept	0.3538	1.167

The calibration equations over theses ranges are I_{pa} (µA)=1.21×C (µM)+30.81, R^2=0.9944, and I_{pa} (µA)=0.53 C (µM)+53.30, R^2=0.9975, respectively. LOD and LOQ were calculated as 5.0 nM and 10.6 nM *(S/N=3)*, respectively. The relative standard deviation (RSD) for MD and 5 repeated measurements was less than 3%.

Figure 8. The increasing concentration of methyldopa (0.01, 0.015, 0.020, 0.025, 0.030, 0.035 mM) with 0.5 mM ascorbic acid at poly (*p*-aminobenzene sulfonic acid) modified sensor in 0.1 M phosphate buffer solution (pH 3.0)
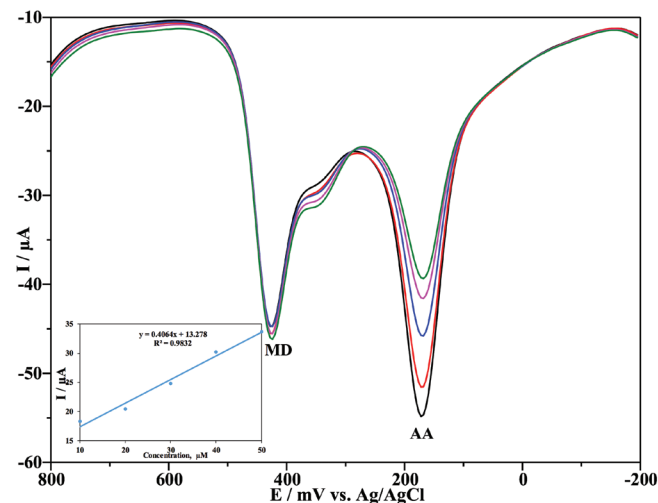
Figure 9. The increasing concentration of ascorbic acid (0.1, 0.2, 0.3, 0.4, 0.5 mM) in the presence of 0.01 mM methyldopa at poly (*p*-aminobenzene sulfonic acid) in 0.1 M phosphate buffer solution (pH 3.0)

It is readily seen from Figure 8 that peak currents increase linearly with increasing MD concentration even in the presence of AA. In addition, the MD peak current was unaffected by the increasing AA concentration (Figure 9). Moreover, from the successive runs of the modified electrode in the binary mixture, it was observed that the voltammetric responses were almost invariable. The RSD for MD and 5 repeated measurements was less than 3%. This reflects that the stability of the modified electrode was satisfactory.

Analytical applications
Five Alfamet tablets containing 250 mg of MD in each tablet were directly weighed and powdered in a mortar. The calculated amount of MD corresponding to 100 mM concentration stock solution was weighed and transferred to a 10-mL volumetric flask and the volume was supplemented with ultrapure water.

Table 2. Detection of methyldopa in commercial tablets

Parameters	Labeled, mM	Found, mM	RSD*, %	Bias, %	Recovery, %	RSD* of recovery, %	Bias of recovery, %
Proposed method	1	0.979	0.14	0.84	97.9	0.77	1.98
Blood serum	1	0.764	0.22	0.79	76.4	0.82	2.00

Each value is an average of five determinations.
*RSD: Relative standard deviation

The contents of the flask were subjected to centrifugation at 5000 rpm for 15 min to effect complete dissolution. The prepared mixture was filtered using paper filter and diluted using appropriate amounts of double distilled water. The serum samples were collected from a research hospital and were centrifuged (15 min at 5000 rpm) and then diluted 10 times with double distilled water without any additional pretreatment. Before the voltammetric determination, appropriate amounts of prepared real samples were added to 10 mL of phosphate buffer solution with optimum pH (pH 3.0) and then transferred to the electrochemical cell for electrochemical measurements. The standard addition method was used to determine MD in the real and spiked samples.

The quantity of MD in the tablets was computed from the suitable calibration graphs. Furthermore, the accuracy of the proposed techniques was checked by carrying out recovery studies. Recovery results obtained from the calibration graph can be seen in Table 2. The proposed method was successfully performed on real samples in the presence of interferences.

CONCLUSION

A poly (*p*-ABSA) modified electrode was applied for electrocatalytic assay of MD. The modified GCE indicated high electrocatalytic activity for MD. The modified GCE provides much sensitivity and selectivity in the assay of MD. Moreover, the modified electrode showed easy regeneration and good repeatability and stability. The modified GCE can be used under the selected conditions (in PBS, pH 3) for the determination of MD. The results show that the proposed method can be easily used in the determination of MD in drug samples and clinical analyses. It has been observed that this method can be used to identify MD in blood serum.

ACKNOWLEDGEMENTS

Conflict of Interest: No conflict of interest was declared by the authors.

REFERENCES

1. Hoffman BB, Lefkowitz RJ. In: Gilman AG, Hardman JG, Limbird LE, Molinoff PB, Ruddon RW, eds. The Pharmacological Basis of Therapeutics (9th ed). New York; McGraw-Hill; 1996:1908-1984.

2. Katzung EG, Masters SS, Trevor AJ. In: Katzung BG, ed. Basic and Clinical Pharmacology (12th ed). New York; McGraw-Hill; 2012:79-96.

3. Zecevic M, Zivanovic L, Agatonovic SK, Minic D. The use of a response surface methodology on HPLC analysis of methyldopa, amiloride and hydrochlorothiazide in tablets. J Pharm Biomed Anal. 2001;24:1019-1025.

4. Ballantine J, Woolfson AD. Determination of catecholamines in pharmaceutical preparations by differential pulse polarography at the glassy carbon electrode. Int J Pharmaceutics. 1979;3:239-246.

5. Badawy SS, Issa YM, Tag-Eldin AS. Potentiometric determination of L-dopa, carbidopa, methyldopa and aspartame using a new trinitrobenzenesulfonate selective electrode. Electroanalysis. 1996;8:1060-1064.

6. Wahbi AM, Abdine H, Korany M, Abdel-Hay MH. Sodium cobaltinitrite as a reagent for determining some phenolic drugs. J Ass Anal Chem. 1978;61:1113-1117.

7. Nagaraja P, Vasantha RA, Sunitha KR. A new sensitive and selective spectrophotometric method for the determination of catechol derivatives and its pharmaceutical preparations. J Pharm Biomed Anal. 2001;25:417-424.

8. Abdulrahman LK, Al-Abachi AM, Al-Qaissy MH. Flow injection-spectrophotometric determination of some catecholamine drugs in pharmaceutical preparations via oxidative coupling reaction with p-toluidine and sodium periodate. Anal Chim Acta. 2005;538:331-335.

9. Levine M. New concepts in the biology and biochemistry of ascorbic acid. N Engl J Med. 1986;314:892-902.

10. Kajiya Y, Sugai H, Iwakura C, Yoneyama H. Glucose sensitivity of polypyrrole films containing immobilized glucose oxidase and hydroquinonesulfonate ions. Anal Chem. 1991;63:49-54.

11. Arrigan DWM, Lowens MJ. Polypyrrole films doped with an electroactive sulfonated chelating reagent: electrochemical characterization and the detection of metal ions. Electroanalysis. 1999;11:647-652.

12. Gholiv MB, Amiri M. Preparation of polypyrrole/nuclear fast red films on gold electrode and its application on the electrocatalytic determination of methyl-dopa and ascorbic acid. Electroanalysis. 2009;21:2461-2467.

13. Gao Z, Ivaska A. Electrochemical behaviour of dopamine and ascorbic acid at overoxidized polypyrrole(dodecyl sulphate) film-coated electrodes. Anal Chim Acta. 1993;284:393-404.

14. Gao Z, Zi M, Chen B. Permeability controllable overoxidised polypyrrole film modified glassy carbon electrodes. Anal Chim Acta. 1994;286:213-218.

15. Saeed S, Reyhaneh-Sadat S, Zahra K. Sensitive electrochemical sensor for determination of methyldopa based on polypyrrole/

carbon nanoparticle composite thin film made by in situ electropolymerization. Electroanalysis. 2011;23:2248.

16. Behzad R, Neda A, Ali AE. Adsorptive stripping voltammetry determination of methyldopa on the surface of a carboxylated multiwall carbon nanotubes modified glassy carbon electrode in biological and pharmaceutical samples. Colloids and Surfaces B Biointerfaces. 2013;109:253-258.

17. Seyed ZM, Hadi B, Malihe J, Ali A. Nanomolar determination of methyldopa in the presence of large amounts of hydrochlorothiazide using a carbon paste electrode modified with graphene oxide nanosheets and 3-(4'-amino-3'-hydroxy-biphenyl-4-yl)-acrylic acid. Electroanalysis. 2015;27:2421-2430.

18. Diaz A, Bargon J, Handbook of Conducting Polymers, Skotheim, TA, ed, New York; Marcel Dekker Inc. 1986:1:81-82.

Rapid Stability Indicating HPLC Method for the Analysis of Leflunomide and Its Related Impurities in Bulk Drug and Formulations

Bulk İlaç ve Formülasyonlarda Leflunomid ve İlgili Safsızlıklarının Analizi için Hızlı Stabilite Göstergeli YBSK Yöntemini

 Useni Reddy MALLU, Venkateswara Rao ANNA, Bikshal Babu KASIMALA*

Koneru Lakshmaiah Education Foundation, Department of Chemistry, Guntur, Andhra Pradesh, India

ABSTRACT

Objectives: Leflunomide (LFNM) is a drug that belongs to isoxazole derivatives and has immunosuppressive and anti-inflammatory activities. A literature search confirms that there is no method reported for the simultaneous estimation of LFNM and its related impurities A and B in pharmaceutical dosage forms or in bulk drug. Hence the present work aimed to develop a simple stability indicating RP-HPLC method for the separation and quantification of LFNM and its impurities A and B.

Materials and Methods: Systematic trials of method conditions like mobile phase ratio, pH, flow rate, stationary phase, and detector wavelength were performed for the simultaneous analysis of LFNM and its related impurities A and B. The developed method was validated as per the ICH guidelines including forced degradation studies in different stress conditions.

Results: Optimized separation was achieved on a Thermo Scientific Hypersil ODS C18 column (250 mm×4.6 mm; 5 µm id) using mobile phase composition of acetonitrile, methanol, and 0.1 M sodium perchlorate in the ratio of 40:30:30 (v/v), pH 4.6, at a flow rate of 1.0 mL/min in isocratic elution. UV detection was carried out at a wavelength of 246 nm. Well-resolved peaks were observed with high numbers of theoretical plates, lower tailing factor, and reproducible relative retention time and response factor. The method was validated and all the validation parameters were found to be within the acceptance limits. Stability tests were done through exposure of the analyte solution to five different stress conditions, i.e. 1 N HCl, 1 N NaOH, 3% H_2O_2, thermal degradation of powder, and exposure to UV radiation. The method can successfully separate the degradation products along with both the impurities studied. The % degradation was also found to be less.

Conclusion: The method developed for LFNM is simple and precise and can be applied for the separation and quantification of LFNM and its related impurities in bulk drug and pharmaceutical formulations.

Key words: Leflunomide, impurity A, impurity B, stress degradation, HPLC

ÖZ

Amaç: Leflunomid (LFNM), izoksazol türevine ait ve immüne süpresif ve antienflamatuvar aktiviteye sahip bir ilaçtır. Literatür taraması, farmasötik dozaj formlarında ve bulk ilaçlarda LFNM ve ilgili safsızlık A ve B'nin değerlendirilmesi için rapor edilen bir yöntemin olmadığını doğrulamaktadır. Bu nedenle bu çalışma, LFNM'nin ve A ve B safsızlıklarının ayrıştırılması ve miktarının belirlenmesi için hızlı stabilite göstergeli RP-YBSK yöntemini geliştirmeyi amaçlamıştır.

Gereç ve Yöntemler: LFNM ve ilgili safsızlık A ve B'nin eş zamanlı analizi için mobil faz oranı, pH, akış hızı, stasyoner faz ve detector dalga boyu gibi metod koşullarının sistematik testleri gerçekleştirilmiştir. Geliştirilen yöntem farklı stress koşullarında zoraki bozunma çalışmalarını içeren ICH yönergelerine göre valide edilmiştir.

Bulgular: Optimal ayrıştırma, Thermo Scientific Hypersil ODS C18 kolonu (250 mm×4,6 mm; 5 µm id) üzerinde, 40:30:30 (h/h) oranında asetonitril, methanol ve 0,1 M sodium perklorat bileşiminden oluşan mobil faz kullanılarak elde edilmiştir; izokratik elüsyonda 1,0 mL/dak akış hızında pH 4,6 idi. UV saptaması 246 nm dalga boyunda gerçekleştirilmiştir. İyi-kararlı pikler, çok sayıda teorik plaka, daha az kuyruklama faktörü ve tekrarlanabilir göreceli retansiyon süresi ve tepki faktörü ile elde edilmiştir. Yöntem valide edilmiştir ve tüm validasyon parametreleri kabul limitinde bulunmuştur. Stabilite testleri, analit çözeltisinin beş farklı stress koşuluna, yani 1 N HCl, 1 N NaOH, %3 H_2O_2, tozun termal degradasyonuna ve UV radyasyonuna

maruz kalması yoluyla gerçekleştirilmiştir. Yöntem, bozunma ürünlerini çalışılan safsızlıklarla birlikte başarılı bir şekilde ayırabilmiştir. Yüzde degradasyon da daha az bulunmuştur.

Sonuç: LFNM'nin ayrılması ve miktar tayini için geliştirilen yöntem basit ve kesindir ve bulk ilaç ve farmasötik formülasyonlarda LFNM'nin ve ilgili safsızlıklarının ayrıştırılması ve analizi için uygulanabilir.

Anahtar kelimeler: Leflunomide, safsızlık A, safsızlık B, stress bozulması, YBSK

INTRODUCTION

Leflunomide (LFNM) is an isoxazole derivative having both immunosuppressive and anti-inflammatory activities.[1] LFNM acts as a dihydroorotate dehydrogenase inhibitor used for the treatment of rheumatoid arthritis.[2,3] It is also used to treat psoriasis, psoriatic arthropathy,[4] and other inflammatory conditions like bullous pemphigoid, Felty syndrome, Sjögren syndrome, Wegener granulomatosis, and vasculitis.[5] The most common side effects associated with LFNM are nausea, vomiting, diarrhea, abdominal pain, alopecia, and hypertension.[6]

The literature reveals that methods are reported for the estimation of LFNM in pharmaceutical formulations using high performance liquid chromatography (HPLC),[7-14] UPLC,[15] and spectrophotometer.[16,17] Only one HPLC method was reported for the simultaneous estimation of LFNM with other NSAIDs.[18] Bioanalytical methods are reported for estimation of LFNM in biological samples using HPLC,[19] HPTLC,[20] and liquid chromatography.[21] The other methods reported were determination of the active metabolite of LFNM in biological samples using HPLC.[22-24] No methods are reported for the estimation of LFLM and its USP related impurities in pharmaceutical formulations. Hence in the present study we attempted to develop a simple method for the estimation of LFLM (5-methyl-N-[4-(trifluoromethyl) phenyl]-isoxazole-4-carboxamide) and its related impurities A (α,α,α-trifluoro-p-toluidine, 4-(trifluoromethyl)aniline, 4-aminobenzotrifluoride) and B (2-cyano-3-hydroxy-N-(4-trifluoromethylphenyl) crotonamide) in pharmaceutical formulations. The molecular structure of LFNM and its related compounds in the study are given in Figure 1.

MATERIALS AND METHODS

Instrumentation
The separation and estimation of LFNM with impurities A and B were conducted on a PEAK HPLC (India) system. The mobile phase was pumped into the column using an LC-P7000 isocratic pump. A 20-μL fixed volume sample was injected for the analysis using a Rheodyne injector (model 7725) with a fixed 20-μL loop. A variable wavelength programmable (Waters 486) ultraviolet (UV)-visible detector was used for detecting the compounds. The detector response signals were monitored and integrated using Young Lin Autochro-3000 software (Korea). Samples were injected using a Hamilton (USA) manual HPLC syringe. A double beam UV-visible spectrophotometer (Teccomp UV-2301, India) was used for the spectral analysis. A Denver electronic analytical balance (SI-234) was used for weighing the standards and samples. pH of the mobile phase was adjusted using a Systronics (India) digital pH meter (Sr No: S 1326).

Chemicals and reagents
The active pharmaceutical ingredient LFNM with 99.20% purity and its two impurities A and B were obtained as gift samples from Torrent Pharmaceuticals Limited, Secundrabad, Telangana, India. The marketed formulation of LFNM (Lefno©–10 mg) was purchased in a local pharmacy. Laboratory reagent grade sodium perchlorate monohydrate ($NaClO_4.H_2O$) and perchloric acid ($HClO_4$) were purchased from SD Fine Chem. Limited, Mumbai. HPLC grade methanol, acetonitrile, and water were purchased from Merck Chemicals, Mumbai, and 0.2-μm nylon membrane filter papers were used for filtration of samples and mobile phase and were purchased from Millipore (India).

Preparation of solutions

Sodium perchlorate solution (0.1 M)
First 14.046 g of $NaClO_4.H_2O$ was weighed accurately and dissolved in 500 mL of water (HPLC grade). Then it was sonicated for 2-5 min to dissolve the compound completely in the water. The final volume was made up to the mark in a 1000-mL volumetric flask using water. The solution was filtered through a 0.45-μm nylon membrane filter paper.
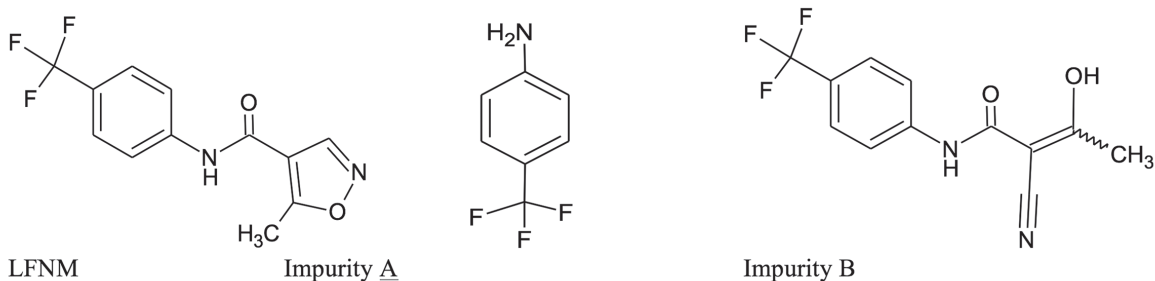
Figure 1. Molecular structure of LFNM and its related compounds in the study

LFNM: Leflunomide

Perchloric acid solution (0.1 M)

First 70% perchloric acid having molarity 11.6 M was used for the preparation of 0.1 M solution. Then 8.6 mL of $HClO_4$ was pipetted and was further made up to 1000 mL using water. The solution was sonicated and filtered through 0.45-µm nylon membrane filter paper.

Standard drug and impurity solutions

First 100 mg of standard drug LFNM was weighed accurately and then put in a 100-mL volumetric flask. The drug was dissolved in approximately 75 mL of methanol. Then the final volume was made up to 100 mL with methanol. LFNM standard stock solution of 1000 µg/mL was obtained and 1 mL of it was accurately pipetted into a 100-mL volumetric flask and the final volume was made up to the mark to get LFNM working standard solution of 10 µg/mL.

The procedure explained for the preparation of LFNM standard solution was followed for the preparation of 10 µg/mL Imp A and Imp B separately. Ten milliliters of LFNM, Imp A, and Imp B were mixed separately and the mixture solution was used for method development.

Formulation solution

Ten tablets of LFNM (Lefno©–10 mg) were powdered using a sterile mortar and pestle to get a fine powder. From the tablet powder an amount of drug equivalent to 10 mg of LFNM was weighed accurately and was dissolved in 10 mL of methanol. The solution was kept in an orbital shaker for 15 min to dissolve the drug completely in solvent. Then it was filtered through 0.45-µm nylon membrane filter paper. Sample solution containing 1000 µg/mL LFNM was obtained. The sample stock solution was further diluted to get a working sample solution having a LFNM concentration of 250 µg/mL. This solution was used for the identification and estimation of LFNM and its impurities A and B in pharmaceutical formulations.

Method development

The standard drug solution containing 10 µg/mL concentrations of both impurities and LFNM was initially used for method development studies. The wavelength of the detector was maintained based on the iso-absorption wavelength obtained by UV spectrophotometer for LFNM and impurities A and B. System suitability, resolution, response factor (RF), and peak symmetry are the key factors that are taken into consideration for optimization of the mobile phase. The mobile phase was confirmed by changes in different solvent ratios, strength of organic modifiers, and pH. Separation was performed on different column configurations and manufactures. The flow rate of the mobile phase also changed in order to get better resolution. The conditions that give the best resolution, response, and peak symmetry were considered suitable conditions and these conditions were further validated for the applicability of the method for the estimation of LFNM and its related impurities A and B in pharmaceutical formulations.

Method validation

The method was validated as per ICH guidelines.[25]

System suitability

System suitability tests were carried out on a freshly prepared standard solution at three concentrations (10, 20, and 30 µg/mL) of the LFNM, Imp A, and Imp B to scrutinize the various optimized parameters such as retention time, relative RF (RRF), resolution, tailing factor, and USP plate count.

Linearity and range

Standard calibration curves were prepared with six calibrators over a concentration range of 0.5-3.0 µg/mL for LFNM, Imp A, and Imp B. The solutions were analyzed in triplicate in the optimized conditions. The data of peak area vs. drug concentration were analyzed using linear least square regression.

Precision

Precision was determined using six standard solutions containing 2 µg/mL LFNM, Imp A, and Imp B that were prepared and analyzed in the optimized method conditions. For intraday precision the solutions were prepared and analyzed six times on the same day at different time intervals and for interday precision the solutions were analyzed on three different days. Peak area responses of six replicate analyses were calculated in terms of relative standard deviation (RSD).

Ruggedness

Ruggedness of the method was studied by different analysts analyzing standard solutions containing 8 µg/mL LFNM, Imp A, and Imp B in the optimized conditions in the same laboratory conditions. %RSD values of peak area responses of six replicate analyses were calculated.

Robustness

Robustness of the proposed method was tested by slight variation in optimized method conditions. Change in ±5 nm of detector wavelength, ±5 mL variation in mobile phase organic and pH modifier, ±0.1 mL mobile phase flow rate, and ±0.1 factor of pH was studied. In each of the changed conditions, standard solutions containing 8 µg/mL LFNM, Imp A, and Imp B were analyzed in triplicate. The percentage change was calculated.

Recovery

The standard addition method was carried out for determining the accuracy of the method. For this, 50%, 100%, and 150% level concentrations were spiked into a known concentration of 1 µg/mL. Accuracy was determined by comparing the difference between the spiked value and the actual found value.

Force degradation studies

Acid hydrolysis

First 50 mg of drug was mixed with 50 mL of 0.1 N HCl solutions. After incubation for 12 h (AH 1) and 24 h (AH 2), the sample solution was neutralized and diluted up to standard concentration of 250 µg/mL and was analyzed in the developed method conditions.

Base hydrolysis

First 50 mg of drug was mixed with 50 mL of 0.1 N NaOH solutions. After incubation for 12 h (BH 1) and 24 h (BH 2),

the sample solution was neutralized and diluted up to standard concentration of 250 µg/mL and was analyzed in the developed method conditions.

Oxidative degradation

First 50 mg of drug was mixed with 50 mL of 3% H_2O_2 solution. After incubation for 12 h (OD1) and 24 h (OD2), the sample solution was neutralized and diluted up to standard concentration of 250 µg/mL and was analyzed in the developed method conditions.

Photolytic degradation

First 50 mg of drug sample was kept in UV light (254 nm). After incubation for 12 h (PD 1) and 24 h (PD2), the sample solution was neutralized and diluted up to standard concentration of 250 µg/mL and was analyzed in the developed method conditions.

Thermal degradation

First 50 mg of drug sample was kept in an oven at 60˚C. After incubation for 12 h (TD 1) and 24 h (TD 2), the sample solution was neutralized and diluted up to standard concentration of 250 µg/mL and was analyzed in the developed method conditions.

Formulation analysis

Formulation sample solution of 250 µg/mL prepared from marketed formulation tablets of LFNM (Lefno©–10 mg) was analyzed in triplicate in the optimized conditions. The peak area response obtained in the formulation analysis was used to determine the applicability of the developed method for the estimation of LFNM in pharmaceutical formulations.

RESULTS AND DISCUSSION

The aim of the present work was to develop a simple, accurate reverse phase-HPLC-UV method for the quantification of LFNM and its related impurities A and B in pharmaceutical formulations. A literature survey reveals that no method was reported previously for the separation and qualitative and quantitative analysis of LFNM and its related impurities A and B. Hence the attempt made here is novel and has significant importance in simultaneous detection and quantification of LFNM and its related impurities A and B.

The mobile phase was confirmed by change in different solvent ratios, expected peak shape, and resolution achieved using the mobile phase composition of acetonitrile, methanol, and 0.1 M sodium perchlorate in the ratio of 40:30:30 (v/v). The pH of the mobile phase was adjusted to 4.6 using 0.1 M perchloric acid. The mobile phase was pumped at a flow rate of 1.0 mL/min in isocratic elution. UV detection was carried out at a wavelength of 246 nm and separation was achieved on a Thermo Scientific Hypersil ODS C18 column (250 mm×4.6 mm; 5 µm id). In the optimized conditions, well retained, resolved, and symmetric peaks are observed in the standard chromatogram containing 10 µg/mL LFNM, imp A, and imp B. The standard chromatogram obtained in the optimized conditions is given in Figure 2. The blank analysis was performed by analyzing the mobile phase and it confirmed that no detection was observed in the blank chromatogram (Figure 3). This proved that the method

developed was specific and no mobile phase interference was observed in the chromatogram.

Prior to validation of the developed method, repeatability and system suitability were determined at standard solution concentrations of 10, 15, and 20 µg/mL. The standard solutions were prepared and were analyzed in the developed method conditions in triplicate. The system suitability conditions like plate count, asymmetric factor, and resolution were determined and found to be within the acceptance limits. The RF, RRF, and relative retention time were also calculated and found to be reproducible. Hence the developed method was found to be reproducible and all the system suitable parameters were within the acceptable limits (Table 1).

A six point linear calibration curve was obtained in the concentration range of 0.5-3.0 µg/mL. The linear regression equation was found to be y=50344x+2396.2 (R=0.999), y=33020x - 169.16 (R=0.999), and y=42853x + 606.76 (R=0.999) for LFNM, imp A, and imp B, respectively. A very high correlation coefficient value (more than 0.999) was observed for LFNM and both impurities, confirming that the method follows a linear relation accurately within the concentration range studied. The linearity results are given in Table 2 and the calibration curve is shown in Figure 4.

Precision of the developed method was tested by analyzing the standard solution at a concentration of 2.0 µg/mL. The
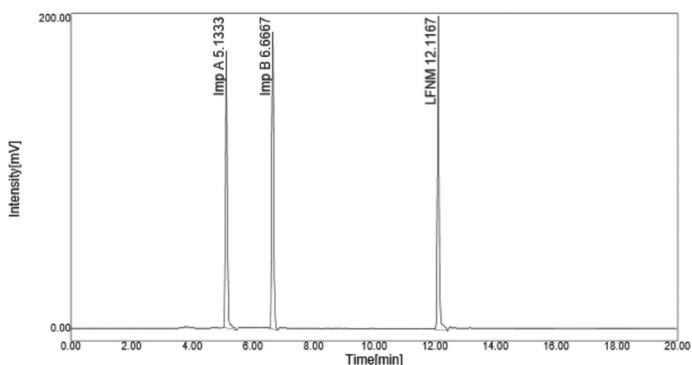
Figure 2. Standard chromatogram of LFNM, Imp A, and Imp and B at a concentration of 10 µg/mL

LFNM: Leflunomide
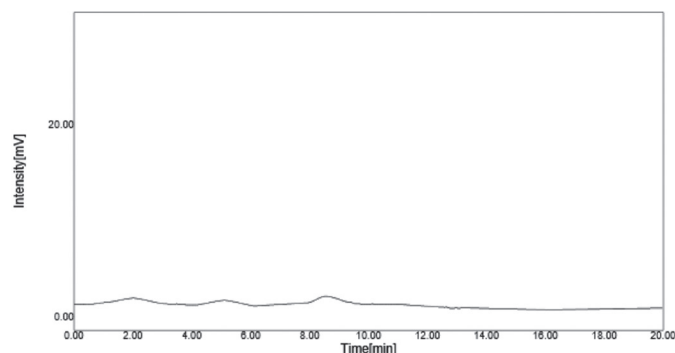
Figure 3. Blank (mobile phase) chromatogram of LFNM, Imp A, and Imp B

LFNM: Leflunomide

solution was analyzed six times on the same day for intraday precision and on three different days for interday precision. The same concentration of solution was prepared and analyzed on three days by three different analysts for ruggedness. The %RSD was calculated and was found to be 0.383, 0.394, and 0.915 in intraday precision, 0.258, 0.236, and 0.281 in interday precision, and 0.578, 0.458, and 0.491 in the ruggedness study for impurities A and B and LFNM, respectively. The results confirm that the developed method was rugged and precise.

Robustness was tested by analyzing the standard solution in the optimized conditions that were changed deliberately. The percentage change in each changed condition was calculated and was found to be less than 2 (Table 3). This confirms that a small change in the analytical conditions did not influence the chromatographic separation and detection of LFNM and its related impurities A and B. Hence the method was found to be robust.

Accuracy of the method was determined by spiked recovery studies. For this, 50%, 100%, and 150% concentrations were spiked and analyzed in triplicate into a known concentration of 1 µg/mL. The percentage recovery was found to be within the acceptance limit of 98-102% (Table 4). The %RSD in each spiked level was calculated and was found to be within the

acceptance limit of <2. Hence the proposed method was found to be accurate.

The standard drug was exposed to different stress conditions and was analyzed in the optimized conditions and the results were compared with those of an unstressed standard (Figure 5). The percentage degradation was found to be very high in the acid degradation study. In this condition the drug was found to be degraded up to 2.518% in 12 h and 10.808% in 24 h of stress exposure. The number of degradation products was also found to be high in this condition. Three additional peaks along with both impurities and LFNM were detected in acid condition (Figure 6). In the base degradation study, the drug was found to be degraded up to 2.19% and 8.619% after 12 and 24 h of stress exposure, respectively. One additional peak after 12 h and two additional peaks after 24 h (Figure 7) of stress exposure along with LFNM and both impurities were detected in base conditions. In oxidative degradation, very low degradation of 1.14% was observed at 12 h with no additional degradation compounds, whereas after 24 h one additional peak was detected and the % degradation was found to be 5.289 (Figure 8). In the photolytic degradation, 3.13% degradation with one additional detection was observed at 12 h and two additional degradation products with % degradation of 8.887 (Figure 9) were observed. In the thermal degradation, 5.581% degradation was observed and the

Table 1. System suitability results

Compound	Concentration in µg/mL	Retention time (min)	RRT	RRF	Theo plate*	Tail factor*	Resolution*
LFNM	10	12.109±0.008	---	---	9933	0.745	11.524
	15	12.155±0.019	---	---	9862	0.740	11.607
	20	12.144±0.010	---	---	9863	0.757	11.850
Impurity A	10	5.132±0.001	0.423±0.004	0.649±0.005	4270	1.157	---
	15	5.133±0.028	0.422±0.002	0.647±0.001	4277	1.160	---
	20	5.137±0.010	0.423±0.003	0.651±0.002	4333	1.163	---
Impurity B	10	6.654±0.018	0.050±0.002	0.843±0.001	6055	1.540	5.980
	15	6.672±0.009	0.549±0.001	0.834±0.005	6157	1.485	5.877
	20	6.611±0.009	0.544±0.003	0.846±0.002	6086	1.540	5.893

*Values given in table are the average values of three replicate experiments
RRT: Relative retention time, RRF: Relative response factor, LFNM: Leflunomide, min: Minute

Table 2. Linearity results

| S. no.	Concentration in µg/mL	Peak area observed		
		Imp A	Imp B	LFNM
1	0.5	16243±198.596	22220±314.079	26647±185.176
2	1	32607±533.094	42538±227.027	52314±254.161
3	1.5	50051±109.768	65490±173.463	80610±109.587
4	2	65467±360.266	86523±253.997	102530±1945.648
5	2.5	82575±117.091	108259±1057.730	128587±2427.108
6	3	98748±152.533	128567±761.748	152506±1489.122

*Values given in table are the average±standard deviation of three replicate experiments
LFNM: Leflunomide
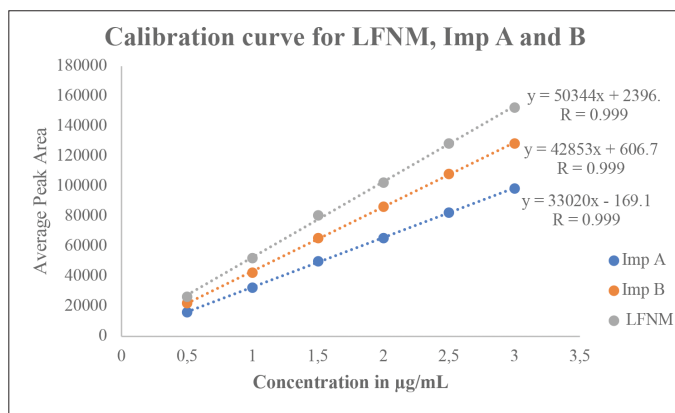
Figure 4. Linear calibration curve for LFNM, Imp A, and Imp B in the developed method

LFNM: Leflunomide

chromatogram shows one additional detection along with LFNM and both impurities (Figure 10). In all degradation conditions, the % degradation was found to increase with an increase in time. The % degradation and the formation of a number of degradation products increased with an increase in the stress degradation time from 12 h to 24 h in all the conditions studied. The additional detection observed in the stress degradation study along with LFNM and both impurities studied may be unknown impurities formed or the compound degraded due to the stress study. These additional compounds were not observed in the standard unstressed chromatogram. Both the impurities and the degradation products were successfully separated in the optimized conditions and hence the method can separate and quantify the potential impurities in LFNM. The forced degradation results are given in Table 5.

Table 3. Robustness results

S. no.	Condition	Robustness at 2 µg/mL					
		Imp A		Imp B		LFNM	
		Peak area	% Change	Peak area	% Change	Peak area	% Change
1	Optimized	65467	---	86523	---	102530	---
2	MP 1	65633	0.253	85901	0.719	102981	0.439
3	MP 2	65782	0.481	85257	1.464	103102	0.557
4	WL 1	64990	0.728	85637	1.024	103392	0.840
5	WL 2	64628	1.281	86030	0.569	103782	1.221
6	pH 1	65125	0.522	86132	0.451	103075	0.531
7	pH 2	64528	1.434	85998	0.606	102903	0.363
8	FR 1	64593	1.335	85813	0.820	102745	0.209
9	FR 2	64520	1.446	86121	0.464	102134	0.386

MP (Mobile Phase) 1: acetonitrile, methanol and 0.1 M sodium perchlorate in the ratio of 34:35:30 (v/v), MP 2: acetonitrile, methanol and 0.1 M sodium perchlorate in the ratio of 45:25:30 (v/v); WL (Wavelength) 1: 241 nm, WL 2: 251 nm; pH 1: 4.5, pH 2: 4.7; FR (Flow rate) 1: 0.9 mL/min, FR 2: 1.1 mL/min.
LFNM: Leflunomide

Table 4. Recovery results

S. no.	Compound	Recovery level	Concentration in µg/mL				% Recovery*
			Target	Spiked	Final	Amount recovered*	
1	Imp A	50%	1	0.5	1.5	1.491±0.003	99.359±0.165
2		100%	1	1	2	1.980±0.010	99.011±0.522
3		150%	1	1.5	2.5	2.464±0.009	98.548±0.373
4	Imp B	50%	1	0.5	1.5	1.489±0.004	99.254±0.243
5		100%	1	1	2	1.979±0.002	98.977±0.116
6		150%	1	1.5	2.5	2.487±0.004	99.504±0.183
7	LFNM	50%	1	0.5	1.5	1.497±0.006	99.803±0.409
8		100%	1	1	2	1.974±0.003	98.699±0.141
9		150%	1	1.5	2.5	2.495±0.017	99.838±0.685

*Values given in table are the average±standard deviation for three replicate experiments
LFNM: Leflunomide
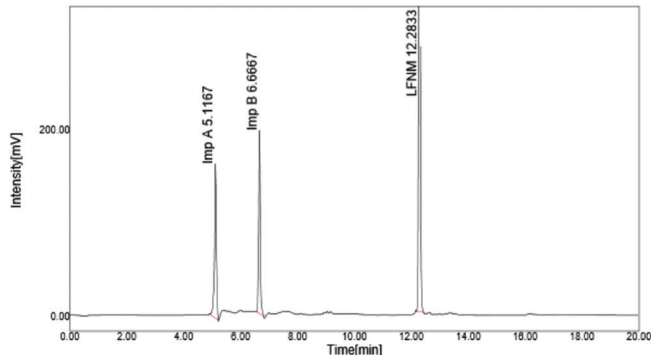
Figure 5. Unstressed (standard) chromatogram of LFNM
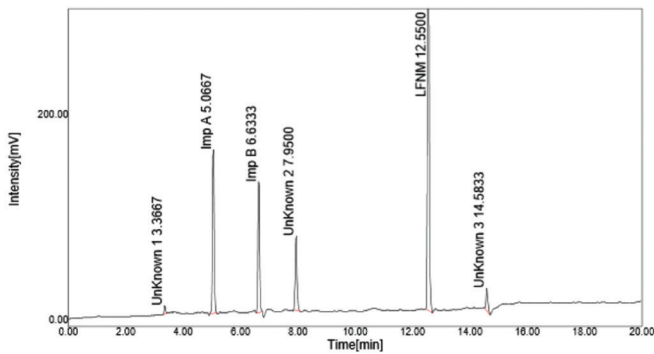
LFNM: Leflunomide

Figure 6. Acid degradation chromatogram of LFNM
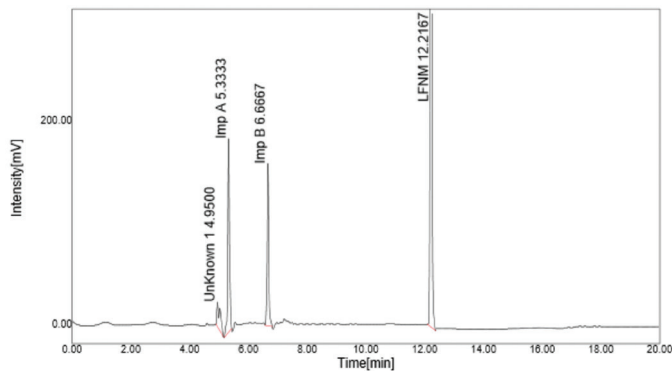
LFNM: Leflunomide

Figure 7. Base degradation chromatogram of LFNM
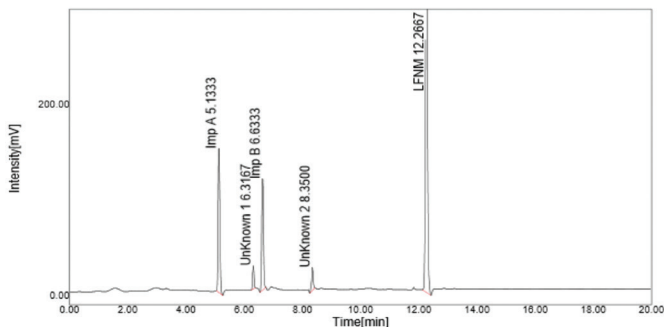
LFNM: Leflunomide

Figure 8. Oxidative degradation chromatogram of LFNM

LFNM: Leflunomide

S. no.	Condition	Number of additional peaks observed	Peak area	% Amount remaining	% Amount degraded
1	AH 1	1	12371397	97.481	2.518
2	AH 2	3	11319358	89.191	10.808
3	BH 1	1	12412803	97.807	2.192
4	BH 2	2	11597145	91.380	8.619
5	OD 1	0	12546917	98.864	1.136
6	OD 2	1	12019823	94.710	5.289
7	PD 1	1	12293071	96.864	3.135
8	PD 2	2	11563280	91.113	8.887
9	TD 1	0	12481397	98.350	1.652
10	TD 2	1	11982822	94.419	5.581

Table 5. Forced degradation results
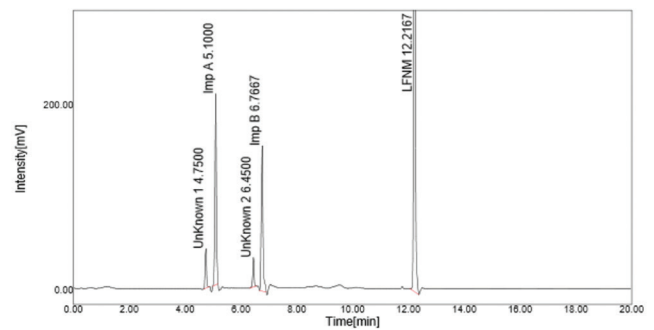
Figure 9. Photolytic degradation chromatogram of LFNM
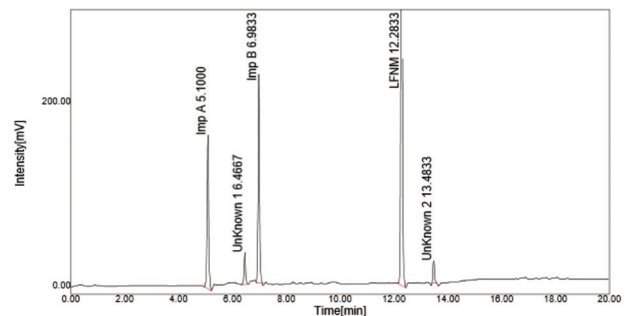
LFNM: Leflunomide

Figure 10. Thermal degradation chromatogram of LFNM

LFNM: Leflunomide

The formulation sample solution of LFNM was analyzed in the developed method conditions in triplicate. The peak area response of LFNM was used for determination of the applicability of the developed method for the analysis of LFNM in pharmaceutical formulations. A standard regression equation was used for the determination of formulation assay and the % assay was found to be 98.735%. In the formulation chromatogram both the impurities were detected (Figure 11) and other chromatographic impurities and formulation excipients did not interfere with the results. Hence the developed method
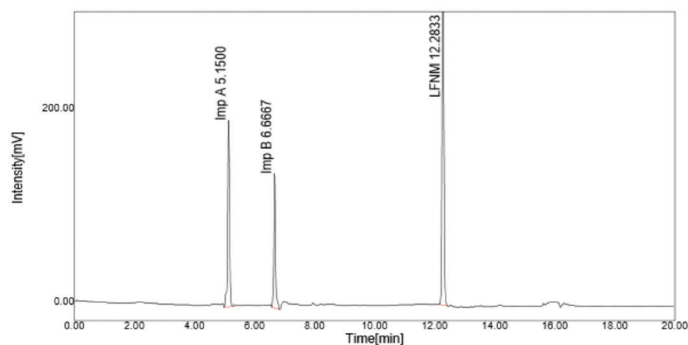
Figure 11. Formulation chromatogram of LFNM (Lefno©–10 mg)

LFNM: Leflunomide

was found to be suitable for the quantification of LFNM and can separate and analyze impurities A and B.

CONCLUSION

A simple, validated, and fast stability indicating HPLC method is established for quantification of LFNM and its potential USP impurities A and B. In the literature no method was found to be established for the simultaneous quantification of LFNM and its potential impurities A and B. Hence the method represents the first report about a stability indicating method for the determination of LFNM in the presence of impurities. The proposed method achieves satisfactory separation of LFNM from impurities and the degradation products, an extended linear range, and rapid analysis time. A high recovery of LFNM in formulation was obtained. The proposed method ensured precise and accurate determination of LFNM in pharmaceutical formulations. The excipients present in the formulation were not interfering in the method. Hence the method is simple, convenient, and suitable for analyzing LFNM in bulk and in pharmaceutical formulations in the presence of its potential impurities A and B.

Conflict of Interest: No conflict of interest was declared by the authors.

REFERENCES

1. Anthony CA. Immunosuppressive drugs: the first 50 years and a glance forward. Immunopharmacology. 2000;47:63-83.

2. Reuben A. Hepatotoxicity of Immunosuppressive Drugs. In: Kaplowitz N, DeLeve LD, eds. Drug-Induced Liver Disease (3rd ed). New York; Academic Press; 2013:569-591.

3. Li EK, Tam LS, Tomlinson B. Leflunomide in the treatment of rheumatoid arthritis. Clin Ther. 2004;26:447-459.

4. Nash P, Thaci D, Behrens F, Falk F, Kaltwasser JP. Leflunomide improves psoriasis in patients with psoriatic arthritis: an in depth analysis of data from the TOPAS Study. Dermatology. 2006;212:238-249.

5. Sanders S, Harisdangkul V. Leflunomide for the treatment of rheumatoid arthritis and autoimmunity. Am J Med Sci. 2002;323:190-193.

6. Konemann S, Dorr M, Felix SB. The Heart in Rheumatic, Autoimmune and Inflammatory Diseases, Cardiac Immunomodulation, Pathophysiology. Clinical Aspects and Therapeutic Approaches. New York; Academic Press; 2017:681-714.

7. Palled MS, Padmavathi YD, Bhat AR. Development and validation of RP-HPLC method for the estimation of leflunomide in bulk drug and tablets. RJPBCS. 2014;5:659-667.

8. Saini B, Bansal G. Isolation and characterization of a degradation product in leflunomide and a validated selective stability-indicating HPLC-UV method for their quantification. JPA. 2015;5:207-212.

9. Miron DS, Soldattelli C, Schapoval EES. HPLC with diode-array detection for determination of leflunomide in tablets. Chromatographia. 2006;63:283-287.

10. Yeniceli D, Ak D, Tuncel M. Determination of leflunomide in tablets by high performance liquid chromatography. J Pharm Biomed Anal. 2006;40:197-201.

11. Govind JK, Vijay RR, Kapil LD, Atul HB, Hitendra SJ. Validation of a stability-indicating LC method for assay of leflunomide in tablets and for determination of content uniformity. Int J Chemtech Res. 2011;3:523-530.

12. Prathyusha Naik CN, Chandra Sekhar KB, Muneer S. A novel stability indicating RP-HPLC method development and validation of leflunomide in bulk and its dosage form. Int J Res Pharm Sci. 2016;7:47-51.

13. Srinivas Rao V, Sunanda KK, Narasimha Rao M, Allam Appa Rao, Maheswari IL, Srinubabu G. Development and validation of LC method for the determination of leflunomide in pharmaceutical formulations using an experimental design. Afr J Pure Appl Chem. 2008;2:010-017.

14. Patel SK, Patel KH, Karkhanis VV, Captain AD. Development and validation of analytical method for estimation of leflunomide in bulk and their pharmaceutical dosage form. Austin J Anal Pharm Chem. 2015;2:1046-1056.

15. Govind JK, Vijay RR, Gaurang PP, Hitendra SJ. Development and validation of a stability indicating UPLC assay method for determination of Leflunomide in tablet formulation. Der Chemica Sinica. 2011;2:65-74.

16. Lakshmana Prabu S, Suriya Prakash TNK, Shanmugarathinam A. Development of difference spectrophotometric method for the estimation of leflunomide in tablet dosage form. Chem Ind Chem Eng Q. 2012;18:407-410.

17. Pal NR, Chakraborty M, Debnath R, Gupta BK. Spectrophotometric method for estimation of leflunomide in bulk and tablets. Asian J Chem. 2010;22:1649-1651.

18. Sultana N, Arayne MS, Khan MM, Ali SN. Development of liquid chromatography UV method for simultaneous determination of leflunomide and NSAIDs in API and pharmaceutical formulations: It's application to *in vitro* interaction studies. Med Chem. 2013;3:262-270.

19. Schmidt A, Schwind B, Gillich M, Brune K, Hinz B. Simultaneous determination of Leflunomide and its active metabolite, A77 1726, in human plasma by high performance liquid chromatography. Biomed Chromatogr. 2003;17:276-281.

20. Sola KA, Dedhiya PP, Shah SA. Development and validation of HPTLC method for estimation of leflunomide in its pharmaceutical dosage form. IJDRA. 2017;5:60-67.

21. Talaat W. Bioanalytical method for the estimation of co-administered esomeprazole, leflunomide and ibuprofen in human plasma and in pharmaceutical dosage forms using micellar liquid chromatography. Biomed Chromatogr. 2017;31. Epub 2016 Nov 15.

22. Sobhani K, Garrett DA, Liu DP, Rainey PM. Rapid and simple high-performance liquid chromatography assay for the leflunomide metabolite teriflunomide (A77 1726), in renal transplant recipients. Am J Clin Pathol. 2010;133:454-457.

23. Chan V, Charles BG, Tett SE. Rapid determination of the active leflunomide metabolite A77 1726 in human plasma by high-performance liquid chromatography. Journal of Chromatography B. 2004;803:331-335.

24. Pawiñski T, Gralak B. HPLC determination of active metabolite of leflunomide in plasma. Chem Anal. 2005;50;785.

25. ICH Harmonised Tripartite Guideline, Validation of Analytical Procedures. Text and Methodology. ICH Q2(R1). The European Agency for the Evaluation of Medicinal Products (CPMP/ICH/381/95), 1995.

Phytochemical Screening and Toxicological Evaluation of *Sargassum wightii* Greville in Wistar Rats

Sargassum wightii Greville'nin Fitokimyasal Taraması ve Wistar Sıçanlardaki Toksikolojik Değerlendirmesi

[ID] Sathiya RAMU*, [ID] Anita MURALI, [ID] Anbu JAYARAMAN

M. S. Ramaiah University of Applied Sciences, Faculty of Pharmacy, Department of Pharmacology, Bangalore, Karnataka, India

ABSTRACT

Objectives: The present study was conducted to identify the phytoconstituents present in different extracts of *Sargassum wightii* and to assess the toxicity of its ethanol extract.

Materials and Methods: Successive solvent extraction and total ethanol extraction of *S. wightii* were performed and preliminary phytochemical screening was carried out. The acute toxicity of ethanol extract of *S. wightii* (ESW) was studied. The subchronic toxicity of ESW was tested with doses of 100, 200, and 400 mg/kg. The animals were observed for changes in body weight and food and water intake. At the end of the study, the relative weights of vital organs were noted, followed by histopathological examinations. Various hematological and biochemical estimations were also carried out.

Results: Phytochemical screening of *S. wightii* revealed the presence of alkaloids, carbohydrates, glycosides, phenolic compounds, and tannins. ESW did not induce any mortality or pre-terminal death in the acute toxicity study. There were no significant differences in body weight, relative weight of vital organs (except the brain), or food or water intake compared to the control group. The histopathological examination showed normal architecture, suggesting absence of pathological lesions. Hematological and biochemical parameters were also comparable to those of the control group except for reductions in glucose and cholesterol levels, which are postulated to be beneficial.

Conclusion: The presence of various phytoconstituents in *S. wightii* is evidence that it could be a potential source for treating different ailments. No significant toxic effects were observed after treatment with ESW. Thus, it is proposed to be safe and can be recommended for long-term treatment.

Key words: *Sargassum wightii*, phytochemical screening, acute toxicity, subchronic toxicity

ÖZ

Amaç: Bu çalışma, *Sargassum wightii*'nin farklı ekstrelerinde bulunan fitokimyasalları tanımlamak ve etanol ekstresinin toksisitesini değerlendirmek için yapılmıştır.

Gereç ve Yöntemler: *S. wightii*'den total etanol ekstraksiyonu ve ardışık çözücü ekstraksiyonu yapılarak ekstreler üzerinde ön fitokimyasal tarama yapılmıştır. *S. wightii*'nin etanol ekstresinin (ESW) akut toksisitesi araştırılmıştır. ESW'nin subkronik toksisitesi, 100, 200 ve 400 mg/kg'lık dozlarla test edilmiştir. Hayvanlar, vücut ağırlığındaki ve yiyecek ve su alımındaki değişiklikler için gözlenmiştir. Çalışmanın sonunda, hayati organların relatif ağırlıkları, ardından histopatolojik incelemeler yapılmıştır. Çeşitli hematolojik ve biyokimyasal değerlendirmeler de yapılmıştır.

Bulgular: *S. wightii*'nin fitokimyasal taraması, alkaloitler, karbonhidratlar, glikozitler, fenolik bileşikler ve tanenlerin varlığını ortaya koymuştur. ESW, akut toksisite çalışmasında mortalite veya terminal öncesi ölüme neden olmamıştır. Hayvanlar, vücut ağırlığındaki ve yem ve su tüketimindeki değişiklikler yönünden gözlenmiştir. Çalışmanın sonunda, hayati organların (beyin hariç) relatif ağırlıkları, yem ve su tüketiminde kontrol grubuna kıyasla anlamlı farklılıklar bulunamamıştır. Histopatolojik incelemede patolojik lezyonların olmadığını gösteren normal bir yapı izlenmiştir. Hematolojik ve biyokimyasal parametreler, yararlı olduğu düşünülen glukoz ve kolesterol seviyelerinde azalma haricinde, kontrol grubu ile de karşılaştırılabilir düzeyde bulunmuştur.

Sonuç: *S. wightii*'de çeşitli fitokimyasalların varlığı, farklı hastalıkların tedavisi için potansiyel bir kaynak olabileceğinin kanıtıdır. ESW ile tedaviden sonra önemli bir toksik etki gözlenmemiştir. Bu nedenle, güvenli olduğu ve uzun süreli tedavide kullanılabilirliği önerilmiştir.

Anahtar kelimeler: *Sargassum wightii*, fitokimyasal tarama, akut toksisite, subkronik toksiste

INTRODUCTION

Sargassum is a significant genus of brown marine algae belonging to the family *Sargassaceae*. The well-known bioactive compounds of *Sargassum* include meroterpenoids, phlorotannins, fucoidans, sterols, and glycolipids. It is reported to possess antioxidant, hypolipidemic, hypoglycemic, neuroprotective, antimicrobial, anticancer, anti-inflammatory, anticoagulant, antimelanogenic, and hepatoprotective activities.[1-9]

Sargassum wightii Greville (*S. wightii*) is an abundant marine brown alga commonly found on the shorelines of India. It is dark brown, 21-40 cm in height, richly branched, and the midrib is spherical to ellipsoidal and 5-8 mm long and 2-4 mm wide.[10] It is a macroscopic, multicellular, photosynthetic, nonvascular, pelagic marine species rich in sulfated polysaccharides that manifest potent free radical scavenging and antioxidant effects and hypolipidemic and anti-inflammatory effects.[11-13] Fucoidan is one of the well-known components of *S. wightii* with diverse biological activities including anti-inflammatory, anticancer, antimicrobial, and α-D-glucosidase inhibitory activity.[14] The present study was designed to screen the phytoconstituents present in different extracts of *S. wightii* and to assess the toxicity of total ethanol extract of *S. wightii.* Ethanol extract was chosen for the toxicity study as it is known to possess various potent bioactive phytoconstituents compared to other solvent extracts and also because of interest in further pharmacological studies with ethanol extract of *S. wightii*.

MATERIALS AND METHODS

Study material

Fresh seaweed of *S. wightii* was collected from coastal regions of Rameshwaram, Tamil Nadu, India, during October 2015. It was authenticated by Dr. Yoganarasimhan, a taxonomist, and a voucher specimen (#52) was prepared as per the guidelines and deposited at the Herbarium of the Faculty of Pharmacy, M. S. Ramaiah University of Applied Sciences, Bangalore, for future reference.

During collection, the seaweed was washed thoroughly with sea water to get rid of any superfluous matter such as sand particles, salt, epiphytes, or any other foreign materials. Later, the seaweed was thoroughly washed with running tap water and then distilled water. It was shade dried at room temperature, powdered, and then packed in airtight containers. The study material was stored in a refrigerator for further study. Macroscopic analysis including the size, shape, color, base, and margin of *S. wightii* was carried out.[4]

Extraction

Successive solvent extraction

Successive solvent extraction of *S. wightii* was carried out using a Soxhlet apparatus. The solvent order was according to their polarity such as petroleum ether, toluene, chloroform, 95% ethanol, and cold maceration. The extract with each solvent was filtered and dried to concentrate. The color and consistency of the extracts were noted and the percentage yield was calculated.

Total alcohol extraction

The coarsely powdered plant material was defatted using petroleum ether (60-80°C) and extracted using 95% v/v ethanol in a Soxhlet apparatus. The extract was filtered and evaporated and accurate weight of the extract was recorded. The color and consistency of the extracts were noted and percentage yield was calculated.

Phytochemical screening

Preliminary phytochemical screening was carried out for the extracts obtained from successive solvent extraction and total alcohol extraction according to standard procedures.[15]

Toxicity studies

Experimental animals

All the animals used for this study were obtained from the Animal House Facility, Faculty of Pharmacy, M. S. Ramaiah University of Applied Sciences (Registration number: 220/PO/ReBi/S/2000/CPCSEA/ 02.05.2016). Acute toxicity was carried out on three female Wistar rats. For the subchronic toxicity study, Wistar rats of either sex weighing between 195 and 235 g were used in the present study. They were divided into four groups, each group consisting of six animals.

The animals were housed in polypropylene cages. The temperature in the experimental animal room was maintained at 22°C (±3°C), with relative humidity 50-60% and artificial lighting, the sequence being 12 h light, 12 h dark. Each animal in the cage was marked on the tail with methylene blue dye for appropriate identification. Food but not water was withheld overnight for the experimental animals. The experimental procedures were conducted in accordance with the guidelines provided by the Institutional Animal Ethics Committee and prior approval was obtained with the approval no. MSRFPH/PFP-59/2015.

Acute toxicity study

The acute toxicity study was designed as per the OECD Guidelines 423.[16] Although *S. wightii* is a traditional medicine, with no reports of mortality[17,18] even in large doses, a limit test was carried out. A single oral dose (2000 mg/kg) of ethanol extract of *S. wightii* (ESW) was given to three female Wistar rats.

After dosing, for the first 30 min, the animals were monitored individually. They were given special attention for the first 4 h for any toxic signs. The observation was extended first to 24 h and then daily thereafter for a total of 14 days. The animals were observed individually for any toxic signs or pre-terminal deaths and they were recorded if they occurred. Once a week, individual body weight was monitored in all the animals to determine any drastic changes. The color and consistency of feces and changes in fur and skin, mucous membranes (nasal), and eyes of the animal were observed on a weekly basis.

Physical observations such as changes in the circulatory (heart rate), respiratory (rate), autonomic (piloerection, lacrimation, salivation, urinary incontinence, and defecation), and central nervous system (drowsiness, ptosis, gait, eye prominence,

eyelid closure, convulsions, biting, Straub's test, motor in-coordination, writhing, stereotypy, aggression, righting reflex, pinnal reflex, corneal reflex, tremors, and convulsions) were monitored and recorded if present.

Subchronic toxicity

The subchronic toxicity study was carried out as per OECD guidelines 407.[19] The animals were divided into four groups, each group consisting of six animals. The grouping of animals was as follows:

Group I – Normal control vehicle treated 1% sodium CMC.

Group II – Ethanol ESW 100 mg/kg (low dose).

Group III – Ethanol ESW 200 mg/kg (medium dose).

Group IV – Ethanol ESW 400 mg/kg (high dose).

Group I received 1% sodium CMC, while groups II-IV received ESW in doses of 100, 200, and 400 mg/kg orally once daily for 28 days. The doses were selected depending on the results obtained from the acute toxicity study. Dosing time was kept constant to minimize any biological variation among animals.

At the end of the study, the animals were anesthetized and a blood sample was collected through the retro-orbital plexus into nonheparinized tubes for biochemical parameters and heparinized tubes for hematological parameters. Biochemical analysis was carried out to explore major toxic effects in tissues, specifically the liver and kidney. Biochemical investigations included sodium, potassium,[20] glucose,[21] total protein and albumin,[22-24] urea,[25] creatinine,[26] total cholesterol,[27,28] alanine amino transferase (ALT), and aspartate amino transferase (AST).[29] Hematological parameters such as hemoglobin content, total leucocyte count, erythrocyte count, and platelet count were estimated.[30] Urine analysis was carried out during the last week of the study and included timed urine volume and pH.[31]

All animals in the study were subjected to a complete, detailed gross necropsy. It included thorough examination of the external surface of the body, all orifices, and thoracic, cranial and abdominal cavities. The vital organs such as the liver, lungs, spleen, brain, kidneys, and heart were isolated and adherent tissue was cleared. The wet weight of organs was recorded immediately after dissection to avoid drying. Individual organs were also examined macroscopically for any gross lesions in all the animals. The following tissues were preserved in the fixation medium for histopathological examination: brain, stomach, small intestines, liver, kidneys, spleen, heart, lungs, bone, testes, ovary, and pancreas.

Statistical analysis

The data were expressed as mean ± standard error of the mean (n=6). Significant differences between groups were determined using one-way ANOVA, followed by Tukey's multiple comparison test. $P < 0.05$ was considered significant.

RESULTS

The macroscopic characters of *S. wightii* leaves were as follows: 4 to 8 cm length, linear to oval, dark brown, with tapering base and entire margin. The color, consistency, and percentage yield of various extracts are presented in Table 1. The color of extracts varied from dark green and greenish brown to brown. Consistency was mostly semisolid except for the extract of cold maceration, which was solid. Percentage yield of extract ranged from 0.69 to 2.98. The highest yield was from cold maceration (2.98%) and the least was from toluene extraction (0.69%). Phytochemical screening revealed the presence of alkaloids, phenolic compounds, carbohydrates, glycosides, and tannins.

Acute toxicity study

ESW did not induce any mortality or pre-terminal death. No changes were observed in salivation, lacrimation, perspiration, piloerection, micturition, or defecation. The animals were observed for ptosis, drowsiness, stereotypy, aggression, tremors, convulsion, Straub's test, motor in-coordination, and writhing and no abnormalities were observed in any of the treated animals. Gait, righting reflex, and corneal reflex were normal. Skin, fur, eyes, and body weight of the animals were also normal. Tremors, lethargy, diarrhea, and coma were not observed during the study.

Subchronic toxicity study

Body weight changes were documented on a weekly basis and the results are presented in Table 1. The body weights of animals treated with 100, 200, and 400 mg/kg extract showed no significant changes and were comparable with those of the control group. The results of the subchronic toxicity study on food and water intake are presented in Tables 2 and 3, respectively. Food as well as water intake was monitored in all the groups on a daily basis and the results are presented on a weekly basis. There were no significant changes in food or water intake between the control and extract-treated groups.

Table 1. Body weight changes in ESW-treated rats				
Groups	Group I (Control) (g)	Group II (100 mg/kg) (g)	Group III (200 mg/kg) (g)	Group IV (400 mg/kg) (g)
Day 0	199.67±17.47	202.33±4.37	195.33±4.80	235.33±8.40
Day 7	218.16±15.27	214±4.03	214±1.79	238.33±9.98
Day 14	216.33±14.61	217.66±7.42	210.83±5.52	232.83±10.60
Day 21	219.33±14.61	218.83±6.18	211.66±9.90	232±13.53
Day 28	224.66±5.65	224.67±5.65	215.33±16.95	234.5±15.56

Values are expressed as mean ± standard error of the mean; (n=6)
ESW: Extract of *S. wightii*

The results of the biochemical analysis are reported in Table 4. There were no significant changes in parameters such as albumin, total protein, urea, creatinine, sodium, or potassium at the end of 28 days of treatment. AST and ALT did not show any significant difference in the extract-treated groups and were comparable with those in the control group.

There was a statistically significant decrease in blood glucose levels in the extract-treated groups. Cholesterol level was significantly reduced in the animals treated with doses of 100 and 200 mg/kg extract, whereas 400 mg/kg did not show any significant differences.

Hematological parameters were estimated at the end of 28 days and the results are presented in Table 5. There were slight variations but no significant changes in the levels of red blood cells (RBC), white blood cells (WBC), platelets, or hemoglobin in the extract-treated groups when compared to the normal group. The results of urine analysis (Table 6) were comparable with those of the control group.

The gross anatomy of every organ was examined macroscopically by direct observation. The macroscopic architecture of organs was normal in all the treatment groups and there were no signs of abnormalities. The organ weight of the control and extract-treated animals were noted at the end of the study (Table 7). There were no significant changes in the weights of vital organs including the heart, kidney, liver, spleen, and lungs, whereas there was a slight increase in the weight of the brain with the dose of 400 mg/kg.

Table 2. Food intake in ESW-treated rats

Groups	Group I (Control) (g)	Group II (100 mg/kg) (g)	Group III (200 mg/kg) (g)	Group IV (400 mg/kg) (g)
Week 1	22.68±0.64	24.26±0.49	23.41±0.97	23.1±1.08
Week 2	22.61±0.77	23.17±0.99	21.1±1.20	23.17±1.20
Week 3	21.58±1.89	20 ±1.12	19.95±1.59	19.05±1.57
Week 4	21.21±1.35	20.52±0.58	21.15±1.52	21.84±1.14

Values are expressed as mean ± standard error of the mean; (n=6)
ESW: Extract of *S. wightii*

Table 3. Water intake in ESW-treated rats

Groups	Group I (Control) (mL)	Group II (100 mg/kg) (mL)	Group III (200 mg/kg) (mL)	Group IV (400 mg/kg) (mL)
Week 1	46.7±2.71	49.77±1.57	48.78±2.78	46.32±3.28
Week 2	50.02±2.40	52.66±1.93	51.21±4.2	53.69±2.77
Week 3	55.64±1.70	55.84±2.31	56.3±1.87	54.15±1.37
Week 4	55.69±1.73	57.92±0.99	58.43±2.30	52.83±1.49

Values are expressed as mean ± standard error of the mean; (n=6)
ESW: Extract of *S. wightii*

Table 4. Biochemical parameters in ESW-treated rats

Groups	Group I (Control)	Group II (100 mg/kg)	Group III (200 mg/kg)	Group IV (400 mg/kg)
Glucose (mg/dL)	82.98±2.80	46.17±2.56[a]	47.75±1.61[a]	36.49±1.74[a]
Cholesterol (mg/dL)	78±1.78	51.83±1.64[b]	52.5±1.92[b]	61.83±7.86
Albumin (g/dL)	3.92±0.09	3.68±0.13	3.48±0.09	3.73±0.16
Total protein (g/dL)	7.02±0.20	7±0.14	6.92±0.19	6.45±0.29
Creatinine (mg/dL)	0.57±0.02	0.55±0.03	0.57±0.01	0.55±0.02
ALT (U/L)	53.83±2.69	57.5±2.87	53.67±1.41	51.5±1.48
AST (U/L)	221.5±4.15	221±3.25	213.33±2.81	218.5±1.89
Urea (mg/dL)	30.67±1.26	34.83±0.91	33±1.21	32.5±1.06
Sodium (mEq/L)	150.83±1.68	151.17±1.78	150.33±1.08	150.17±1.35
Potassium (mEq/L)	4.83±0.23	4.88±0.24	4.80±0.24	4.92±0.21

Values are expressed as mean±standard error of the mean (SEM); **[b]p<0.01** ([b]p<0.01 indicates significance with p value less than 0.01 when compared to control); **[a]p<0.001** ([a]p<0.001 indicates high significance with P value less than 0.001 when compared to control); (n=6)
ESW: Extract of *S. wightii,* ALT: Alanine amino transferase, AST: Aspartate amino transferase

A histopathological evaluation was conducted on various organs such as the kidney, lungs, testes, ovary, bone, stomach, brain, pancreas, spleen, intestine, liver, and heart. The testes showed seminiferous tubules with normal spermatogenesis in the low dose-treated groups. An increase in spermatogenesis with normal architecture was observed in the medium and high dose-treated groups (Figure 1a-d). With low dose, the glomeruli appeared normal with mild tubular epithelial damage. Medium dose-treated animals showed mild infiltrations in the glomeruli with tubular epithelial cell damage and the damage was comparable to that in the control group (Figure 2a-d). All the groups showed functionally efficient nerve fibers with normal astrocytes (Figure 3a-d). Normal pancreatic acini and pancreatic islet cells with intercalated and lobular ducts were observed in all the groups (Figure 4a-d). All the groups showed normal cardiac muscle bundles with myocytes and no signs of damage or changes were observed (Figure 5a-d). Congestion of alveolar tissue with normal alveolus was observed with low doses, whereas mild infiltrations were observed in alveolar tissue with normal alveolar epithelium, alveolus, and air spaces in high doses (Figure 6a-d). All the treated groups showed normal spleens with lymphoid

Table 5. Hematological parameters in ESW-treated rats

Groups	Group I (Control)	Group II (100 mg/kg)	Group III (200 mg/kg)	Group IV (400 mg/kg)
RBC (10^6/mm³)	11.44±0.25	12.32±0.24	11.86±0.38	11.06±0.19
WBC (10^3/mm³)	10.13±0.34	11.58±0.87	12.75±1.02	13.18±0.95
Platelets (Lakhs/cu.mm)	4.27±0.26	4.30±0.21	4.19±0.17	4.50±0.12
Hb (g/dL)	13.63±0.439	13.83±0.45	14.88±0.55	14.47±0.52

Values are expressed as mean ± standard error of the mean; (n=6) RBC: Red blood cells, WBC: White blood cells, ESW: Extract of *S. wightii*, Hb: Hemoglobin

Table 6. Urine analysis of ESW-treated rats

Sl. no.	Animal groups	Urine volume	pH	Appearance
1	Group I (control)	1.5 mL	7	Clear, pale yellow
2	Group II (100 mg/kg)	2 mL	7	Clear, pale yellow
3	Group III (200 mg/kg)	1.5 mL	7	Clear, pale yellow
4	Group IV (400 mg/kg)	1 mL	7	Clear, pale yellow

ESW: Extract of *S. wightii*

Table 7. Organ weights in ESW-treated rats

Groups	Group I (Control)	Group II (100 mg/kg)	Group III (200 mg/kg)	Group IV (400 mg/kg)
Heart (g)	0.833±0.042	0.792±0.044	0.733±0.038	0.742±0.022
Kidney (g)	0.71±0.029	0.841±0.019	0.818±0.042	0.873±0.064
Liver (g)	8.41±0.572	7.40±0.425	7.81±0.701	8.60±0.972
Spleen (g)	0.853±0.058	0.855±0.103	0.812±0.058	0.795±0.064
Brain (g)	1.65±0.047	1.88±0.030	1.80±0.094	1.90±0.050[c]
Lungs (g)	1.69±0.096	1.95±0.153	2.16±0.305	2.04±0.277

Values are expressed as mean ± standard error of the mean. [c]$p<0.05$ ([c]$p<0.05$ indicates significance with p value less than 0.05 when compared to control), ESW: Extract of *S. wightii*

1a) Normal control   **1b) SW 100 mg/kg**   **1c) SW 200 mg/kg**   **1d) SW 400 mg/kg**
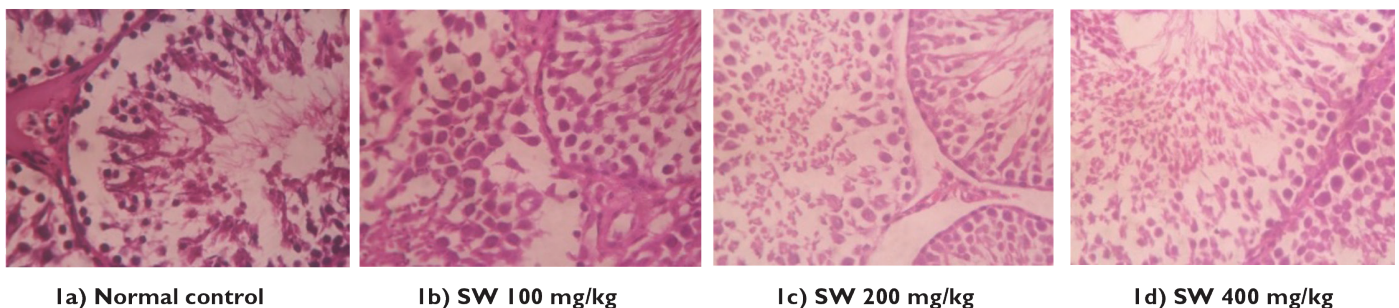
Figure 1. Histopathology of testes

aggregation (Figure 7a-d). Normal ovarian stroma with corpus luteum and follicles were seen in all the treatment groups (Figure 8a-d). Extract-treated groups showed gastric glands with normal parietal cells and gastric mucosa (Figure 9a-d). Normal columnar epithelial cells, intestinal villi, and goblet cells were observed in the intestine (Figure 10a-d). The bone showed normal osteoblasts with bone matrix in all the extract-treated

groups (Figure 11a-d). Control group animals showed normal hepatocytes with a central vein, whereas those treated with a low dose showed normal hepatocytes with mild congestion of blood vessels and edema. Dilatation of sinusoids with normal hepatocytes was seen in the medium dose-treated animals. High dose group animals showed eosinophilic cytoplasm with mild infiltrations of mononuclear cells/heterochromatic nuclei

| 2a) Normal control | 2b) SW 100 mg/kg | 2c) SW 200 mg/kg | 2d) SW 400 mg/kg |
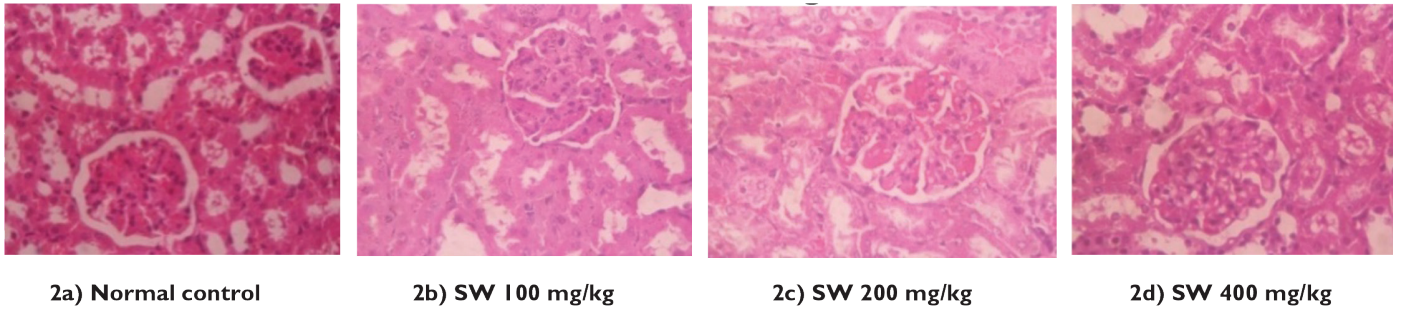
Figure 2. Histopathology of kidney

| 3a) Normal control | 3b) SW 100 mg/kg | 3c) SW 200 mg/kg | 3d) SW 400 mg/kg |
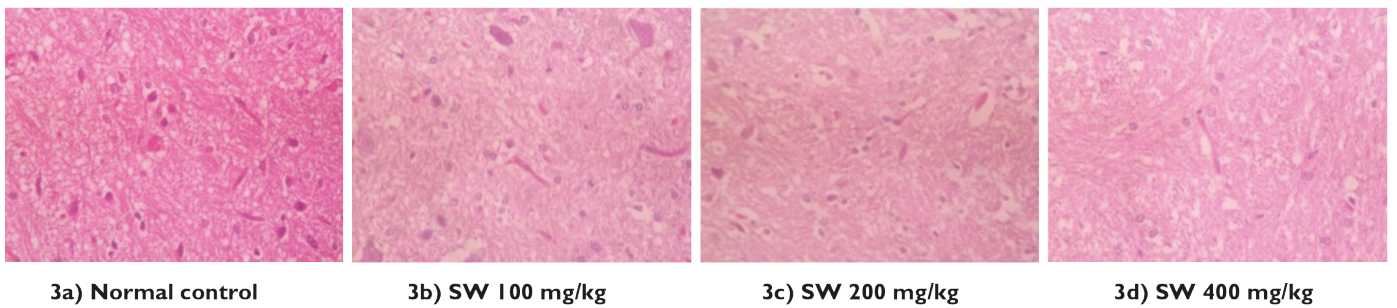
Figure 3. Histopathology of brain

| 4a) Normal control | 4b) SW 100 mg/kg | 4c) SW 200 mg/kg | 4d) SW 400 mg/kg |
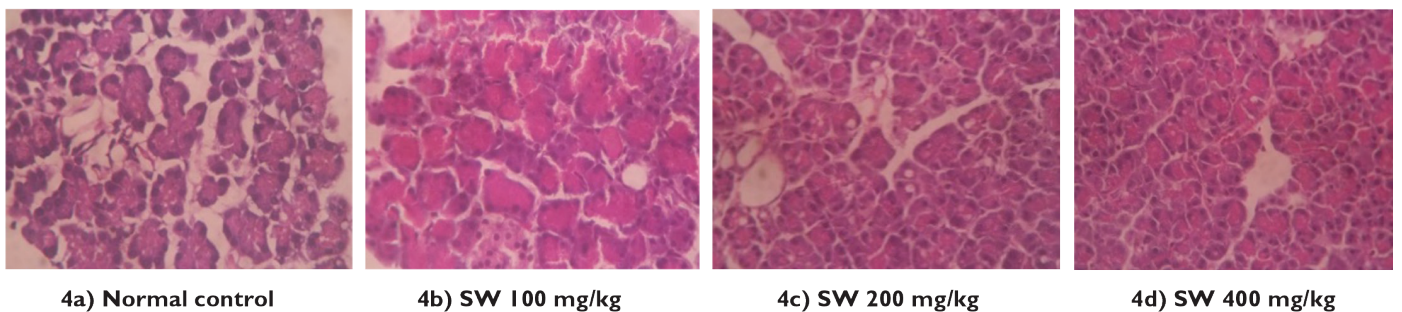
Figure 4. Histopathology of pancreas

| 5a) Normal control | 5b) SW 100 mg/kg | 5c) SW 200 mg/kg | 5d) SW 400 mg/kg |
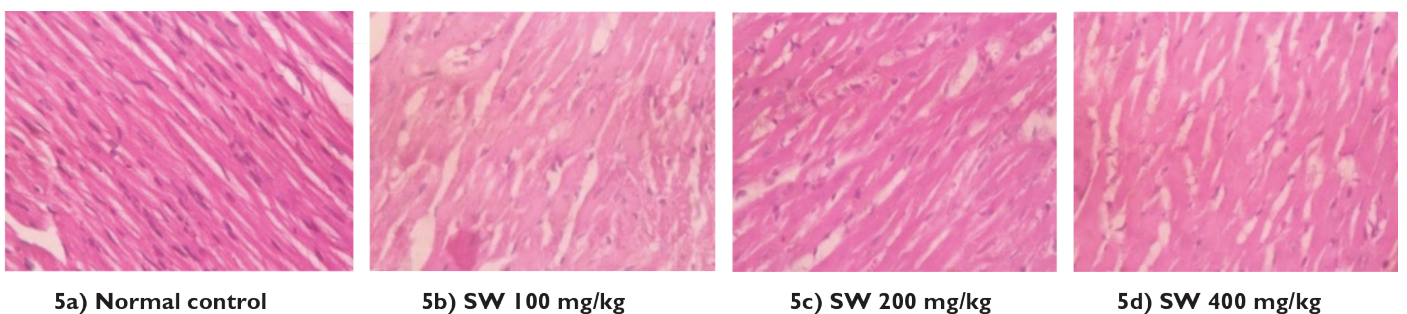
Figure 5. Histopathology of heart

6a) **Normal control**   6b) **SW 100 mg/kg**   6c) **SW 200 mg/kg**   6d) **SW 400 mg/kg**
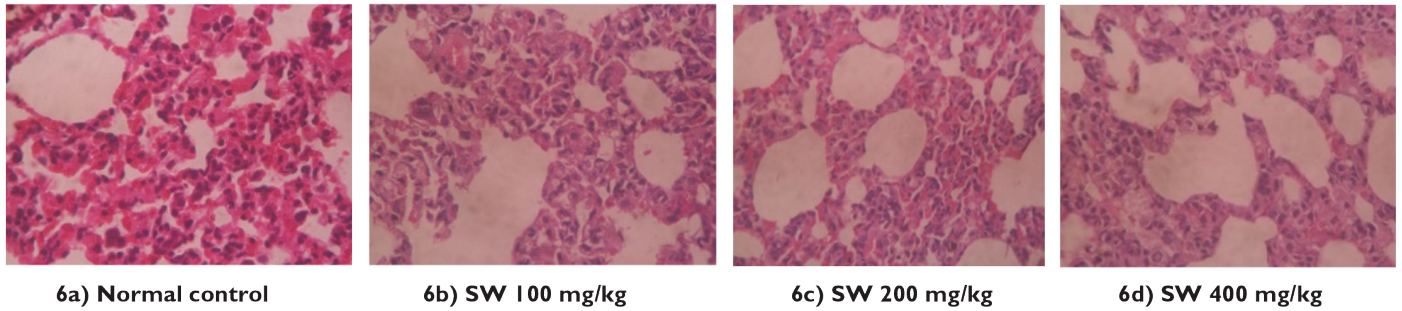
Figure 6. Histopathology of lungs

7a) **Normal control**   7b) **SW 100 mg/kg**   7c) **SW 200 mg/kg**   7d) **SW 400 mg/kg**
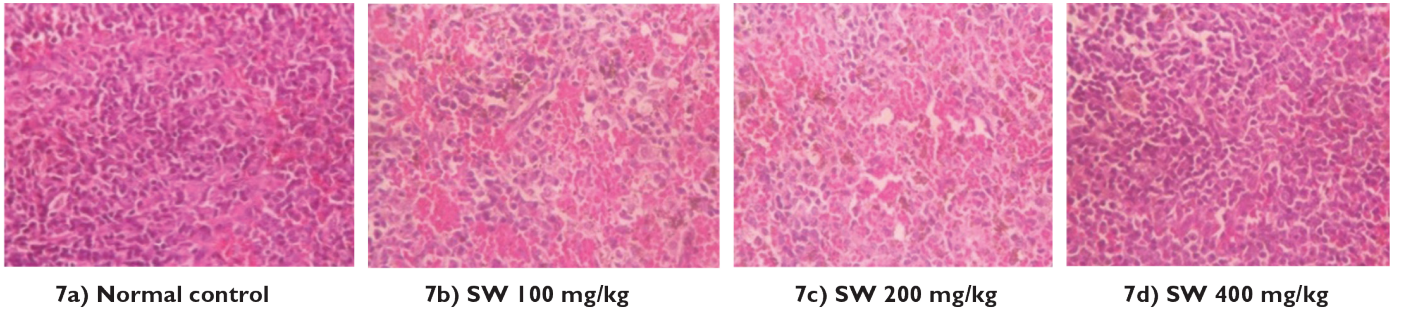
Figure 7. Histopathology of spleen

8a) **Normal control**   8b) **SW 100 mg/kg**   8c) **SW 200 mg/kg**   8d) **SW 400 mg/kg**
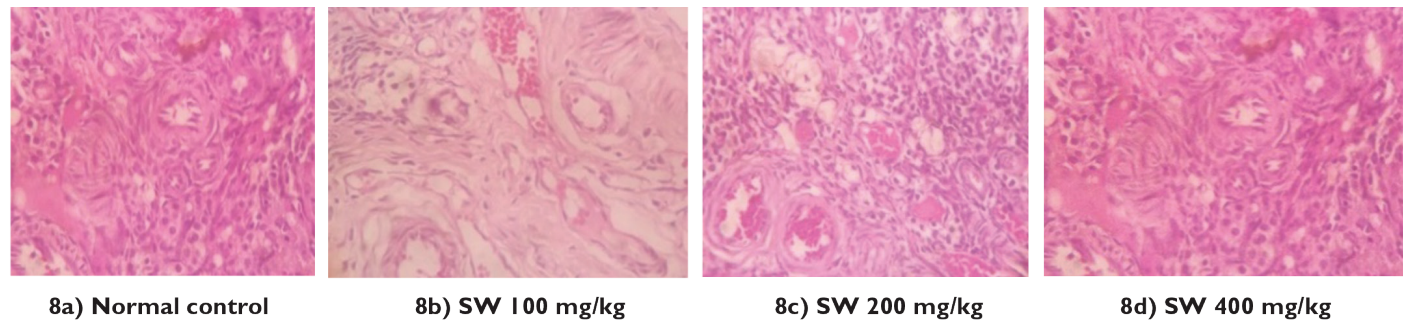
Figure 8. Histopathology of ovary

9a) **Normal control**   9b) **SW 100 mg/kg**   9c) **SW 200 mg/kg**   9d) **SW 400 mg/kg**
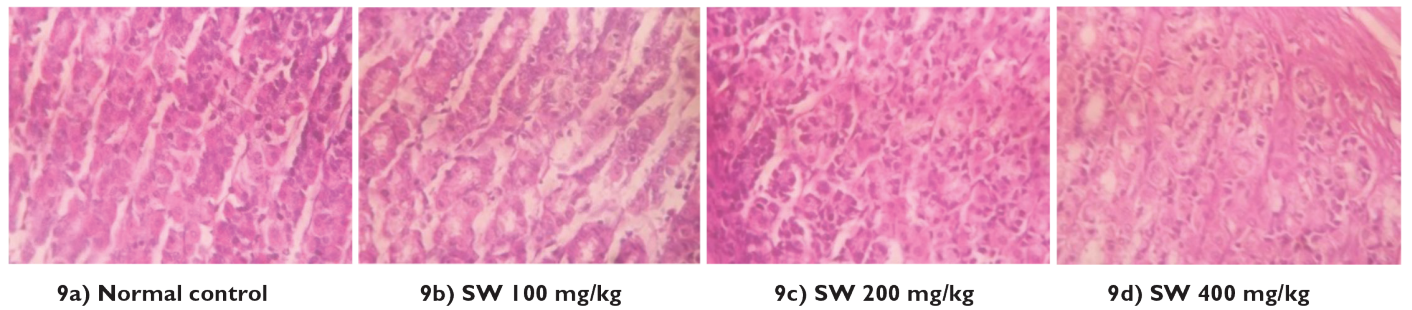
Figure 9. Histopathology of stomach

10a) **Normal control**   10b) **SW 100 mg/kg**   10c) **SW 200 mg/kg**   10d) **SW 400 mg/kg**
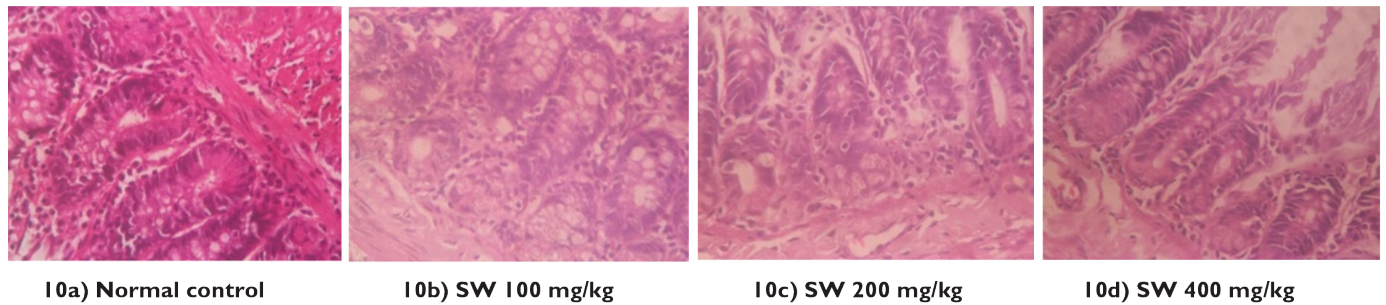
Figure 10. Histopathology of intestine

(Figure 12a-d). The interpretations of all the treated groups were done in comparison with the control group.

DISCUSSION

Herbal medicines are thought to have lower risk compared to synthetic drugs, but the concept is becoming outdated since it is evident that herbal medicines also have potential risks. Various studies have reported the toxicity of herbal compounds and it becomes mandatory to rule out any such possible toxicity profile.[32]

The preliminary phytochemical analysis revealed the presence of many active constituents that may be pharmacologically beneficial. The animals were found to be free of any major toxic signs during as well as at the end of the acute and subchronic toxicity study. There were no abnormal signs of any motor or sensory functions.

Reduction in body weight is known to be one of the most common indices to understand the toxicity profile of drugs.[33] Minor insignificant changes in body weight were observed throughout the treatment period. Any changes in food intake or water drinking pattern indicate a toxic impact on or abnormality in metabolism.[32] Statistically insignificant changes in food and water intake indicate that the extract was safe for long-term administration and did not induce any alteration in the metabolic system.

The normal ranges of electrolytes, creatinine, and urea indicate that ESW has no deleterious effect on the renal system. Generally increased levels of AST and ALT are considered to be an index of liver damage. Changes can occur in the levels of these enzymes when there are changes in hepatic cellular permeability, damage to the hepatocytes, or necrosis.[34] Statistically insignificant results for ALT and AST ruled out any such toxic effects on the liver. The reduction in glucose level seen in the present study is correlated to already reported alpha glucosidase as well as alpha amylase inhibitory activity of *S. wightii* and fucoidan.[35-37] Therefore, it is concluded that the hypoglycemic potential of ESW is comparable to that in studies previously reported on *S. wightii* or fucoidan.[38,39]

Cholesterol is known to be one of the major lipids that can provide information about lipid metabolism.[40] Previous studies have already reported the hypolipidemic property of sulfated polysaccharides, which could be correlated to the reduction in cholesterol level observed in the present study. Another study correlated the hypolipidemic effect of fucoidan to reduction in HMG CoA reductase expression and an upregulation of LDL receptor.[41] Thus these results are consistent with previous studies available on the hypoglycemic property of sulfated polysaccharides, which are expected to be the major compounds present in *S. wightii* extract.[42]

11a) Normal control   **11b) SW 100 mg/kg**   **11c) SW 200 mg/kg**   **11d) SW 400 mg/kg**
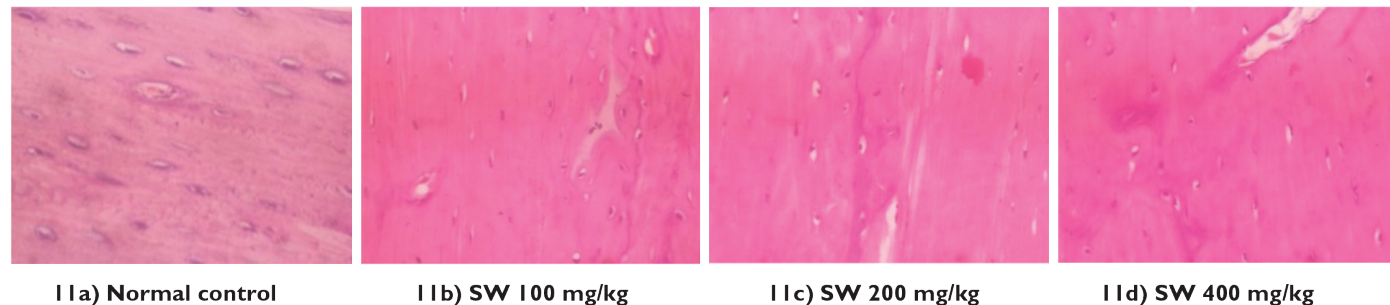
Figure 11. Histopathology of bone

12a) Normal control   **12b) SW 100 mg/kg**   **12c) SW 200 mg/kg**   **12d) SW 400 mg/kg**
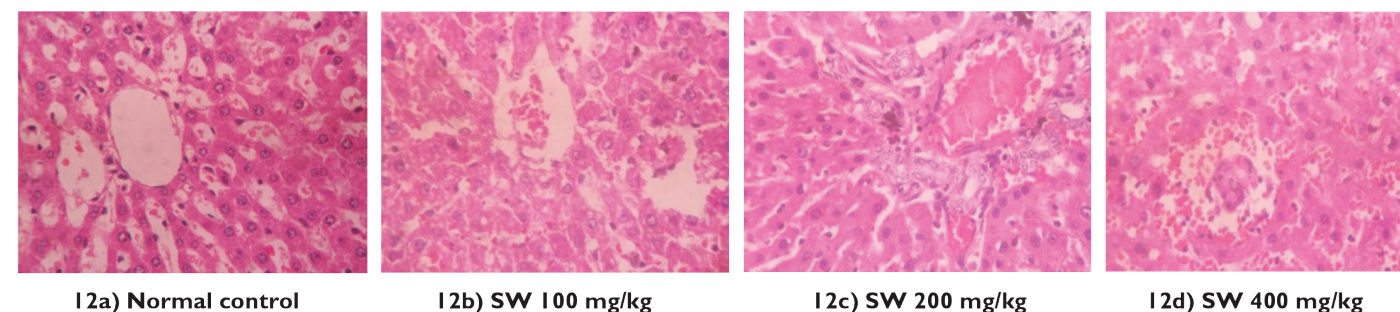
Figure 12. Histopathology of liver

Groups

Group I – Normal control vehicle treated 1% sodium CMC.

Group II – Ethanol extract of *S. wightii* 100 mg/kg (low dose).

Group III – Ethanol extract of *S. wightii* 200 mg/kg (medium dose).

Group IV – Ethanol extract of *S. wightii* 400 mg/kg (high dose).

The hematological system is one of the most important systems serving as an indicator of health status. It is also known to be an easy target for most toxic compounds.[43] The results indicate that the ESW is nontoxic to the hematopoietic system.

Organ weight is known to be one of the main indices to derive any targeted organ toxicity. The absence of any significant differences in organ weight eliminates any such organ level toxicity. No signs of abnormality or organ level damage were observed in the macroscopic examination of gross anatomy. In the histopathological examination, all the organs showed normal architecture. Although some changes were observed, they were minimal and comparable with the observations in the control group.

Thus, the present study reveals that ESW is safe up to 2000 mg/kg administered as a single oral dose and long-term administration of ESW does not cause toxicity to vital organs at submaximal doses, which encourages the long-term use of ESW for any further pharmacological investigations.

ACKNOWLEDGEMENTS

Conflict of Interest: No conflict of interest was declared by the authors.

REFERENCES

1. Immanuel G, Sivagnanavelmurugan M, Marudhupandi T, Radhakrishnan S, Palavesam A. The effect of fucoidan from brown seaweed *Sargassum wightii* on WSSV resistance and immune activity in shrimp *Penaeus monodon*. Fish Shellfish Immunol. 2012;32:551-564.

2. Cho SH, Kang SE, Cho JY, Kim AR, Park SM, Hong YK, Ahn DH. The antioxidant properties of brown seaweed (*Sargassum siliquastrum*) extracts. J Med Food. 2007;10:479-485.

3. Kim S, Lee W, Bae G, Kim G. Anti-diabetic and hypolipidemic effects of *Sargassum yezoense* in *db/db* mice. Biochem Biophys Res Communications. 2012;424:675-680.

4. Jin W, Zhang W, Wang J, Yao J, Xie E, Liu D, Duan D, Zhang Q. A study of neuroprotective and antioxidant activities of heteropolysaccharides from six *Sargassum* species. Int J Biol Macromolec. 2014;67:336-342.

5. Moubayed N, Houri H, Khulaifi M, Farraj D. Antimicrobial, antioxidant properties and chemical composition of seaweeds collected from Saudi Arabia (Red Sea and Arabian Gulf). Saudi J Biol Sci. 2017;24:162-169.

6. Zandi K, Ahmadzadeh S, Tajbakhsh S, Rastian Z, Yousefi F, Farshadpour F. Anticancer activity of *Sargassum oligocystum* water extract against human cancer cell lines. Eur Rev Med Pharmacol Sci. 2010;14:669-673.

7. Jeong DH, Kim KB, Kim MH, Kanq BK, Ahn DH. Anti-inflammatory activity of ethanolic extract of *Sargassum micracanthum*. J Microbiol Biotechnol. 2013;23:1691-1698.

8. Dore C, Alves M, Will L, Costa T, Sabry D, Rego L. A sulfated polysaccharide, fucans, isolated from brown algae *Sargassum vulgare* with anticoagulant, antithrombotic, antioxidant and anti-inflammatory effects. Carbohydr Polym. 2013;91:467-475.

9. Hira K, Sultana V, Ara J, Haque SE, Athar M. Hepatoprotective potential of three *Sargassum* species from Karachi coast against carbon tetrachloride and acetaminophen intoxication. J Coast Life Med. 2016;4:10-13

10. Michael MD, Guiry GM, Algae Base. World-wide electronic publication, National University of Ireland, Galway; 2015. http://www.algaebase.org; searched on 01 September 2015.

11. Rupérez P, Ahrazem O, Leal JA. Potential antioxidant capacity of sulfated polysaccharides from the edible marine brown seaweed *Fucus vesiculosus*. J Agric Food Chem. 2002;50:840-845.

12. Kolsi RBA, Salah HB, Jardak N, Chaaben R, Jribi I, Feki AE, Rebai T, Jamoussi K, Allouche N, Blecker C, Belghith H, Belghith K. Sulphated polysaccharide isolated from *Sargassum vulgare*: Characterization and hypolipidemic effects. Carbohydr Polym. 2017;170:148-159.

13. Coura CO, DeAraujo IW, Vanderlei ES, Rodriques JA, Quindere AL, Fontes BP, de Queiroz IN, de Menezes DB, Bezerra MM, e Silva AA, Chaves HV, Jorge RJ, Evangelista JS, Benevides NM. Antinociceptive and anti-inflammatory activities of sulphated polysaccharides from the red seaweed *Gracilaria cornea*. Basic Clin Pharmacol Toxicol. 2012;110:335-341.

14. Murugaiyan K, Sivakumar K. Seasonal variation in elemental composition of *Stoechospermum marginatum* (Ag.) Kutz and *S. wightii* (Greville Mscr.) J.G. Agardh in relation to chemical composition of seawater. Colloids Surf B Biointerfaces. 2008;64:140-144.

15. Devi J, Balan GS, Periyanayagam K. Pharmacognostical study and phytochemical evaluation of brown seaweed *Sargassum wightii*. J Coast Life Med. 2013;1:199-204.

16. OECD Guideline for Testing of Chemicals, 2001. Acute Oral Toxicity - Fixed Dose Procedure.

17. Li N, Zhang Q, Song J. Toxicological evaluation of fucoidan extracted from *Laminaria japonica* in Wistar rats. Food Chem Toxicol. 2005;43:421-426.

18. Lakshmanasenthil S, Vinothkumar T, Geetharamani D, Marudhupandi T, Suja G, Sindhu NS. Fucoidan - a novel alpha amylase inhibitor from *Turbinaria ornata* with relevance to NIDDM therapy. Biocatal Agric Biotechnol. 2014;3:66-70.

19. OECD Guideline for Testing of Chemicals, 2008. Repeated Dose 28-Day Oral Toxicity Study in Rodents.

20. Ogbonnia SO, Nkemehule FE, Anyika EN. Evaluation of subchronic toxicity of *Stachytarpheta angustifolia* (Mill) Vahl (Fam. Verbanaceae) extract in animals. Afr J Biotechnol. 2009;8:1793-1799.

21. Trinder P. Determination of glucose in blood using glucose oxidase with an alternative oxygen receptor. Ann Clin Biochem. 1969;6:24-27.

22. Brobeck JR. Physiological Basis of Medical Practice (9th ed). Baltimore; Wilkins and Wilkins; 1973.

23. Doumas BT. Standards for total serum protein assays - a collaborative study. Clin Chem. 1975;1159-1166.

24. Webster BT. Estimation of protein in liquid and solid sample. Clin Chem. 1977;21:1159.

25. Chaney AL, Marbach EP. Determination of urea in liquid samples. Clin Chem. 1962;8:130.

26. Tietz NW. Fundamentals of Clinical Chemistry. Philadelphia: WB Saunders; 1976.

27. Assmann G. At what levels of total low- or high-density lipoprotein cholesterol should diet/drug therapy be initiated? European guidelines. Am J Cardiol. 1990;65:11F-15F.

28. Assmann G, Schriewer H, Schmitz G. Qualification of high density lipoprotein cholesterol by precipitation with phosphotungstic acid/Mg/Cl$_2$. Clin Chem. 1983;29:2026-2030.

29. Bergmayer HU. Methods of Enzymatic Analysis. New York; Academic Press; 1974:1196.

30. Ghai CL. A Textbook of Practical Physiology (5th ed). New Delhi; Jaypee Brothers Medical Publishers; 2003.

31. Ghosh R, Murali, A, Sathiya R. Diuretic effects of *Mitragyna parvifolia* Korth. root extract and its therapeutic efficacy against experimental urolithiasis in rats. Spatula DD. 2015;5:113-121.

32. Christapher PV, Parasuraman S, Asmawi MZ, Murugaiyah V. Acute and subchronic toxicity studies of methanol extract of *Polygonum minus* leaves in Sprague Dawley rats. Regul Toxicol Pharmacol. 2017;86:33-41.

33. Attanayake AP, Jayatilaka K, Pathirana C, Mudduwa L. Efficacy and toxicological evaluation of *Coccinia grandis* (Cucurbitaceae) extract in male Wistar rats. Asian Pac J Trop Dis. 2013;3:460-466.

34. Sujith K, Darwin R, Suba V. Toxicological evaluation of ethanol extract of *Anacyclus pyrethrum* in albino Wistar rats. Asian Pac J Trop Dis. 2012;2:437-441.

35. Senthil LS, Kumar TV, Geetharamani D, Suja G, Yesudas R, Chacko A, Fucoidan - An alpha amylase inhibitor from *S. wightii* with relevance to NIDDM. Int J Biol Macromol. 2015;81:644-647.

36. Kim K, Yoon K, Lee B. Fucoidan regulate blood glucose homeostasis in C57BL/KSJ m+/+ db and C57BL/KSJ db/db mice. Fitoterapia. 2012;83:1105-1109.

37. Hu S, Xia G, Wang J, Wang Y, Li Z, Xue C. Fucoidan from sea cucumber protects against high-fat high sucrose diet induced hyperglycaemia and insulin resistance in mice. J Funct Foods. 2014;10:128-138.

38. Wang D, Zhao X, Liu Y. Hypoglycemic effects of a polysaccharide from flower buds of *Lonicera japonica* in streptozotocin induced diabetic rats. Int J Biol Macromol. 2017;102:396-404.

39. Wang Y, Wang J, Zhao Y, Hu S, Shi D, Xue C. Fucoidan from sea cucumber *Cucumaria frondosa* exhibits anti-hyperglycemic effects in insulin resistant mice via activating the PI3K/PKB pathway and GLUT4. J Biosci Bioeng. 2016;121:36-42.

40. Poornima K, Krishnan R, Aswathi KV, Gopalakrishnan VK. Toxicological evaluation of ethanol extract of *Tabernaemontana coronaria* (L) R. Br. Asian Pac J Trop Dis. 2012;S679-S684.

41. Park J, Yeoam M, Hahm D. Fucoidan improves serum lipid levels and atherosclerosis through hepatic SREBP-2-mediated regulation. J Pharmacol Sci. 2016;131:84-92.

42. Li S, Li J, Zhi Z, Wei C, Wang W, Ding T, Ye X, Hu Y, Linhardt RJ, Chen S. Macromolecular properties and hypolipidemic effects of four sulphated polysaccharides from sea cucumbers. Carbohydr Polym. 2017;173:330-337.

43. Lynch N, Berry D. Differences in perceived risks and benefits of herbal, over-the-counter conventional, and prescribed conventional, medicines and implication of this for the safe and effective use of herbal products. Complement Ther Med. 2007;15:84-91.

ORIGINAL ARTICLE

Cytotoxic Activity of Sesquiterpenoids Isolated from Endemic *Ferula tenuissima* Hub.-Mor & Peşmen

Endemik *Ferula tenuissima* Hub.-Mor & Peşmen'den Elde Edilen Seskiterpenoidlerin Sitotoksik Etkisi

🆔 Fadime AYDOĞAN[1]*, 🆔 Şura BAYKAN[1], 🆔 Bilge DEBELEÇ BÜTÜNER[2]

[1]Ege University, Faculty of Pharmacy, Department of Pharmaceutical Botany, İzmir, Turkey
[2]Ege University, Faculty of Pharmacy, Department of Pharmaceutical Biotechnology, İzmir, Turkey

ABSTRACT

Objectives: This was a phytochemical study of endemic *Ferula tenuissima* roots and determined the cytotoxic activity of pure compounds on PC-3.

Materials and Methods: Air-dried and powdered roots of *F. tenuissima* (1 kg) were extracted consecutively with n-hexane, chloroform ($CHCl_3$), and methanol (MeOH) (3×2 L, each) by sonication at 30°C for 24 h. The extracts were then filtered. The solvents were separately evaporated under reduced pressure to dryness. The compounds were isolated by chromatographic methods and their structures were determined by spectral methods (1D and 2D NMR and LC-MS). The compounds were tested for their cytotoxic activities versus the PC-3 cell line by WST assay.

Results: A phytochemical investigation of the dried roots of endemic *F. tenuissima* was performed and three sesquiterpene esters were isolated. The daucane-type sesquiterpenes teferidin, ferutinin, and elaeochytrin-A were identified. In the bioactivity study, ferutinin exhibited the highest cytotoxic activity, with an IC_{50} value of 19.7 µM.

Conclusion: The results indicate that the main compounds of *F. tenuissima* roots are daucane sesquiterpenes and ferutinin has a potential effect on PC-3 cells.

Key words: *Ferula tenuissima*, daucane sesquiterpene esters, cytotoxicity, prostate cancer

ÖZ

Amaç: Endemik *Ferula tenuissima* köklerinin fitokimyasal yönden incelenmesi ve elde edilen saf bileşiklerin PC-3 üzerinde sitotoksik etkilerinin belirlenmesidir.

Gereç ve Yöntemler: *F. tenuissima* 'nın açık havada kurutulmuş ve toz haline getirilmiş kökleri (1 kg, 24 saat boyunca 30°C'de sonikasyonda n-hexane, kloroform ($CHCl_3$) ve metanol (MeOH) (3×2 L, her biri) ile sırasıyla ekstre edilmiştir. Ekstraktlar daha sonra süzülmüştür. Sıvı ekstreler, vakum altında kuruluğa kadar uçurulmuştur. Kromatografik yöntemler ile bileşikler elde edilmiş ve bileşiklerin yapıları spektral yöntemler ile belirlinmiştir (1D-, 2D NMR ve LC-MS). Bileşiklerin PC-3 üzerindeki sitotoksik aktiviteleri WST yöntemi ile test edilmiştir.

Bulgular: Endemik *F. tenuissima*'nın kurutulmuş köklerinin fitokimyasal incelemesi yapılmış ve üç seskiterpen esteri izole edilmiştir. Teferidin, ferutinin ve elaeochytrin-A daukan tip seskiterpen esterleri olarak belirlenmiştir. Biyoaktivite çalışmasında, ferutinin en yüksek sitotoksik aktiviteyi IC_{50}: 19.7 µM ile göstermiştir.

Sonuç: *F. tenuissima* köklerinin ana bileşiklerinin daukan seskiterpenler ve ferutininin PC-3 hücreleri üzerinde potansiyel bir etkiye sahip olduğunu göstermektedir.

Anahtar kelimeler: *Ferula tenuissima*, daukan seskiterpen ester, sitotoksite, prostat kanseri

INTRODUCTION

In recent years, cancer has become the main cause of public health problems and the second leading cause of death in the world despite advanced imaging and molecular diagnostic techniques.[1] Prostate cancer is the most common cancer in men and is the second leading cause of cancer deaths in the United States after lung cancer.[1] Today, most cancer drugs used as cytotoxic agents are obtained directly from natural products like plants, marine organisms, and microorganisms or indirectly by the semisynthesis of molecules from these sources. As a result, cancer research on natural products is expanding.[2]

The genus *Ferula* L. of the family Apiaceae (Umbelliferae) is represented by about 185 species worldwide and 23 taxa in Turkey.[3] Several species, such as the roots of *Ferula gummosa* and *Ferula asafeotida*, have been used in folk medicine as an antidote in poisonings and as an aphrodisiac, antimicrobial, expectorant, and antihemorrhoidal, as well as to treat stomachache, colitis in infants, asthma, and urinary tract disorders.[4] Monoterpenes, sesquiterpenes (especially daucane-, humulane-, and guaiane-type sesquiterpene esters and sesquiterpene lactones), and coumarins were found to be the main constituents of the genus *Ferula* by phytochemical studies.[5-8] Phenylpropanoid, sulfur-containing derivates, and triterpenes and their glycosides were also reported.[9-11] Recent pharmacological research has demonstrated that different extracts of *Ferula* species contain sesquiterpene derivatives that have in particular proven to be cytotoxic on several cancer cell lines.[2,12] In addition, the extracts have been reported to have antimicrobial, anthelmintic, anticonvulsant, antispasmodic, antihyperglycemic, antihyperlipidemic, and antioxidant activities.[13-18]

EXPERIMENTAL

Plant material

The roots of *Ferula tenuissima* Hub.-Mor & Peşmen were collected in the Yarpuz Region, Osmaniye, Turkey (940 m) in June 2013. The whole plant was identified by Assoc. Prof. Serdar Gokhan Senol from the Section of Botany, Department of Biology, Faculty of Science, Ege University. A voucher specimen (IZEF 6046) was deposited in the Herbarium of Ege University, Faculty of Pharmacy, İzmir, Turkey (www.izef.ege.edu.tr).

Extraction and isolation

Air-dried and powdered roots of *F. tenuissima* (1 kg) were extracted consecutively with n-hexane, chloroform (CHCl$_3$), and methanol (MeOH) (3×2 L, each) by sonication at 30°C for 24 h. The extracts were then filtered. The solvents were separately evaporated under reduced pressure to dryness. Yields were 44.31 g, 9.90 g, and 45.89 g, respectively. Next 9.27 g of the CHCl$_3$ extract was submitted to silica gel column chromatography and eluted consecutively with n-hexane: EtOAc gradient (100:0-0:100, v/v, 10% decreasing polarity, each 500 mL), EtOAc: acetone (100:0-0:100, v/v, 10% decreasing polarity), and then acetone: MeOH (100:0-0:100, v/v, 10% decreasing polarity)

to give 15 fractions, named A-O, and monitored by thin-layer chromatography (TLC). Based on the TLC profiles 3 fractions, i.e. fractions B (210 mg), E (233 mg), and G (200 mg), were selected for further purification. Fraction B was chromatographed over a silica gel column (150 g) with n-hexane: EtOAc (100:0-87.5:12.5, with 2.5% increasing polarity) to afford five fractions (B1-B5). Fraction B3 (83 mg) was rechromatographed over a silica gel column (75 g) with n-hexane: EtOAc (100:0-90:10, 2% decreasing polarity) to yield compound **1** (40 mg) purely. Then 33 mg of fraction E was further purified by preparative TLC (n-hexane:EtOAc, 80:20, silica gel) and isolated and yielded 17 mg of compound **3**. Fraction G was submitted to silica gel column chromatography, eluted with n-hexane: EtOAc (95:5-50:50; 5% increasing polarity) solvent, and yielded compound **2** (33 mg).

Cytotoxicity assay and cells

Cell toxicity was analyzed by using WST-1 according to the manufacturer's protocol. PC-3 and RWPE-1 cell lines were obtained from the American Type Culture Collection (ATCC, Manassas, VA, USA). PC3 cells were propagated using DMEM F-12 supplemented with 5% FBS, L-glutamine (2 mM), penicillin (100 U/mL), and streptomycin (100 μg/mL), while RWPE-1 cells were propagated in keratinocyte growth medium supplemented with bovine pituitary extract and 5 μM EGF at 37°C with 5% CO$_2$. Molecules were dissolved in DMSO and treatments were done so that DMSO volume would not exceed 0.5% of the culture media volume. Control cells were treated with the same volume of DMSO used during the molecule treatments. PC-3 "(8x103)" and RWPE-1 cells "(104)" were seeded and grown in 96-well plates and incubated for 24 h. Molecule treatments were performed for 48 h and WST-1 cell proliferation reagent (roche cat no: 05015944001) was used as recommended. Briefly, WST-1 (1:10 final dilution) was added to the cells at the end of treatments, and the cells were incubated for an additional 3 h. At the end of the incubation, absorbance was measured at 450 and 690 nm using a SpectraMaxPlus 384 spectrophotometer (Molecular Devices). IC$_{50}$ concentrations of the molecules were calculated through nonlinear regression analysis in GraphPad Prism 6. All experiments were performed in triplicate. Doxorubicin was used as the positive control.

Chemicals and other materials

Mass spectra (Thermo-Scientific TSQ Quantum Access Max LC-MS/MS, ESI). Nuclear magnetic resonance (NMR) spectra were recorded on a Varian Oxford AS400 and a Bruker DRX-500. The chemical shifts were measured relative to the residual solvent peak and are expressed in δ (ppm) and the coupling constants (J) are reported in Hertz (Hz). Column chromatography was carried out on silica gel 60 (40-63 mm, Merck), Sephadex LH-20 (GE Healthcare), and Micropore RP-18 (25-40 mm, Merck) using analytical grade purity solvents (Merck and Sigma). TLC analyses were carried out on silica gel 60 F254 and RP-18 F254s (Merck) precoated aluminum plates. Compounds were detected by UV (244-366 nm) and 10% vanillin ethanol solution/ H$_2$SO$_4$ reagent followed by heating at 105°C for 1-2 min.

RESULTS AND DISCUSSION

The powdered roots of *F. tenuissima* were extracted consecutively with n-hexane, $CHCl_3$, and MeOH (3×2 L, each) by sonication at 30°C for 24 h. The $CHCl_3$-soluble fraction was subjected to repeated column chromatography (CC) to afford three known compounds (see Figure 1). All of them were daucane-type sesquiterpenoids; their structures were established by NMR and MS and by comparison with published data. Compounds **1** (teferidin),[19] **2** (ferutinin),[19] and **3** (elaeochytrin-A)[20] were also identified by comparison of their spectral data with those in the literature.[19,20]

Compound 1 (Teferidin)

4β-Hydroxy-6α-benzoyloxy-5α(H)-dauc-8-ene: Yellow residue, EI MS/MS, [M]+ at m/z=342.16 for $C_{22}H_{30}O_3$; ^1H, ^{13}C NMR spectroscopic data, see Table 1.

Compound 2 (Ferutinin)

4β-Hydroxy-6α-(*p*-hydroxy benzoyloxy)-5α(H)-dauc-8-ene: Yellow residue, EI MS/MS [M+H]+ at m/z=359.06, [M+NH$_4$]+ m/z=376.11, [M+Na]+ m/z=381.06, [M+K]+ m/z=397.03 for $C_{22}H_{30}O_4$; ^1H, ^{13}C NMR spectroscopic data, see Table 1.

Compound 3 (Elaeochytrin-A)

4β-Hydroxy-6α-(*o*-amino benzoyloxy)-5α(H)-dauc-8-ene. Yellow residue, EI MS [M+Na]+ m/z=380.34 for $C_{22}H_{31}NO_3$; ^1H, ^{13}C NMR spectroscopic data, see Table 1.

All compounds isolated from *F. tenuissima* were evaluated for their cytotoxic activity against the PC-3 cancer cell and normal prostate RWPE cell lines. The IC_{50} values of compounds that are active on at least one cell line at concentration are given in Table 2.
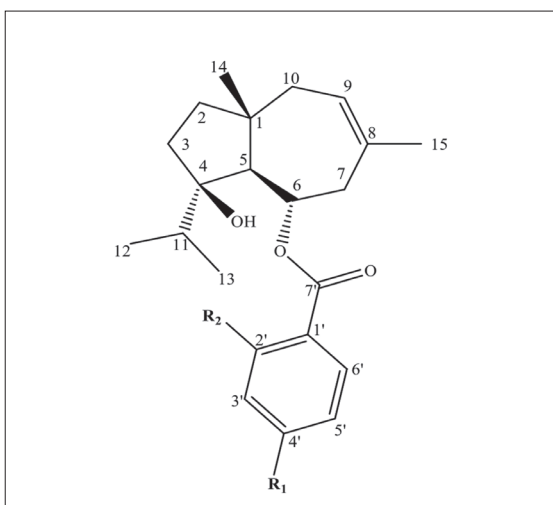
Compound	R$_1$	R$_2$
1-Teferidin	H	H
2-Ferutinin	O	H
	H	
3-Elaeochytrin-A	H	NH$_2$

Figure 1. Structure of compounds 1-3

CONCLUSION

Mono-, di-, triesters of humulane, germacrane, eudesmane, and especially daucane-type sesquiterpenes and coumarin and lactone derivates are major components of the genus *Ferula* L.[21] It was observed that the location of the double bond in the daucane ring affected activity, which was at positions 7-8, 8-9, and 9-10. Furthermore, the presence of hydroxyl groups at different positions on the daucane ring and the formation of mono-, di-, and tri-ester structures of this hydroxyl group, especially benzoic, angelic, cinnamic, and vanillic acid, increases the variability in biological activity.[21] The isolated teferidin compound is jaeschkeanadiol benzoic acid ester isolated from *F. tenuisecta* roots for the first time in 1976.[2] It has also been reported from *F. hermonis*, *F. pallida*, *F. elaeochytris*, *F. rigidula*, and *F. jaeschkeana* roots.[21] Ferutinin was first described in 1973 by Saidkozev as jaeschkeanadiol p-hydroxy benzoic ester.[23] It was isolated from different *Ferula* species previously.[23] Elaeochytrin-A was first reported from *F. elaeochytris* roots.[20]

In our study, it was determined that all compounds were moderately effective on the PC-3 and RWPE-1 cell lines. The affinity of the compounds for RWPE-1 cells also indicated that the selectivity of the compound is not as high as expected.

In a previous study, elaeochytrin-A showed cytotoxic effects on K562R (imatinib-resistant) human chronic myeloid leukemia and DA1-3b/M2BCR-ABL (dasatinib-resistant) mouse leukemia cell lines at IC_{50} 12.4 and 7.8 μM concentrations, respectively.[20] In the same study, ferutinin showed cytotoxic activity at IC_{50} 25.3 and 29.1 μM and teferidin at IC_{50} 55.1 and 29.5 μM. When the molecular structures were examined, the double bond between C8 and C9 positions decreased cytotoxic activity.[20] Ferutinin has been shown to have an antiproliferative effect on colon cancer cell lines of WiDr, COLO320-HSR, and LS-174T[24] and to induce apoptosis and intracellular Ca^{+2} pathway in human Jurkat cells.[25] Ferutinin showed ERα and ERβ agonist and antagonist receptor activity with improving sexual function in male and female rats.[26] It has been found that the hydroxyl group at position 3 increases the estrogen-like effect of the presence of oxygen and the presence of electrophilic groups in the *p*-position of the benzene ring (hydroxyl, oxo, etc.).[26] Prostate cancer formation, especially androgenic hormones, is the main cause of uncontrolled proliferation of cells. Ferutinin molecule studies suggest that both the effects on sexual function and the activity of *in vitro* cytotoxicity studies may be specific antagonist/agonist effects on androgen hormone receptors.[26] As a result of our bioactivity studies on the PC-3 cell line with compounds isolated from *F. tenuissima* roots, the most active cytotoxic agent of ferutinin synthesis emerged (IC_{50}: 19.69 μM), in addition to the potential phototherapeutic results of phytochemical and bioactivity studies of other genus-related species due to the biological activity of the root extracts of *Ferula* taxa and daucane-type sesquiterpenoids.

ACKNOWLEDGEMENTS

Table 1. NMR spectroscopic data for compounds 1-3 in CDCl$_3$ (δ$_H$ 7.26 ppm, δ$_C$ 77.1 ppm)

Positions	Compound 1		Compound 2		Compound 3	
	δ$_H$ (δ ppm, *J*=Hz)	δ$_C$	δ$_H$ (δ ppm, *J*=Hz)	δ$_C$	δ$_H$ (δ ppm, *J*=Hz)	δ$_C$
1	-	43.9 (*s*)	-	44.0 (*s*)	-	44.2 (*s*)
2	1.43 (*m*) 1.20 (*m*)	41.0 (*t*)	1.56 (*m*) 1.26 (*m*)	41.2 (*t*)	1.54 (*m*) 1.30 (*m*)	41.5 (*t*)
3	1.92 (*m*) 1.50 (*m*)	32.4 (*t*)	1.92 (*m*) 1.65 (*m*)	31.4 (*t*)	1.91 (*m*) 1.60 (*m*)	31.8 (*t*)
4	-	85.1 (*s*)	-	87.0 (*s*)	-	86.5 (*s*)
5	1.96 (*d, J*=9.6)	59.4 (*d*)	2.02 (*d, J*=10.8)	60.1 (*d*)	2.00 (*d, J*=10.8)	60.1 (*d*)
6	5.09 (*td, J*=10.2, 2.4)	70.9 (*d*)	5.27 (*td, J*=10.4, 2.8)	71.2 (*d*)	5.27 (*ddd, J*=10.8, 10.4, 2.8)	70.7 (*d*)
7	2.39 (*dd, J*=12.8, 10.8) 2.16 (*dd, J*=14.0, 12.8)	41.5 (*t*)	2.56 (*dd, J*=12.4, 11.2) 2.29 (*dd, J*=14.0, 2.8)	41.4 (*t*)	2.54 (*dd, J*=12.4, 11.6) 2.27 (*dd, J*=14.0, 2.4)	41.6 (*t*)
8	-	133.7 (*s*)	-	133.5 (*s*)	-	134.4 (*s*)
9	5.50 (*bs*)	125.3 (*d*)	5.55 (*bt, J*=5.6)	125.3 (*d*)	5.55 (*bs*)	125.4 (*d*)
10	1.96 (*m*) 1.85 (*m*)	40.9 (*t*)	2.06 (*m*) 1.98 (*m*)	41.0 (*t*)	2.05 (*m*) 1.91 (*m*)	41.2 (*t*)
11	2.10 (*sept, J*=6.8)	36.5 (*d*)	1.86 (*sept, J*=6.8)	37.0 (*d*)	2.04 (*m*)	37.4 (*d*)
12	0.75 (*d, J*=6.8)	18.1 (*q*)	0.85 (*d, J*=6.8)	17.6 (*q*)	0.85 (*d, J*=6.8)	17.7 (*q*)
13	0.94 (*d, J*=6.8)	18.8 (*q*)	0.94 (*d, J*=6.8)	18.5 (*q*)	0.95 (*d, J*=6.8)	18.7 (*q*)
14	1.01 (*s*)	20.6 (*q*)	1.10 (*s*)	20.2 (*q*)	1.11 (*s*)	20.3 (*q*)
15	1.75 (*s*)	26.6 (*q*)	1.81 (*s*)	26.4 (*q*)	1.82 (*s*)	26.6 (*q*)
1'	-	131.3 (*s*)	-	121.9 (*s*)	-	111.0 (*s*)
2'	7.89 (*d, J*=7.2)	129.3 (*d*)	7.92 (*d, J*=8.8)	132.0 (*d*)	-	151.1 (*s*)
3'	7.50 (*dd, J*=8.0, 7.2)	129.0 (*d*)	6.88 (*d, J*=8.8)	115.5 (*d*)	6.67 (*dd, J*=8.0, 0.8)	117.0 (*d*)
4'	7.61 (*t, J*=7.2)	133.3 (*d*)	-	161.1 (*s*)	7.27 (*ddd, J*=7.2, 6.8, 1.6)	133.7 (*d*)
5'	7.50 (*dd, J*=8.0, 7.2)	129.0 (*d*)	6.88 (*d, J*=8.8)	115.5 (*d*)	6.64 (*td, J*=8.0, 1.2)	116.4 (*d*)
6'	7.89 (*d, J*=7.2)	129.3 (*d*)	7.92 (*d, J*=8.8)	132.0 (*d*)	7.78 (*dd, J*=8.0, 1.6)	131.0 (*d*)
7'	-	165.2 (*s*)	-	167.3 (*s*)	-	168.3 (*s*)

F. tenuissima showed a profile of chloroform extracts with ultraviolet active at 254 and 366 nm, blue-green color visible spots with vanillin/H$_2$SO$_4$ reagent for all compounds
NMR: Nuclean magnetic resonance

Table 2. Cytotoxicity (IC$_{50}$ in μM[a]) of isolated jaeschkeanadiol esters against prostate cancer cell lines *in vitro*

	PC-3	RWPE-1
Teferidin	65.3±4.10	21.77±1.20
Ferutinin	19.69±2.22	3.295±0.80
Elaeochytrin-A	44.23±3.27	8.299±0.9
Doxorubicin[b]	1.17±0.12	0.468±0.038

[a] Data are mean values ± standard deviation of three experiments, [b] IC$_{50}$ μM, positive control, [c] PC-3 (Prostate cancer cell line), RWPE-1 (Normal prostate epithelial cell line)

Conflict of Interest: No conflict of interest was declared by the authors.

REFERENCES

1. Siegel RL, Miller KD, Jemal A. Cancer statistics, 2016. CA Cancer J Clin. 2016;66:7-30.

2. Valiahdi SM, Iranshahi M, Sahebkar A. Cytotoxic activities of phytochemicals from *Ferula* species. Daru. 2013;21:39.

3. Sağıroğlu M. Türkiye *Ferula* L. (Umbelliferae) Cinsinin Revizyonu [Doktora]. Ankara: Gazi Üniversitesi, Fen Bilimleri Enstitüsü; 2005.

4. Baytop T. Türkiye'de Bitkilerle Tedavi (Geçmişte ve Bugün). 2. Baskı ed. İstanbul: Nobel Tıp Kitabevleri; 1999.

5. Abd El-Razek MH, Ohta S, Hirata T. Terpenoid coumarins of the genus *Ferula* L. Heterocycles. 2003;60:689-716.

6. Zhi-Qiang Wang, Chao Huang, Jian Huang, Hong-Ying Han, Guo-Yu Li, Jin-Hui Wang, Tie-Min Sun. The stereochemistry of two

monoterpenoid diastereomers from *Ferula dissecta*. RSC Advances. 2014;4:14373-14377.

7. Alkhatib R, Hennebelle T, Joha S, Roumy V, Güzel Y, Biabiany M, Idziorek T, Preudhomme C, Quesnel B, Sahpaz S, Bailleul F. Humulane and germacrane sesquiterpenes from *Ferula lycia*. J Nat Prod. 2010;73:780-783.

8. Galal AM, Abourashed EA, Ross SA, ElSohly MA, Al-Said MS, El-Feraly FS.Daucane sesquiterpenes from *Ferula hermonis*. J Nat Prod. 2001;64:399-400.

9. Iranshahi M, Amin GR, Amini M, Shafiee A. Sulfur containing derivatives from *Ferula persica* var. *latisecta*. Phytochemistry. 2003;63:965-966.

10. Duan H, Takaishi Y, Tori M, Takaoka S, Honda G, Ito M, Takeda Y, Kodzhimatov OK, Kodzhimatov K, Ashurmetov O. Polysulfide derivatives from *Ferula foetida*. J Nat Prod. 2002;65:1667-1669.

11. Diaz JG, Fraga BM, Gonzalez AG, Gonzalez P, Hernandez MG, Miranda JM. Triterpenes from *Ferula linkii*. Phytochemistry. 1984;23:1471-1473.

12. Suzuki K, Okasaka M, Kashiwada Y, Takaishi Y, Honda G, Ito M, Takeda Y, Kodzhimatov OK, Ashurmetov O, Sekiya M, Ikeshiro Y. Sesquiterpene lactones from the roots of *Ferula varia* and their cytotoxic activity. J Nat Prod. 2007;70:1915-1918.

13. Bagheri SM, Rezvani ME, Vahidi AR, Esmaili M. Anticonvulsant effect of *Ferula assa-foetida* oleo gum resin on chemical and amygdala-kindled rats. N Am J Med Sci. 2014;6:408-412.

14. Liu T, Osman K, Kaatz GW, Gibbons S, Mu Q.Antibacterial sesquiterpenoid derivatives from *Ferula ferulaeoides*. Planta Med. 2013;79:701-706.

15. Bashir S, Alam M, Adhikari A, Shrestha RL, Yousuf S, Ahmad B, Parveen S, Aman A, Choudhary MI. New antileishmanial sesquiterpene coumarins from *Ferula narthex* Boiss. Phytochemistry Letters. 2014;9:46-50.

16. Yusufoglu HS, Soliman GA, Abdel-Rahman RF, Abdel-Kader MS, Ganaie MA, Bedir E, Baykan S, Ozturk B. Antihyperglycemic and antihyperlipidemic effects of *Ferula duranii* in experimental type 2 diabetic rats. International Journal of Pharmacology. 2015;11:532-541.

17. Yusufoglu HS, Soliman GA, Abdel-Rahman RF, Abdel-Kader MS, Ganaie MA, Bedir E, Baykan Erel S, Ozturk B. Antihyperglycemic and antihyperlipidemic effects of *Ferula assa-foetida* and *Ferula tenuissima* extracts in diabetic rats. Pakistan Journal of Biological Sciences. 2015;18:314-323.

18. Yusufoglu HS, Soliman GA, Abdel-Rahman RF, Abdel-Kader MS, Genaie MA, Bedir E, Baykan Erel S, Ozturk B. Antioxidant and antihyperglycemic effects of *Ferula drudeana* and *Ferula huber-morathii* in experimental diabetic rats. International Journal of Pharmacology. 2015;11:738-748.

19. Al-Oqail M, Hassan WH, Ahmad MS, Al-Rehaily AJ. Phytochemical and biological studies of *Solanum schimperianum* Hochst. Saudi Pharm J. 2012;20:371-379.

20. Alkhatib R, Hennebelle T, Joha S, Idziorek T, Preudhomme C, Quesnel B, Sahpaz S, Bailleul F. Activity of elaeochytrin A from *Ferula elaeochytris* on leukemia cell lines. Phytochemistry. 2008;69:2979-2983.

21. Saidkhodzhaev A, Nikonov GK. The structure of teferidin - A new ester from the fruit of *Ferula tenuisecta*. Chemistry of Natural Compounds. 1976;12:96-97.

22. Shakhnoza S, Azimova AIS. Natural Sesquiterpene Esters; Plant Sources, Structure and Properties. Springer; New York; 2013.

23. Saidkhodzhaev A, Nikonov GK. The structure of ferutinin. Chemistry of Natural Compounds. 1975;9:25-26.

24. Poli F, Appendino G, Sacchetti G, Ballero M, Maggiano N, Ranelletti FO. Antiproliferative effects of daucane esters from *Ferula communis* and *F. arrigonii* on human colon cancer cell lines. Phytother Res. 2005;19:152-157.

25. Macho A, Blanco-Molina M, Spagliardi P, Appendino G, Bremner P, Heinrich M, Fiebich BL, Muñoz E. Calcium ionophoretic and apoptotic effects of ferutinin in the human Jurkat T-cell line. Biochem Pharmacol. 2004;68:875-883.

26. Appendino G, Spagliardi P, Cravotto G, Pocock V, Milligan S. Daucane phytoestrogens: A structure-activity study. J Nat Prod. 2002;65:1612-1615.

Nanocarriers Used Most in Drug Delivery and Drug Release: Nanohydrogel, Chitosan, Graphene, and Solid Lipid

İlaç Dağıtım ve İlaç Salımında En Çok Kullanılan Nanotaşıyıcılar: Nanohidrojel, Kitosan, Grafen ve Katı Lipit

🄳 Sibel Ayşıl ÖZKAN[1]*, 🄳 Aylin DEDEOĞLU[1], 🄳 Nurgül KARADAŞ BAKIRHAN[2], 🄳 Yalçın ÖZKAN[3]

[1]Ankara University, Faculty of Pharmacy, Department of Analytical Chemistry, Ankara, Turkey
[2]University of Health Sciences, Gülhane Faculty of Pharmacy, Department of Analytical Chemistry, Ankara, Turkey
[3]University of Health Sciences, Gülhane Faculty of Pharmacy, Department of Pharmaceutical Technology, Ankara, Turkey

ABSTRACT

Over the past few years, nanocarriers have become an ideal solution for safe and efficient drug delivery and release. This is mainly due to the extraordinary characteristics that nanomaterials exhibit when compared with their larger scaled forms. A variety of these carriers are more popular due to their high biocompatibility, ensuring greater efficacy especially in cancer treatments. Nanocrystal, liposomal, and micelle designs of these materials as nanocarriers for drug delivery and release have been extensively researched throughout the past 50 years. Successful applications have not only ensured a greater focus on therapeutic development but also created a new solution available in the pharmaceutical market. Herein, a brief review of research studies focused on nanocarrier materials and designs to achieve superior benefits of drugs for disease treatments is presented. Nanohydrogels, chitosan, graphene oxide, and solid lipid nanoparticle nanocarrier designs and applications are selectively given due to the great attention they have gained from being highly biocompatible and easy-to-manipulate nanocarrier options from organic and inorganic nanocarrier materials. Each summary exhibits the progress that has been achieved to date. With greater understanding of the current state in the development process of these nanomaterials, there is a rising chance to provide better treatment to patients, which is a desperate need in pharmaceutical technologies.

Key words: Nanocarrier, drug delivery, nanomaterials, controlled drug release, targeting

ÖZ

Geçtiğimiz yıllarda, nanotaşıyıcılar güvenli ve verimli ilaç dağıtımı ve salımı için ideal bir çözüm haline geldi. Bu, temel olarak nanomalzemelerin daha büyük ölçekli formlarıyla karşılaştırıldığında sergiledikleri olağanüstü özelliklerden kaynaklanmaktadır. Bu taşıyıcıların çeşitliliği yüksek biyouyumluluk nedeniyle daha popüler olup, özellikle kanser tedavilerinde daha fazla etkinlik sağlar. Son 50 yıl boyunca, nanokristal, lipozomal ve misel tasarımları bu malzemelerin ilaç dağıtımı ve salınımı için çok araştırılmıştır. Başarılı uygulamalar sadece terapötik gelişimde daha fazla odaklanma sağlamakla kalmadı, aynı zamanda farmasötik pazarda da mevcut yeni bir çözüm yarattı. Bu çalışmada, nanotaşıyıcılar araştırmaların kısa bir derlemesi ve ilaç tedavisi için ilaçların üstün yararlarını elde etmek için nanohidrojel, kitosan, grafen/grafen oksit ve katı lipid nanoparçacık tasarımları sunulmuştur. Bu malzemeler biyouymululuğu yüksek ve manipülasyonu kolay olmaları sebebi ile son yıllarda en çok tercih edilen nanotaşıyıcı malzemeleri olmuştur. İlaç dağıtımı ve salınmasında en fazla ilgi çeken bu nanotaşıyıcı malzemeleri, bugüne kadar olan gelişimleri özetlenmiştir. İlaç dağıtımı için nanotaşıyıcı ihtiyacının ve bu nano malzemelerin gelişim sürecinde mevcut durumun daha iyi anlaşılmasıyla, farmasötik teknolojilerinde hastalara daha iyi tedavi sağlama şansı artmaktadır.

Anahtar kelimeler: Nanotaşıyıcı, ilaç dağıtımı, nanomalzemeler, kontrollü ilaç salımı, hedefleme

INTRODUCTION

Materials that have one or more dimensions lower than 100 nm are considered nanomaterials.[1] To be more specific, in 2011 the European Commission defined a nanomaterial as follows:

"A natural, incidental or manufactured material containing particles, in an unbound state or as an aggregate or as an agglomerate and where, for 50% or more of the particles in the number size distribution, one or more external dimensions is in the size range 1 nm-100 nm."[2]

Nanomaterials have great research and development/product development potential in medical applications. Some of these applications include DNA/RNA nanotechnology, diagnosis by molecular imaging, biosensing, nanomedicine, and nanocarriers for drug delivery.[3] A considerable number of nanomaterials have been developed, produced, and utilized for these application fields, such as nanohydrogels, chitosan/starch/cellulose nanoparticles, graphene (GR)/GR oxide (GO) nanosheets, iron oxide nanoparticles, gold nanoparticles, cerium oxide nanoparticles, and carbon nanotubes/nanoparticles.

Nanomaterials exhibit extraordinary optical, electronic, and/or mechanical properties when compared with their greater scaled forms. They can differ in color, conductivity, reactivity, surface area to volume ratio, and surface tension from macro forms. Due to this, nanomaterials have attracted the attention of scientists for their potential utilization in vaccines, drug development, and drug delivery.[4] Over many years, many nanomaterials have been adopted as nanocarriers, i.e. nanohydrogels, oil-in-water (O/W) emulsions, liposomes, and nanoparticles based on synthetic polymers or natural macromolecules.[5] The very first studies were conducted by Couvreur et al.[6] and Kreuter and Speiser.[7] in the late 70s, where the team exploited polymeric nanocapsules as lysosomotropic carriers and adjuvants.

Drug nanocarriers usually serve two main purposes: targeted drug delivery to specific tissue, organ, or cells and controlled drug release. The foundation of drug delivery is based on biocompatible nanoparticles or nanocapsules and targeting molecules. Biocompatible materials are selected and incorporated to enhance the hydrophilicity of hydrophobic carrier systems or drugs. Targeting molecules are generally antibodies or avidin/biotins that directly target tissue, organs, or cells. Drug release features of nanocarrier systems are provided by the environmentally sensitive structure of the carrier. Controlling drug release ensures paramount therapeutic effect by releasing the delivered drug with high efficiency in the targeted area and preventing any healthy tissue damage that could be caused by some drugs such as chemotherapy agents.[8] Nanocarriers that have been designed from polymer-based nanoparticles are solid colloidal particles that are approximately 10-500 nm in size.[4] Drug incorporation into nanocarriers is based on 5 methods: dissolution, entrapment, adsorption, attachment, or encapsulation.[9] Herein a brief review of nanocarrier systems is given. A summary of the literature including easily manipulated popular nanomaterials that have been adopted as nanocarriers (nanohydrogels, chitosan (CS) nanoparticles, GR/GO nanocarriers, and solid lipid nanoparticles) is given. Nanohydrogels and CS nanoparticle derivatives are the most heavily rotated amphiphilic nanocarrier materials. GR/GO nanomaterials are favored nanocarriers since they are present in a wide range of carrier designs. Finally, solid lipid nanocarriers (SLNs) are currently the most promising and novel lipophilic drug carriers.[10]

NANOHYDROGEL CARRIERS

Nanohydrogels can be defined starting with the descriptions of macro-scaled hydrogels. Hydrogels are three-dimensional hydrophilic polymer chain networks that are crosslinked. These networks can consist of natural or synthetic polymers and display swelling behavior when introduced to water or physiological fluids. Moreover, they are able to revert to their initial state when removed from the presence of water/biological fluids.[11-13] Due to this unique behavior, hydrogels have gained attention and been adopted in biomedical applications such as drug delivery, drug release, and vaccine design.[14]

Drug delivery and drug release system designs that utilize hydrogels have been and are still considered appealing in medicine due to their crosslink-controlled pore structures. Moreover, physiochemically, hydrogels are very similar to the extracellular matrix of the human body. With also a very high content of water, hydrogels are known to have very high biocompatibility. A main disadvantage is their viscosity, which created an alternative solution: nanohydrogels. These submicron particles made excellent drug carriers that could easily be extruded through an injector needle. In addition, decreasing size ensures an increase in surface area that provides further bioconjugation.[11,15]

Nanogels, in the range of 10-100 nm size, are small enough to be used as systemic drug carriers. For designs that include clearance of nanogel carriers by kidney filtration the diameter is lower than 10 nm. Drug release to tissue, organs, or cells is through the meshes of nanohydrogels, which are typically between 5 and 100 nm in size.[16] Mesh sizes in environmentally dependent designs such as temperature- and pH-sensitive ones change with the stimuli according to the crosslink bond concentration that forms or breaks.[15] Regulating the breakages of crosslinking bonds that form the initial mesh size of the carriers will provide control of drug release acceleration. Other designs include utilization of the swelling capacity of nanohydrogels.[17] As swelling continues, mesh sizes increase and gradually release the encapsulated drug.[15]

Nanohydrogel carriers that are environmentally dependent include designs sensitive to pH, temperature, electric field, light, enzyme, calcium, glucose, redox, etc.[18] In this paper, some of these designs are summarized according to their sensitivity features as below. From this summary, it can be stated that as nanohydrogel carriers there are several popular materials that are prominent when compared with others. In Table 1, materials that receive the greatest attention from scientists are listed.

Temperature-sensitive nanohydrogel carriers

Temperature-sensitive nanohydrogel carriers are systems that exhibit swelling behavior that is dependent on temperature changes and are a widely studied field.[19] A temperature-sensitive drug-release design was reported by Ichikawa and Fukumori[20] in 1999. The design consists of a water-soluble hemostatic drug core inside a thermosensitive poly[N-isopropylacrylamide (NIPAAm)] nanohydrogel containing an ethyl cellulose shell. Ichikawa and Fukumori[20] stated that the mentioned shell could change and revert to its initial size with temperature changes between 30°C and 50°C in water and that nanohydrogels exhibit positive thermosensitive swelling. The drug release rate is reported to be not only temperature dependent but also nanohydrogel concentration dependent.[20] A very recent study introduced thermosensitive 5-fluorouracil (5-FU; a chemotherapeutic drug employed for solid tumor treatments) containing methyl cellulose (MC) nanohydrogels for decreased side effects of chemotherapy. In this 2018 study Dalwadi and Patel[21] produced MC nanohydrogels by a tip probe-sonicator method from MC hydrogels. 5-FU release depends on both temperature and its biodegradability. Within 48 h the drug is released in the injected area, preventing a cytotoxic drug burst in a very large area as in conventional chemotherapy.[21]

pH- and/or ionic-strength-sensitive nanohydrogel carriers

pH and/or ionic strength sensitivity allows nanocarriers' mesh size to be manipulated according to the environmental pH. Elsaeed et al.[22] synthesized poly(NIPA-co-AAC) nanohydrogels by inverse microemulsion polymerization method in 2010. On average, the diameter of these nanohydrogels is reported to range between 60 and 80 nm. The team delivers a possible drug release methodology that is pH dependent through poly (NIPA-co-AAC) nanohydrogel by characterizing its swelling behavior between the pH values of 4.00 and 8.00 (ionic strength=0.4). That study shows that the nanohydrogels' swelling capacity increased with environmental pH.[22] In an earlier study, in 2004, Dufresne et al.[23] reported pH-sensitive poly (N-isopropylacrylamide) derivative copolymers or poly(alkyl(meth)acrylate) diblock copolymers were produced as indomethacin (a nonsteroidal anti-inflammatory drug), fenofibrate (a drug for treating abnormal blood lipid levels), and doxorubicin (DOX) and aluminum chloride phthalocyanine carriers. PNIPAM copolymers were stated to be synthesized by free radical polymerization while the poly[alkyl(meth)acrylate] diblock copolymers were synthesized by atom transfer radical polymerization. The team carried out both *in vitro* and *in vivo* assays. Dufresne et al.[23] refer to the PNIPAM derivatives as a potential safe alternative to Cremophor®EL, a common carrier for various poorly water-soluble drugs. Furthermore, poly[alkyl(meth)acrylate] derivative [polyethylene glycol (PEG)-b-(EA-co-MAA)] nanoparticles were stated to be excellent carriers for hydrophobic drugs that could be used orally. The carrier system is reported to exhibit dissociation behavior with increasing pH.[23]

CHITOSAN NANOCARRIERS

Chitin is a long-chain polymer derivative [poly (b-(1-4)-N-acetyl-D-glucosamine)] of glucose with significance as the raw material of CS nanocarriers (CSNs). When chitin is deacetylated up to about 50%, it transforms into CS, which has a linear backbone linked through glycosidic bonds.[24,25] CS's efficient bio-adhesiveness and permeabilization capacity make it one of the most popular nanocarrier materials amongst other hydrophilic polymers.[26] Moreover, CS is a nanocarrier that has a high loading efficiency of drugs. Based on the protonation of -NH$_2$ at the C-2 position of the D-glucosamine repeat, one of the most important characteristics of CS is its solubility in aqueous acidic media as given in Figure 1.[24] Thus, CS nanocapsules provide an effective solution for the delivery of hydrophobic drugs.[27] All the mentioned features of CS nanoparticles make it an excellent nanocarrier material.

Moreover, CS exhibits pH-sensitive behavior due to the percentage of its acetylated monomers and their distribution in the chains.[28] This behavior is utilized for controlled drug release by scientists. A common example for this is drug delivery to tumor cells and controlling release since the pH of tumor cells is significantly lower than that of healthy cells.[29] A summary of the literature that features CSNs as drug delivery systems is provided in Table 2 in chronological order. Production methods for CS carriers differ however, the most common method used being ionotropic gelation, which is based on the capability of polyelectrolytes to crosslink in the presence of counter ions.[30]

As can be seen in Table 2, Fernández-Urrusuno et al.[31] proposed the use of CS nanoparticles as potential drug carriers for transmucosal delivery in 1999. In their design the team loads insulin into CS nanoparticles to be given nasally to conscious normoglycemic rabbits. It is reported that there was a 40% reduction in the serum glucose levels.[31] Aktaş et al.[34] reported the use of PEG-grafted CS nanoparticles as peptide drug carriers. They observed nanoparticle formation through intermolecular hydrogen bonding in an aqueous solution. The incorporation and release of insulin were dependent on the degree of introduction of the PEG chain on CS and observed sustained release phenomenon over time.[52,53] Pérez-Álvarez et al.[51] reported one of the most recent studies in this field revealing the state of art in 2019. Their work exploits the designed CSN as a great candidate for polyoxometalate delivery into tumoral
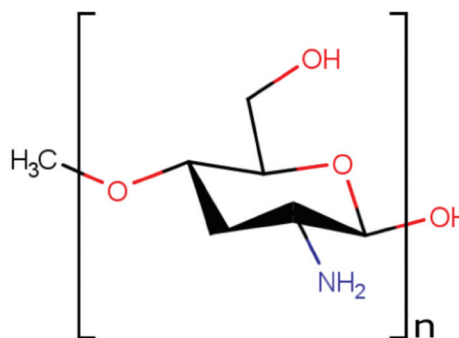
Figure 1. Chitosan monomer
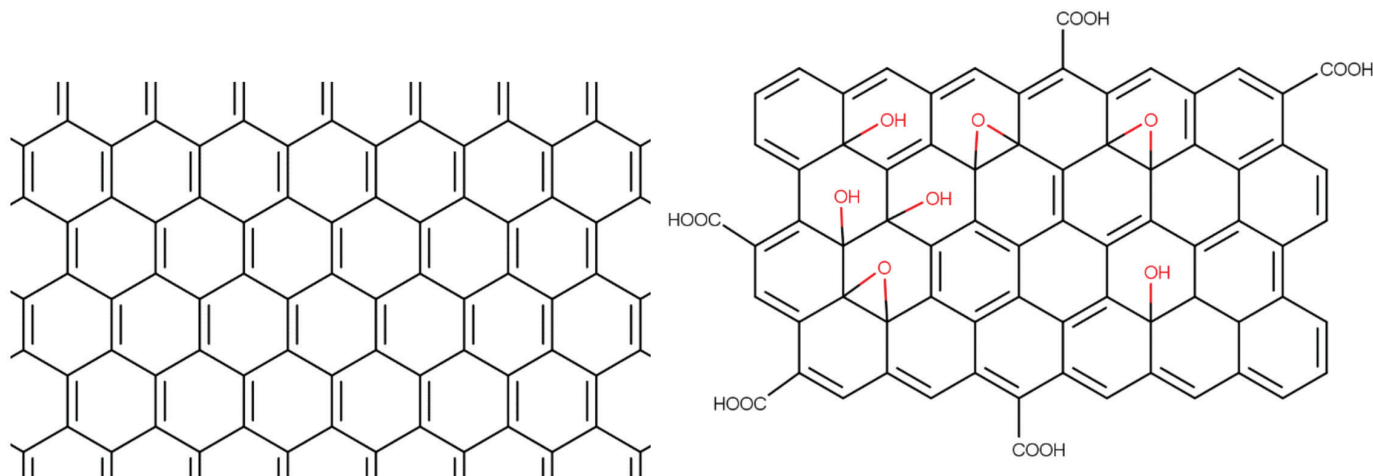
Figure 2. Molecular structure of graphene and graphene oxide

cells. CSN production is achieved by dissolving low molecular weight CS in 1% (v/v) acetic acid solutions for crosslinking in inverse microemulsion medium, which results in the attainment of nanometric CS gel particles. Utilizing the pH-sensitive characteristics the team managed to inhibit cytotoxic drug release.[51]

GRAPHENE AND GRAPHENE OXIDE NANOCARRIERS

Professor Andre Geim and Professor Kostya Novoselov made a groundbreaking disclosure by finally discovering a production method for GR in 2004. The research was outstanding since it had not been possible previously to produce a single layer of graphite (carbon atoms with sp2 bonds in the shape of honeycomb). Later, GR became known as the basic building block of graphitic materials such as spherical nanoparticles that are also known as 0D fullerenes, 1D carbon nanotubes, and 3D graphite.[54-58]

Following the discovery, scientists began to reveal GR's unique characteristics provided by its submicron dimension and the π-conjugation in its structure. GR is revealed to exhibit extraordinary thermal, mechanical, and electrical properties.[57] Further research provided a better understanding of the physical and chemical structure of GR's surface, which has created interest in medical and pharmaceutical technologies as well as other fields of science. GR is researched and utilized for nanoscaffolds, chemical/biosensing, imaging, drug delivery and controlled drug release.[59] In the area of nanomedicine and nanocarriers, GR and its composites are important due to its large surface area where every single atom is exposed on the surface ($2600 \text{ m}^2\text{ g}^{-1}$), layer number, lateral dimension, surface chemistry, and purity.[60-62] Hereby, GR could be considered a superior candidate as an ideal nanocarrier with the mentioned characteristics that allows a high drug load capacity.[58]

One of the most popular derivatives of GR is GO, GR with oxygen-containing functionalities (epoxide, carbonyl, carboxyl, and hydroxyl groups). GR and GO have a major difference

that affects their drug delivery performance when used as nanocarriers: GO is highly hydrophilic, whereas GR is hydrophobic so that it requires surface modifications for use in biological fluids. Thus, any nanocarrier design that uses GR should take into consideration the possible impurities and negative effects such as cytotoxicity.[61,63] This leads researchers to gravitate towards GO-containing designs rather than GR nanocarrier designs.

In Table 3, a summary of GR/GO nanocarrier designs is given. As can be seen, Hummer's method for production is the most popular choice, where graphite oxidative exfoliation is applied with $NaNO_3$. Although Hummer's production method is usually opted for rather than other complicated methods, over the years it can be seen that nanocarrier designs have evolved into more complex systems that apply chemotherapy and photothermal therapy for treating cancer.

In 2008, Liu et al.[87] published a study that demonstrates PEG-functionalized GO nanocarriers used as a noncovalent physisorption chemotherapy drug delivery system. The team reveals that the nanocarriers have an adequate *in vitro* cellular uptake capacity.[87] A very recent study by Bullo et al.[88] examined the state of the art in GO nanocarriers. GO is reported to be synthesized by Hummer's method. GO is modified with PEG for higher biocompatibility and loaded with two chemotherapeutic drugs: protocatechuic acid and chlorogenic acid. The carrier is then coated with folic acid to target cancer cells since tumor surface membranes have a greater number of folate receptors. The final size of the nanocarrier system is stated to be 9-40 nm with a median of 8 nm. The team reveals that drug release of this design took more than 100 h, which ensures a steady therapeutic effect.[88]

SOLID LIPID NANOPARTICLES

Nanocarriers designed with a polymer foundation have a certain advantage in terms of the wealth of possible chemical modifications, including the synthesis of block and comb polymers.[89] Designs that use SLNs exploit this advantage by combining the advantages and avoiding the disadvantages of

Table 1. Popular nanohydrogel materials utilized as nanocarriers	
Nanohydrogel carrier material	**Structure**
Xyloglucan	
Glycerophosphate	
Poly (N-isopropylacrylamide)	
Poly (N-isopropylacrylamide-co-acrylic acid)	
Poloxamer (Pluronic)	
Poly (Organo phosphazene)	
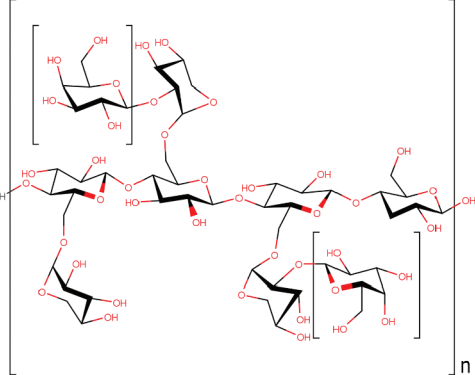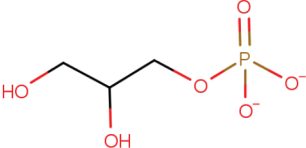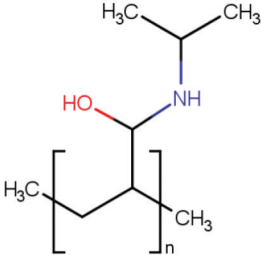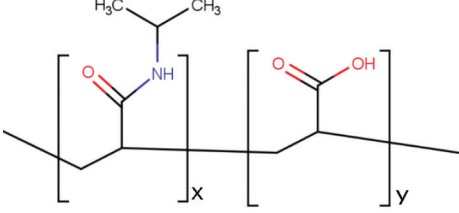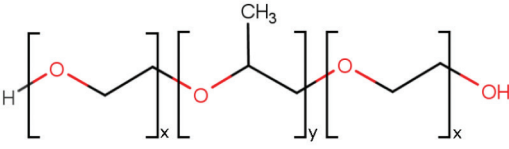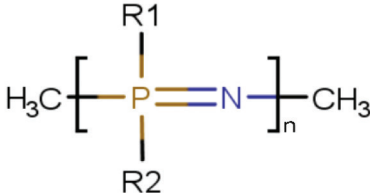
Table 2. A literature summary of CSNs

Date	Drug	Nanocarrier design & advantages	CS nanoparticle production	Reference
1999	Insulin	Blood glucose control nasal absorption pH selective release	Ionotropic gelation with Penta-sodium tri-polyphosphate	31
2005	Epirubicin	Chemotherapy chitosan-bound magnetic nanocarrier	Carboxymethylated Chitosan covalently bound onto Fe_3O_4 nanoparticles	32
2005	BSA	Carboxymethyl konjac glucomannan–chitosan nanoparticles	Dropping method	33
2005	Z-DEVD-FMK	Cerebral Ischemia Therapy CS-PEG-BIO-SA/OX26	Chitosan acetylation 13.7%	34
2005	Insulin	Oral/Nasal Drug Carrier CS nanoparticles, CS nanocapsules and CS-coated lipid nanoparticles	Ionotropic gelation	35
2006	Triclosan Furoscmide	Higher solubility in water hydroxypropyl cyclodextrin containing chitosan nanocarrier	Ionotropic gelation	36
2006	Protein complex P1	Transmucosal drug carrier glucomannan-coated chitosan nanoparticles	Ionotropic gelation	37
2006	Salmon calcitonin	Oral drug carrier carrier for peptide drugs through the intestinal epithelium	Ionotropic gelation	38
2007	-	Transmucosal drug carrier hydrophilic cyclodextrin-chitosan core and chitosan coating	Ionotropic gelation	39
2008	Indomethacin	Ophthalmic Drug Delivery	Ionotropic gelation by addition of TPP anions	40
2009	HP-b-CD complex simvastatin	Oral delivery of drugs that are insoluble in water	Ionotropic gelation with Penta-sodium tri-polyphosphate	41
2010	Bleomycin	Chemotherapy Fe_3O_4 containing chitosan nanoparticles	Ionotropic gelation with Penta-sodium tri-polyphosphate	42
2010	siRNA	PEGylated Chitosan Nanocarriers Imidazole-modified chitosan-IAA nanoparticles	Complex coacervation of nonmodified chitosan or chitosan-IAA with siRNA	43
2010	Glutathione	Oral Drug Carrier Chitosan and Chitosan/cyclodextrin NPs	Ionotropic gelation	44
2010	Mesalazine	Colon Specific Drug Delivery Superparamagnetic chitosan–dextran sulfate NPs	Ionotropic gelation	45
2011	Silver NPs	Colon Cancer Apoptosis Chitosan-based nanocarrier of silver NPs	Ionotropic gelation with Penta-sodium tri-polyphosphate	46
2011	Curcumin	Hydrophobic drug delivery for cancer treatment Carboxymethyl chitosan nanocarriers	Ionic cross linking between carboxyl group	47
2014	100% iron saturated-bovine lactoferrin	Osteoarthritis treatment	-	48
2014	Rosmarinic acid	Antioxidant delivery	Ionotropic gelation with Penta-sodium tri-polyphosphate	49
2015	Paclitaxel	Chitosan based glycolipid-like nanocarrier		50
2019	Polyoxometalates	Breast cancer therapy pH selective release	Crosslinked in inverse microemulsion medium	51

CSN: Chitosan nanocarriers

Table 3. A literature summary of GR/GO nanocarriers

Date	Drug	Nanocarrier	Nanocarrier design & advantages	GR or go synthesis	Nanocarrier size on average	Reference
2010	Camptothecin (CPT) Doxorubicin (DOX)	FA-GONS-p-amino benzenesulfonic acid	Sulfonic acid groups render stability in physiological solutions Target: human breast cancer cells	Hummer's method	GONS (thickness) ⟨ 150 nm	64
2011	Ellagic acid (EA)	GONS-Pluronic F38(F38), GONS - Tween 80(T80), GONS–Maltodextrin (MD)	High drug loading (For GO-T80, 1.22 g per 1 g)	Hummer's method	GONS-F38 (thickness)=6-7 nm GONS-T80 (thickness)=7-8 nm GONS-MD (thickness) =5-6 nm	65
2011	Doxorubicin (DOX)	PEG-GONS	Both chemotherapy and near infrared (NIR) photothermal therapy Lower systematic toxicity	Hummer's method	-	66
2011	Tamoxifen Citrate (TmC)	Pyridinium bromide (PY+-Chol)-Graphene (GR)	Enhanced the apoptosis of cancer cells	-	PY+-Chol-GR (hydrodynamic diameter)=150-200 nm	67
2013	Doxorubicin (DOX)	Polyethylene Glycol-Branched Polyethyleneimine-Reduced GO (PEG-BPEI-rGO)	Photothermally controlled anti-cancer drug delivery Higher cancer cell death	Reduction by hydrazine monohydrate	100-200 nm	68
2013	5-fluorouracil (5-FU)	Fe_3O_4-GONS	pH dependent chemotherapy High drug loading capacity of up to 0.35 mg mg^{-1}	Hummer's method	-	69
2013	Doxorubicin (DOX)	PVP-GONS-FA	pH sensitive nanocarrier Both chemotherapy and near infrared (NIR) photothermal therapy	Hummer's method	GONS=100 nm	70
2013	Doxorubicin (DOX)	FA-GONS-Chitosan (CHI)	High drug loading efficiency (0.98 mg/mg) & prolonged drug release rate pH sensitive drug release	Hummer's method	-	71
2014	Doxorubicin (DOX)	GO/integrin aVb3 mono-antibody (Abs)/polyethyleneimine (PEI)/citraconic anhydride functionalized poly(allylamine) (PAH-Cit)	Charge-reversal, target specific nanocarrier Drug release in acidic intracellular organelles	Hummer's method	GO/PEI/PAH-Cit/ DOX=20-200 nm	72
2014	Doxorubicin (DOX)	Hyaluronic acid (HA)-GONS	Targeted and pH sensitive drug delivery High loading efficiency of drug (42.9%)	Hummer's method	GONS (lateral)=10-200 nm	73

2014	Doxorubicin (DOX)	PEG-Poly (allylamine hydrochloride) (PAH)-2,3-dimethylmaleic anhydride (DA)-GONS	pH sensitive drug release Both chemotherapy and photothermal therapy	Hummer's method	PEG-PAH-DA-GONS=70 nm	74
2015	Paclitaxel (PTX)	PEG-GO	Nontoxic chemotherapy carrier Increased biocompatibility and physiological stability	Hummer's method	PEG-GO-PTX (lateral)=50-200 nm	75
2015	Irinotecan (IRI) Doxorubicin (DI)	Poloxamer 188-GONS	Photothermal therapy with dual chemotherapies in one system	Hummer's method	GONS=200 nm	76
2015	Indomethacin (IMC) Doxorubicin (DOX)	poly(N-isopropylacrylamide) (PNIPAM)-GO	Enhanced thermal stability Improved dispersibility in aqueous and cell medium	Hummer's method	GONS=0.85 nm NIPAM-GONS=3.2 nm	77
2016	Doxorubicin (DOX)	Gold Nanoparticle (AuNP) - Folic Acid - GONS	Targeted chemotherapy and photothermal ablation	-	AuNP-FA-GONS (Hydrodynamic size)=188.2±7.2 nm AuNP-GO (diagonal)=135 nm	78
2018	Doxorubicin (DOX) Camptothecin (CPT)	Folic acid (FA)-Graphene Oxide Nanosheet (GONS)	FA linked GONS for high affinity to folate receptor	Hummer's method	2.7 nm	79
2018	Tetracycline (TC)	Carboxymethylcellulose (CMC)-Zn-Based Metal-Organic Framework (MOF-5)-GO	Efficient oral drug delivery Effective protection against stomach pH	Hummer's method	CMC/MOF-5/GO (diameter)=344 nm	80
2018	Doxorubicin (DOX)	Carboxymethylcellulose (CMC)-Zn-Based Metal-Organic Framework (MOF-5)-GONS	Targeted delivery and controlled release of chemotherapy human blood cancer cell lines	Hummer's method	GONS (Thickness)=30 nm CMC/MOF-5/GONS=80 nm	81
2019	Quercetin (QSR) Gefitinib (GEF)	Polyvinylpyrrolidone (PVP)-GO	High biocompatibility Enhanced anticancer activity within a dosage range	Hummer's method	GO=166.5 nm PVP-GO=300-400 nm	82
2019	Cis-diamminedichloroplatinum (II) (CisPt)	Maghemiteγ-Fe$_2$O$_3$-GO	Efficient Malignant glioma chemotherapy GONP accumulates in U87 human glioblastoma subcutaneous tumor xenografts	Hummer's method	GO (width)=80-100 nm GO (thickness)=6.3 nm	83
2019	Methotrexate (MTX)	Polyethylene Glycol bis Amin (PEGA)- GO Magnetic NS (GOMNS)	Magnetic Iron NPs Increased efficacy in chemotherapy with pH dependent drug release and biocompatibility	Hummer's method	-	84
2019	5-Fluorouracil (5-FU) Curcumin (CUR)	Chitosan-rGO	Increased efficiency of chemotherapy against colon cancer	-	-	85
2019	Doxorubicin (DOX)	κ-Carrageenan (κ-Car)-GONS-biotin	Targeted therapy for cervical cancer pH-sensitive drug release	Hummer's method	ϰ-Car-GONS-biotin (thickness)=219 nm	86

other colloidal carriers.

Lipids are defined as molecules that are hydrophobic or consisting of both hydrophilic and hydrophobic parts that are insoluble in water and soluble in organic solvents.[90] IUPAC gave the following further detailed definition in 1995:

"A loosely defined term for substances of biological origin that are soluble in nonpolar solvents. They consist of saponifiable lipids, such as glycerides (fats and oils) and phospholipids, as well as nonsaponifiable lipids, principally steroids."[91]

SLNs are developed by researchers as a substitute colloidal carrier with a spherical morphology for drug delivery and drug release.[5] SLNs have an average size of between 150 and 300 nm but could reach up to 1000 nm according to the surfactant used during production and are composed of roughly 0.1-30 (% w/w) solid fat.[92] Size and solid to liquid fat ratio affect the long-term stability, drug-loading capacity, and drug-release behavior of SLNs.[93] As mentioned, SLNs have several favored assets such as low to no toxic effect on healthy tissue and ease of production in greater units of production, ability to load both lipophilic and hydrophilic therapeutic agents, and high drug load capacity.[5] The most common use of SLNs as nanocarriers is for oral drug delivery. Other than this example, several drugs have been loaded using SLNs for drug delivery, such as doxorubicin and idarubicin,[94] thymopentin,[95] and camptothecin.[96]

DISCUSSION AND CONCLUSION

Nanocarriers provide researchers with a highly applicable alternative method for targeted drug delivery and controlled drug release. The first and foremost reason that nanocarriers have become such a great focus in pharmaceutical technologies is that nanomaterials demonstrate extraordinary characteristics when compared with their larger scaled forms. These characteristics are summarized in this review as color, visible light, reactivity, surface area to volume ratio, conductivity, and surface tension. A variety of these carriers are more popular due to their high biocompatibility, ensuring greater efficacy especially in cancer treatments. Successful applications have not only ensured a greater focus on therapeutic development but also created a new solution available in the pharmaceutical market. In this paper, nanocarrier materials that have gained the most attention in drug delivery and release are summarized under the titles of nanohydrogels carriers, CSNs, GR and GO nanocarriers, and SLNs. Besides these nanomaterials there are also a great number of different nanocarrier designs that are not included in this review, such as gold nanocarriers,[97] starch and/or cellulose nanocarriers,[98] cerium oxide nanocarriers,[99] and carbon nanotube incorporated nanocarriers.[100] It is clear that, with further information gathered on nanocarriers for drug delivery and the current state in the development process of these nanomaterials, there is a high possibility to deliver better treatment to patients desperate in need of efficient treatment strategies.

Conflict of interest: No conflict of interest was declared by the authors.

REFERENCES

1. Grimsdale AC, Müllen K. The chemistry of organic nanomaterials. Angew Chem Int Ed Engl. 2005;44:5592-5629.

2. EU Definition of a Nanomaterial [Internet]. [cited 2019 May 27]. Available from: https://www.safenano.org/knowledgebase/regulation/substances/eu-definition-of-a-nanomaterial/

3. Nalwa HS. A special issue on reviews in nanomedicine, drug delivery and vaccine development. J Biomed Nanotechnol. 2014;10:1635-1640.

4. Han J, Zhao D, Li D, Wang X, Jin Z, Zhao K. Polymer-based nanomaterials and applications for vaccines and drugs. Polymers (Basel). 2018;10(1).

5. Müller RH, Mäder K, Gohla S. Solid lipid nanoparticles (SLN) for controlled drug delivery - a review of the state of the art. Eur J Pharm Biopharm. 2000;50:161-177.

6. Couvreur P, Kante B, Roland M, Guiot P, Bauduin P, Speiser P. Polycyanoacrylate nanocapsules as potential lysosomotropic carriers: preparation, morphological and sorptive properties. J Pharm Pharmacol. 1979;31:331-332.

7. Kreuter J, Speiser PP. *In vitro* studies of poly(methyl methacrylate) adjuvants. J Pharm Sci. 1976;65:1624-1627.

8. De Jong WH, Borm PJ. Drug delivery and nanoparticles: applications and hazards. Int J Nanomedicine. 2008;3:133-149.

9. Ochekpe NA, Olorunfemi PO, Ngwuluka NC. Nanotechnology and Drug Delivery Part 2: Nanostructures for Drug Delivery. Trop J Pharm Res. 2009;8:275-287.

10. Lombardo D, Kiselev MA, Caccamo MT. Smart nanoparticles for drug delivery application: development of versatile nanocarrier platforms in biotechnology and nanomedicine. Journal of Nanomaterials. 2019;2019:1-26.

11. Hoare TR, Kohane DS. Hydrogels in drug delivery: progress and challenges. Polymer. 2008;49:1993-2007.

12. Choudhary B, Paul SR, Nayak SK, Qureshi D, Pal K. Synthesis and biomedical applications of filled hydrogels. In: Pal K, Banerjee I, eds. Polymeric Gels: Characterization, Properties and Biomedical Applications (1st ed). United Kingdom; Elsevier, 2018:283-302.

13. Klouda L, Mikos AG. Thermoresponsive hydrogels in biomedical applications. Eur J Pharm Biopharm. 2008;68:34-45.

14. Wang ZG, Ding B. DNA-based self-assembly for functional nanomaterials. Adv Mater. 2013;25:3905-3914.

15. Li J, Mooney DJ. Designing hydrogels for controlled drug delivery. Nat Rev Mater. 2016;1:16071.

16. Lin CC, Metters AT. Hydrogels in controlled release formulations: network design and mathematical modeling. Adv Drug Deliv Rev. 2006;58:1379-1408.

17. Brannon-Peppas L, Peppas NA. Equilibrium swelling behavior of pH-sensitive hydrogels. Chemical Engineering Science. 1991;46:715-722.

18. Garg T, Singh S, Goyal AK. Stimuli-sensitive hydrogels: an excellent carrier for drug and cell delivery. Crit Rev Ther Drug Carrier Syst. 2013;30:369-409.

19. Liu J, Yin Y. Temperature responsive hydrogels: construction and applications. Polym Sci. 2015;1:1.

20. Ichikawa H, Fukumori Y. A novel positively thermosensitive controlled-release microcapsule with membrane of nano-sized poly(N-isopropylacrylamide) gel dispersed in ethylcellulose matrix. J Control Release. 2000;63:107-119.

21. Dalwadi C, Patel G1. Thermosensitive nanohydrogel of 5-fluorouracil for head and neck cancer: preparation, characterization and cytotoxicity assay. Int J Nanomedicine. 2018;13(T-NANO 2014 Abstracts):31-33.

22. Elsaeed SM, Farag RK, Maysour NS. Synthesis and characterization of pH-sensitive crosslinked (NIPA-co-AAC) nanohydrogels copolymer. J Appl Polym Sci. 2012;124:1947-1955.

23. Dufresne MH, Garrec DL, Sant V, Leroux JC, Ranger M. Preparation and characterization of water-soluble pH-sensitive nanocarriers for drug delivery. Int J Pharm. 2004;277:81-90.

24. Rinaudo M. Chitin and chitosan: properties and applications. Progress in Polymer Science. 2006;31:603-632.

25. Ravi Kumar MNV. A review of chitin and chitosan applications. React Funct Polym. 2000;46:1-27.

26. de la Fuente M, Csaba N, Garcia-Fuentes M, Alonso MJ. Nanoparticles as protein and gene carriers to mucosal surfaces. Nanomedicine (Lond). 2008;3:845-857.

27. Calvo P, Remuñán-López C, Vila-Jatu JL, Alonso MJ. Novel hydrophilic chitosan-polyethylene oxide nanoparticles as protein carriers. J. Appl. Polym. Sci. 1997;63:125-132.

28. Csaba N, Garcia-Fuentes M, Alonso MJ. The performance of nanocarriers for transmucosal drug delivery. Expert Opin Drug Deliv. 2006;3:463-478.

29. Zhang X, Lin Y, Gillies RJ. Tumor pH and its measurement. J Nucl Med. 2010;51:1167-1170.

30. Giri TK. Alginate containing nanoarchitectonics for improved cancer therapy. In: Holban AM, Grumezescu AM, eds. Nanoarchitectonics for Smart Delivery and Drug Targeting. Elsevier, 2016;565-588.

31. Fernández-Urrusuno R, Calvo P, Remuñán-López C, Vila-Jato JL, Alonso MJ. Enhancement of nasal absorption of insulin using chitosan nanoparticles. Pharm Res. 1999;16:1576-1581.

32. Chang YC, Shieh DB, Chang CH, Chen DH. Conjugation of monodisperse chitosan-bound magnetic nanocarrier with epirubicin for targeted cancer therapy. J Biomed Nanotechnol. 2005;1:196-201.

33. Du J, Sun R, Zhang S, Zhang LF, Xiong CD, Peng YX. Novel polyelectrolyte carboxymethyl konjac glucomannan-chitosan nanoparticles for drug delivery. I. Physicochemical characterization of the carboxymethyl konjac glucomannan-chitosan nanoparticles. Biopolymers. 2005;78:1-8.

34. Aktaş Y, Yemisci M, Andrieux K, Gürsoy RN, Alonso MJ, Fernandez-Megia E, Novoa-Carballal R, Quiñoá E, Riguera R, Sargon MF, Celik HH, Demir AS, Hincal AA, Dalkara T, Capan Y, Couvreur P. Development and brain delivery of chitosan–PEG nanoparticles functionalized with the monoclonal antibody OX26. Bioconjug Chem. 2005;16:1503-1511.

35. Prego C, García M, Torres D, Alonso MJ. Transmucosal macromolecular drug delivery. J. Control. Release. 2005;101:151-162.

36. Maestrelli F, Garcia-Fuentes M, Mura P, Alonso MJ. A new drug nanocarrier consisting of chitosan and hydoxypropylcyclodextrin. Eur J Pharm Biopharm. 2006;63:79-86.

37. Cuña M, Alonso-Sandel M, Remuñán-López C, Pivel JP, Alonso-Lebrero JL, Alonso MJ. Development of phosphorylated glucomannan-coated chitosan nanoparticles as nanocarriers for protein delivery. J Nanosci Nanotechnol. 2006;6:2887-2895.

38. Prego C, Fabre M, Torres D, Alonso MJ. Efficacy and mechanism of action of chitosan nanocapsules for oral peptide delivery. Pharm Res. 2006;23:549-556.

39. Trapani A, Garcia-Fuentes M, Alonso MJ. Novel drug nanocarriers combining hydrophilic cyclodextrins and chitosan. Nanotechnology. 2008;19:185101.

40. Badawi AA, El-Laithy HM, El Qidra RK, El Mofty H, El dally M. Chitosan based nanocarriers for indomethacin ocular delivery. Arch Pharm Res. 2008;31:1040-1049.

41. Vyas A, Saraf S, Saraf S. Encapsulation of cyclodextrin complexed simvastatin in chitosan nanocarriers: a novel technique for oral delivery. J Incl Phenom. 2009;66:251-259.

42. Kavaz D, Odabaş S, Güven E, Demirbilek M, Denkbaş EB. Bleomycin loaded magnetic chitosan nanoparticles as multifunctional nanocarriers. J. Bioact. Compat. Polym. 2010;25:305-318.

43. Ghosn B, Singh A, Li M, Vlassov AV, Burnett C, Puri N, Roy K. Efficient gene silencing in lungs and liver using imidazole-modified chitosan as a nanocarrier for small interfering RNA. Oligonucleotides. 2010;20:163-172.

44. Trapani A, Lopedota A, Franco M, Cioffi N, Ieva E, Garcia-Fuentes M, Alonso MJ. A comparative study of chitosan and chitosan/cyclodextrin nanoparticles as potential carriers for the oral delivery of small peptides. Eur J Pharm Biopharm. 2010;75:26-32.

45. Saboktakin MR, Tabatabaie R, Maharramov A, Ramazanov MA. Synthesis and characterization of superparamagnetic chitosan-dextran sulfate hydrogels as nano carriers for colon-specific drug delivery. Carbohydr. Polym. 2010;81:372-376.

46. Sanpui P, Chattopadhyay A, Ghosh SS. Induction of apoptosis in cancer cells at low silver nanoparticle concentrations using chitosan nanocarrier. ACS Appl Mater Interfaces. 2011;3:218-228.

47. Anitha A, Maya S, Deepa N, Chennazhi KP, Nair SV, Tamura H, Jayakumar R. Efficient water soluble O-carboxymethyl chitosan nanocarrier for the delivery of curcumin to cancer cells. Carbohydr. Polym. 2011;83:452-461.

48. Samarasinghe RM, Kanwar RK, Kanwar JR. The effect of oral administration of iron saturated-bovine lactoferrin encapsulated chitosan-nanocarriers on osteoarthritis. Biomaterials. 2014;35:7522-7534.

49. da Silva SB, Amorim M, Fonte P, Madureira R, Ferreira D, Pintado M, Sarmento B. Natural extracts into chitosan nanocarriers for rosmarinic acid drug delivery. Pharm Biol. 2015;53:642-652.

50. Hu YW, Du YZ, Liu N, Liu X, Meng TT, Cheng BL, He JB, You J, Yuan H, Hu FQ. Selective redox-responsive drug release in tumor cells mediated by chitosan based glycolipid-like nanocarrier. J Control Release. 2015;206:91-100.

51. Pérez-Álvarez L, Ruiz-Rubio L, Artetxe B, Vivanco MD, Gutiérrez-Zorrilla JM, Vilas-Vilela JL. Chitosan nanogels as nanocarriers of polyoxometalates for breast cancer therapies. Carbohydr Polym. 2019;213:159-167.

52. Kumar MN, Muzzarelli RA, Muzzarelli C, Sashiwa H, Domb AJ. Chitosan chemistry and pharmaceutical perspectives. Chem Rev. 2004;104:6017-6084.

53. Ahmed TA, Aljaeid BM. Preparation, characterization, and potential application of chitosan, chitosan derivatives, and chitosan metal nanoparticles in pharmaceutical drug delivery. Drug Des Devel Ther. 2016;10:483-507.

54. Geim AK, Novoselov KS. The rise of graphene. Nat Mater. 2007;6:183-191.

55. Geim AK. Graphene: status and prospects. Science. 2009;324:1530-1534.

56. Stankovich S, Dikin DA, Dommett GH, Kohlhaas KM, Zimney EJ, Stach EA, Piner RD, Nguyen ST, Ruoff RS. Graphene-based composite materials. Nature. 2006;442:282-286.

57. Allen MJ, Tung VC, Kaner RB. Honeycomb carbon: a review of graphene. Chem Rev. 2010;110:132-145.

58. Liu J, Cui L, Losic D. Graphene and graphene oxide as new nanocarriers for drug delivery applications. Acta Biomater. 2013;9:9243-9257.

59. Shao Y, Wang J, Wu H, Liu J, Aksay IA, Lin Y. Graphene based electrochemical sensors and biosensors: A review. Electroanalysis 2010;22:1027-1036.

60. Shen H, Zhang L, Liu M, Zhang Z. Biomedical applications of graphene. Theranostics. 2012;2:283-294.

61. Wang Y, Li Z, Wang J, Li J, Lin Y. Graphene and graphene oxide: biofunctionalization and applications in biotechnology. Trends Biotechnol. 2011;29:205-212.

62. Liu Z, Sun X, Nakayama-Ratchford N, Dai H. Supramolecular chemistry on water-soluble carbon nanotubes for drug loading and delivery. ACS Nano. 2007;1:50-56.

63. Pumera M. Nanotoxicology: the molecular science point of view. Chem Asian J. 2011;6:340-348.

64. Zhang L, Xia J, Zhao Q, Liu L, Zhang Z. Functional graphene oxide as a nanocarrier for controlled loading and targeted delivery of mixed anticancer drugs. Small. 2010;6:537-544.

65. Kakran M, Sahoo NG, Bao H, Pan Y, Li L. Functionalized graphene oxide as nanocarrier for loading and delivery of ellagic acid. Curr Med Chem. 2011;18:4503-4512.

66. Zhang W, Guo Z, Huang D, Liu Z, Guo X, Zhong H. Synergistic effect of chemo-photothermal therapy using PEGylated graphene oxide. Biomaterials. 2011;32:8555-8561.

67. Misra SK, Kondaiah P, Bhattacharya S, Rao CN. Graphene as a nanocarrier for tamoxifen induces apoptosis in transformed cancer cell lines of different origins. Small. 2012;8:131-143.

68. Kim H, Lee D, Kim J, Kim TI, Kim WJ. Photothermally triggered cytosolic drug delivery via endosome disruption using a functionalized reduced graphene oxide. ACS Nano. 2013;7:6735-6746.

69. Fan X, Jiao G, Zhao W, Jin P, Li X. Magnetic Fe_3O_4-graphene composites as targeted drug nanocarriers for pH-activated release. Nanoscale. 2013;5:1143-1152.

70. Qin XC, Guo ZY, Liu ZM, Zhang W, Wan MM, Yang BW. Folic acid-conjugated graphene oxide for cancer targeted chemo-photothermal therapy. J Photochem Photobiol B. 2013;120:156-162.

71. Wang Z, Zhou C, Xia J, Via B, Xia Y, Zhang F, Li Y, Xia L. Fabrication and characterization of a triple functionalization of graphene oxide with Fe_3O_4, folic acid and doxorubicin as dual-targeted drug

nanocarrier. Colloids Surf B Biointerfaces. 2013;106:60-65.

72. Zhou T, Zhou X, Xing D. Controlled release of doxorubicin from graphene oxide based charge-reversal nanocarrier. Biomaterials. 2014;35:4185-4194.

73. Song E, Han W, Li C, Cheng D, Li L, Liu L, Zhu G, Song Y, Tan W. Hyaluronic acid-decorated graphene oxide nanohybrids as nanocarriers for targeted and pH-responsive anticancer drug delivery. ACS Appl Mater Interfaces. 2014;6:11882-11890.

74. Feng L, Li K, Shi X, Gao M, Liu J, Liu Z. Smart pH-responsive nanocarriers based on nano-graphene oxide for combined chemo- and photothermal therapy overcoming drug resistance. Adv Healthc Mater. 2014;3:1261-1271.

75. Xu Z, Zhu S, Wang M, Li Y, Shi P, Huang X. Delivery of paclitaxel using pegylated graphene oxide as a nanocarrier. ACS Appl Mater Interfaces. 2015;7:1355-1363.

76. Tran TH, Nguyen HT, Pham TT, Choi JY, Choi HG, Yong CS, Kim JO. Development of a graphene oxide nanocarrier for dual-drug chemo-phototherapy to overcome drug resistance in cancer. ACS Appl Mater Interfaces. 2015;7:28647-28655.

77. Kundu A, Nandi S, Das P, Nandi AK. Fluorescent graphene oxide via polymer grafting: an efficient nanocarrier for both hydrophilic and hydrophobic drugs. ACS Appl Mater Interfaces. 2015;7:3512-3523.

78. Chauhan G, Chopra V, Tyagi A, Rath G, Sharma RK, Goyal AK. "Gold nanoparticles composite-folic acid conjugated graphene oxide nanohybrids" for targeted chemo-thermal cancer ablation: *in vitro* screening and *in vivo* studies. Eur J Pharm Sci. 2017;96:351-361.

79. He H, Li S, Shi X, Wang X, Liu X, Wang Q, Guo A, Ge B, Khan NU, Huang F. Quantitative nanoscopy of small blinking graphene nanocarriers in drug delivery. Bioconjug Chem. 2018;29:3658-3666.

80. Karimzadeh Z, Javanbakht S, Namazi H. Carboxymethylcellulose/ MOF-5/graphene oxide bio-nanocomposite as antibacterial drug nanocarrier agent. Bioimpacts. 2019;9:5-13.

81. Javanbakht S, Pooresmaeil M, Namazi H. Green one-pot synthesis of carboxymethylcellulose/Zn-based metal-organic framework/ graphene oxide bio-nanocomposite as a nanocarrier for drug delivery system. Carbohydr Polym. 2019;208:294-301.

82. Tiwari H, Karki N, Pal M, Basak S, Verma RK, Bal R, Kandpal ND, Bisht G, Sahoo NG. Functionalized graphene oxide as a nanocarrier for dual drug delivery applications: the synergistic effect of quercetin and gefitinib against ovarian cancer cells. Colloids Surf B Biointerfaces. 2019;178:452-459.

83. Makharza SA, Cirillo G, Vittorio O, Valli E, Voli F, Farfalla A, Curcio M, Iemma F, Nicoletta FP, El-Gendy AA, Goya GF, Hampel S. Magnetic graphene oxide nanocarrier for targeted delivery of cisplatin: a perspective for glioblastoma treatment. Pharmaceuticals (Basel). 2019;12(2).

84. Abdollahi Z, Taheri-Kafrani A, Bahrani SA, Kajani AA. PEGAylated graphene oxide/superparamagnetic nanocomposite as a high-efficiency loading nanocarrier for controlled delivery of methotrexate. J Biotechnol. 2019;298:88-97.

85. Dhanavel S, Revathy TA, Sivaranjani T, Sivakumar K, Palani P, Narayanan V, Stephen A. 5-Fluorouracil and curcumin co-encapsulated chitosan/reduced graphene oxide nanocomposites against human colon cancer cell lines. Polym Bull. 2019 Mar 15. doi:10.1007/s00289-019-02734-x

86. Vinothini K, Rajendran NK, Munusamy MA, Alarfaj AA, Rajan M. Development of biotin molecule targeted cancer cell drug delivery of doxorubicin loaded ϰ-carrageenan grafted graphene oxide nanocarrier. Mater Sci Eng C Mater Biol Appl. 2019;100:676-687.

87. Liu Z, Robinson JT, Sun X, Dai H. PEGylated nanographene oxide for delivery of water-insoluble cancer drugs. J Am Chem Soc. 2008;130:10876-10877.

88. Bullo S, Buskaran K, Baby R, Dorniani D, Fakurazi S, Hussein MZ. Dual drugs anticancer nanoformulation using graphene oxide-PEG as nanocarrier for protocatechuic acid and chlorogenic acid. Pharm Res. 2019;36:91.

89. Mehnert W, Mäder K. Solid lipid nanoparticles. Advanced Drug Delivery Reviews. 2012;64:83-101.

90. Gordillo-Galeano A, Mora-Huertas CE. Solid lipid nanoparticles and nanostructured lipid carriers: a review emphasizing on particle structure and drug release. Eur J Pharm Biopharm. 2018;133:285-308.

91. Moss GP, Smith PAS, Tavernier D. Glossary of class names of organic compounds and reactivity intermediates based on structure (IUPAC Recommendations 1995). Pure &App Chem. 1995;67:1307-1375.

92. Naseri N, Valizadeh H, Zakeri-Milani P. Solid lipid nanoparticles and nanostructured lipid carriers: structure, preparation and application. Adv Pharm Bull. 2015;5:305-313.

93. Yoon G, Park JW, Yoon IS. Solid lipid nanoparticles (SLNs) and nanostructured lipid carriers (NLCs): recent advances in drug delivery. J Pharm Investig. 2013;43:353-362.

94. Cavalli R, Caputo O, Gasco MR. Solid lipospheres of doxorubicin and idarubicin. Int J Pharm. 1993;89:R9-R12.

95. Morel S, Ugazio E, Cavalli R, Gasco MR. Thymopentin in solid lipid nanoparticles. Int J Pharm. 1996;132:259-261.

96. Yang S, Zhu J, Lu Y, Liang B, Yang C. Body distribution of camptothecin solid lipid nanoparticles after oral administration. Pharm Res. 1999;16:751-757.

97. Choi WI, Kim JY, Kang C, Byeon CC, Kim YH, Tae G. Tumor regression *in vivo* by photothermal therapy based on gold-nanorod-loaded, functional nanocarriers. ACS Nano. 2011;5:1995-2003.

98. Kang B, Okwieka P, Schöttler S, Winzen S, Langhanki J, Mohr K, Opatz T, Mailänder V, Landfester K, Wurm FR. Carbohydrate-based nanocarriers exhibiting specific cell targeting with minimum influence from the protein corona. Angew Chem Int Ed Engl. 2015;54:7436-7440.

99. Sack M, Alili L, Karaman E, Das S, Gupta A, Seal S, Brenneisen P. Combination of conventional chemotherapeutics with redox-active cerium oxide nanoparticles—a novel aspect in cancer therapy. Mol Cancer Ther. 2014;13:1740-1749.

100. Hampel S, Kunze D, Haase D, Krämer K, Rauschenbach M, Ritschel M, Leonhardt A, Thomas J, Oswald S, Hoffmann V, Büchner B. Carbon nanotubes filled with a chemotherapeutic agent: a nanocarrier mediates inhibition of tumor cell growth. Nanomedicine (Lond). 2008;3:175-182.

2019 Author Index

2019 Author Index

2019 Subject Index

2019 Subject Index